The Fracture Toughness of

Fibre Concretes

By

Kenneth Lai-Wing Liu, B.Sc.

A thesis submitted for the degree

of Doctor of Philosophy

C.N.A.A. LONDON

January

1982.

Department of Civil Engineering and Building,

The Polytechnic of Wales

Treforest,

Mid Glamorgan,

In collaboration with E.H.Bradley & Sons Ltd

Certification of Research

This is to certify that, except when specific reference is made, the work described in this Dessertation is the result of the investigation of the candidate.

Candidate

Director of Studies

This is to certify that neither of this Dissertation, nor any part of it, has been presented, or is being concurrently submitted, in candidature for any degree at any other University.

K. L. Wong

Candidate

Acknowledgments

The work presented in this thesis was carried out in the Civil Engineering Department of The Polytechnic of Wales, Treforest, under supervision of Dr. B.I.G. Barr, Dr. D.C. McDowall and Dr. J. Watkins, to whom the author wishes to express his greatest gratitude for their constant encouragement, interest and advice.

My thanks are also due to E.H. Bradley & Sons Ltd for the preparation and supply of test samples.

The author also wishes to thank the technical staff in the Department of Civil Engineering and Building at the Polytechnic of Wales for their invaluable assistance during the course of this work.

The Polytechnic of Wales provided funds for this project, which the author gratefully acknowledges.

Finally the effort of Mr. T.T. Lee for his typing of this thesis is gratefully acknowledged.

CONTENTS

SUMMARY

This thesis presents experimental and numerical results on the application of Fracture Mechanics to concrete materials. In the experimental work, a study of the general properties of plain and fibre-reinforced concrete has been carried out with particular emphasis on Mode II as well as Mode I failure. A numerical study of the test specimens used in the experimental work has been carried out using constant strain triangular elements.

Three new fracture toughness tests are proposed. Two of these tests are based on the traditional standard concrete quality control specimens. The tests are relatively easy to apply requiring a minimum of specimen preparation.

The fracture toughness values have been determined from the finite element results. Stress intensity factor is readily determined from a knowledge of the load at failure and the configuration of the test specimen.

The effect of the test specimen geometry has been investigated. The results indicate that the fracture toughness value was independent of the proposed specimen geometry. A good correlation of results was obtained in the split cube specimens with the coefficient of variation generally within ten percent.

The effect of varying the modulus of elasticity in concrete was also investigated. The results show that K_{Ic} is dependent on the modulus of elasticity value for the Finite Element Analysis used in this work.

The tests developed in this study have been applied to polypropylene fibre reinforced concrete and glass fibre reinforced cement composites. The effects of varying quantities of fibre on the stress intensity factor have been investigated.

Conclusions from this project and possible future work are summarised in the last chapter.

CHAPTER ONE

INTRODUCTION

In the design of engineering structures, an engineer has to consider many types of failure. The types of failure include bending, shear, buckling and fracture. In recent years an increasing effort has been made to try to understand more regarding the problems of buckling and fracture. To some extent this increased interest and research activity in these areas has come about as a result of service failures.

Brittle fracture of structural steels has created problems for engineers ever since the late 1800's when steel became available for constructional use. During World War II, the brittle fracture of all welded ships became a major problem particularly the Liberty Ships built in the United States. The first sign of trouble occurred in the late 1942 when several reports were received of serious fractures in some ships. These occurrences were not immediately recognised as a serious structural problem until the failure of the S.S.Schenectady on January 16, 1943. Other examples of brittle fracture failures include an oil drilling rig, liquid storage tanks, gas pressure vessels, bridges and standpipes.

Many years ago, A.A.Griffith (1920) found that if glass was drawn into thin fibres, the tensile stress required to cause failure was higher than that for rods of larger cross-sections. He observed that the larger sections

often contained flaws, cracks or discontinuities in the structures and that the greater the length of the crack, the lower the tensile strength. The Griffith Theory has been expanded by Irwin and Orowan and is commonly known as the 'Fracture Mechanics Theory'. This theory has been used extensively to study the fracture of brittle materials, particularly high strength materials used in aerospace.

Concrete when not reinforced has considerable strength in compression but very little strength in tension. The actual strength of cement paste is very much lower than the theoretical strength. This is due to the presence of microcracks, voids, poor bonds and flaws in the concrete. The flaws vary in size and it is the major ones that cause failure under loading. This plays a major part in the fracture machanics of concrete.

In the early days of Fracture Mechanics, research workers concentrated on the fracture mechanism of metallic materials. Kaplan (1961) was one of the first to apply Fracture Mechanics theory in the study of the failure of concrete. He used concrete beams with crack - simulating notches to determine the critical strain energy release rate with the extension of the crack. Similar testing arrangements have been used later by other research workers to evaluate the effect of concrete parameters on fracture toughness. In recent years, most of the research effort has been directed towards developing testing methods which

could be employed to evaluate the fracture toughness of cement, mortar and concrete.

The technology for the improvement of cementitious mixtures by the incorporation of fibres is not a new idea. In ancient time, natural fibres and materials such as jute, hair, wood and bamboo have been used extensively to bind together the matrix of a wide range of materials to improve their physical properties. In the early 1960s, investigations were carried out on the effect of the addition of steel, glass, polypropylene, carbon and nylon fibres to reinforce cement paste, mortar and concrete mixes. In the early years, the main purpose of adding fibre to concrete was to increase its tensile strength. However, there has been an increasing recognition that increased ductility or toughness in fibre concrete is the most important parameter to study.

The addition of fibre to concrete offers improvement in many engineering properties of the material such as fracture toughness, fatigue resistance, impact resistance and flexural strength. These advantages have encouraged the world-wide industries in the use of fibre reinforcement for concrete, either in precast concrete or cast insitu concrete. Currently fibre concrete has been applied successfully in a number of countries especially in the United States, Canada, Japan and Western Europe. Most of the applied areas are in bridge decks, pavements,

airfields, maintenance and repair works etc.

In recent years, the finite element method has been widely accepted by the engineering professions as an extremely powerful tool of analysis. Its application has enabled satisfactory solutions to be obtained for many problems. With the advent of large digital computers, the finite element method enjoys a steady rise in popularity. The accuracy of the method has been improved by use of more sophisticated elements. The finite element method is suggested as the best candidate at the present time for obtaining approximate stress intensity factors, whenever exact solutions are not available. For given specimen geometry and loading conditions, stress intensity factors can be obtained from the basic law of displacement together with the experimental results.

The aim of this study is to investigate the properties of polypropylene fibre-reinforced concrete and the toughness of glass-reinforced cement composite materials and to develop a testing system suitable to determine the resistance of concrete materials subjected to shear failure.

To investigate the properties of polypropylene fibre-reinforced concrete several tests including two standard and three non-standard tests were carried out. Compressive strength and flexural strength were determined

using the standard procedure as described in BS 1881:Part 4. The three non-standard tests used in the experimental work were the torsion test, impact test and the split cube test. The effect of variation of polypropylene fibre content is also reported in this thesis.

Most of the research work in Fracture Mechanics has concentrated on Mode I failure. It is necessary to extend the application of Fracture Mechanics into Mode II failure. Shear failure has been produced by using a loading system similiar to the short beam shear test which has been developed to investigate interlaminar shear strength. The effects of polypropylene fibre contents in concretes and slot separations in the specimens which influence the fracture toughness have been studied.

The compact tension test is one of the recommended geometries for testing high-strength metallic materials. A similar testing system has been employed to determine the fracture toughness of glass fibre-reinforced cement composite materials. Varying specimen sizes and notch-depths have been investigated. The fracture toughness index of this material is also discussed.

In addition to the above study, finite element analysis has been employed to look at the effect of eccentricity of loading in the split-cube test and the stress distribution set up along the slot separation of the

shear specimen. In Fracture Mechanics, stress intensity factors are traditionally expressed in terms of polynomial functions of specimen geometry. The polynomial functions are derived from the finite element method using the compliance technique in this study. The stress intensity factor can be determined from the experimental and finite element results.

Unlike metallic materials which have a high modulus of elasticity, concretes have a comparatively low modulus of elasticity. The effect of varying the modulus of elasticity of concrete in the numerical work is discussed.

CHAPTER TWO

REVIEW OF LITERATURE

2.1 GRIFFITH'S THEORY

Most of the initial theoretical work on brittle fracture was developed on the basis of the concept introduced by A.A.Griffith(1) in the 1920's. His work on the theory of rupture introduced two basic ideas. The first was the presence of flaws in all real materials and the second was the relationship between the work to spread a crack and the surface energy of the new surfaces formed. Griffith(1) calculated the strain energy per unit plate thickness resulting from a crack length of 2c in a thin plate under normal stress σ, Fig.(2.1), as follows:

$$\text{Strain energy} = \frac{\pi c^2 \sigma^2}{E} \qquad (2.1)$$

The surface energy associated with the crack is given by

$$\text{Surface energy} = 2(2C)S \qquad (2.2)$$

where S is the surface energy per unit area.

Hence the total net change of potential energy of the system due to the presence of the crack is

$$4CS - \frac{\pi C^2 \sigma^2}{E} \qquad (2.3)$$

The condition that the crack may extend is

$$\frac{\partial}{\partial C}\left(4CS - \frac{\pi C^2 \sigma^2}{E}\right) = 0 \qquad (2.4)$$

From equation (2.4) Griffith (1) obtained the expression

$$\sigma_{cr} = \sqrt{\frac{2SE}{\pi C}} \qquad (2.5)$$

where σ_{cr} is the critical stress for crack extension.

The Griffith theory gives good results for a truely brittle material such as glass. When a crack propagates in glass there is negligible plastic work done even at the crack tip zone.

2.2 EXTENSION TO NON-BRITTLE MATERIALS

Orowan(2) studied X-ray pictures of the surface of a brittle crack obtained in a ship plate. Although the cracked surface showed no visible signs of plastic deformation the X-ray photographs showed that considerable plastic yielding had occurred at the crack surface. Irwin (3) pointed out that for metals, the work done against surface tension was not significant compared with the work done in plastic deformation of the atomic layers adjacent to the crack surface. Orowan(2) and Irwin(3) independently suggested that the energy of this plastic layer should be included in the effective surface energy. Thus equation (2.5) becomes

$$\sigma_{cr} = \sqrt{\frac{2Ey}{\pi c}} \qquad (2.6)$$

where y is the effective surface energy.

2.3 LINEAR ELASTIC FRACTURE MECHANICS (LEFM)

Linear elastic fracture mechanics is the study of stress and displacement fields near a crack tip in an isotropic, homogeneous, elastic material at the onset of rapid, unstable crack propagation which leads to fracture. The theory essentially provides a means of predicting the fracture stress of structures or their components, containing sharp flaws or cracks of known size and location, in terms of a single parameter. The concepts of the theory are most applicable to brittle materials in which the inelastic region near the crack tip is small compared to the flaws and specimen dimensions. The theory can be developed in terms of either an energy approach or a stress-intensity approach. Both approaches are closely related and yield identical results.

2.3.1 ENERGY APPROACH

In the energy approach, the criterion for crack propagation of a crack in a body is expressed in terms of the rate of change, with respect to crack extension, of the various energy terms involved in the process. Although the energy absorbed in crack growth, dQ, is influenced by many unknown parameters, the available energy for crack extension, dU, depends only on the elastic properties of the specimen and the applied load. If the development of

kinetic energy is negligible, then dU = dQ, and the rate of energy absorption at any stage in the crack growth can be determined by the instantaneous value of the rate of supply of available energy. The latter, dU/dA, where dA is the increase in crack area, is denoted by the symbol G. Irwin(3) first gave the formal definition of G as a fracture parameter and referred as the "strain energy release rate" measured in unit of KN/m. G is also referred to as the crack driving force or crack extension force. During stable crack propagation, G is entirely absorbed by the work involved in plastic flow and other energy dissipating mechanisms as well as the relatively smaller surface energy increase. The critical value of G at instability of the crack, or the onset of fast extension is denoted by Gc, the unstable condition for plane stress conditions. For the case of a crack length 2C in an infinite plate, as shown in Fig. (2.1), the relationship is

$$G_I = \frac{\pi C \sigma^2}{E} \qquad (2.7)$$

From the equation(2.7) we see that the strain energy release rate is proportional to the product of the crack length and the square of the stress.

The "strain energy release rate" provides a convenient parameter to include all supplemmtary energy-dissipating terms, such as plastic flow, which could

in turn produce heat or sound, in addition to the work required to fracture the atomic bonds. Gc is thus a measure of a material's resistance to fracture and became known as the material's toughness or the crack-resistance force of the material.

2.3.2 STRESS INTENSITY FACTOR APPROACH

Consider a crack having a shape defined by a simple curve or straight line where crack extension occurs in the crack plane. Irwin(4) developed a series of linear elastic crack stress field solutions using the mathematical procedures of Westerg aard(5). In Fracture Mechanics, there are three basic modes or types of crack extension. They are :

Mode I — The opening mode — crack surface displacements normal to the crack plane.

Mode II — The edge sliding mode — crack surface displacements in the crack plane and normal to the crack border.

Mode III — The tearing mode — crack surface displacements in the crack plane and parallel to the crack border.

The three modes are illustrated in Fig.(2.2).

Associated with the three modes of crack extension there are three sets of equations which give the direct and shear stress distribution surrounding a crack tip. The equations also give the expressions for the displacements surrounding the crack tip. The three sets of equations are as follows :

Mode I

$$\sigma_x = \frac{K_I}{(2\pi r)^{1/2}} \cos\frac{\theta}{2}\left(1 - \sin\frac{\theta}{2}\sin\frac{3\theta}{2}\right)$$

$$\sigma_y = \frac{K_I}{(2\pi r)^{1/2}} \cos\frac{\theta}{2}\left(1 + \sin\frac{\theta}{2}\sin\frac{3\theta}{2}\right) \qquad (2.8)$$

$$\tau_{xy} = \frac{K_I}{(2\pi r)^{1/2}} \cos\frac{\theta}{2}\sin\frac{\theta}{2}\cos\frac{3\theta}{2}$$

$$u_x = \frac{K_I}{2G}\left(\frac{r}{2\pi}\right)^{1/2} \cos\frac{\theta}{2}\left(\mu - 1 + 2\sin^2\frac{\theta}{2}\right)$$

$$u_y = \frac{K_I}{2G}\left(\frac{r}{2\pi}\right)^{1/2} \sin\frac{\theta}{2}\left(\mu + 1 - 2\cos^2\frac{\theta}{2}\right)$$

$$w = 0$$

Mode II

$$\sigma_x = \frac{K_{II}}{(2\pi r)^{1/2}} \sin\frac{\theta}{2}\left(2 + \cos\frac{\theta}{2}\cos\frac{3\theta}{2}\right)$$

$$\sigma_y = \frac{K_{II}}{(2\pi r)^{1/2}} \sin\frac{\theta}{2}\cos\frac{\theta}{2}\cos\frac{3\theta}{2}$$

$$\tau_{xy} = \frac{K_{II}}{(2\pi r)^{1/2}} \cos\frac{\theta}{2}\left(1 - \sin\frac{\theta}{2}\sin\frac{3\theta}{2}\right) \qquad (2.9)$$

$$u_x = \frac{K_{II}}{2G_1}\left(\frac{r}{2\pi}\right)^{1/2} \sin\frac{\theta}{2}\left(\mu + 1 + \cos^2\frac{\theta}{2}\right)$$

$$u_y = \frac{K_{II}}{2G_1}\left(\frac{r}{2\pi}\right)^{1/2} \cos\frac{\theta}{2}\left(1 - \mu - \sin^2\frac{\theta}{2}\right)$$

$$w = 0$$

Mode III

$$\tau_{xz} = -\frac{K_{III}}{(2\pi r)^{1/2}} \sin\frac{\theta}{2}$$

$$\tau_{yz} = \frac{K_{III}}{(2\pi r)^{1/2}} \cos\frac{\theta}{2} \qquad (2.10)$$

$$\sigma_x = \sigma_z = \tau_{xy} = 0$$

$$w = \frac{K_{III}}{G_1}\left(\frac{2r}{\pi}\right)^{1/2} \sin\frac{\theta}{2}$$

$$u_x = u_y = 0$$

The stress intensity factor, K_I, is a measure of the stress intensity near the crack tip subjected to mode I loading. The stress intensity factor is directly proportional to the applied load and the specimen geometry. For a crack of length 2C, subjected to a uniform tensile stress σ in an infinite plate as shown in Fig.(2.1), the stress intensity factor is given by

$$K_I = \sigma\sqrt{\pi C} \qquad (2.11)$$

In the case of finite width specimens a correction factor α_1, known as the stress intensity coefficient is included in equation (2.11).

$$K_I = \alpha_1 \sigma\sqrt{\pi C} \qquad (2.12)$$

By similar considerations it can be shown that Mode II and Mode III stress intensities have the general forms

$$K_{II} = \alpha_2 \tau\sqrt{\pi C} \qquad (2.13)$$

and

$$K_{III} = \alpha_3 \tau\sqrt{\pi C} \qquad (2.14)$$

where αi, i=1,2,3, are the relevant geometric functions and τ is the in-plane (Mode II) and out of plane (Mode III)

shear stresses at infinity.

The notion of K implies that the higher the value of K, the more severe the stress distribution around the crack. When K reaches a critical value Kc, sufficient energy is being supplied to the crack tip for crack propagation to occur. Kc is a useful measure of fracture toughness of a material or its resistance to brittle fracture. The advantage of using K is that it provides a single parameter characterisation and its evalution is a normal stress analysis problem involving the applied stress, crack length and specimen configuration.

2.3.3 EQUIVALENCE OF ENERGY BALANCE AND STRESS INTENSITY APPROACHES

For linear elastic loading conditions, the stress intensity factor of a through-thickness crack of length 2C in an infinite plate loaded by a remote tensile stress transverse to the crack plane is given by

$$K = \sigma\sqrt{\pi C} \qquad (2.11)$$

Similarly from equation(2.1), it can be shown that the corresponding "fixed grip" Griffith(1) strain energy release rate for plane stress conditions is given by

$$\frac{dU}{dC} = \frac{\sigma^2 \pi C}{E} \qquad (2.15)$$

Hence

$$\frac{dU}{dC} = \frac{K^2}{E} \qquad (2.16)$$

Irwin (4) showed that the strain energy release rate G could be regarded as the force tending to cause crack extension. Thus the following commonly used relationships are obtained :

For plane stress,

$$K^2 = EG \quad \text{and} \quad Kc^2 = EGc \qquad (2.17)$$

and for plane strain

$$K_I^2 = \frac{EG}{1-\nu^2} \quad \text{and} \quad K_{Ic}^2 = \frac{EG_{Ic}}{1-\nu^2} \qquad (2.18)$$

similar relationships may be written for Mode II and Mode III crack surface displacements.

Measured values of Kc or Gc are found to vary with the cross-section of the specimen used, and this variation is related to fracture surfaces. The range of values

depends on the stress condition at the tip of the crack and decreases with increase of sheet thickness. As the sheet thickness increases, the state of stress in the vicinity of the crack changes from plane stress to plane strain conditions, and Kc and Gc approach minimum limiting values as shown in Fig.(2.3). These minimum values are denoted by K_{Ic} and G_{Ic} and are considered to be material properties. The distinction between K_{Ic} and Kc is important and can be compared to the distinction between strength and stress.

Because of the change from plane stress to plane strain conditions, K_{Ic} is often referred to as the plane strain fracture toughness, and represents a basic material property. K_{Ic} and G_{Ic} are thus independent of specimen dimensions in contrast to Kc and Gc which depend to some extent on geometry. K_{Ic} and G_{Ic} provide an invariant fracture characteristic for many materials and are therefore of more interest for general evaluation of material property than Kc and Gc.

2.4 APPLICATION OF FRACTURE TOUGHNESS TO HIGH STRENGTH METALLIC MATERIALS — K CALIBRATION METHOD

In structural design, designers have tended in recent years to use higher strength materials which can give economic benefits. As the strength increases, the sensitivity to inherent flaws also increases i.e. brittleness increases. Therefore it is necessary to be aware of the fracture toughness of high strength materials.

The most commonly used method to determine the plane strain crack toughness of high strength materials is based on the work of Irwin and Kies (6) and is known as the K calibration method. The K calibration method measures the reciprocal of stiffness(compliance) of a notched specimen which is incrementally extended. The specimen compliance can be expressed as a function of crack length and then the derivative of this function with respect to crack length is determined. The main advantage of this compliance calibration method is that the actual configuration and loading condition of a K_{Ic} test specimen can be closely modelled by the K calibration specimens as shown in Fig.(2.4). The results of the K-calibration under various methods and specimens of testing are illustrated in Fig.(2.5).

Tetelman and McEvily(7) carried out tests on various

plate thickness with respect to fracture toughness Gc and plane strain fracture S in high strength alluminum alloy plate as shown in Fig.(2.6). For thin sheets where the thickness $t < t_o$, fracture occurs by plane stress and Gc increases approximately linear with thickness. Increasing the thickness increases the relative amount of plane strain fracture, decreases the amount of microscopic slow crack growth and causes the toughness to decrease and approach a limiting value.

Brown and Srawley(8) showed that $(K_{Ic} / \sigma_{ys})^2$ is a characteristic dimensions of the plastic zone and should be useful in estimating specimen dimensions. In order to obtain a valid K_{Ic} test, the crack length and thickness should be greater than some multiple of $(K_{Ic}/\sigma_{ys})^2$ and this multiple should not be less than about 2.5. The initial specimen size may be obtained based on an estimated value of K_{Ic} for the material. This K_{Ic} value should be overestimated so that a larger specimen size than necessary will be used for the initial trial tests. The initial specimen size may be reduced to an appropriate size provided the crack length and thickness are not less than about $2.5\ (K_{Ic}/\sigma_{ys})^2$ for further testing. A ratio of crack length to width greater than 0.5 is not suitable for the tests because the K-calibration curves increase rapidly at high a/w values. Hence small errors in measured crack length can lead to large errors in the calculated K_{Ic} values.

2.5 EFFECT OF PLASTIC ZONE IN LESS BRITTLE MATERIALS

For high strength materials the plastic zone can often be ignored since the plastic zone around the crack tip is small relative to the specimen and flaw size. However, for less brittle materials a region of plasticity is developed near the crack tip whenever the stresses exceed the yield strength of the materials. Thus linear elastic fracture mechanics theory cannot be applied to evaluate the fracture toughness of such materials unless the crack tip plastic zone size is known.

The simplest method of determining the plastic zone size is to treat the problem as plane stress and to assume that yielding occurs in those regions and also the material is assumed to be non-strain hardening. From the linear elastic fracture machanics analysis,

$$\sigma_y = K(2\pi r)^{-1/2} \cos\frac{\theta}{2}\left[1 + \sin\frac{\theta}{2}\sin\frac{3\theta}{2}\right] \qquad (2.19)$$

Considering stresses directly ahead of the crack where $\theta=0$, the elastic stress $\sigma_y = K(2\pi r)^{-1/2}$ will exceed the yield strength at some distance r from the crack tip as shown in Fig.(2.7). Irwin (9) assumed that the distance ry from the central location to the elastic-plastic boundary could be estimated by inserting a critical yield stress σ_{ys} for σ_y and r = ry. Thus

$$\sigma_{ys} = K(2\pi r_y)^{-1/2} \tag{2.20}$$

and

$$r_y = \frac{1}{2\pi}\left(\frac{K}{\sigma_{ys}}\right)^2 \tag{2.21}$$

or

$$R = 2r_y = \frac{1}{\pi}\left(\frac{K}{\sigma_{ys}}\right)^2 \tag{2.22}$$

A more precise method for determine the plastic zone size for the sharp tensile crack under plane stress condition has been given by Dugdale(10). He assumed that $a = R + c$ is the distance from the centre of the crack to the elastic-plastic zone boundary as shown in Fig.(2.8). The combined crack and plastic zone was treated as a flattened ellipse. To determine R Dugdale(10) assumed that the crack length 2c has spread elastically to a distance 2a but that the crack has been closed up in the plastic zone by an internal tensile stress which acts across the crack faces in the region $|a| > |x| > |c|$ as shown in Fig.(2.8). Since internally applied forces are in static equilibrium, this internal tensile stress must equal σ_y because σ_y is the tensile stress existing in the plastic zone. When this internal stress field is superimposed on the elastic stress

field of the crack in the presence of an externally applied tensile stress σ, and the restriction is imposed that the stress at the end of the plastic zone (x=a) be finite. Then the plastic zone size is determined by the relation

$$\frac{R}{C} = \frac{\pi^2}{8}\left(\frac{\sigma}{\sigma_y}\right)^2 \qquad (2.23)$$

which is approximately the same as equation(2.22).

2.6 THE R-CURVES ANALYSIS

The fracture process in a cracked thin metal sheet will not cause sudden failure. As the load increases considerable slow stable crack growth takes place prior to catastrophic failure. The amount of slow crack growth depends mainly on the specimen configuration and this configuration together with the applied loads determine the stress intensity factor which indicates the magnitude of the stresses around the plastic zone at the crack tip. The relationship between the amount of crack growth and the applied stress intensity factor can be employed as a basis for useful testing methods applicable to the less brittle materials and is known as crack growth resistance curve (R-curve).

The concept was introduced by Irwin and Kies(6) in 1954, using the energy approach, and concluding that the strain energy release rate and the fracturing work rate must be equal at onset of instability, and that they are unlikely to differ widely in magnitude as fracture continues. This concept was further developed by other research workers as applied to fracturing different types of specimens.

Typical curves were shown in Fig.(2.9) by McCabe and Heyer(11) in which the K_R-curve rises sharply from a starting crack length a_o. The K-curve is calculated from $K = \frac{P\sqrt{a}}{BW} Y$ for a centre notched specimen, where Y is a a function of a/W. The intercept between the crack driving force K, and the crack growth resistance of the material K_R, determines the incremental stable crack extension. The point at which the K and K_R curves are tangential determines the instability conditions for Kc.

2.7 THE J-INTEGRAL EVALUATION OF FRACTURE TOUGHNESS

The J-integral can be treated as a parameter which is an average measure of the crack tip elastic-plastic field. It has been shown by Rice(12) that the J-integral may be

interpreted as the potential energy difference between two identically loaded bodies having neighbouring crack sizes. This can be expressed as

$$J = -dU/dl \qquad (2.24)$$

where U is the potential energy and l is the crack length. An experimental evaluation of the J-integral can be performed readily by consider the load-deflection curves of identical specimens with varying crack lengths as shown in Fig.(2.10). As the crack extends from l to l+Δl under load P_1, the total work done on the body is represented by the area OABCO. The strain energy of the body with crack length l+Δl under load P_1 is the area OBCO. The shaded area, OABO, is the difference between the work done on the body to extend the crack to l+Δl and the strain energy of the body at B. Thus it is the energy available for crack extension and the potential energy difference between cracks of length l+Δl at load P_1.

The J-integral method can be applied to both plane stress and plane strain conditions. Due to elastic-plastic behaviour of the materials, unloading is not permitted during fracturing so that a realistic approximation of elastic-plastic behaviour is obtained. For plane strain conditions, size limitation for the use of the J-integral method is also important. When the length of uncracked ligament is small, the results for J_{1c} would not be

valid(13).

The J-integral method can be used for both elastic and plastic behaviour. For linear elastic materials the J-integral is equivalent to the energy release rate per unit crack extension G. Therefore, a J-integral failure is also equivalent to the K_{Ic} failure criterion. Thus

$$J_{Ic} \equiv G_{Ic} \equiv \frac{1-\nu^2}{E} K_{Ic}^2 \qquad (2.25)$$

2.8 EXPERIMENTAL METHODS TO EVALUATE THE FRACTURE TOUGHNESS OF MATERIALS

During the past fifty years numerous tests have been developed to evaluate the fracture toughness of materials. Almost all of the tests involve the introduction of a notch and the observation of the onset of brittle behaviour. These tests results will give fracture information which may be used by designers in the design process.

2.8.1 PENDULUM IMPACT TESTS ON SMALL SPECIMENS

The principal of these tests is that the specimen is placed in a holder which supports it at its ends as shown in Fig.(2.11). The striker having been initially lifted to a certain height and then released, swings against the specimen and breaks it. The striker, continuing its swing then rises on the other side of the specimen to a height which is less than the initial height. The difference between the two heights multiplied by the mass of the striker is the amount of energy absorbed in producing fracture. The measured energy values cannotbeput into a fracture equation that can be directly used for design purposes. But the energy absorbed in fracture can give an indication of brittleness especially with varying test temperatures so that brittleness of the materials under

varying temperatures particularly low temperature can be assessed.

2.8.2 COMPACT TENSION TEST AND BEND TEST TO MEASURE K_{Ic}

These two methods are accepted as standard methods to evaluate the plane strain fracture toughness K_{Ic}, of metallic materials(14). The "compact tension specimen" is subjected to point loading through pins above and below the crack faces: the bend specimen is deformed under three-point loading. Both specimens are subjected to a bending moment as shown in Fig.(2.12). The compact tension test and the bend test are both specimen geometries dependent. It is required that the specimen thickness, B, and the crack length, a, exceed $2.5(K_{Ic}/\sigma_{ys})^2$. The initial selection of a size of specimen from which valid values of K_{Ic} will be obtained may be based on an estimated value of K_{Ic} for the material. It is recommended that the value of K_{Ic} be overestimated, so that a conservatively large specimen will be employed for the initial tests. After a valid K_{Ic} result is obtained with the conservative size initial specimen, the specimen size may be reduced to an appropriate size (a and $B > 2.5(K_{Ic}/\sigma_{ys})^2$) for subsequent testing. The geometry of standard specimen is illustrated in Fig.(2.12). The crack length, a, is nominally equal to thickness, B, and is between 0.45 and 0.55 times the depth W. Alternatively, bend specimens may have B=0.25W to W and

compact tension specimens may have B=0.25W to 0.5W. Crack length, a, in this case shall be 0.45 to 0.55W, the same as for the standard specimen.

The standard specimens have been calibrated by several methods, which have been refined until complete agreement has been achieved. Information is presented to the user of the standard procedures in terms of a compliance coefficient (the Y-function) which enables the load on a specimen to be converted directly to the K-value. The polynomial forms for K are shown as a function of (a/w) for standard bend and compact tension testpieces. The appropriate expressions for K are given in Fig.(2.12).

2.9 APPLICATION OF FRACTURE MECHANICS TO PLAIN CONCRETE

Kaplan(15) was one of the first to investigate the crack propagation and fracture toughness of concrete. He performed experiments on beam flexure specimens and cylinders in direct and indirect tension to show that microcracks occurred in concrete when loaded. Kaplan(15) discussed two methods to determine the critical strain energy release rate Gc of concrete: the analytical method and direct experimental method.

The analytical method utilises stress analysis to derive a mathematical relationship for the strain energy release rate G in terms of the dimensions of the test specimen, depth of crack, applied load and the modulus of elasticity. The Griffith formula gives the strain energy release rate as

$$G = \frac{\pi \sigma^2 c}{E} \qquad (2.26)$$

For plane strain condition

$$G = \frac{(1-\nu^2)\pi \sigma^2 c}{E} \qquad (2.27)$$

Consider a beam of unit width

$$\sigma = \frac{6M_b}{d^2} \qquad (2.28)$$

and

$$\sigma_n = \frac{6M_b}{h^2} \qquad (2.29)$$

From equations (2.28 and 2.29)

$$\sigma^2 = \sigma_n^2 \frac{h^4}{d^4} \qquad (2.30)$$

Substitute equation(2.30) into (2.27)

$$G_1 = (1-\nu^2)\frac{\sigma_n^2 h^2 \pi c}{E d^4} \qquad (2.31)$$

Equation(2.31) can be rewritten as

$$G_1 = (1-\nu^2)\frac{\sigma_n^2 h}{E} f\left(\frac{c}{d}\right) \qquad (2.32)$$

where $$f\left(\frac{c}{d}\right) = \frac{\pi c}{d}\left(1-\frac{c}{d}\right)^3$$

Kaplan(15) carried out series of tests on concrete

beams with crack-simulating notches subjected to third-point and centre-point loading as shown in Fig.(2.13). He observed that G_c values differed by 38 percent depending on the beam size and loading mechanism. The G_c values were independent with different notch depths and the values obtained by two methods differed by 21 percent.

During the experiments the staining technique was used to observe the slow crack growth prior to fracture. This experiment procedure showed that slow crack growth had taken place prior to instability. Kaplan concluded that Gc could be obtained by these two methods to predict the failure strength of concrete containing cracks.

Concrete consists of cement paste matrix that surrounds fine and coarse aggregates. Microcracks are known to exist in the matrix and at the matrix-aggregate interface. Therefore the fracture toughness of concrete depends on the energy requirement for crack propagation in the matrix and the heterogeneity of the concrete. Lott and Kesler(16) suggested that the actual stress intensity factors of concrete K_c' was the summation of the cement paste, Kpc, and the arresting action of the aggregates on crack growth, f(AAR). This can be written as

$$K_c' = K_{pc} + f(AAR) \qquad (2.33)$$

K_c' is defined as pseudo-fracture toughness for concrete. This value can be obtained experimentally when the concrete body is considered as a homogeneous elastic material . The effects of several concrete parameters on the "pseudo" fracture toughness of concrete was determined by the fabrication and testing of 4" X 4" X 12"(102 X 102 X 305mm) mortar and concrete beams with 0.5", 1.0" and 1.5"(12.7, 25.4 and 38.1mm) crack lengths. The beams were tested in flexure and the critical stress intensity factor, neglecting slow crack growth, was evaluated from

$$K = \frac{6M}{Wd^2}\left[\frac{2d}{\pi} h\left(\frac{a}{d}\right)\right]^{1/2} \qquad (2.34)$$

where $h(a/d) = 10.08(a/d)^2 - 1.225(a/d) + 0.1917$

M = the applied bending moment

W = specimen width

a = notch depth

d = depth of beam

From the experimental results it was found that the critical stress intensity factor was independent of the water-cement ratio(0.50-0.60) for mortars and concretes where the aggregate percentages remained constant; the critical stress intensity factor was independent of fine aggregate percentage for the mortars with the same water-cement ratio; the critical stress intensity factor

varied directly with coarse aggregate for concrete with the same water-cement ratio and fine aggregate content.

Moavenzadeh and Kuguel(17) used notched beams 1" X 1" X 12"(25.4 X 25.4 X 304.8mm) subjected to three-point bending to obtain the surface energy, y, critical strain energy release rate Gc and critical stress intensity factor Kc from the expression

$$U = 2Ay \tag{2.35}$$

and equations(2.31) and (2.34). The surface energy, y, was also determined by using the relationship

$$y = Gc/2 \tag{2.36}$$

and

$$Y = \frac{Kc^2 \pi (1-\nu^2)}{2E} \tag{2.37}$$

The values of surface energy, y, of cement pastes, mortars, and concretes are shown in Table(2.1). The surface energy of concretes was slightly lower than for cement paste as determined by equation(2.35) since the cracks propagated through the paste-aggregate interface which was generally of lower bond strength than the matrix. The surface energy, y, of concretes obtained from equations(2.36-2.37) were higher than the values given by equation(2.35). Equations(2.36-2.37) were subjected to error because slow crack growth and side cracking prior to instability were not taken into account. Cement paste and mortar did not exhibit noticeable side cracking. However, side cracks appeared in the concrete specimens during fracturing. The main crack pattern tended to go around the aggregates rather than through them due to the crack arresting action of the aggregates. This phenomenon indicated that energy required to form the new crack surfaces was greater than the main crack which travelled in a straight line and the strength of concretes depended on the strength of the cement paste and the aggregate-paste interface bond.

Naus and Lott(18) conducted a study to determine the effects of several concrete parameters on the fracture toughness of concrete. The beams were tested in flexure and the fracture toughness at the onset of rapid crack propagation was evaluated from

$$K = \frac{6Ma^{1/2}}{BW} \cdot Y \qquad (2.38)$$

where $Y = 1.99 - 2.47(a/W) + 12.97(a/W)^2 - 23.17(a/W)^3 + 24.80(a/W)^4$

In the analysis, assumptions were made that the material was homogeneous and the crack depth at failure was the cast flaw depth. Naus and Lott(18) concluded that the water-cement ratio did not affect the fracture toughness of concrete; increasing the air content resulted in a decrease in fracture toughness of cement paste, mortar and concrete. Finally the fracture toughness increased with age for all cement materials and also increased gravel content resulted in increased fracture toughness.

Brown(19) described two methods that could be used to measure the fracture toughness of cement pastes and mortars. The first was a notched beam which was subjected to four-point bending and combined with compliance measurements to measure the slow crack growth prior to instability. The change of toughness was measured for separate increments of crack growth as the crack propagated and the value of fracture toughness, Kc, could be calculated from equation(2.38). Brown(19) concluded that the toughness of cement paste was independent of the crack growth and there was no significance between the toughness for sawn and cast notches. It was because the slow crack

growth before the maximum load was reached to ensure that the cracks were naturally sharp when Kc was determined.

The second method developed by Brown(19) used double-cantilever beams, Fig.(2.14), of variable web width such that the length of crack front increased with and exactly compensated for the effect of crack growth so that the slow crack growth problem was avoided. Brown(19) concluded that DCB specimens were more straightforward than the notched beams. The analysis was easier and the toughness value was independent of crack growth and may be expressed as

$$Kc^2 = \frac{12\,Pc^2\,k}{bh^3} \qquad (2.39)$$

where k is a constant

h = DCB height

b = DCB width

Pc = critical load

Higgins and Bailey(20) employed three-point bending specimens to investigate the fracture behaviour of hardened cement paste. The specimens were 9cm long by 1.4cm deep by 2.5cm wide. The stress intensity factor, K, was evaluated using equation(2.38). The authors(20) found that the variation of slit widths of the specimens below about 0.05cm would have no significant change in failure loads.

This indicates that slit widths below 0.05cm were sufficiently narrow to provide a sharp notch. They further concluded that the calculated fracture toughness values varied with the specimen sizes and suggested that tests on larger specimens should produce a constant value of fracture toughness since K_c' appears to tend towards a limiting value when the specimen depth tends to infinity as shown in Fig(2.15).

Barr and Bear(21) described two tests which have been applied to both rock and fine-grained concrete specimens to investigate the fracture toughness of materials. The tests use circumferentially notched round bar specimens which are subjected to two loading systems. In the first case, the notched round bar was subjected to four point bending(CNRBB). In the second case the notched round bar was subjected to an eccentric longitudinal load(CNRBEL). The loading systems are shown in Fig.(2.16).

In the eccentric longitudinal load(CNRBEL) system, the eccentric axial load results in a combination of direct load together with a bending moment. The load is applied via two lengths of 6mm square steel bars and the points of application of the load taken at the inside edge of the steel bars since the load was concentrated to the inside edges as deformation takes place. The stress intensity factor can be calculated from the expression

$$K_I = \frac{P\sqrt{\pi t}}{4d}\left(\frac{3e}{\sqrt{a^3(0.2a+1.38t)}} - \frac{1}{\sqrt{a(0.2a+0.62t)}}\right) \quad (2.40)$$

The CNRBB test system was used by Javan and Dury(22) to compare the fracture toughness of fibre reinforced concrete. They concluded that the CNRBB test was an effective method for comparing the fracture toughness of plain and fibre-reinforced concretes.

Unlike metallic materials, there are still no standard methods for evaluating the fracture toughness behaviour of concretes. In general, most of the research work has concentrated on using either three-point bending or four-point bending methods or tensile specimens to explain the behaviour of fracture toughness of concrete. Swamy(23) summarised the above test geometries and their calculated fracture toughness values which can be used to compare with other researchers' works.

2.10 APPLICATION OF FRACTURE MECHANICS TO FIBRE-REINFORCED CONCRETE

In the past, the main objective of adding various types of fibres to cement based materials was to improve the tensile strength. In recent years, research workers generally agree that increased ductility, or toughness, is the most important property to study in fibre-reinforced concrete. Most of the research work has concentrated on using steel, glass and polypropylene fibres in concretes to investigate the general properties of the composites. The flexural (three-point or four-point loading) and the impact tests are commonly used to determine the fracture toughness of fibre-reinforced concrete. The results generally show that the addition of fibre leads to increase in ductility or toughness strength in the composite materials. In order to improve the toughness strength, a range of different forms of steel fibres were used in the experiments by Hughes and Fattuhi(31). Other methods such as compact tension, J-integral and R-curves analysis(33,34,37) were also used to determine the fracture toughness of fibre-reinforced cementitious materials. The general theory, manufacture and application of fibre-reinforced composite materials are given in the following references(24-26).

Grimer and Ali(27) investigated the general

properties of glass fibre-reinforced cement with respect to flexural strength, tensile strength and impact strength. They concluded that the maximum strength could be obtained when the glass fibre content was about 10 percent by weight; the flexural strength and tensile strength was increased between two to four times of the matrix strength and the impact strength was increased between ten to thirty times of the matrix strength.

Harris et al(28) conducted experiments to determine the fracture behaviour of fibre-reinforced concrete. Two types of steel fibres were used: cold-drawn mild steel wires and cold-drawn high carbon steel wires. The specimens were subjected to three point bending test and the value of fracture toughness was obtained from equation(2.38). Further work had been done to evaluate the work of fracture from the expression

$$\gamma_F = \frac{U}{2(d-c)b} \qquad (2.41)$$

where

γ_F = work of fracture

U = area under the load-deflection curve

d = depth of specimen

b = width of specimen

c = crack length

Harris et al(28) compared the work of fracture of plain concrete with critical strain energy release rate, Gc, which was determined by Kaplan. The results were in good agreement as shown in Fig.(2.17). They concluded that the fracture energy of the steel fibre-reinforced concrete was at least two times the magnitude greater than unreinforced concrete and the mild steel fibres exhibited greater resistance to crack initiation than the high carbon steel fibres. High fracture energy of fibre-reinforced concrete is probably due to the work of pulling fibres out of the matrix after the latter had cracked.

Takagi(29) testing glass fibre-reinforced mortar and concrete, concluded that an increase ocurred in flexural, compressive and tensile strength as the glass fibre content increased; the specimens clearly exhibited an optimum strength at about 0.75 percent reinforcement by weight and the effect of fibre content did not influence Young's modulus both in compression and tension up to 1 percent of fibres by weight.

Hughes and Fattuhi(30) carried out experiments to investigate the effects of steel fibres and polypropylene fibres in concrete. They concluded that the compressive strengths of fibre-reinforced specimens were lower than the unreinforced concrete especially in the case of polypropylene fibres; the flexural strength decreased when

the polypropylene fibres increased and the addition of steel fibres resulted in significant increases of flexural strength.

Failure of the composite is usually due to fibre pull-out, therefore improving the machanical anchorage of fibre is necessary. Hughes and Fattuhi(31) tested a range of forms of fibre to observe the fracture behaviour of fibre-reinforced concrete beams. Round, straight, Duoform, crimped and hooked steel were used in the experiments as shown in Fig.(2.18). It was found that fracture toughness produced by concrete reinforced with Duoform steel and hooked steel fibres was considerably greater than for round and small diameter steel fibres. Hughes and Fattuhi(31) concluded that an efficient form of mechanical anchorge could improve the toughness of fibre-reinforced cement materials.

The properties of the composite materials are often highly dependent on the test techniques used to measure them. Hibbert and Hannant(32) have modifield an impact test machine which can be used to measure energy absorption in concrete beam of 100 X 100 X 500mm. Patterson and Chan(33) reported that fracture toughness of fibre materials can be determined using the load-displacement curve in a tension test of crack-line loaded single-edge crack specimens as shown in Fig.(2.19). The fracture toughness is calculated on the basis of the work required to extend the new crack

per unit length and per unit thickness of the specimen.

Mind ess (34), using the J-integral and four point bending specimens, have evaluated the fracture toughness of fibre-reinforced concrete. The experimental values for J_{Ic} and G_{Ic} were approximately identical for cement paste where $J_{Ic} = 13.13 Nm^{-1}$ and $G_{Ic} = 11.91 Nm^{-1}$ respectively. Mind ess (34) concluded that the J-integral method was a much more sensitive indicator of the effectiveness of fibre additions than G_{Ic} as shown in Fig.(2.20); fibre content which was less than 0.75 percent by volume was not useful as both the flexural strength and the energy required for crack initiation remain unaffected.

Nishioka et al(35) determined the fracture toughness of steel fibre-reinforced concrete by using three-point loading and four-point loading methods. The specimens consisted of randomly distributed steel fibres with various volume percent. The authors(35) concluded that the steel fibre-reinforced concrete with one to two percent in volume fraction of fibre was approximately two to three times greater than the plain concrete. Nishioka et al(35) also recommended that the size of the specimens should be at least ten times larger than the maximum size of the coarse aggregates so that the size of the coarse aggregates would not affect the toughness value during fracturing and provided a more uniform evenly distributed region in the specimens used in the tests.

Ohigashi(36) measured the effective fracture energy of glass fibre-reinforced cement by three-point bending method. The specimen which had been modified with two notches whose depths were different on the compressive and tensile faces of the specimen is shown in Fig.(2.21). The effective fracture energy is then calculated by

$$\gamma = \frac{U}{2(d-c_1-c_2)b} \qquad (2.42)$$

Ohigashi(36) compared the effective fracture energy, γ, with the energy absorbed by impact test as shown in Table(2.2) and concluded that the fracture energy obtained in both methods were in good agreement with each other.

Velazco et al(37) applied various fracture mechanics approaches to obtain a fracture parameter which can be used to predict the effects of fibre addition and is independent of the test specimen geometry. Velazco et al(37) concluded that critical stress intensity factor, J-integral, critical crack opening displacement and compliance methods could not satisfy both requirements except for the R-curves analysis which appeared to be indenpendent of the initial notch

depth and was also sensitive to the fibre content as shown in Fig.(2.22).

Swamy(38) investigated the effect of slow crack growth on the fracture behaviour of various types of fibre concrete beams which were subjected to four-point loading. Steel fibres, alkali-resistant glass fibres and polypropylene fibres were used with volume fractions of 0.5%, 1.0% and 2.0%. The influence of fibre contents on deflection and crack growth of the notched specimen is illustrated in Fig.(2.23). Swamy(38) stressed that three distinct stages of crack growth appeared in fibre cement composites: steady crack growth; quasi-stable crack growth and unstable crack propagation. The apparent fracture toughness was found to increase approximately linearly with crack growth as shown in Fig.(2.24). At low fibre content, little increase in fracture toughness of fibre cement composites was observed. At high fibre content(of about 2.0 percent) there was a considerable increase in fracture toughness, except in polypropylene fibre concrete specimens. Swamy(38) concluded that slow crack growth was greatly influenced on the fracture behaviour of fibre cement composites.

More recently, further development of the circumferentially-notched round bar under eccentric loading(CNRBEL) test(21) was carried out by Dowers(39). He

replaced the round specimen by an ordinary concrete cube, modified by the introduction of two slits and subjected to an eccentric load together with the geometric details of the cube specimen and its notches to give directly the fracture toughness values.

Dowers(39) used 25mm, 30mm and 35mm notch depths to investigate the fracture toughness of concrete. The notches were first introduced by Masonary Clipper and afterwards by lathe for the improvement of accuracy of the notch depth. The fracture toughness values were determined from a finite element solution(40). Dowers(39) concluded that the stress intensity factor was independent of the notch-depth ratios. He also compared the stress intensity factor values determined from equation(2.40) and finite element solution and stressed that equation(2.40) was inaccurate and overestimated K_{Ic} value by 24 percent as shown in Fig.(2.26).

Furtheron, Dowers(39) used water-cement ratios of 0.40, 0.45 and 0.50 to investigate its variations in the effect of fracture toughness of concrete. The results are shown in Fig.(2.27) together with various notch-depth ratios. The ranges of water-cement ratios did not significantly affect the fracture toughness values.

Investigation of various fibre contents (0%-0.30% by weight) in the effect of fracture toughness of concrete

was also included in his thesis(39). Polypropylene fibres of 12,000 denier and 50mm long were used in the experiments. Water-cement ratio was kept constant at 0.50 through the experiments. The notch depths were 30mm in 100mm cube specimen. The fracture toughness values obtained with respect to various polypropylene fibre contents are shown in Fig.(2.28). Dowers(39) concluded that the additions of polypropylene fibres had little or no effect on the value of fracture toughness of concrete.

In order to compare the results of new fracture toughness specimen developed, Dowers(39) used the compact tension specimen as shown in Fig.(2.29) to investigate the fracture toughness of concrete. The fracture toughness values obtained from the compact tension specimen and the DENCEL specimen are shown in Fig.(2.30). Dowers(39) concluded that the compact tension specimen was 15 percent higher than the DENCEL specimen for the fracture toughness values and that the difference was probably due to the undefined crack path of the compact tension specimen and the misali gnment of the loading straps.

2.11 APPLICATION OF FINITE ELEMENT ANALYSIS METHOD TO TWO-DIMENSIONAL PROBLEMS IN FRACTURE MECHANICS

Linear fracture mechanics has been widely used by engineers for the prediction of strength and life of cracked structure. For given geometry and loading conditions, an estimate of the stress intensity factor is obtained from the basic laws of elasticity. Although the stress intensity factors for various shapes and boundary conditions have been calculated, most of the solutions obtained by analytical methods are for the cases in which the shapes and the boundary conditions are rather simple. The finite element method is versatile for the variation of the shapes and boundary conditions.

Numerous reports on fracture toughness of concrete have had a common theme: A single parameter measure of toughness has not yet determined. In particular, it has been alleged repeatedly that resistance to crack growth in cement paste, mortar, and concrete cannot be characterised by a linear elastic fracture mechanics parameter, that is, K_{Ic}. Other research workers used linear elastic fracture mechanics concepts to determine the concrete fracture and concluded that a remarkable independence of measured fracture toughness from variation in specimen geometry was obtained.

In 1971, Kesler et al(58) reported the results of an

experimental investigation which disproved the applicability of linear elastic fracture mechanics to cracking of cement paste, mortar, and concrete. The test specimen is illustrated in Fig.(2.31). The stress intensity factor is determined as follows:

$$K_I = \frac{P}{B\sqrt{\pi a}} \frac{1}{[(W/2\pi a)\sin(2\pi a/W)]^{1/2}} \qquad (2.43)$$

The results are illustrated graphically as shown in Fig.(2.32). The calculated stress intensity factor is decreasing with increasing relative crack length. Thus Kesler et al(58) concluded that linear elastic fracture mechanics concept to concrete fracture was invalid.

Saouma et al(59) used linear elastic fracture mechanics concepts in their numerical analysis for the investigation of the results which were obtained by Kesler et al(58). Saouma et al(59) stressed that the mathematical relationship, equation(2.43), which was used by Kesler et al(58) to compute the stress intensity factor was grossly in error. Equation(2.43) would have been appropriate for crack lengths greater than three or four times the loading hole width, if and only if the ratio H/W was large. However, this ratio H/W ranged from a peak value of 2/3 to as little as 1/3 in the tests which were used by Kesler et al(58). Thus the stress intensity factor determined from equation(2.43) was in error.

Saouma et al(59) indicated that for very small relative crack lengths, 2a/w, the following equation would be applicable if the loading were applied at a point on the crack body as shown in Fig.(2.31).

$$K = \frac{P}{B\sqrt{a}} \qquad (2.44)$$

Saouma et al(59) used the finite element method to evaluate the stress intensity factor. The results are illustrated graphically in Fig.(2.33). A remarkable independence of stress intensity factor against relative crack length is obtained when the corrected stress intensity factor relationship, equation(2.44), was used in the calculation. Thus Saouma et al(59) concluded that linear fracture mechanics concepts could be introduced into analytical tools and numerical analysis codes for the study of crack propagation in concrete structures.

Kobayashi et al(41) showed that numerical methods can be used effectively in the evaluation of the stress intensity factors for most two-dimension problems in fracture mechanics. For most industrial applications, where a ±3-5 percent error is acceptable, numerical solution to two-dimension problems appears to be more effective than a lengthy mathematical solution.

Kobayashi et al(41) considered a crack located in a

large plate which was subjected to an arbitrary in-plane loading condition as shown in Fig(2.34). The elastic state of stress in the vicinity of the crack tip would be expressed in terms of a local polar coordinate system r, θ as given in equation (2.9). The plane stress state of displacement in the vicinity of the crack tip is given by equation(2.8).

If the states of stress or displacement in the vicinity of the crack tip can be determined within a reasonable degree of accuracy, then the stress intensity factors can be computed by equations(2.8 — 2.9). The finite element analysis must then produce sufficiently accurate states of stress or displacement within the local region where equations(2.8 — 2.9) are valid. Kobayashi et al(41) defined this local region as $r < a/20$, where a is the half-crack length.

In order to determine the optimum procedure for evaluating the stress intensity factor, a finite width tension plate with a central notch was considered as shown in Fig.(2.35). A quadrant of this plate was initially divided into 339 rectangular elements for the coarse grid analysis as shown in Fig.(2.36). Using the results of the coarse grid analysis, a portion of the plate surrounding the crack tip was analysed again in a fine grid analysis, Fig.(2.36), with the prescribed force boundary conditions established from the coarse grid analysis. The fine grid

analysis consisted of 798 elements.

In using the approach by stresses or equation(2.8), Kobayashi et al(41) found that the stress intensity factors were underestimated. This is due to the inability of the finite element analysis to handle problems with steep stress gradients, such as those which exist in the vicinity of a crack tip. Part of this inaccuracy was due to the stiffness matrix used which was derived on the basis of uniform strain and uniform stress in the finite element.

The displacement approach in the finite element analysis leads to reasonable results when the crack opening displacement is employed. Using this displacement method, the stress intensity factors have been evaluated for several different problems. Kobayashi et al(41) concluded that the use of COD in place of stress should be a natural approach for the method of direct stiffness which determined the unknown nodal displacements from the known nodal forces through the use of the stiffness matrix.

Chan, Tuba and Wilson(42) have applied the finite element method in linear fracture mechanics problems. The computer program used was based on the displacement method. The program, similar to others, could handle plane stress and plane strain conditions. Displacements and stresses could be determined in arbitrary plane shapes by replacing actual geometry with an assemblage of triangular elements.

The program accepted a variety of boundary conditions and loading systems.

The configuration for the study of mesh size effects and for comparisons with results by the collocation method is shown in Fig.(2.37). Once the numerical solution has been established for a particular finite element representation, crack tip stress intensity factors can be determined by the use of established crack tip relations. Two basic methods have been used: (a)displacement method and (b)stress method. The major emphasis has been placed on the displacement method due to its relative simplicity and ease of interpretation.

(a)Displacement method

This method involves a correlation of the finite element nodal point displacements with the crack tip displacement equations:

$$U_i = \frac{K_I}{G}\left[r/2\pi\right]^{1/2} f_i(\theta,u) \qquad (2.43)$$

where $U_1 = U$ and $U_2 = V$

By substituting a nodal point displacement U_i^* at some point (r,θ) near the crack tip into equation(2.43) a quantity K_I^* could be calculated from equation

$$K_I^* = [2\pi r]^{1/2} G u_i / [f_i(\theta, \mu)] \qquad (2.44)$$

From plots of K_I^* as a function of r for fixed values of θ and a particular displacement component, an estimation of K_I could be made. If the substituted displacements were the exact theoretical values then the value of K_I^* as r approaches zero would be the exact value of K_I. Since the finite element displacements are rather inaccurate at very short distances from the crack tip, thus the tangent extrapolation of K_I^* curve is used to estimate K_I. With a suitable refinement of element size the K_I^* curve rapidly approaches a constant slope with increasing distance(r) from the crack tip. The intercept of the tangent to the constant slope portion of the curve with the K_I^* axis is used as the K_I estimate. The most accurate estimates are obtained from a K_I^* curve corresponding to the 'V' displacement on the crack surface Vc.

$$K_I^* = \frac{(2\pi)^{1/2} E \cdot Vc}{4(1-\nu^2) r^{1/2}} \qquad (2.45)$$

(b) Stress method

The determination of the crack-tip stress intensity factor by the stress method is similar to that by the displacement method. The nodal point stresses are correlated with the crack tip stress equations

$$\sigma_{ij} = \frac{K_I}{(2\pi r)^{1/2}} f_{ij}(\theta) \qquad (2.46)$$

The nodal point stresses σ^{*}_{ij} in the vicinity of the crack tip can be substituted into equation(2.46) and values of K^{*}_{I} may be calculated from

$$K^{*}_{I} = \frac{(2\pi r)^{1/2}}{f_{ij}(\theta)} \sigma_{ij}(r,\theta) \qquad (2.47)$$

From plots of K^{*}_{I} as a function of r for a fixed θ and particular stress component, estimates of K_I are made. If the exact theoretical stresses were substituted into equation(2.47) then the intercept of the curve with K^{*}_{I} axis at r=0 would be the exact value of K_I. Since the finite element method is unable to represent the stress singular conditions at the crack tip, the K^{*}_{I} curve for r>0 must be extrapolated back to r=0. The extrapolated K^{*}_{I} at r=0 is the estimated K_I.

The displacement and stress methods can be extended to obtain Mode II stress intensity factors, or combinations of K_I and K_{II}. To uncouple the mixed mode conditions, K_I estimates are made from the K_I^* curve constructed from the 'V' displacement on the crack surface ($\theta = \pi$) by the displacement method, or from σ_y on the plane $\theta=0$ by the stress method. Similarly K_{II} component can most effectively be obtained from K_{II}^* curves constructed from U displacement on the crack surface by the displacement method

$$K_{II}^* = \frac{(2\pi)^{1/2} E}{4(1-\nu^2)} \frac{u_c}{(r)^{1/2}} \qquad (2.48)$$

Or from τ_{xy} on the $\theta=0$ plane by the stress method

$$K_{II}^* = (2\pi r)^{1/2} \tau_{xy} \qquad (2.49)$$

The displacement method was used by Chan, Tuba and Wilson(42) to study the influence of element size on estimating K_I. The effect of relative element size on the K_I^* curve as calculated by the displacement method is shown in Fig.(2.38). The finite element curves are compared with the K curve calculated from displacements obtained by a boundary collocation solution for the same geometry and loading conditions. From Fig.(2.38), all of the finite element curves approach a constant slope as r/w increases. The higher the degree of element reduction, the more

rapidly the curves approach a constant slope. The best estimate of stress intensity factor can be obtained by extrapolating the straight portion of the K_I^* curves back to the vertical axis as shown in Fig.(2.38).

Chan, Tuba and Wilson(42) compared the theoretical curve of K_I obtained from Westergaard's(5) solution with the finite element curve as shown in Fig.(2.39). The estimated stress intensity factor obtained was 5.5 percent below the exact value.

Watwood(43) used the energy or compliance method for determining K. This method consists of computing the strain energy stored for two or more slightly different crack lengths and making use of the definition of G, i.e.

$$G = (\pm)\, dV/dA \qquad (2.50)$$

\+ if constant load

\- if constant displacement

The easiest method to determine the strain energy is to make use of Clapeyron's theorem i.e., that the strain energy stored for an elastic body is equal to one-half the work that would be done by the applied forces (of the equilibrium state) acting through their total displacements.

From the view of finite element method this statement means a multiplication of the generalized forces at the nodes by one-half the nodal displacements. For problems with small number of external loads, it can be done by hand from the computer output. Alternatively, the strain energy in each element may be calculated directly from the nodal displacements and these summed. After the strain energy is calculated for several crack lengths, numerical differentiation was used to obtain dV/dA.

Dixon and Strannigan(44) demonstrated energy release rate and stress intensity factors can be evaluated by the finite element method. A crack in a body of arbitrary shape subjected to an arbitrary system of applied forces was shown in Fig.(2.40). The forces can be constant, constant displacements or a combination of these. The energy available for an increment of crack area extension dA is provided from work done by the forces Pi dΔi. The release -dV in the total strain energy V stored in the body

$$G_i = P_i \frac{d\Delta_i}{dA} - \frac{dV}{dA} \qquad (2.51)$$

where i, j = 1, 2.....n.

n = number of applied forces.

The displacements of a linear elastic body are related to

the applied forces by

$$\Delta i = \lambda ij\ Pj \qquad (2.52)$$

Where the influence coefficients λij depend upon the geometry of the body including the crack area A.

The strain energy in the body is equal to the work done in loading, that is

$$V = 1/2\ Pi\,\Delta i = 1/2\lambda ij\ Pi\ Pj \qquad (2.53)$$

so

$$G_i = Pi\frac{d\Delta i}{dA} - \frac{1}{2}\frac{d}{dA}(Pi\,\Delta i)$$

$$= Pi\frac{d}{dA}(\lambda ij\ Pj) - \frac{1}{2}\frac{d}{dA}(\lambda ij\ Pi\ Pj)$$

$$= \frac{1}{2}Pi\ Pj\frac{d\lambda ij}{dA} + \frac{1}{2}Pi\,\lambda ij\frac{dPj}{dA} - \frac{1}{2}Pj\,\lambda ij\frac{dPi}{dA}$$

From Maxwell's reciprocal theorem

$$\lambda ij = \lambda ji$$

hence $$G_i = \frac{1}{2}Pi\,Pj\frac{d\lambda ij}{dA} \qquad (2.54)$$

From equation(2.54) it may be deduc ed that the energy release rate G is independent of the type of force

application, for example. constant displacements or constant forces.

For the particular case of a single applied force P or displacement Δ, Fig.(2.40), and equation(2.54) may be written

$$G_I = \frac{1}{2} P^2 \frac{d\lambda}{dA} \qquad (2.55)$$

where $\lambda = \Delta/P$ from equation(2.53) —— compliance

For constant force, P = constant

$$G_I = \frac{1}{2} P \frac{d\Delta}{dA} \qquad (2.56)$$

For constant displacement, Δ = constant

$$G_I = -\frac{1}{2} \Delta \frac{dP}{dA} \qquad (2.57)$$

It has been shown(45) that some direct relationships exist between energy release rates and stress intensity factors. For an isotropic material and plane-strain conditions:

$$G_I = \frac{1-\nu^2}{E} K_I^2 \; ; \; G_{II} = \frac{1-\nu^2}{E} K_{II}^2 \; ; \; G_{III} = \frac{1+\nu}{E} K_{III}^2 \qquad (2.58)$$

For plane-stress conditions

$$G_I = \frac{K_I^2}{E} \quad ; \quad G_{II} = \frac{K_{II}^2}{E} \quad ; \quad G_{III} = \frac{K_{III}^2}{E} \tag{2.59}$$

Where G_I, G_{II} and G_{III} are the energy-release rate contributions of each mode of cracking.

The finite element method has been used by a number of investigators to determine stress intensity factors for cracked bodies(41—44). Nowbray(46) used the compliance or strain energy release rate method to evaluate the single-edge crack (SEC) specimen subjected to uniform, uniaxial tension, Fig.(2.41). The finite element results were then compared with (8) as shown in Table(2.3). The agreement is good and the greatest difference is 3.5 percent.

Nowbray(46) stressed that good results could be obtained with the strain energy release rate method without excessive grid size refinement in the vicinity of the crack tip due to two reasons: First the finite element method would underestimate stresses and displacements close to the crack tip were minimized by examining the strain energy of the entire body through compliance determinations. Second , the calculated compliance across a given gage

section might be underestimated, the magnitude of the underestimate should be relatively independent of crack length. Hence, the slope of the compliance vs crack length curve, which was used for computing G and K should be very close to the true curve.

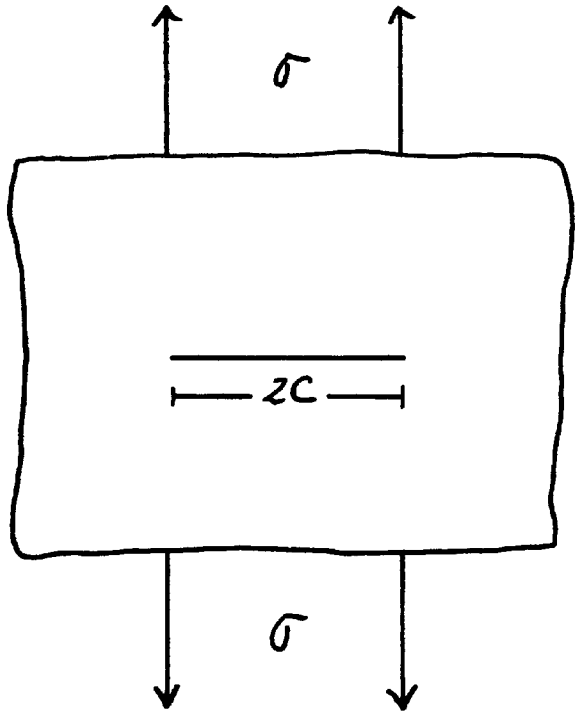

Fig. (2.1) Griffith's model

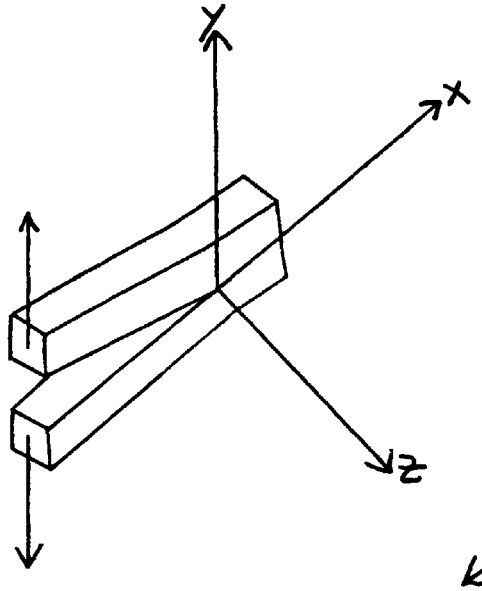

OPENING MODE I

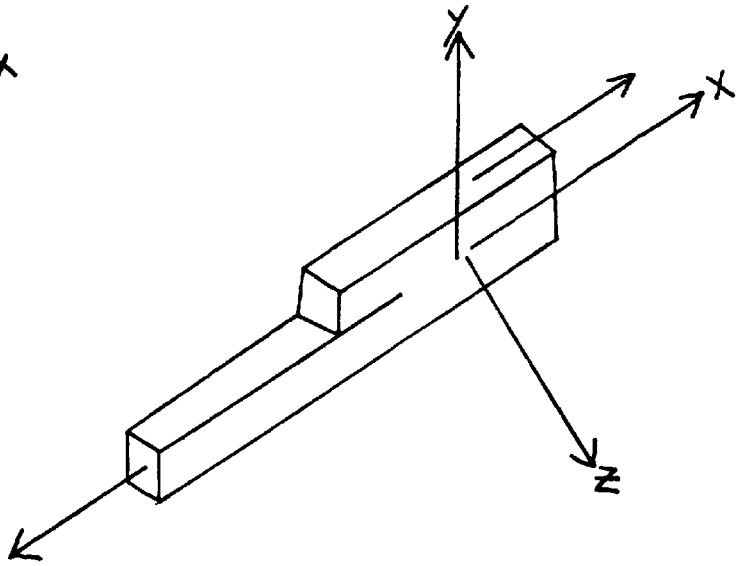

EDGE SLIDING MODE II

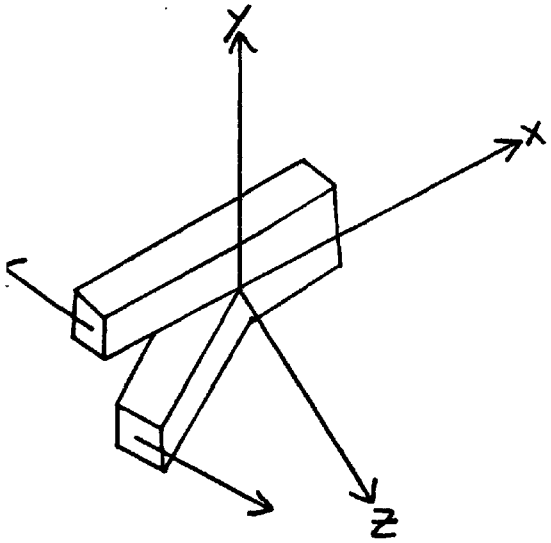

TEARING MODE III

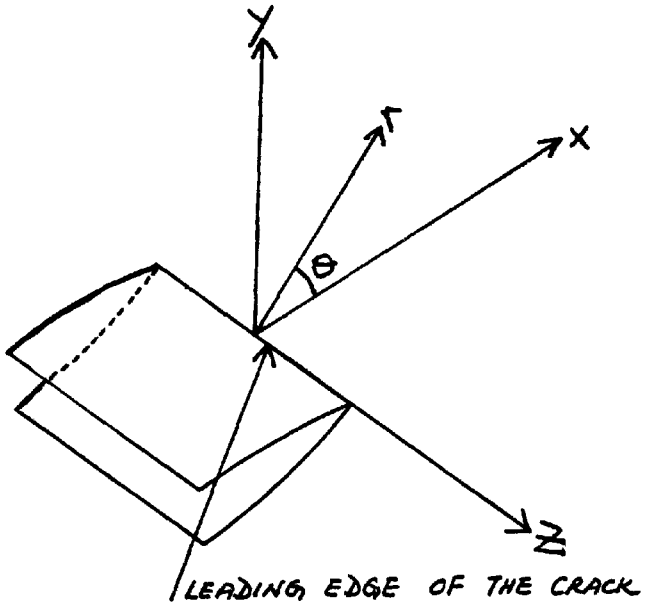

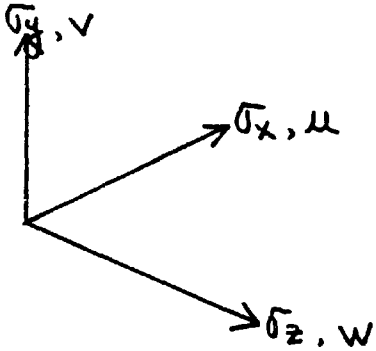

Fig. (2.2) Modes of crack displacement and co-ordinate system

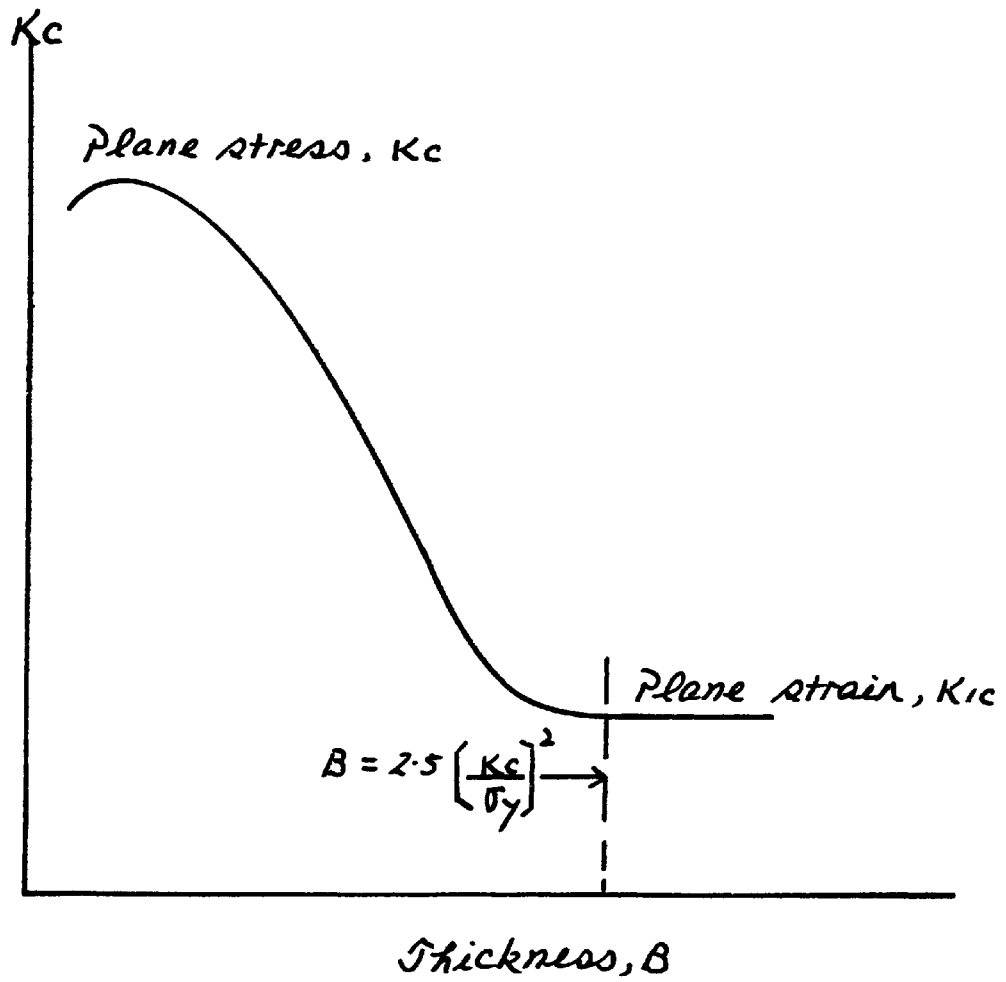

Fig. (2.3) Schematic representation of variation of Kc with specimen thickness

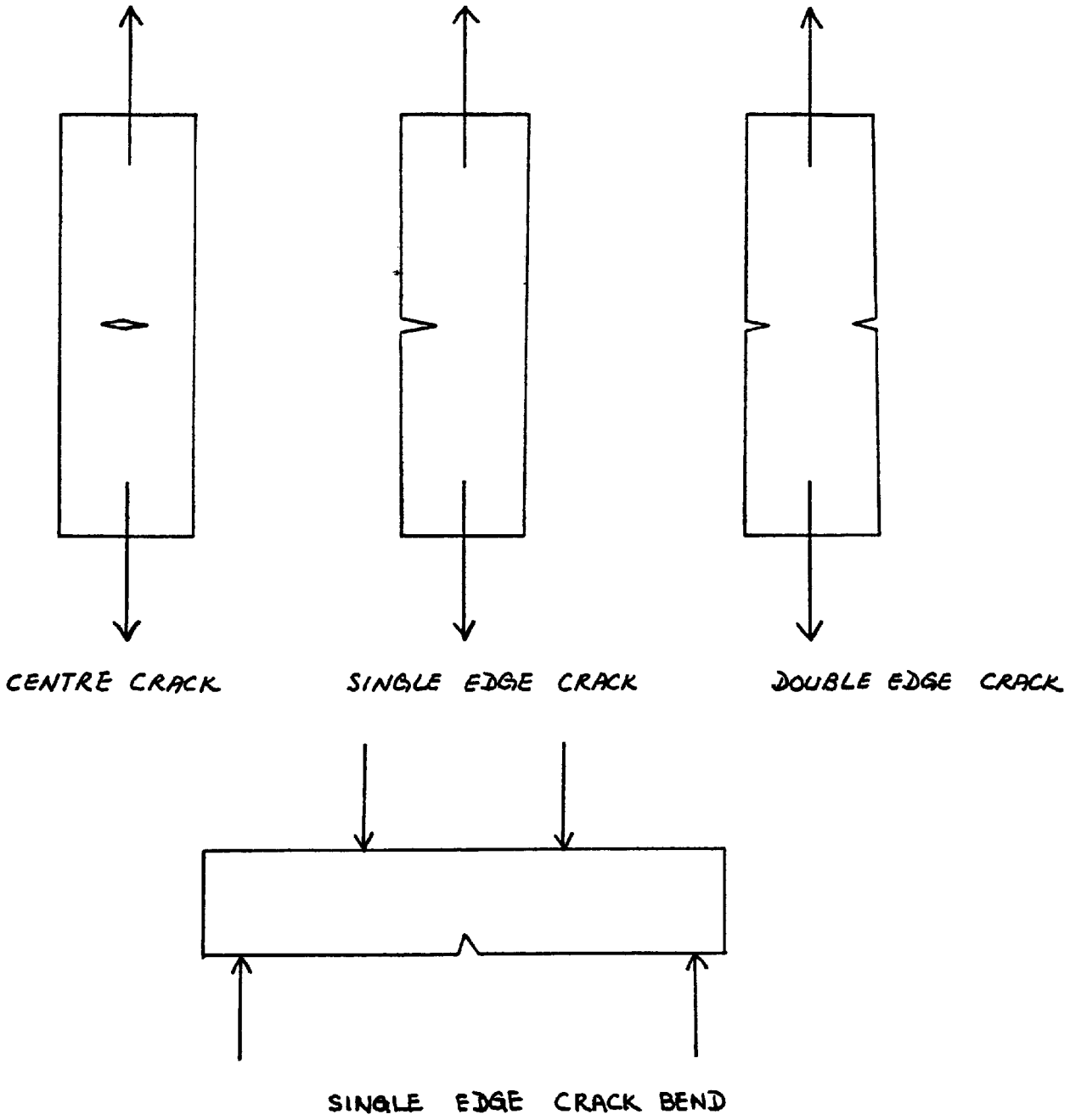

Fig. (2.4) Types of specimens used for K_{IC} testing

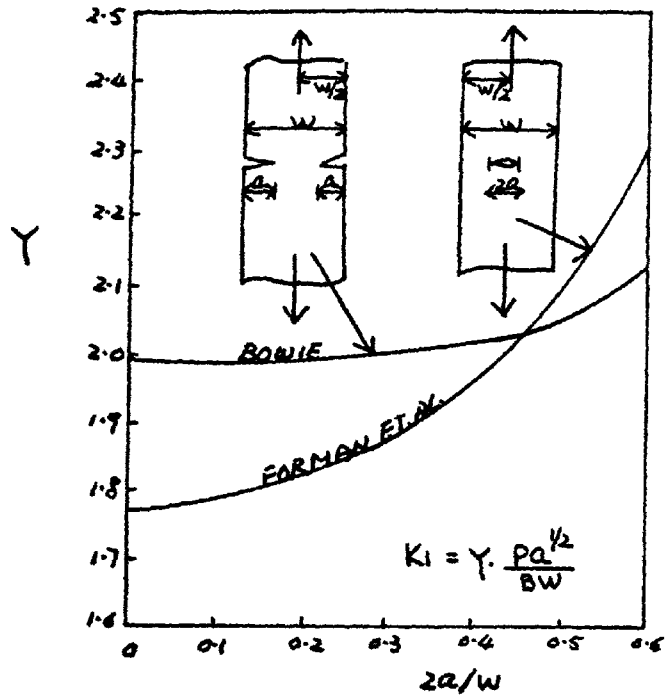

Fig. (2.5 a) K-calibration for the centre-cracked and double-edge-crack specimens

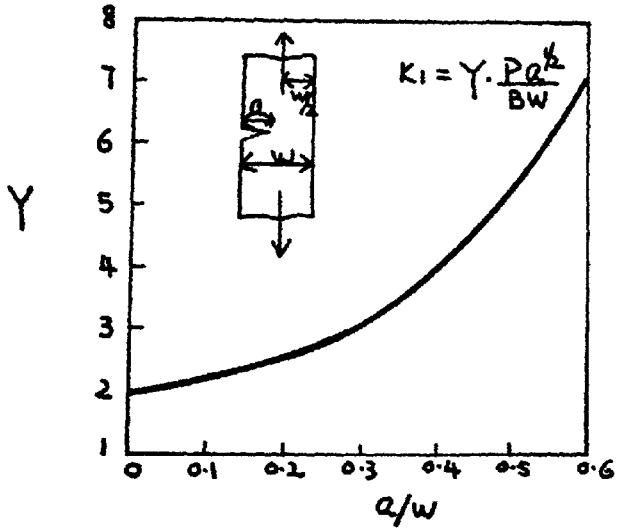

Fig. (2.5 b) K-calibration for single-edge-crack tension specimen

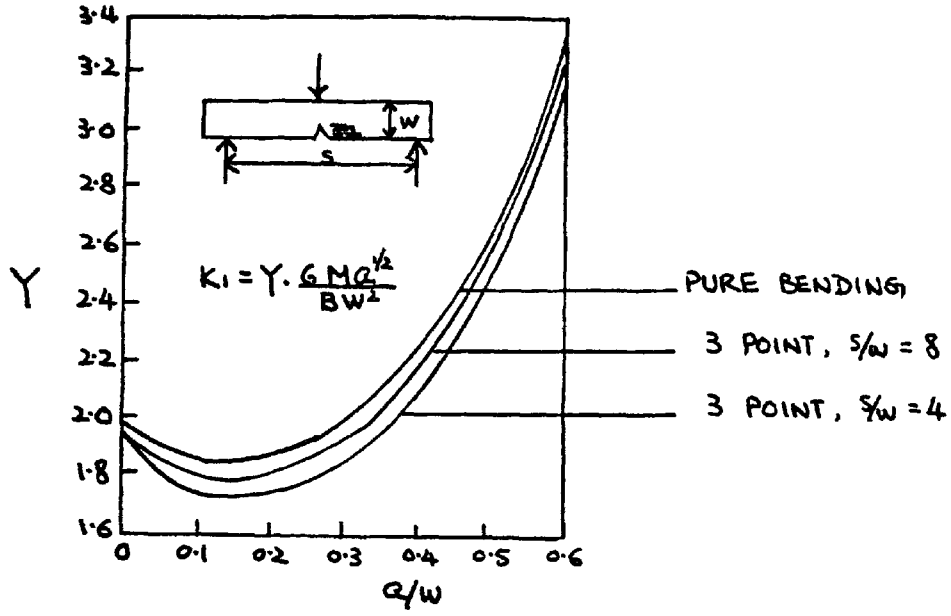

Fig. (2.5 c) K - calibration for bend specimens

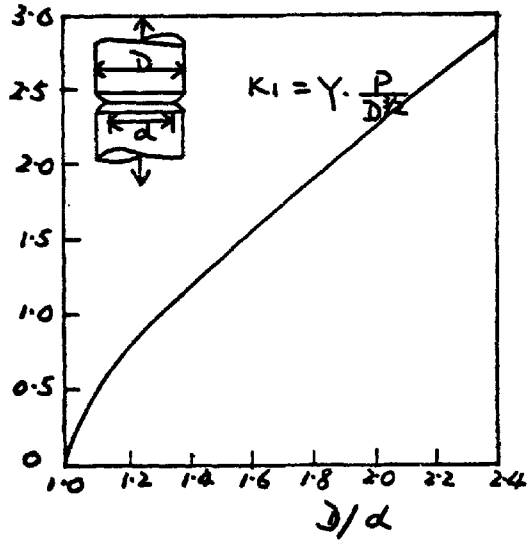

Fig. (2.5 d) K - calibration for circumferentially crack notched round bar

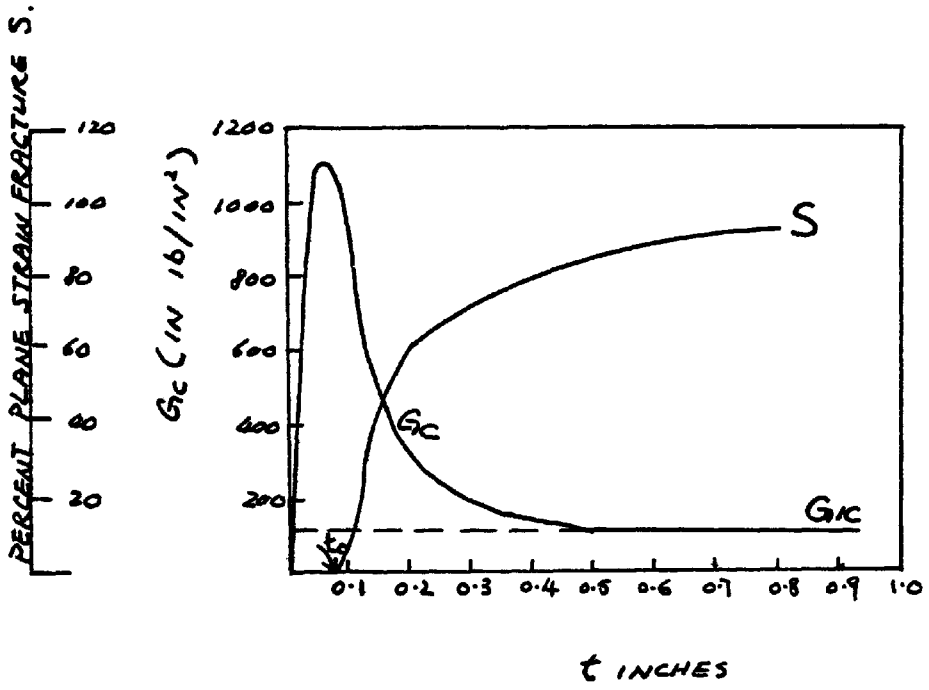

Fig. (2.6) Percent plane strain fracture, S, and Gc as a function of plate thickness (Tetelman et al[7])

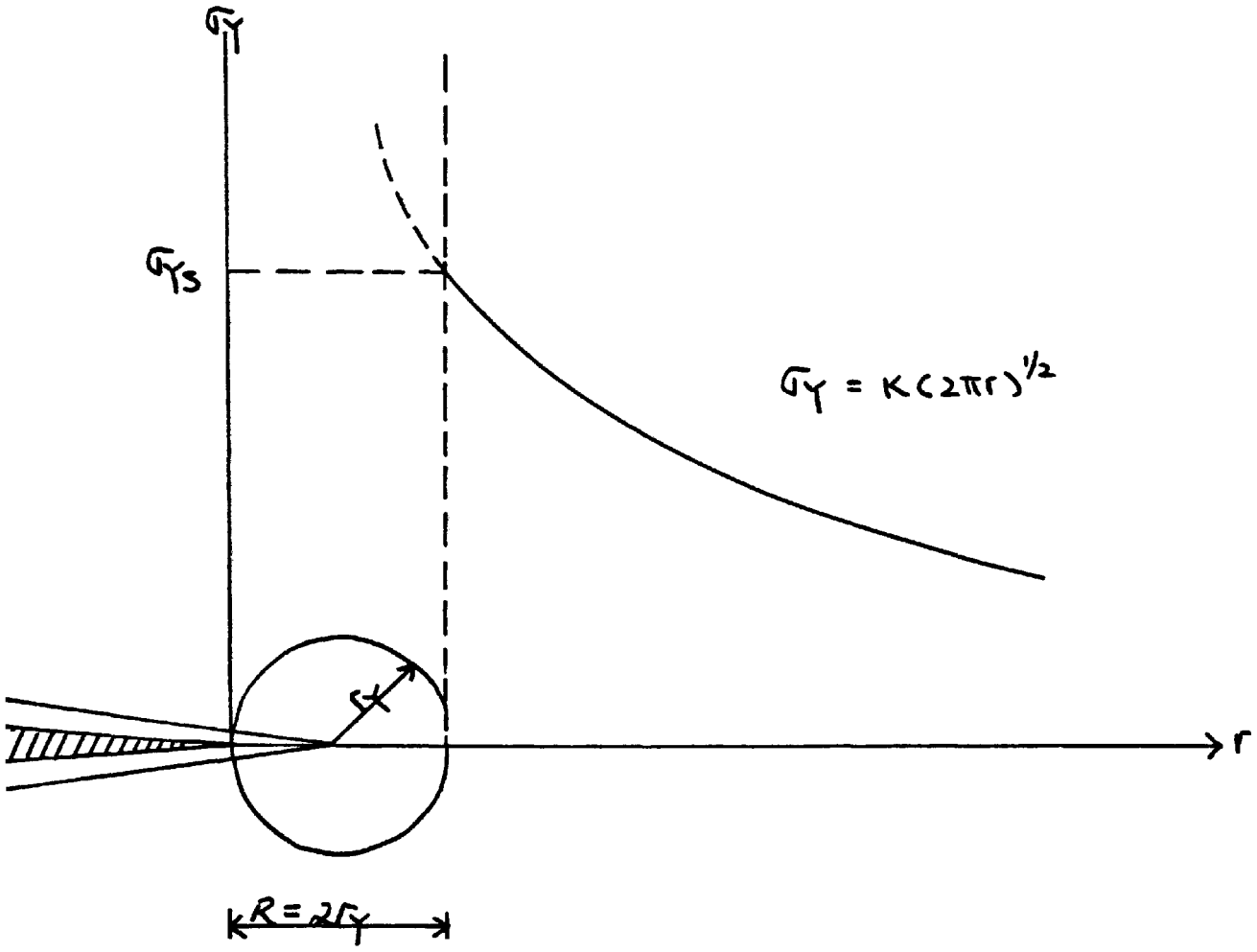

Fig. (2.7) Onset of plastic deformation at the crack tip

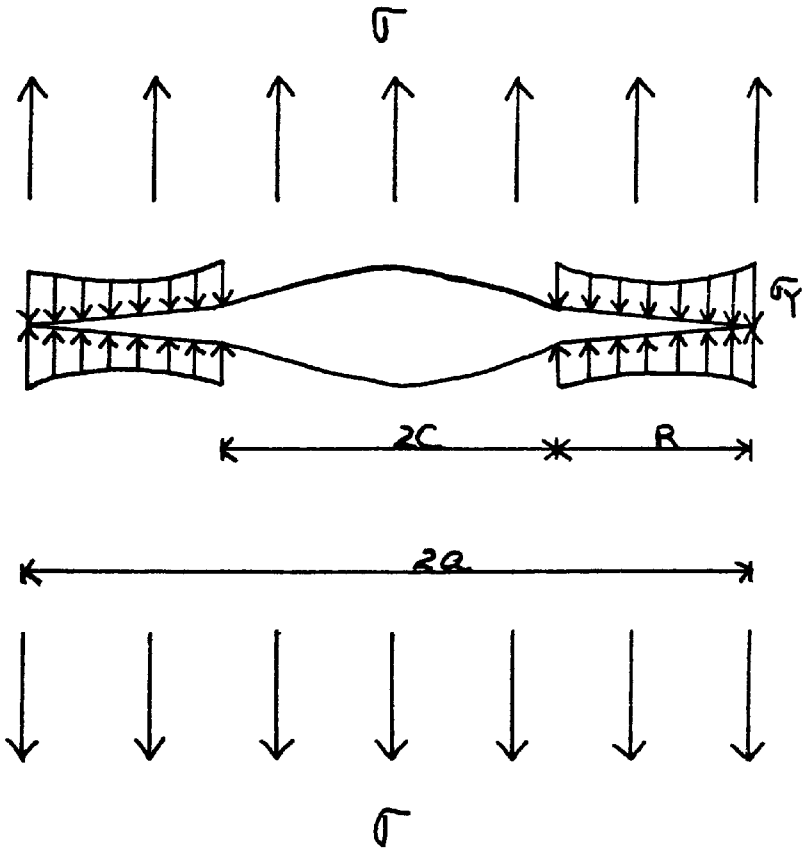

Fig. (2.8) Internal stress distribution used in the Dugdale model

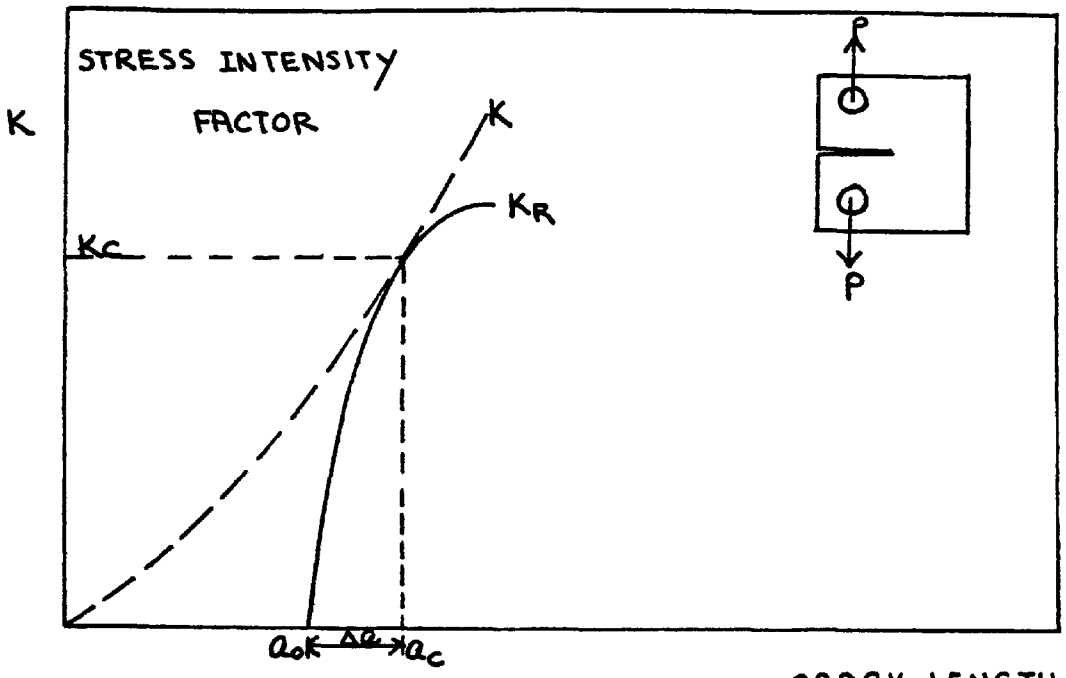

Fig. (2.9) Crack growth resistance curve and crack driving curve (McCabe and Heyer[11])

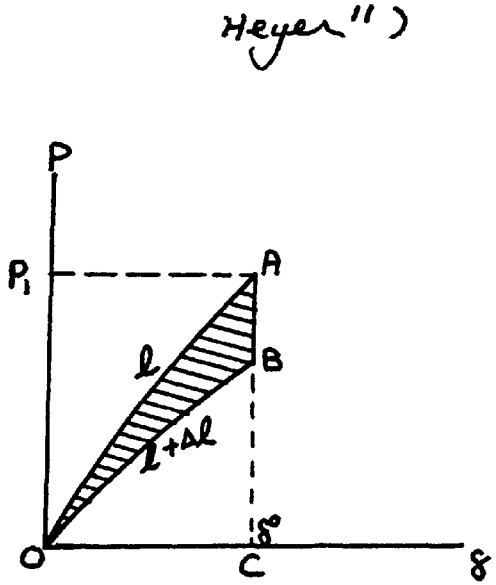

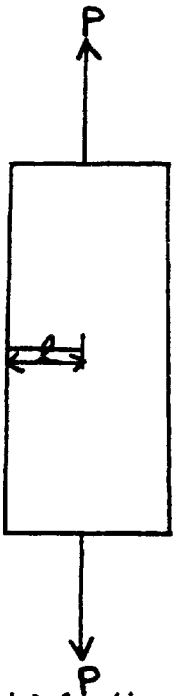

Fig. (2.10) Generalised load - deflection diagram

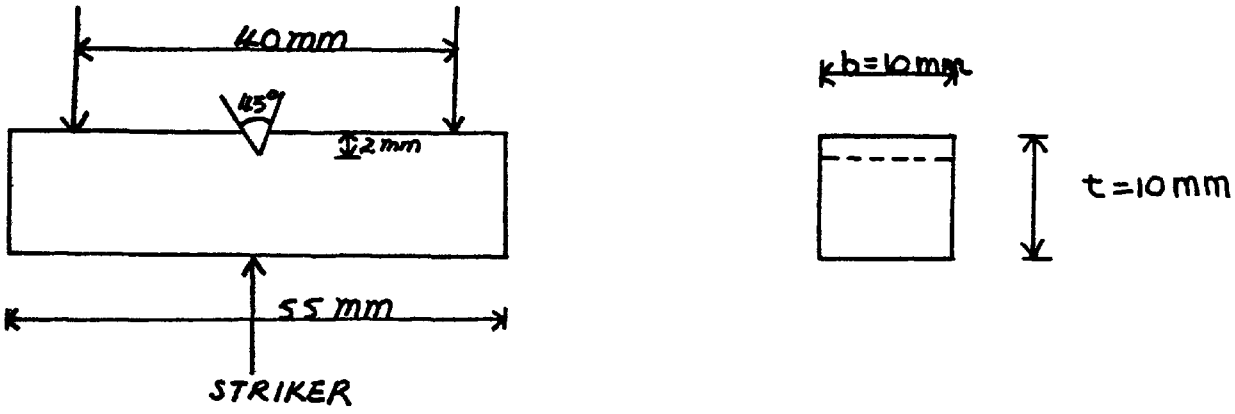

Fig. (2.11) Pendulum impact testing loading

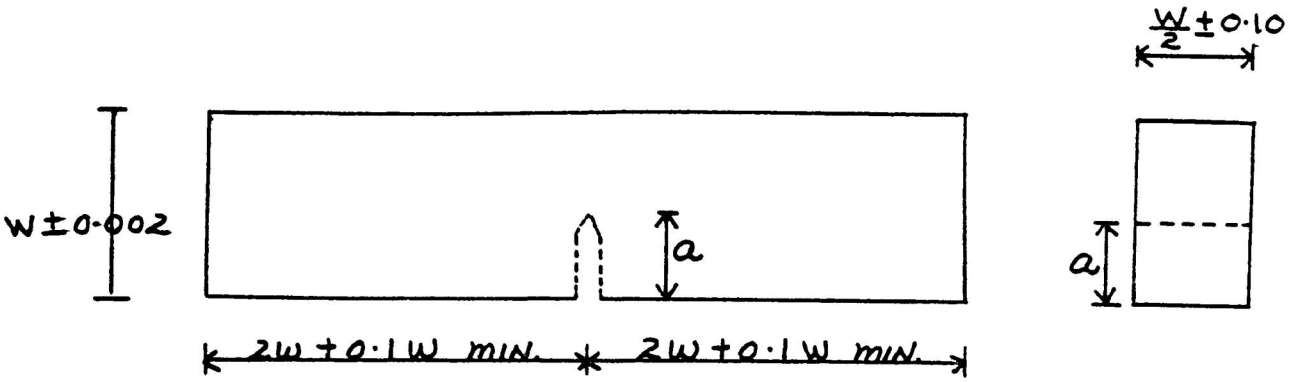

$$K_Q = \frac{P_Q S}{B W^{3/2}} \left[2.9 \left(\frac{a}{W}\right)^{1/2} - 4.6 \left(\frac{a}{W}\right)^{3/2} + 21.8 \left(\frac{a}{W}\right)^{5/2} - 37.6 \left(\frac{a}{W}\right)^{7/2} \right]$$

where S = span length

Bend specimen

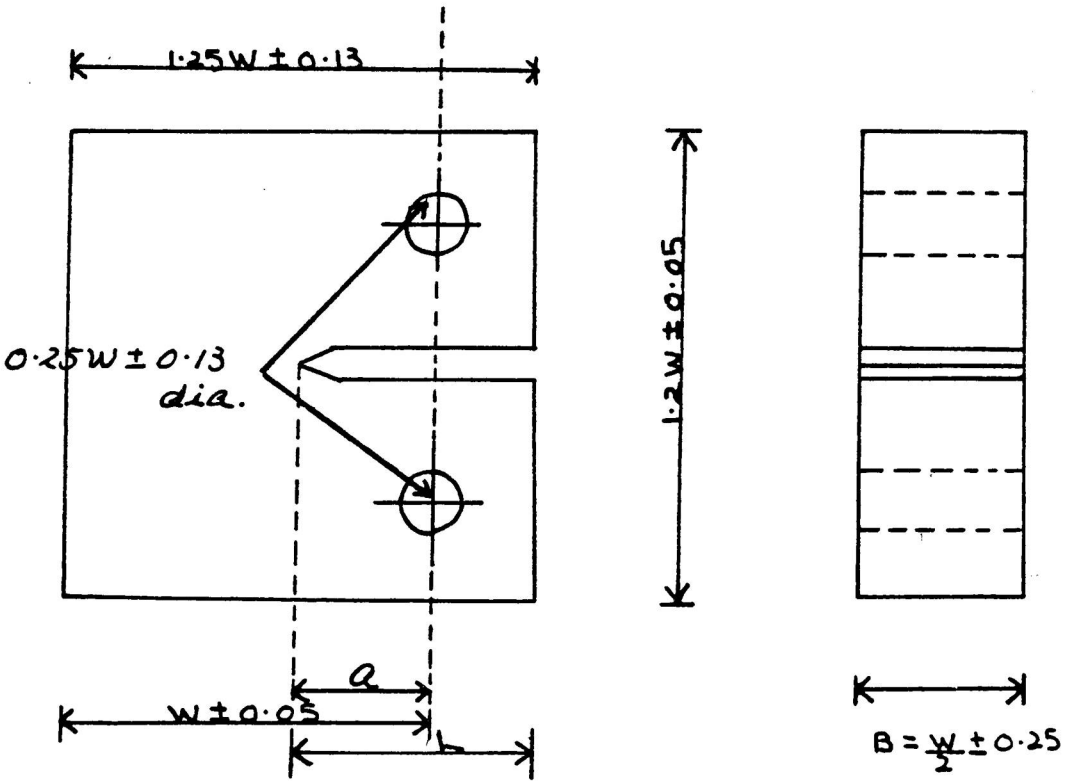

$$K_Q = \frac{P_Q}{B W^{1/2}} \left[29.6 \left(\frac{a}{W}\right)^{1/2} - 185.5 \left(\frac{a}{W}\right)^{3/2} + 655.7 \left(\frac{a}{W}\right)^{5/2} - 1017.0 \left(\frac{a}{W}\right)^{7/2} + 638.9 \left(\frac{a}{W}\right)^{9/2} \right]$$

Compact tension specimen

Fig. (2.12) Bend specimen and compact tension specimen

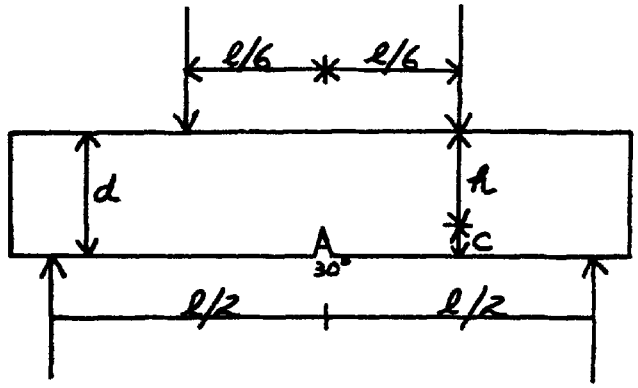

Third point loading

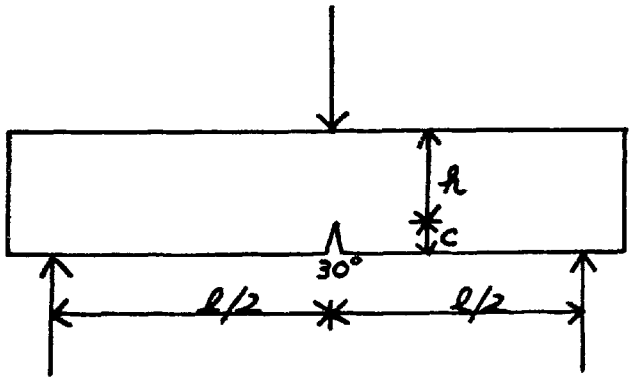

Centre point loading

Fig. (2.13) Details of loading systems used by Kaplan (15)

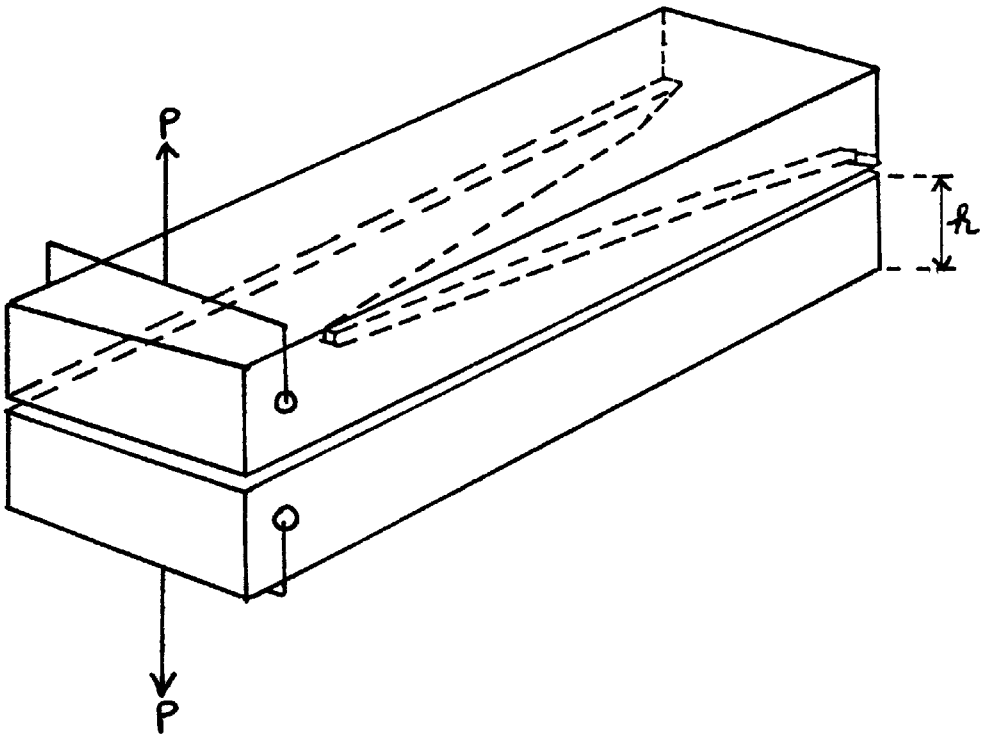

Fig. (2.14) Double cantilever beam (DCB) specimen with tapered web (Brown[19])

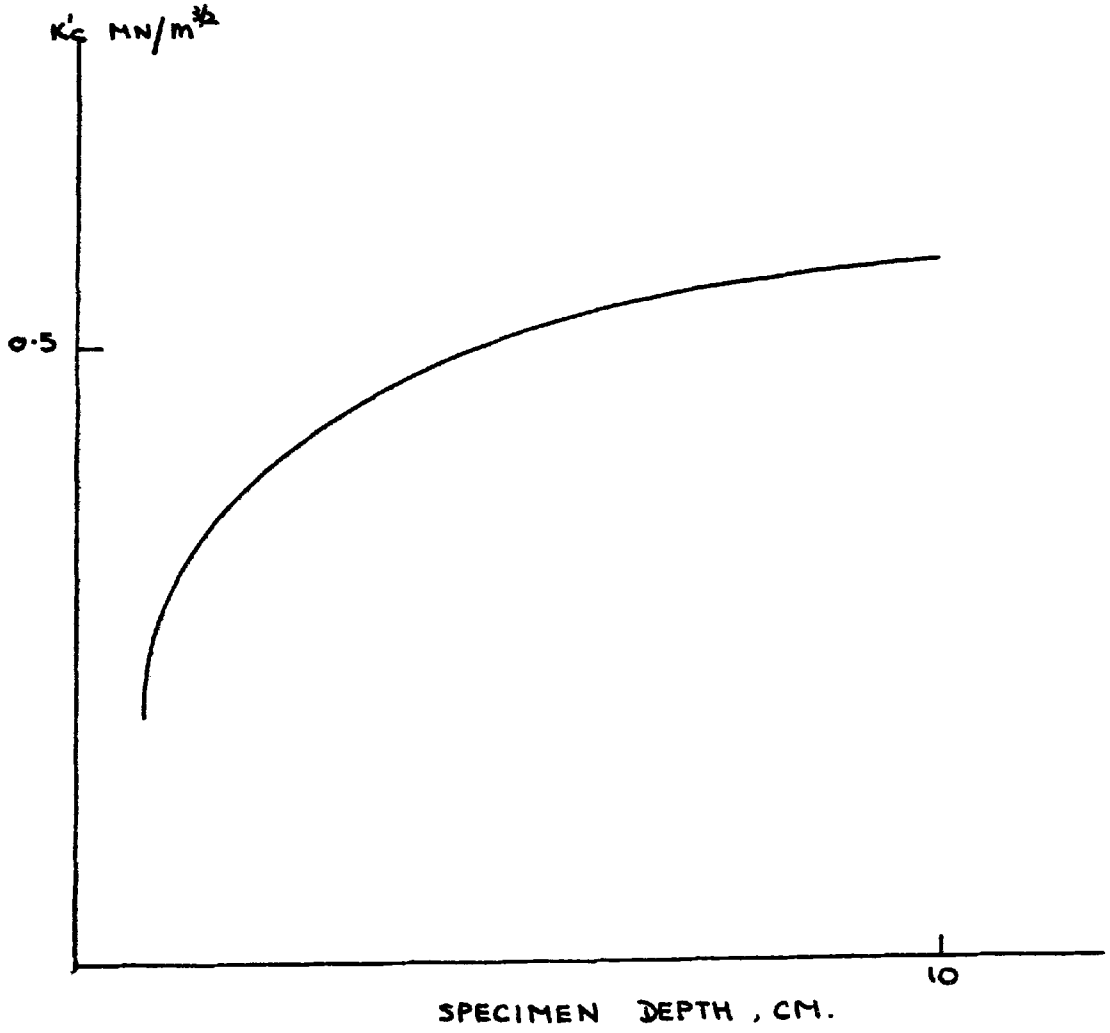

Fig. (2.15) Kć versus specimen depth (Higgens and Bailey[20])

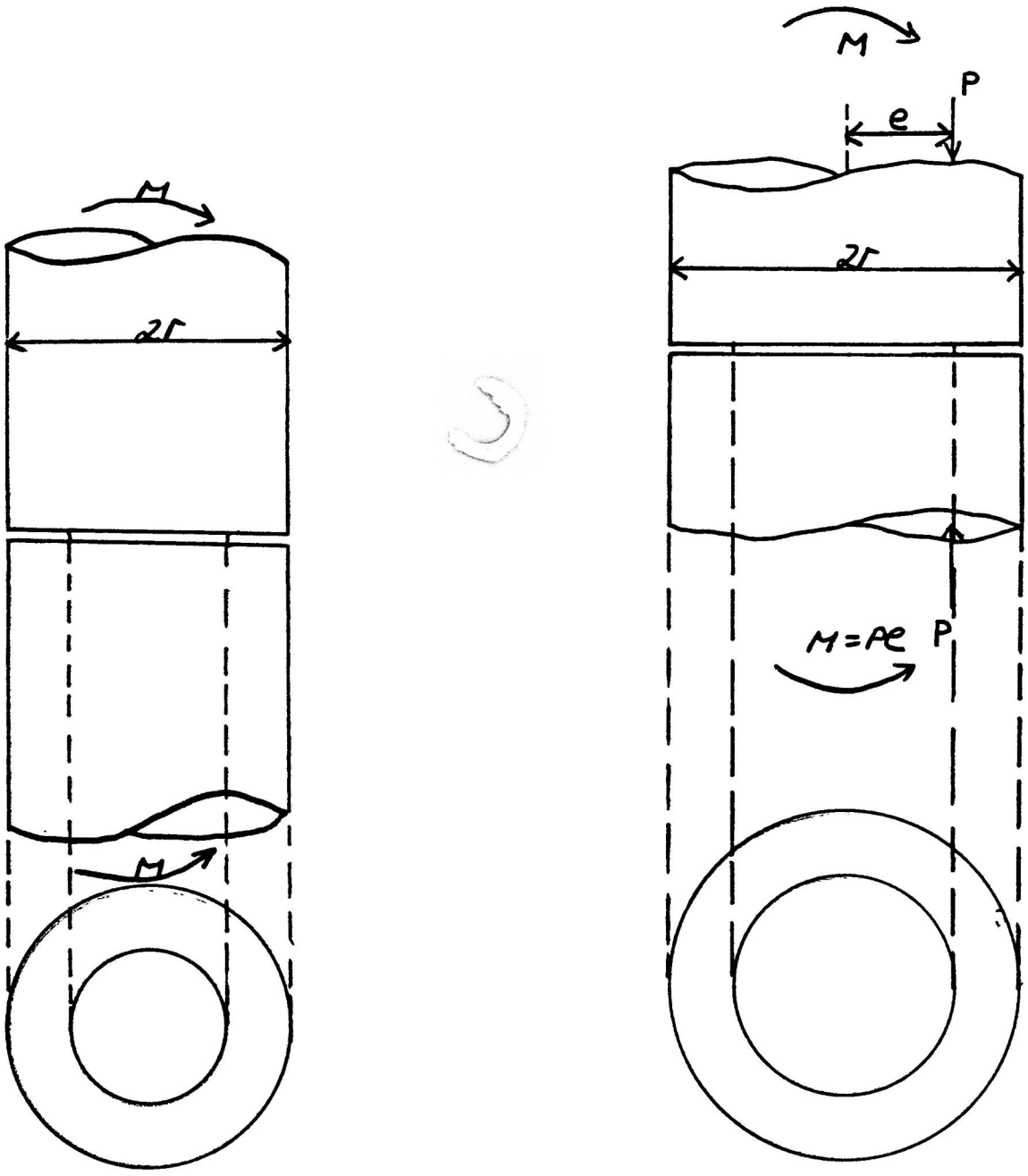

(a) Circumferentially-notched round bar under bending (CNRBB) specimen

(b) Circumferentially-notched round bar under eccentric loading (CNRBEL) specimen

Fig. (2.16) CNRBB specimen and CNRBEL specimen used by Barr and Bear (21)

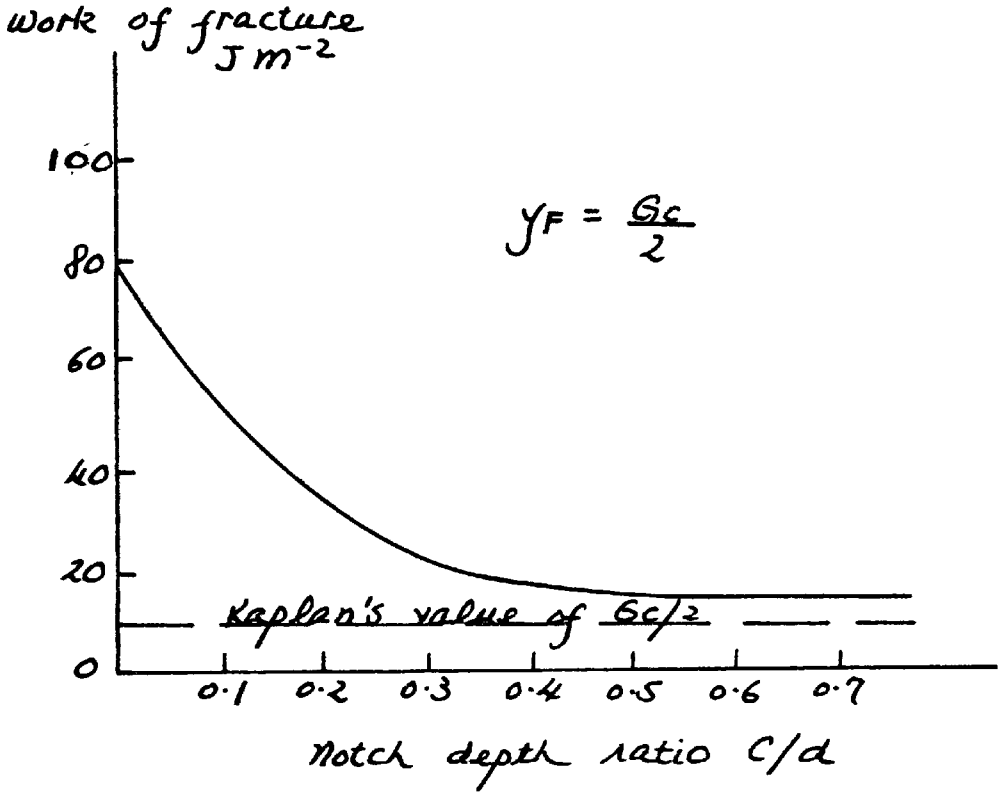

Fig. (2.17) Work of fracture of plain concrete as a function of notch depth (Harris et al [28])

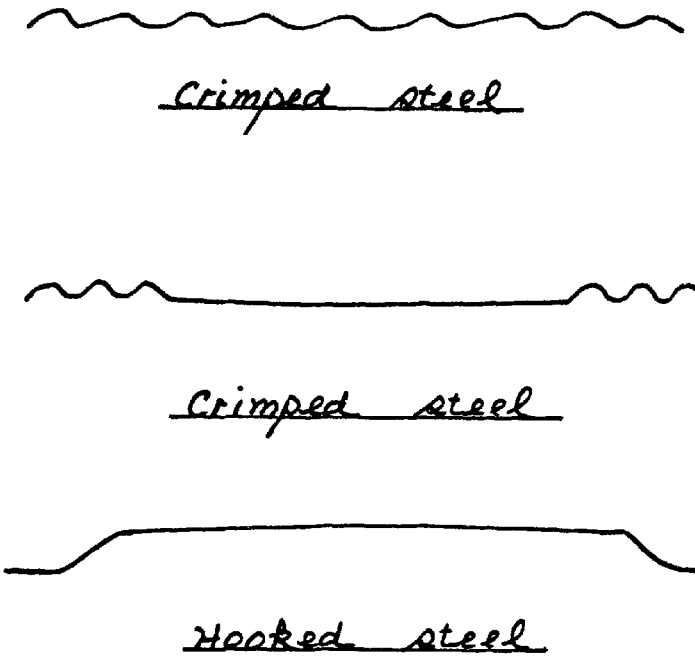

Fig. (2.18) Various forms of steel fibre used by Hughes and Fattuhi (31)

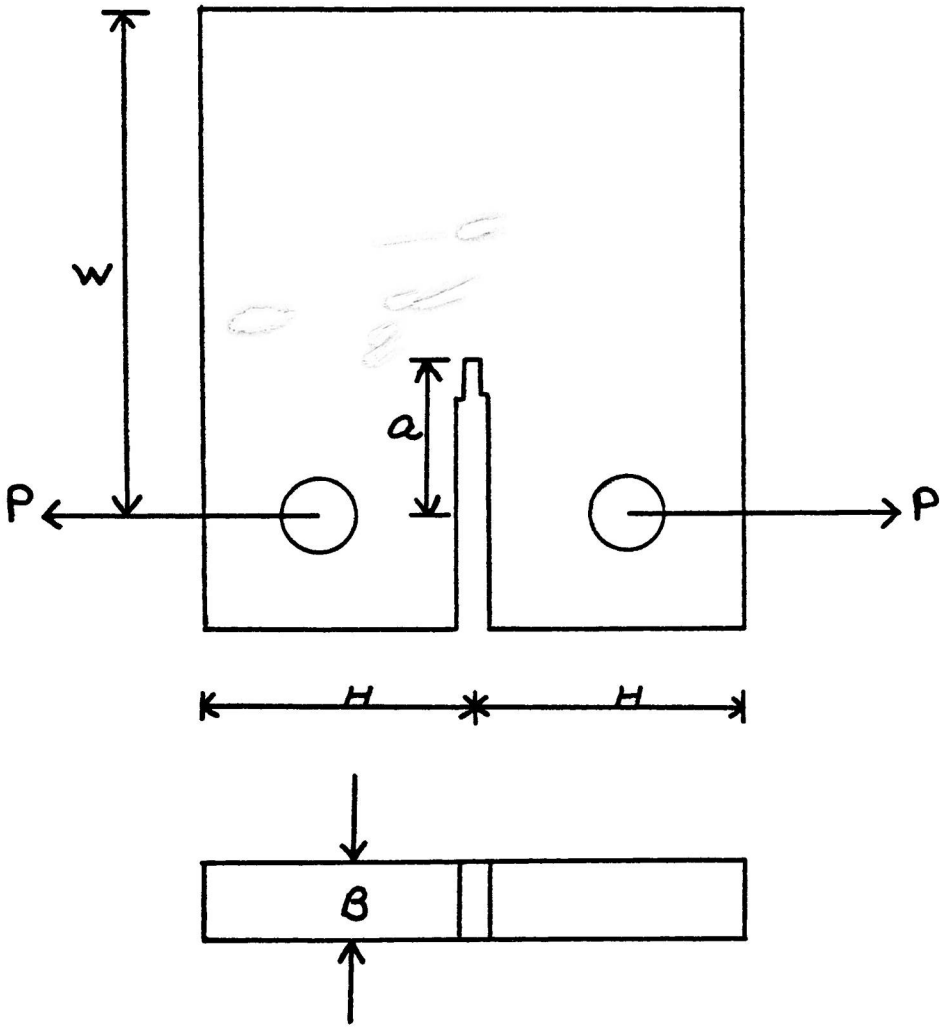

Fig. (2.19) Crack-line loaded single-edge crack specimen (Patterson et al[33])

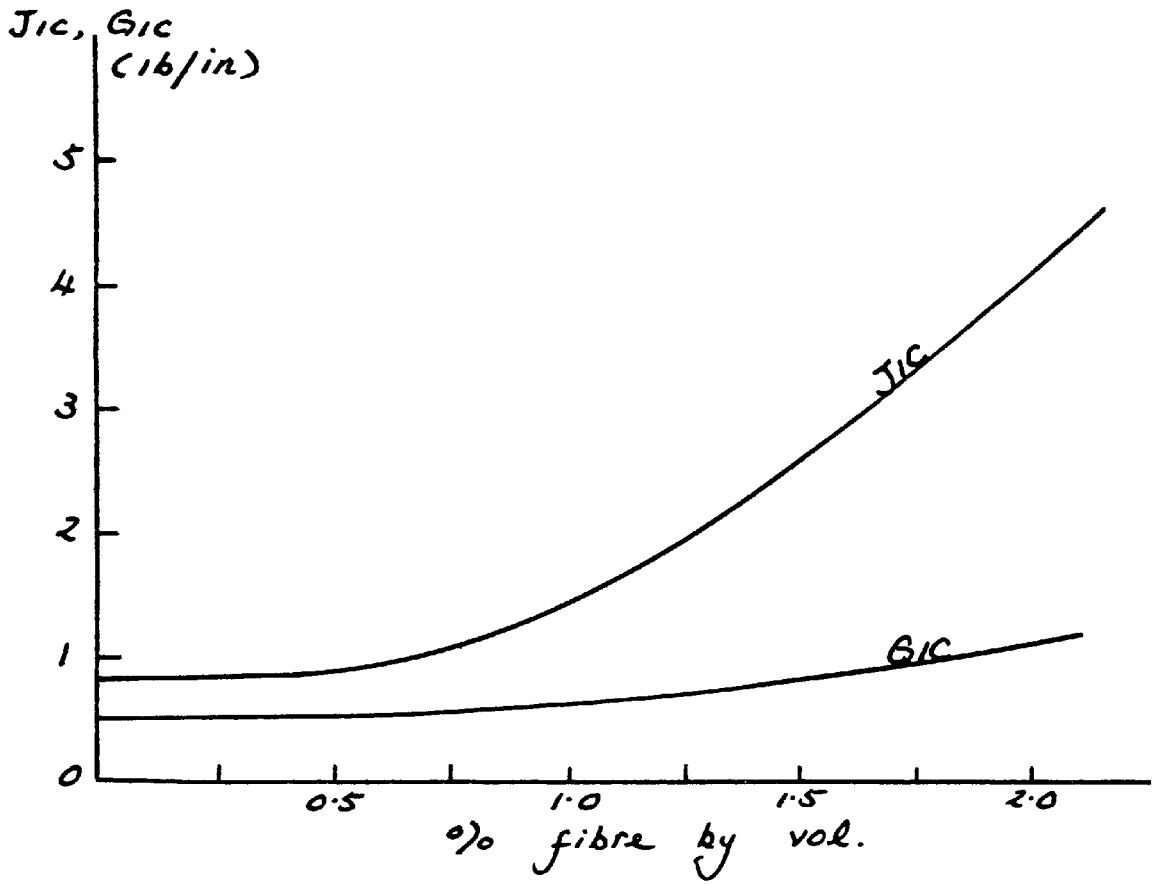

Fig. (2.20) Effect of fibre content on JIc and GIc (Mindess[34])

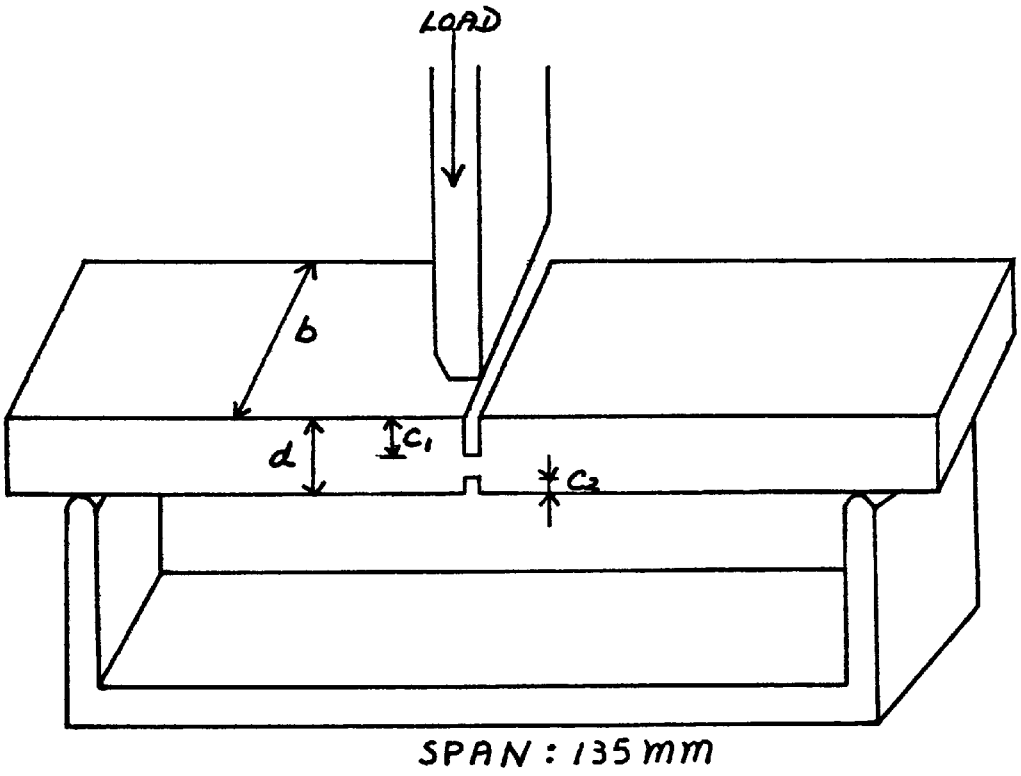

Fig. (2.21) Arrangement of Ohigashi's specimen (36)

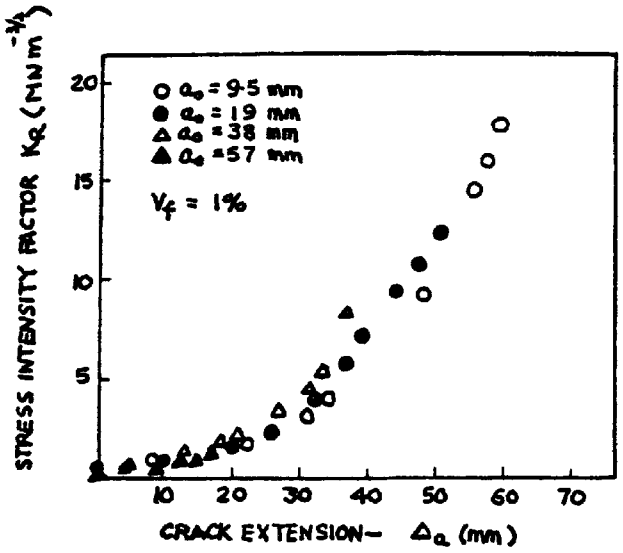

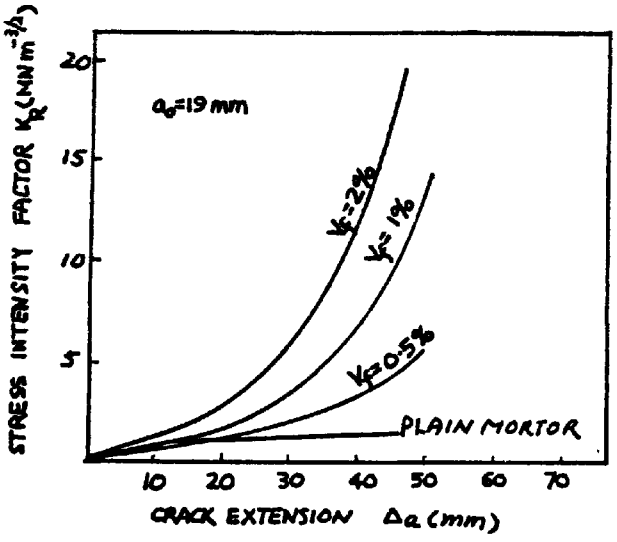

Fig. (2.22) R-curves for different initial notch depth and fibre vol. (Velazco et al [37])

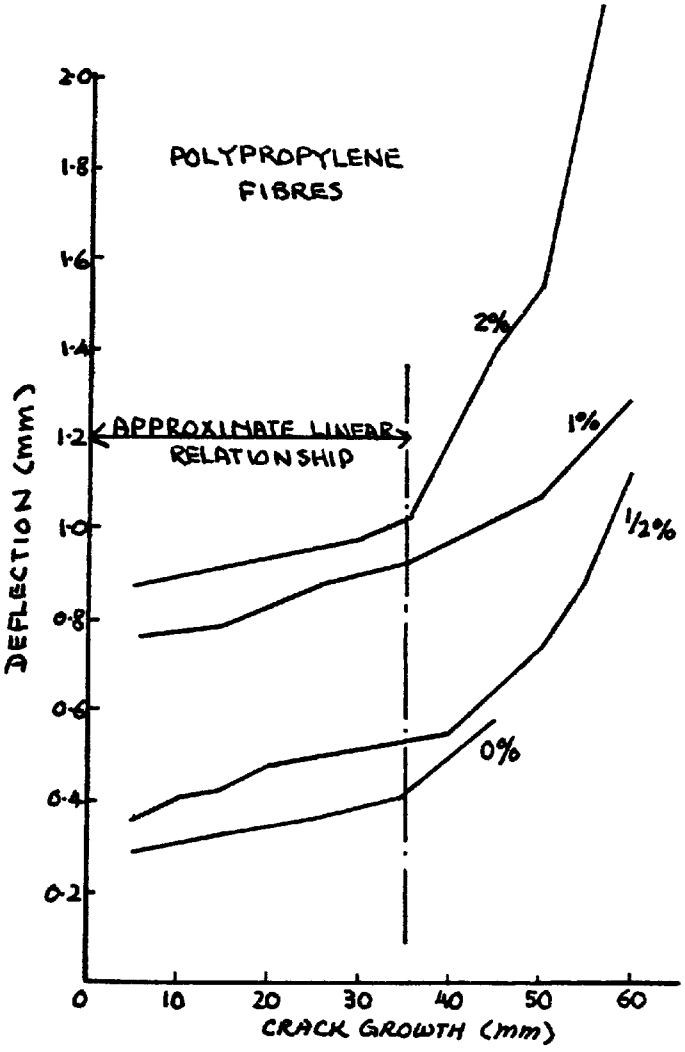

Fig. (2.23) Influence of polypropylene fibres on the deflection - crack growth characteristics of beams in bending (Swamy[38].)

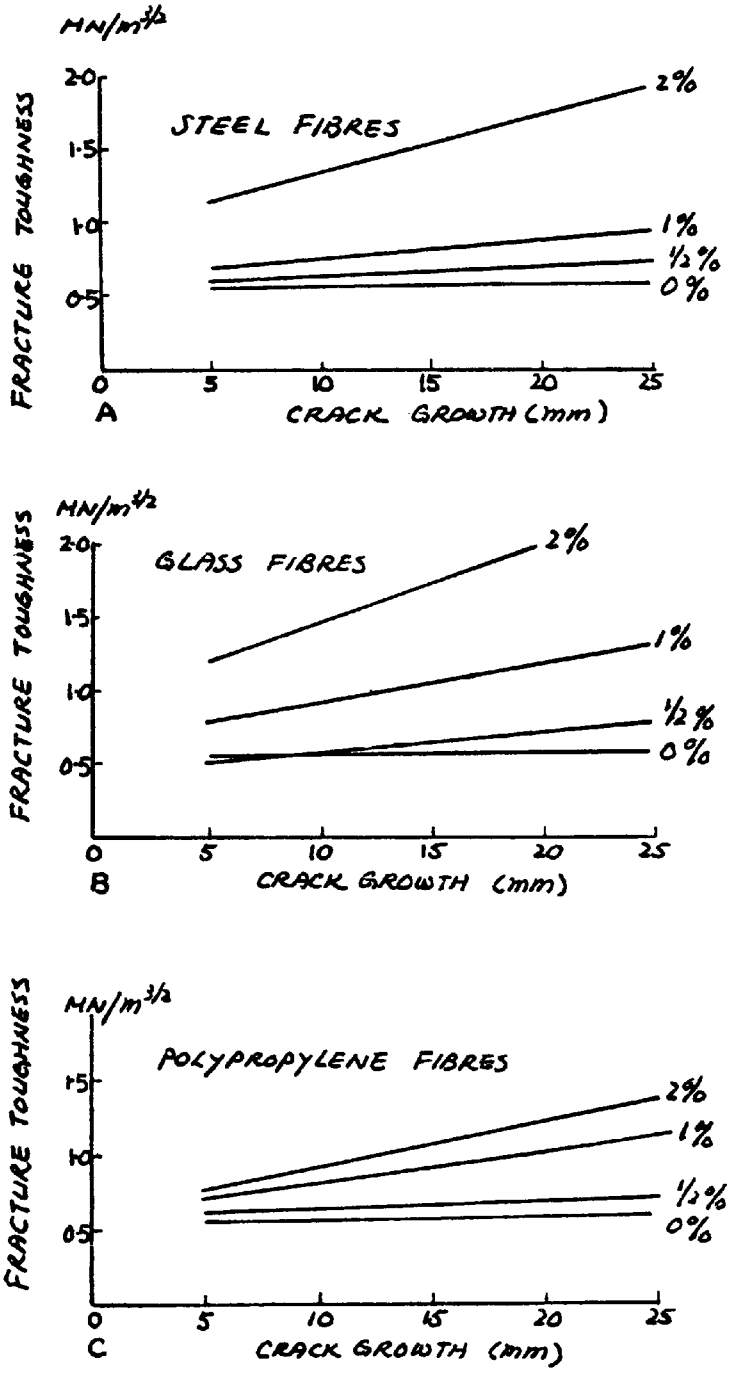

Fig. (2.24) Apparent fracture toughness of fibre concrete composites under slow crack growth (Swamy[38])

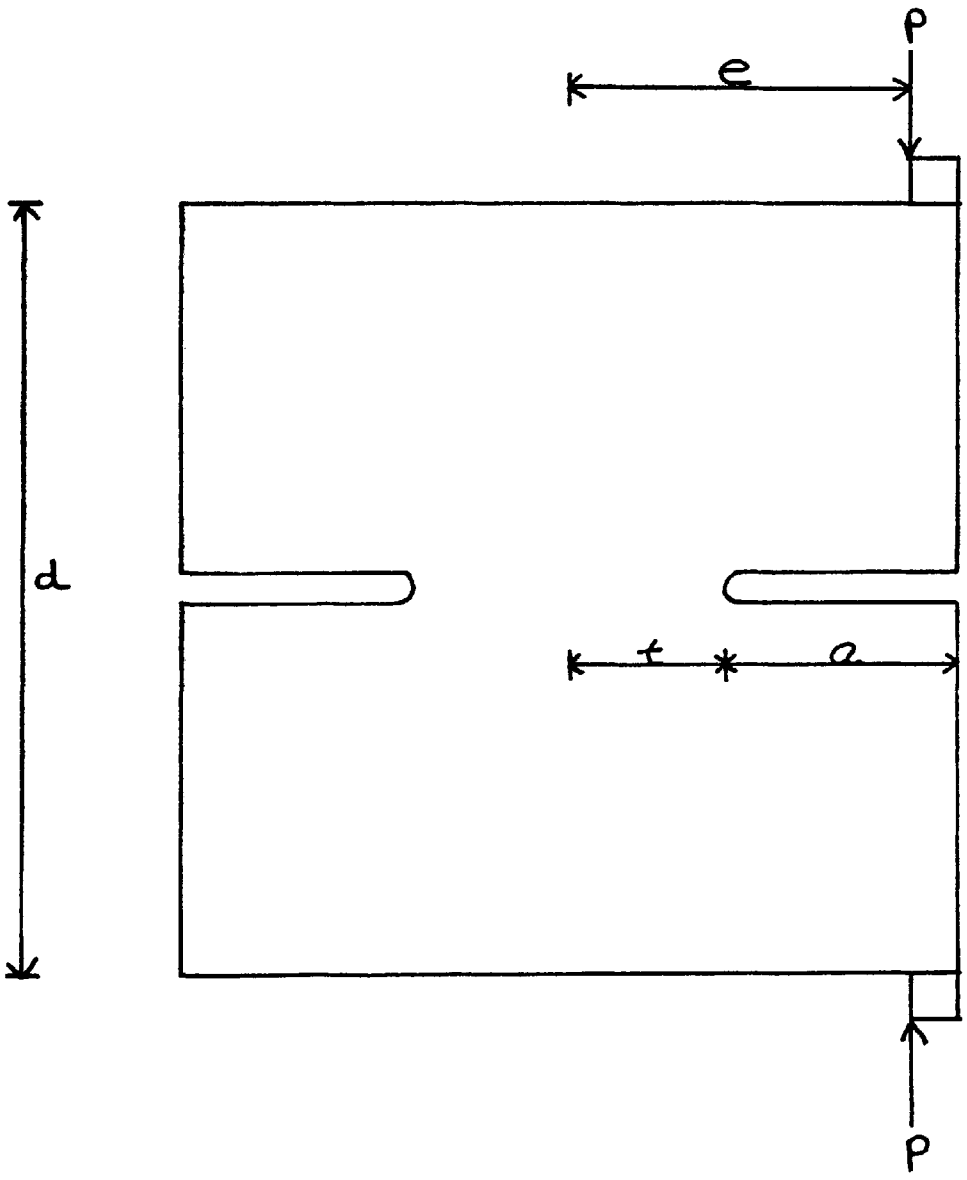

Fig. (2.25) Split cube specimen used by Dowers (39)

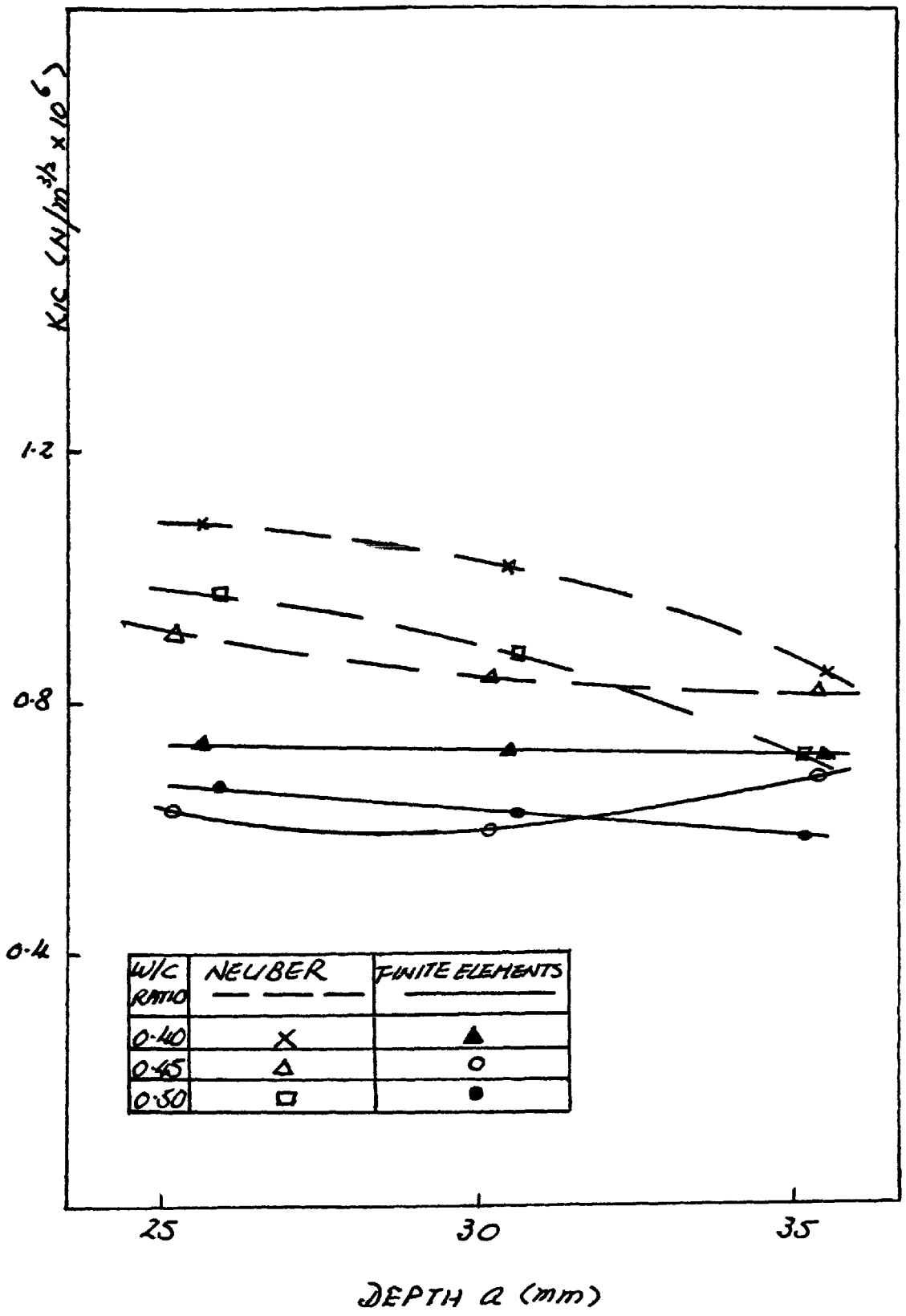

Fig. (2.26) Comparison of K1C values (Dowers [39])

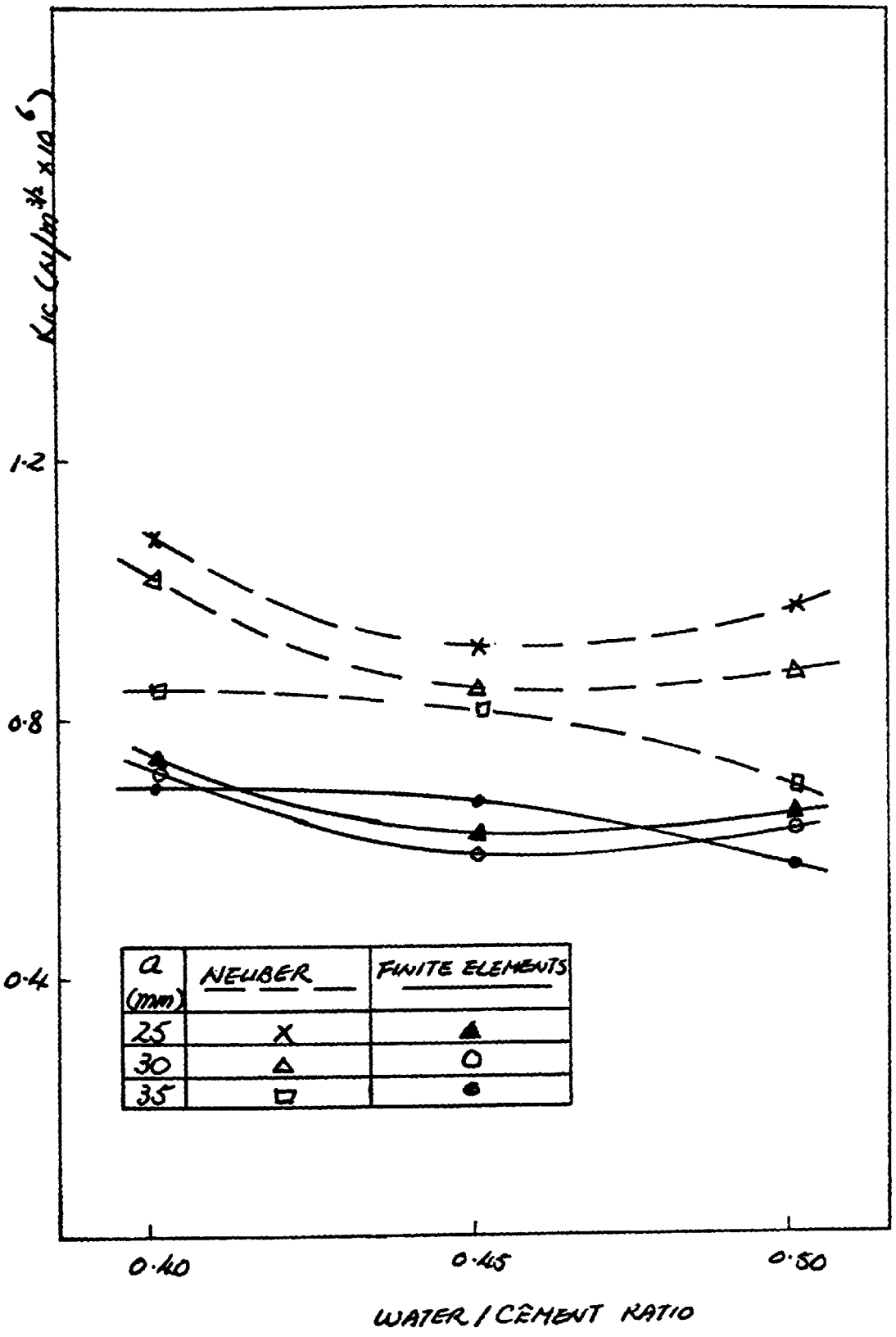

Fig. (2.27) Variation of KIC with water/cement ratio (Dowers[39])

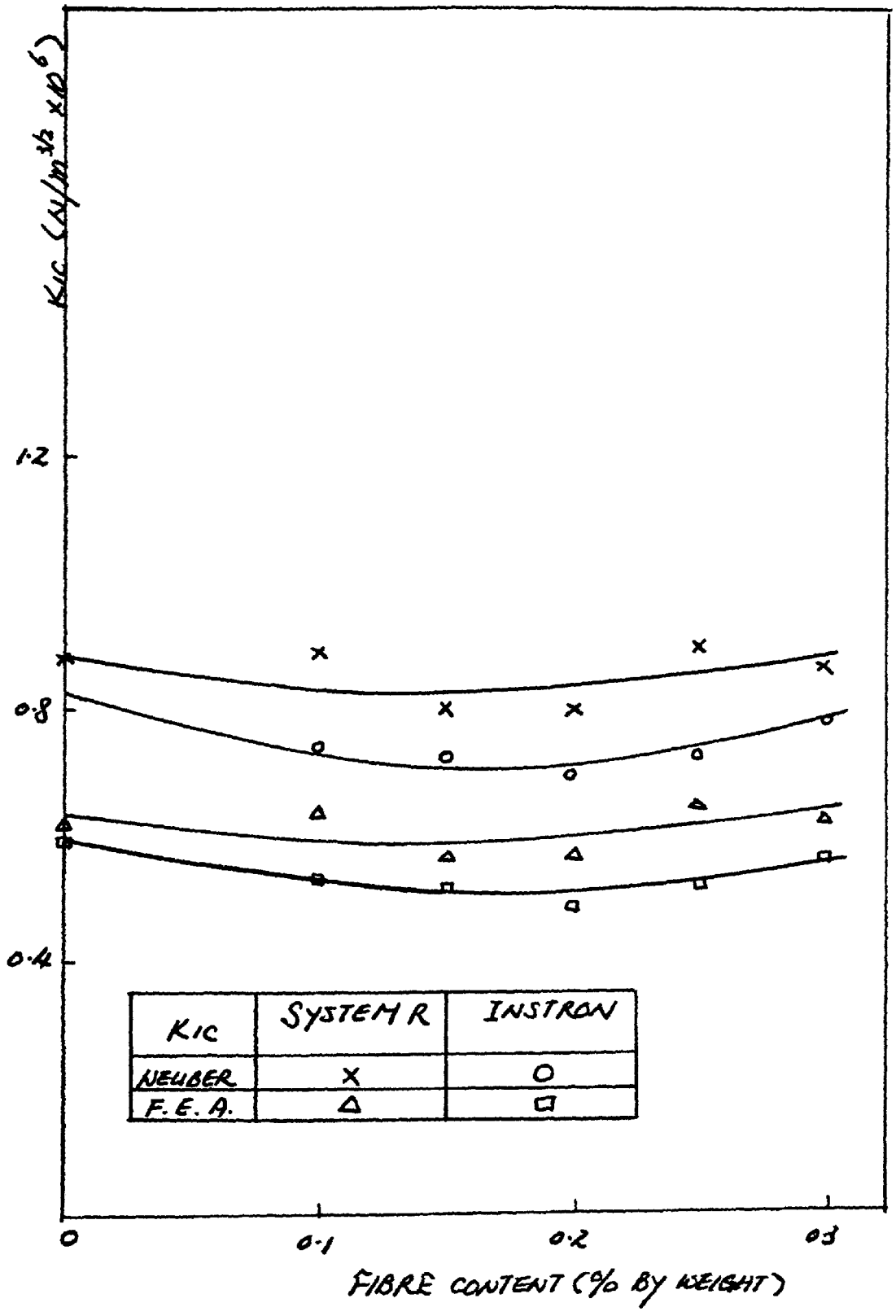

Fig. (2.28) Variation of KIC with fibre content (Dowers[39])

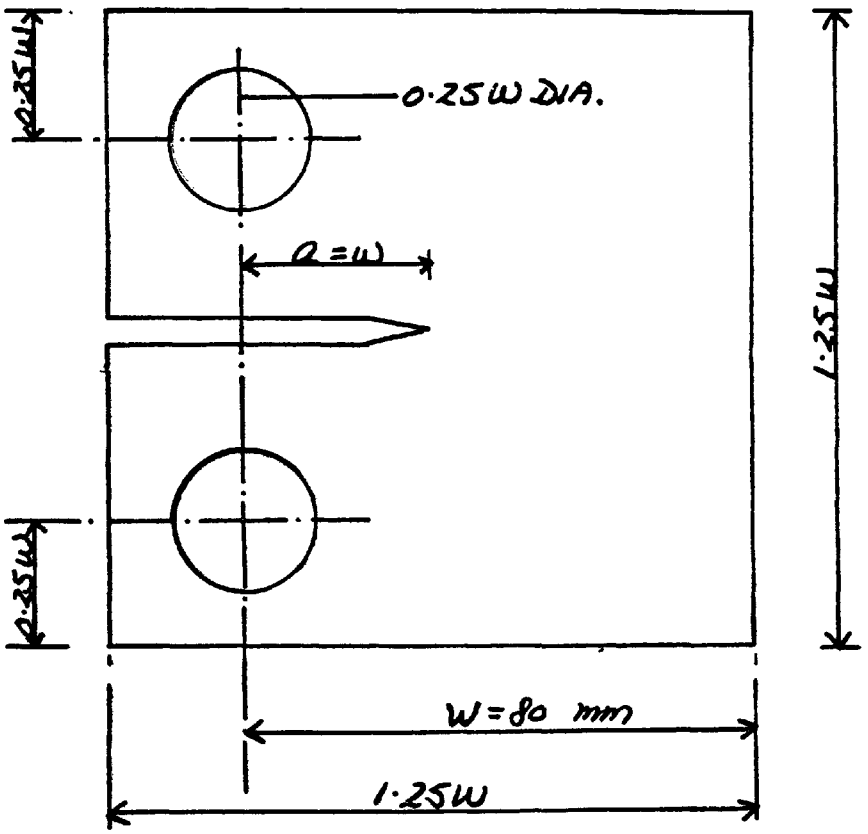

Fig. (2.29) Compact tension specimen used by Dowers (39)

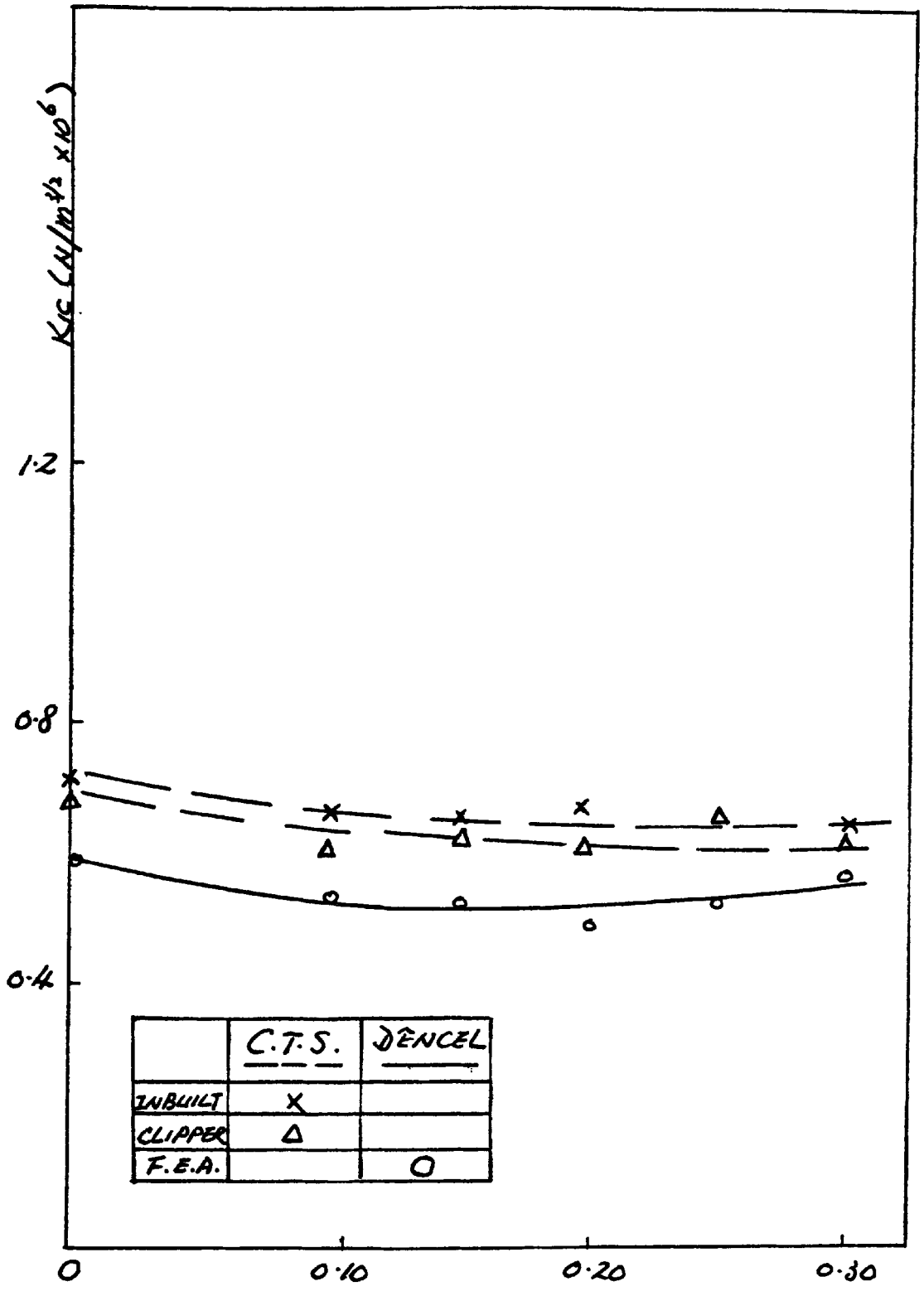

Fig. (2.30) Variation of KIC with fibre content for different specimen geometry (Dowers[39])

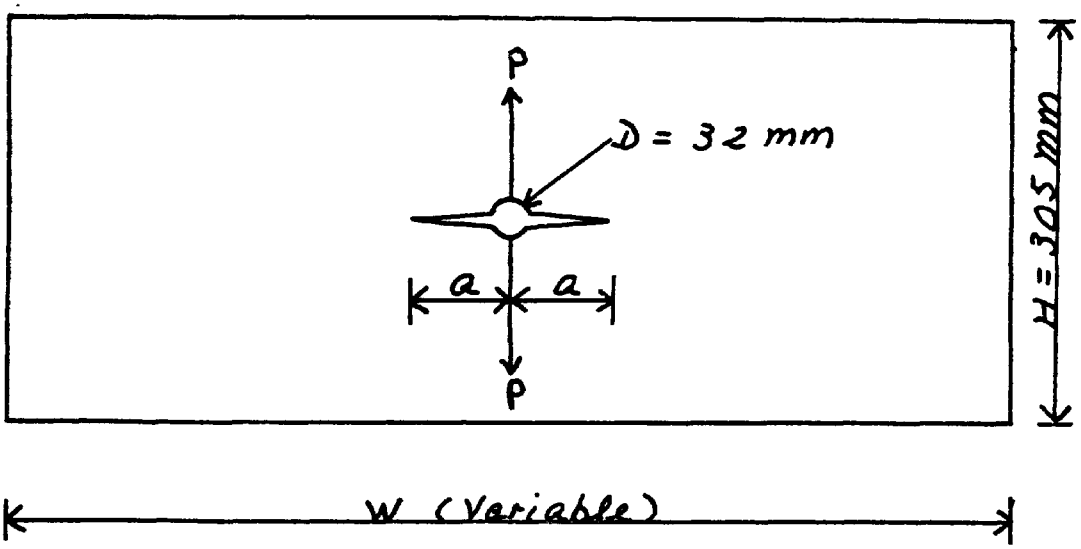

Fig. (2.31) Specimen configuration used by Kesler et al (58)

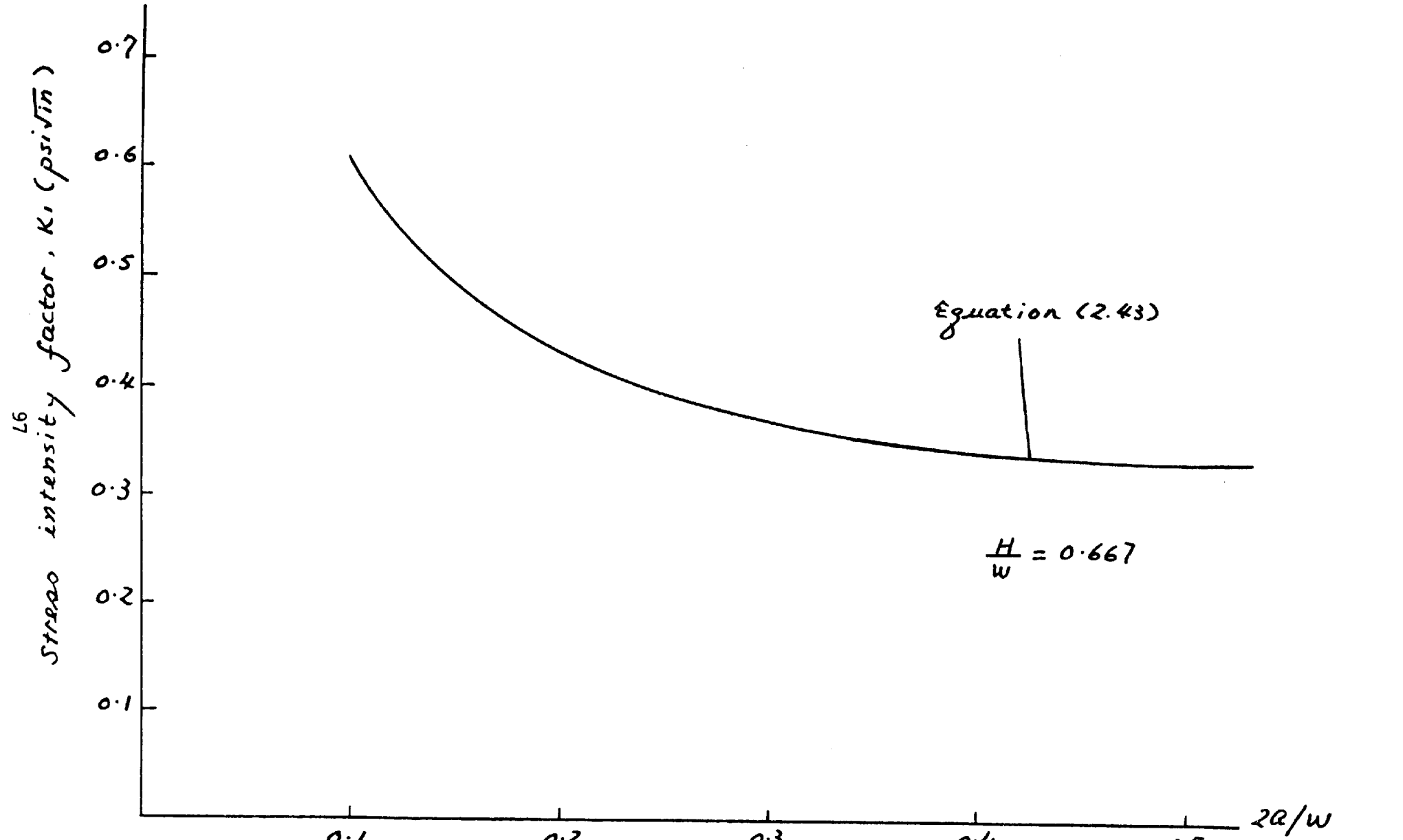

Fig. (2.32) Stress intensity factor versus relative crack length (Kesler et al [58])

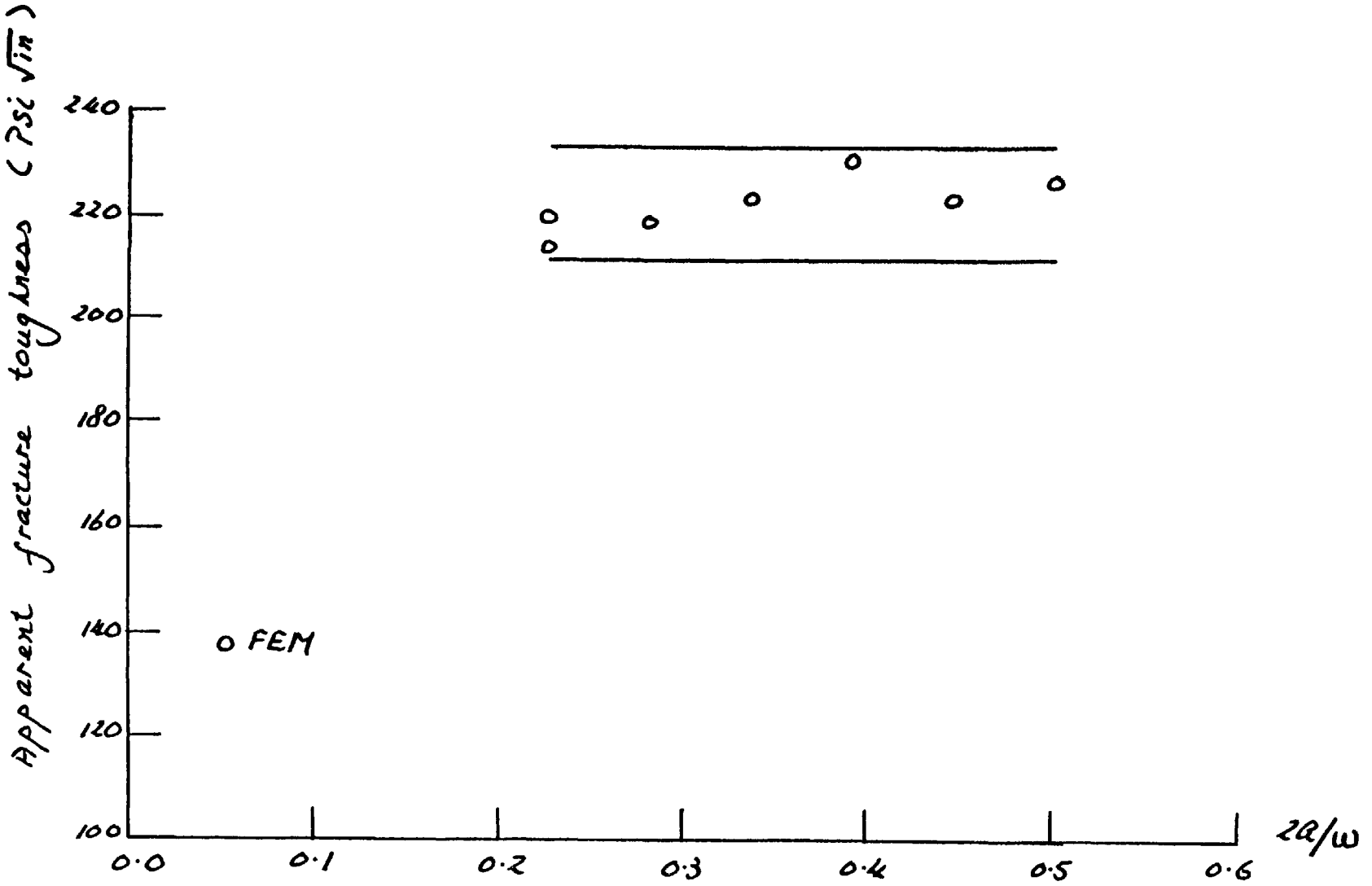

Fig. (2.33) Fracture toughness versus relative crack length — finite element analysis (Saouma et al [59])

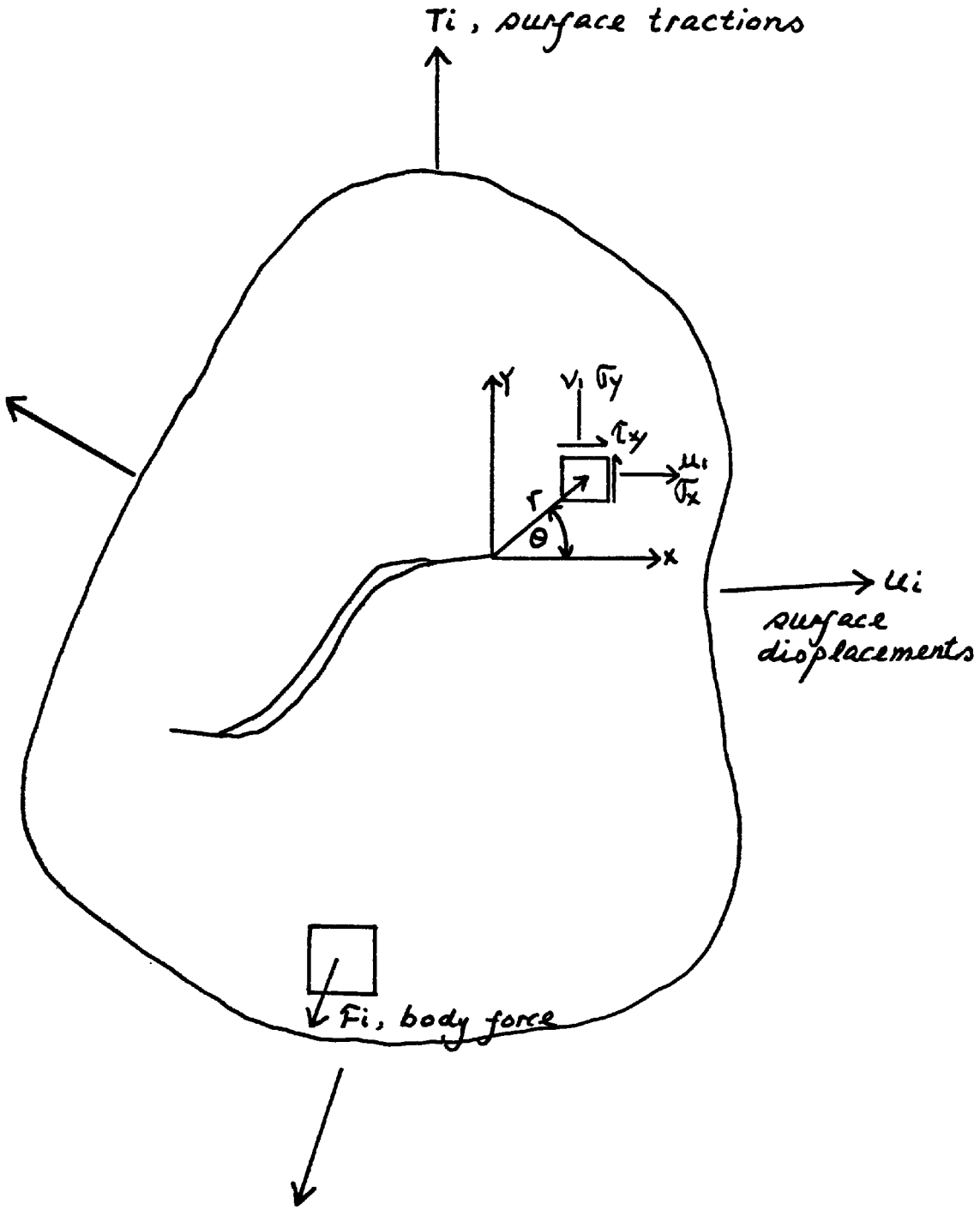

Fig. (2.34) Notched plate subjected to in-plane loading (Kobayashi et al[41])

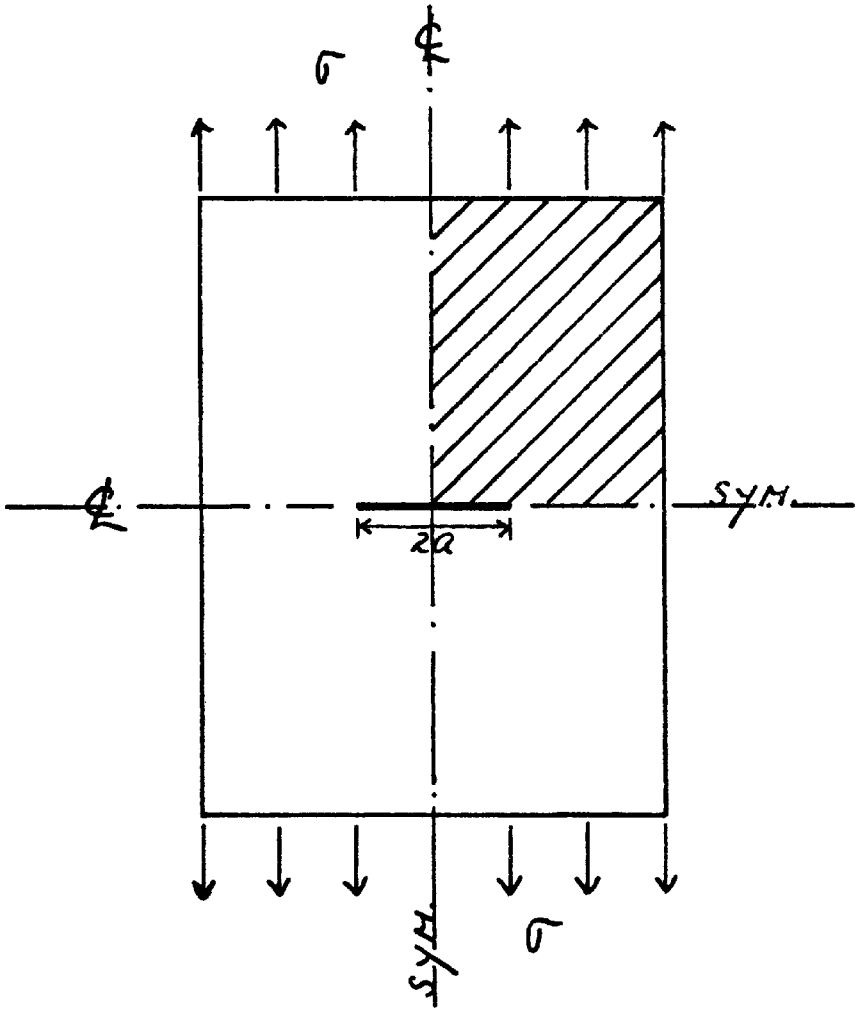

Fig. (2.35) Centrally notched plate subjected to uniaxial tension (Kobayashi et al [41])

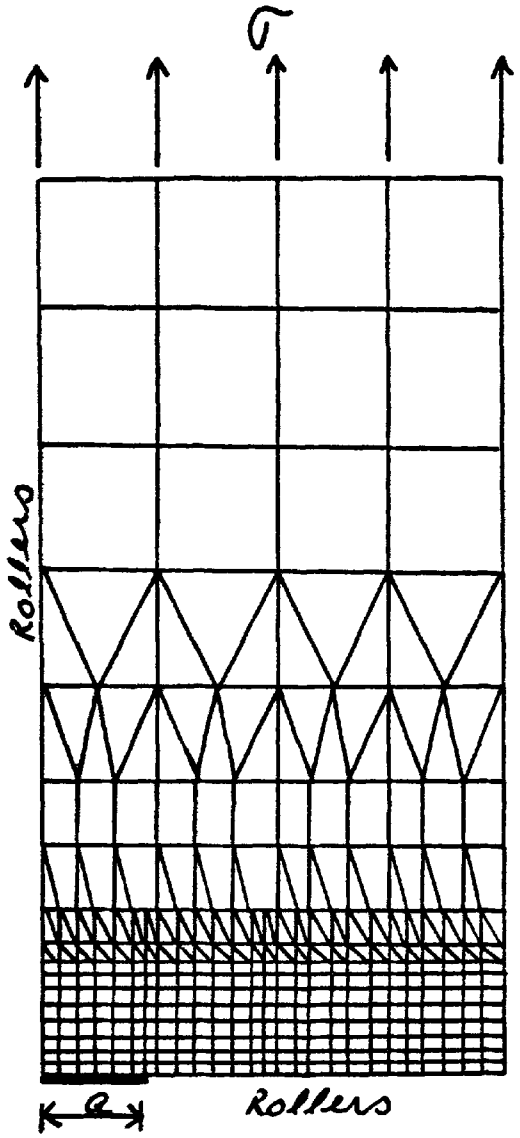

Fig. (2.36) Finite element mesh used by Kobayashi et al (41)

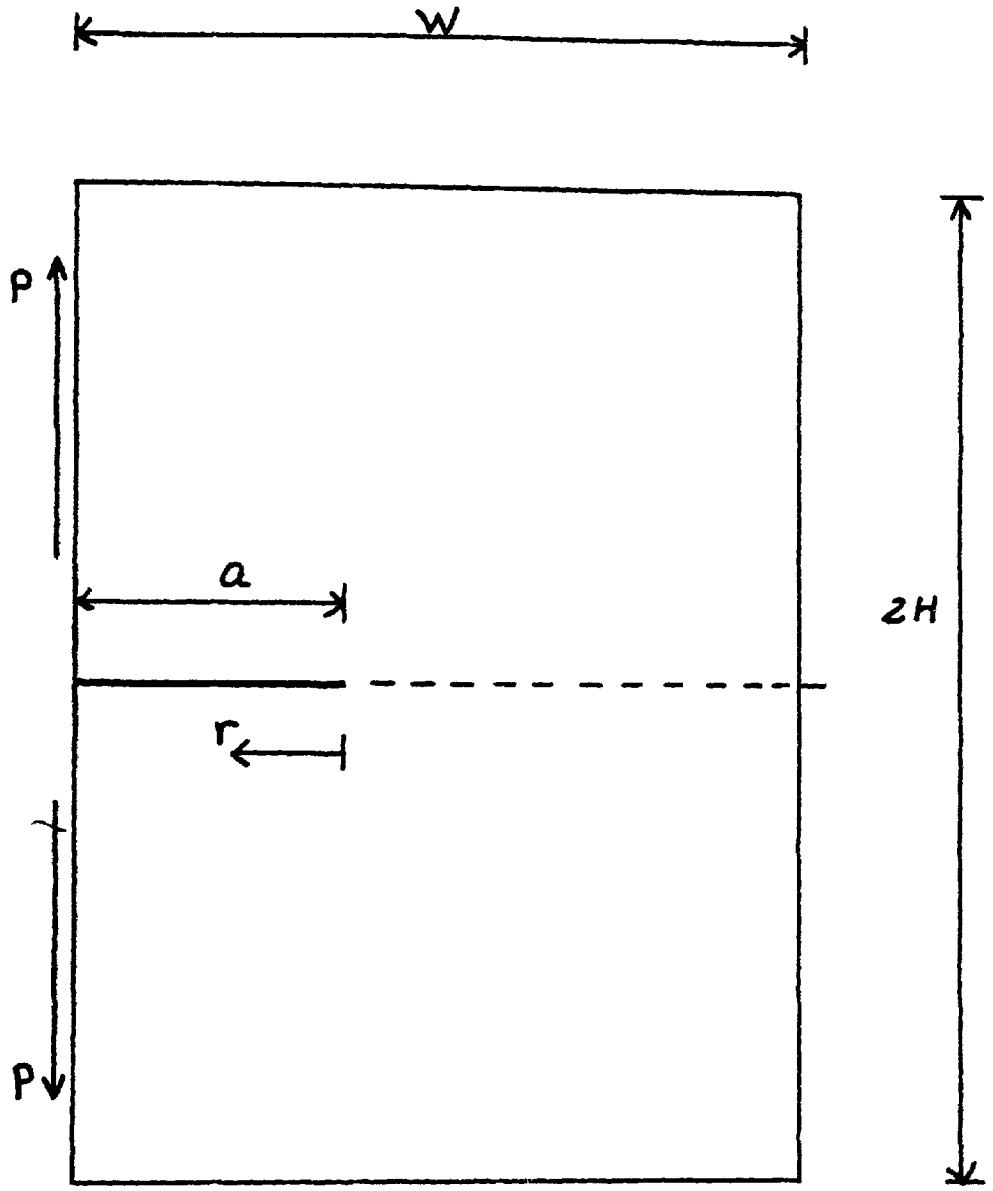

Fig. (2.37) Configuration for the study of mesh size effects and for comparisons with results by the collocation method (Chan et al [42])

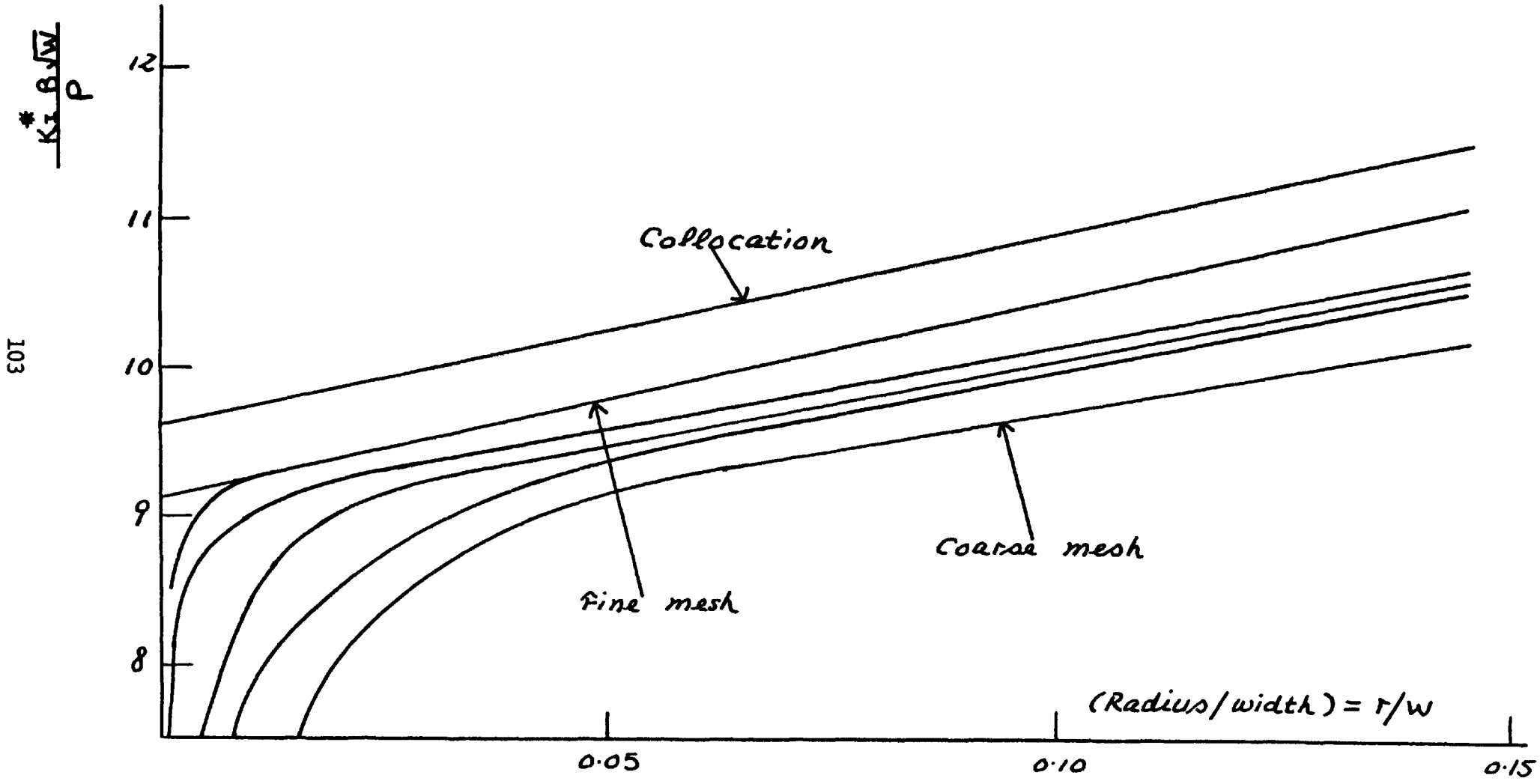

Fig. (2.38) Effect of mesh size on K_I^* (Chan et al [42])

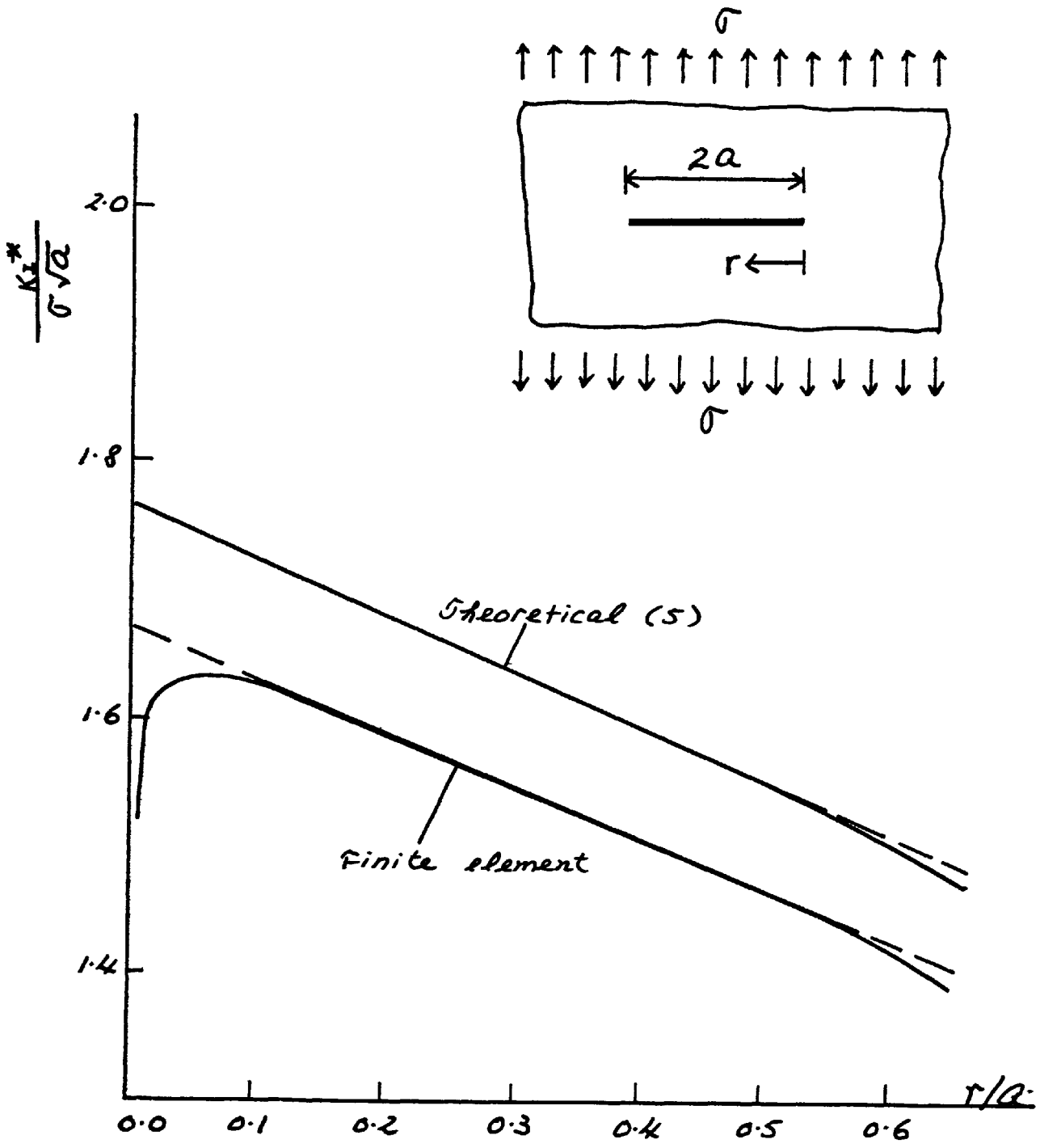

Fig. (2.39) Variation of K_I^* with r/a for finite crack in an infinite medium (Gdar et al [42])

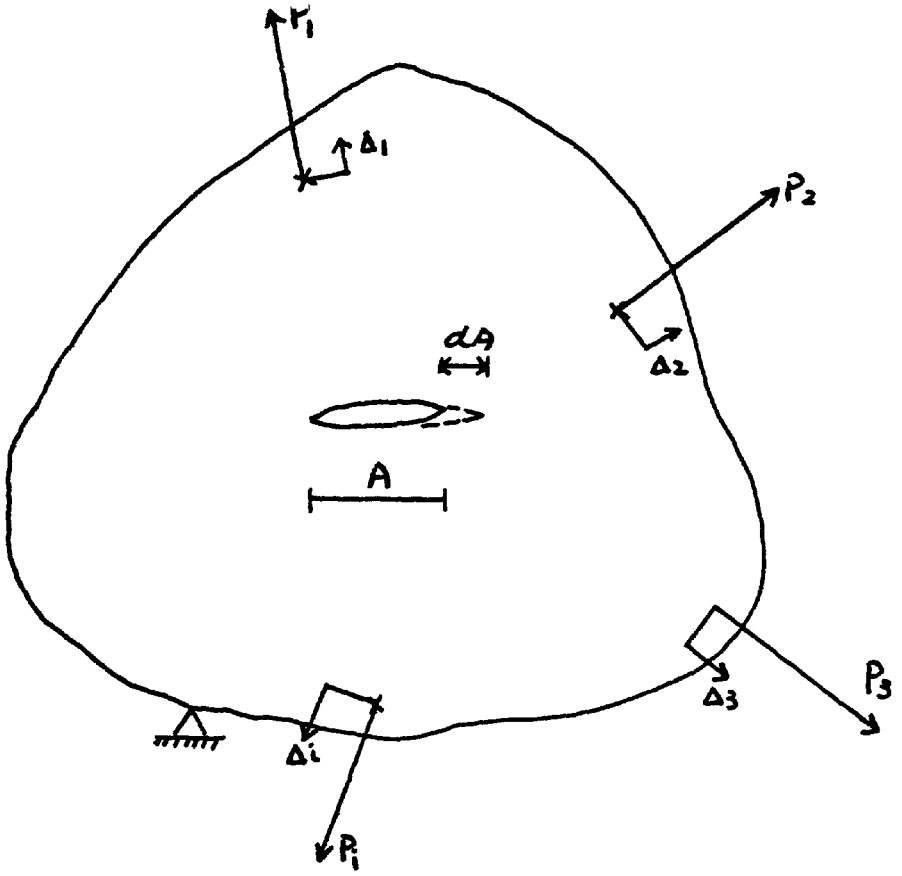

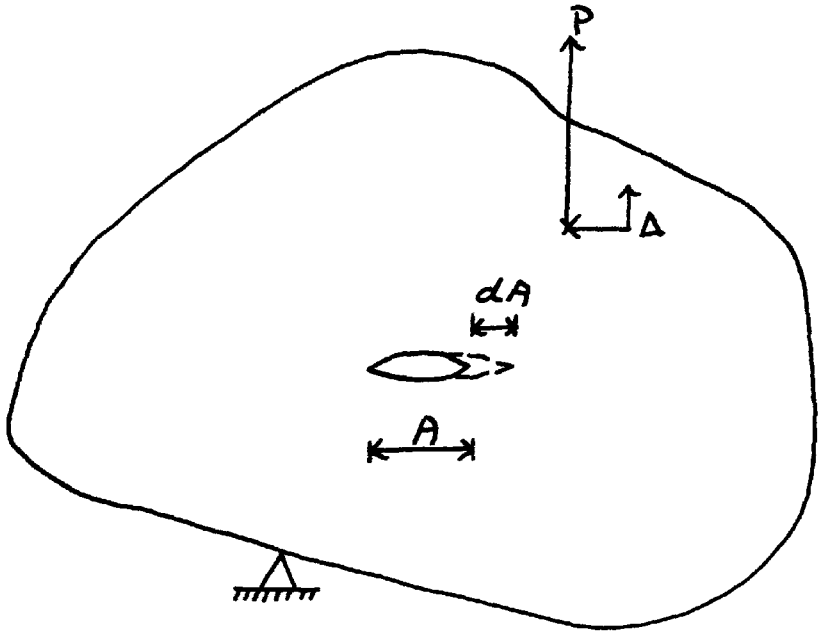

Fig. (2.40) Crack in a body of arbitrary shape (Dixon and Strannigan[44])

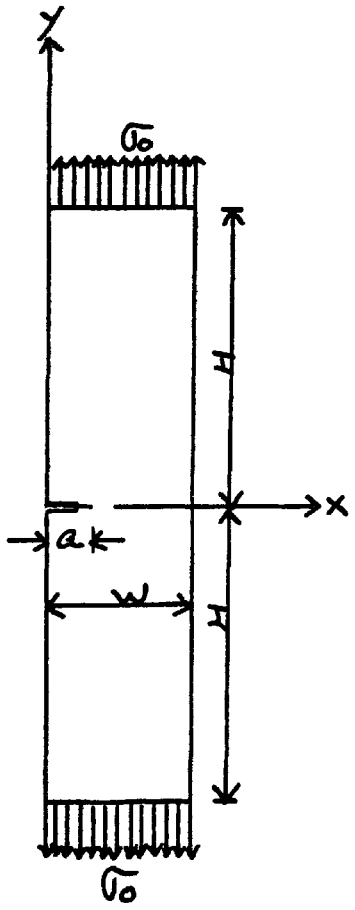

Fig. (2.41) Single edge crack specimen considered in analysis (Nowbray[46])

Table(2.1) Surface energy, Y, term(Moavenzadeh et al(17)).

Materials	Curing Days	Y = U/2A	Y = Gc/2	Y= $Kc^2 \pi /2E$
Cement Paste	3	0.0199	0.0101	0.0133
	7	0.0224	0.0116	0.0153
	14	0.0266	0.0143	0.0188
	28	0.0241	0.0134	0.0176
Mortar	3	0.0240	0.0110	0.0145
	7	0.0270	0.0122	0.0160
Concrete	7	0.0183	0.0239	0.0314
	14	0.0182	0.0257	0.0337
	28	0.0200	0.0273	0.0357

*· w/c = 0.5

Table(2.2) Comparison the fracture energies (2Y) of GRC obtained by the three point bending test and Izod-type impact test (Ohigashi(36)).

Average of 2Y					
(3-point bending) KJ/M	10.5	9.4	9.1	10.0	10.0
Average of 2Y (Impact test) KJ/M	14.9	13.3	13.1	9.8	----

Table(2.3) Comparison of calculated and ASTM recommended K calibration for SEC specimen (Nowbray(46)).

a/W	$K_cW/Pa^{1/2}$		Difference in Percentage
	ASTM(8)	Finite Element	
0.15	2.25	2.33	3.5
0.20	2.44	2.44	0.0
0.25	2.67	2.64	1.1
0.30	2.95	2.92	1.0
0.35	3.30	3.29	0.3
0.40	3.74	3.75	0.3
0.45	4.30	4.29	0.2
0.50	5.02	4.92	2.0

CHAPTER THREE

GENERAL PROPERTIES OF POLYPROPYLENE FIBRE-REINFORCED CONCRETE

3.1 INTRODUCTION

The addition of fibres into cements, mortars, and concretes has been studied extensively for the past twenty years. As a result of these studies there is now available a wide range of fibre composite materials—the most widely used fibres being asbestos, glass, steel and polymer. In the early days, the main objective of adding fibre to concrete was to try to increase its tensile strength. However, in recent years there has been an increasing recognition that increased ductility, or toughness, is the most important property to study in fibre concrete. A comprehensive review of the theory, manufacture and application of fibre-reinforced composite materials has been given by Hannant(26).

This Chapter describes the continuation of the author's(55) work in the final year undergraduate project. Several tests were carried out to investigate the general properties of polypropylene fibre-reinforced concrete. These tests included compression, flexure , torsion and fracture toughness tests. In addition to the above mentioned tests a limited number of impact tests was also carried out. From these tests we have an overall picture of the mechanical properties of polypropylene fibre-reinforced concrete.

3.2 TEST SPECIMEN GEOMETRIES

During the course of the experimental work, two standard and three non-standard tests were carried out. Compressive strength and flexural strength were determined using the standard procedure as described in BS 1881:Part 4. In addition, slump tests were carried out during the manufacture of the cubes and beams. The three non-standard tests used in the experimental work were the split cube test, torsion test and impact test.

The split-cube test(used to evaluate toughness) is a development of two tests used by Bear and Barr(21) to evaluate the fracture toughness of rocks and mortars. In the first test circumferentially notched round bars were subjected to four point loading and in the second test, similar specimens were subjected to an eccentric longitudinal load. The first loading system has been used by Javan and Dury(22) to determine the fracture toughness of fibre-reinforced concrete. Due to the relatively small dimensions of the test specimens described in reference(21), the tests were limited in their application to rocks and mortars. However, the split- cube test developed by Barr et al(40) may be used for ordinary concrete mixes.

The split-cube test was carried out using modified 100mm concrete cubes loaded as shown in Fig.(3.1). The

cubes were notched by means of a Clipper masonry saw which was fitted with a 14 inches(355.6mm) diameter carborundum blade along two opposite faces as shown in Plate (3.1). The notch depth was kept at 30mm for two main reasons. Smaller notch depths often result in shear failures of the specimens near the point of loading while deeper notches result in small areas of uncut concrete which may introduce problems related to the aggregate size(10mm) used in the mix. The load was applied by means of two 6mm square, 100mm long, steel bars. The point of application of the load was assumed to be at the edge of the steel bar nearest the notch-root since, as deformation took place, the load was concentrated to these edges.

The torsion tests were carried out using modified concrete beams(100 X 100 X 500mm). The beams were modified by the introduction of two peripheral notches as shown in Fig.(3.2). The two outer parts of the beams were fixed in position while a torque was applied to the middle part of the beam. The torque necessary to cause shear failure on the two reduced areas of concrete was evaluated from the maximum loaded taken by the system.

The impact tests were carried out using modified concrete cubes(100mm). The cubes were modified by the introduction of peripheral notches as shown in Fig.(3.3). The notched specimens were then fixed in position at one end of the cube while the hammer was released to strike the

remaining part of the specimens. The maximum energy absorbed by the specimens were taken from the system. This testing system gives an indication of the fracture resistance of the fibre-reinforced concrete under Mode II failure.

3.3 EXPERIMENTAL DETAILS

A standard concrete mix was used throughout the experimental work. The mix details were as follows:

Cement : 10 kg
Sand : 18 kg
Aggregate(3/8") : 28 kg

The water-cement ratio was kept constant at 0.50 but with an allowance made for absorption of moisture by the aggregates(0.35 percent). This water/cement ratio gave reasonable workability for the whole range of fibres added. The constituents were mixed in a 2 cubic foot pan mixer and the specimens compacted on a vibrating table.

The polypropylene fibre used was of 12,000 denier(700 m/kg) in 50mm single size strand. The fibres were added in percentages by weight(of the total wet solids) in multiples of 0.05 up to a maximum of 0.30 percent(0.75 percent by volume). The specimens were cured under water and tested at 28 days. In order to prevent "balling" of the fibres during

mixing, the following mixing procedure was adopted. First the dry constituents were mixed in the pan for one minute, the required water being added during the next two minutes. The fibre was then added by means of a sieve(20mm) to shake the fibres into the mix in a random, but uniform manner. The total load was then mixed for a further minute.

The compression tests and flexural tests were carried out using an Avery testing machine. All the split-cube tests were carried out by means of a 1251 Model Instron machine as shown in Plate (3.2). The tests were carried out at nominal room temperature. The torsion tests were carried out in a rig which locked the two ends of the double-notched beams while a jack was used to apply a torque to the middle section of the beams, as illustrated in Plate (3.3). The impact tests were carried out by means of a modified Charpy impact testing machine. The notched specimens were firmly positioned at one end while the striking hammer was released to break the remaining part of the specimens as illustrated in Plate (3.4).

3.4 THEORIES—STRESS INTENSITY FACTOR FOR SPLIT-CUBE TEST

A finite element solution for the split-cube test was developed by Sabir(52). Plane strain conditions were assumed and several notch depths were analysed giving a range of crack length/specimen (a/d) ratios. In fracture machanics, stress intensity factors are traditionally expressed in terms of polynomial functions of (a/d). The five (a/d) ratios considered in the finite element analysis enabled the results to be expressed in terms of five powers of (a/d). For 100mm cubes, the following expression is obtained,

$$K_I = \frac{P}{Bd^{1/2}}\left[18.3(a/d)^{1/2} - 430(a/d)^{3/2} + 3445(a/d)^{5/2} - 11076(a/d)^{7/2} + 12967(a/d)^{9/2}\right] \qquad (3.1)$$

where K_I = stress intensity factor

P = load

B = width (100mm)

d = depth (100mm)

a = depth of slot (30mm)

This expression for K_I reduces to the simple form of

$$K_I = P.Y \qquad (3.2)$$

where Y is a function of notch depth ratio and is constant for constant notch depths. In practice, there were small variations in the notch depths introduced into the cubes and these variations have been taken into account in evaluating the results.

Compressive strength and flexural strength were calculated from the British Standard procedure as described in BS 1881:Part 4. Torsion strength and impact strength were obtained from the corresponding testing systems.

3.5 DISCUSSION OF TEST RESULTS

The slump tests were carried out to measure the workability of the polypropylene fibre-reinforced concrete. Considerable reduction in slump values is clearly seen from these results as shown in Fig.(3.4). These slump results can be classified into three distinct regions of workability: medium; low and very low. These results give information for the use and application of polypropylene fibre-reinforced concrete.

The detailed results for the compressive strength of polypropylene fibre-reinforced concrete is shown in Table (3.1). The compressive strength results are summarised in Table (3.2). Addition of polypropylene fibre does not greatly influence the compressive strength, as shown in Fig.(3.5). However, there is a small drop off in the

compressive strength as the fibre content is increased. This is probably due to the low modulus of fibres which cannot resist compressive forces in the concrete.

There is a small increase in flexural strength as the fibre content is increased. The raw data for the flexural strength results are shown in Table (3.3) and are summarised in Table (3.4). A small addition of polypropylene fibre(0.05 percent) does not affect its flexural strength as shown in Fig.(3.6). The maximum flexural strength obtained from the fibre-reinforced concrete is approximately 7 percent higher than the plain concrete.

The torsional strength result for varying polypropylene fibre content is shown in Table (3.5) and summarised in Table (3.6). A well defined peak value of 0.53 KN-M for the torsional strength was shown to occur at 0.15 percent fibre content, as illustrated in Fig.(3.7). The coefficient of variation for the torsional strength is much greater than the other results obtained. This is probably due to the difficulty in ensuring that no stresses were locked into the test specimens before applying the torque. Furthermore, a comparatively smaller number of tests was carried out in this case.

From the limited number of the tests carried out, it appears that a small addition of polypropylene fibre does

not greatly influence the impact strength. The results are shown in Table (3.7) and Table (3.8). The fibre content of 0.20 percent gives the maximum impact strength as shown in Fig.(3.8). A small number of specimens was carried out in these tests due to the difficulty in ensuring the swinging hammer was not obstructed by the ribs of the supporting A-frame during the fracturing process. Although the tests were not fully investigated, the test results would give some indication of the impact strength of polypropylene fibre-reinforced concrete.

The addition of polypropylene fibres in the small amounts investigated has little effect on the fracture toughness. The detailed results are shown in Table (3.9) and are summarised in Table (3.10). The stress intensity factors were determined using three different equations which included equations (3.1) and (2.40) and the equation derived in Chapter 6 so that a comparison could be made among them. It is seen that the results are similar in all cases as shown in Fig.(3.9) except that the numerical values obtained from equation(3.1) were comparatively lower than the others. This phenomenon will be discussed in Chapter 6 . The fracture toughness is measured from the load at crack initiation and this takes no account of the

post-cracking behaviour. The stress intensity factor, K_I, increases as the fibre content increases up to the optimum value and then decreases as shown in Fig.(3.9).

Typical load-deflection graphs obtained from the Instron System for varying fibre content are illustrated in Fig.(3.10). The curves show a linear response up to the point where the concrete fails and then the load reduces to a constant value. The fracture toughness is calculated from the peak load achieved. The residual load increases with fibre content and is an indication of the residual strength which is provided by the fibres. It has been suggested by a number of research workers, e.g. Henager(48), that the post-cracking behaviour of fibre concrete is best described by a residual strength index. A residual strength index gives a better indication of toughness than the load at initial cracking.

The optimum values of compressive, flexural, torsional, impact and toughness strengths are summarised as shown in Table (3.11). It is seen that the addition of polypropylene fibre has little effect on compressive and flexural strengths. Other researchers(26) found that the compressive and flexural strengths of polypropylene fibre reinforced concrete were increased less than 25 percent and often the strengths of the composite materials were less than that of the matrix alone. The explanation for this

occurrence is probably due to the low modulus of elasticity of the polypropylene fibre in the matrix. Torsional, impact and toughness strengths are comparatively higher than the compressive and flexural strengths. This is partly due to the large amount of energy absorbed in debonding, stretching and pulling out the fibres which occur after the matrix has cracked.

The maximum strengths obtained in this study are within the range 0.15 percent to 0.20 percent of polypropylene fibre content as shown in Table (3.11). The strengths above the 0.20 percent limit were reduced due to the increased difficulty in obtaining good compaction with increasing fibre content. Furthermore, a good quality mix was used with compressive strength of approximately 50 MN/M^2 and hence the strength of the plain concrete itself was reasonably high. From the impact strength results shown in Table (3.8), the impact strength of 0.30 percent polypropylene fibre-reinforced concrete is 55.96 Joules. The rapid drop off of the impact strength beyond 0.25 percent fibre content is very interesting but has not been pursued in this study. However, since impact resistance is greatly improved by the addition of fibres , a number of other research workers(26) have investigated the impact strength of various types of fibre-reinforced concrete. Further investigation of this test has not been carried out in this study. However, in order to improve the efficiency of the impact testing system, modified concrete beams

should be used instead of the concrete cubes. This would result in easier alignment of the impacting face with the concrete specimen being tested.

Many research workers(26,47,48) have used the flexural three-point or four-point loading methods to investigate the general properties of fibre-reinforced concrete. The mix details and the types of polypropylene fibres used(length,denier) are not comparable with the results in this study. So, it is very difficult to compare the results in detail with others. However, the typical load-deflection curves can readily be compared as shown in Fig.(3.10) and Fig.(3.11). It can be seen that the load-deflection curves obtained by other research workers (26,47,48) show a linear response up to the point where the concrete fails and then the load reduces to a constant value(residual strength). The residual strength obtained by Swamy et al(47) increases with the addition of polypropylene fibre content. This phenomenon is in good agreement with the results obtained in this study, Fig.(3.10). In general, the patterns of the load-deflection curves are similar to that obtained by others(26,47,48). The disagreement in magnitude among them is probably due to the types of polypropylene fibres(length,denier) and the loading systems(flexural) used.

Brown(19) modified a double-cantilever beam of variable web width, Fig.(2.14) to determine the fracture toughness of cement pastes and mortars. It is seen that the preparation of the modified double-cantilever beam is not easily done since the required web is variable along the beam. The split-cube tests were carried out using modified 100mm cube specimens. The specimens can be prepared readily using standard moulds and then the notches can be inserted comparatively easier than in the double-cantilever beam (with sufficient accuracy with a Clipper). Provided that standard notch depths are introduced into the cubes, the fracture toughness can be determined from the peak load achieved. The coefficient of variation for the split-cube test results was only marginally greater than that obtained for the compressive test results. The split-cube test has been shown to be a simple test for toughness. The test results may be used either to determine the fracture toughness or to give an indication of toughness from the residual strength of the cracked specimen.

The fracture toughness tests, which have been conducted on concrete, usually use oblong beams(15,19), but the experiments described in this study indicate that the split-cube specimens are more convenient. The test is economic of the material and is suitable for testing in situ concrete (39). There are several practical advantages to the split-cube tests, compared with the flexural tests

and double-cantilever beam tests. The loading of the cube is easy, as there are no problems of parallel loading of flat faces; the specimens can be easily prepared and the experimental method is simple. Thus the fracture toughness can be determined without difficulties using the split-cube specimen.

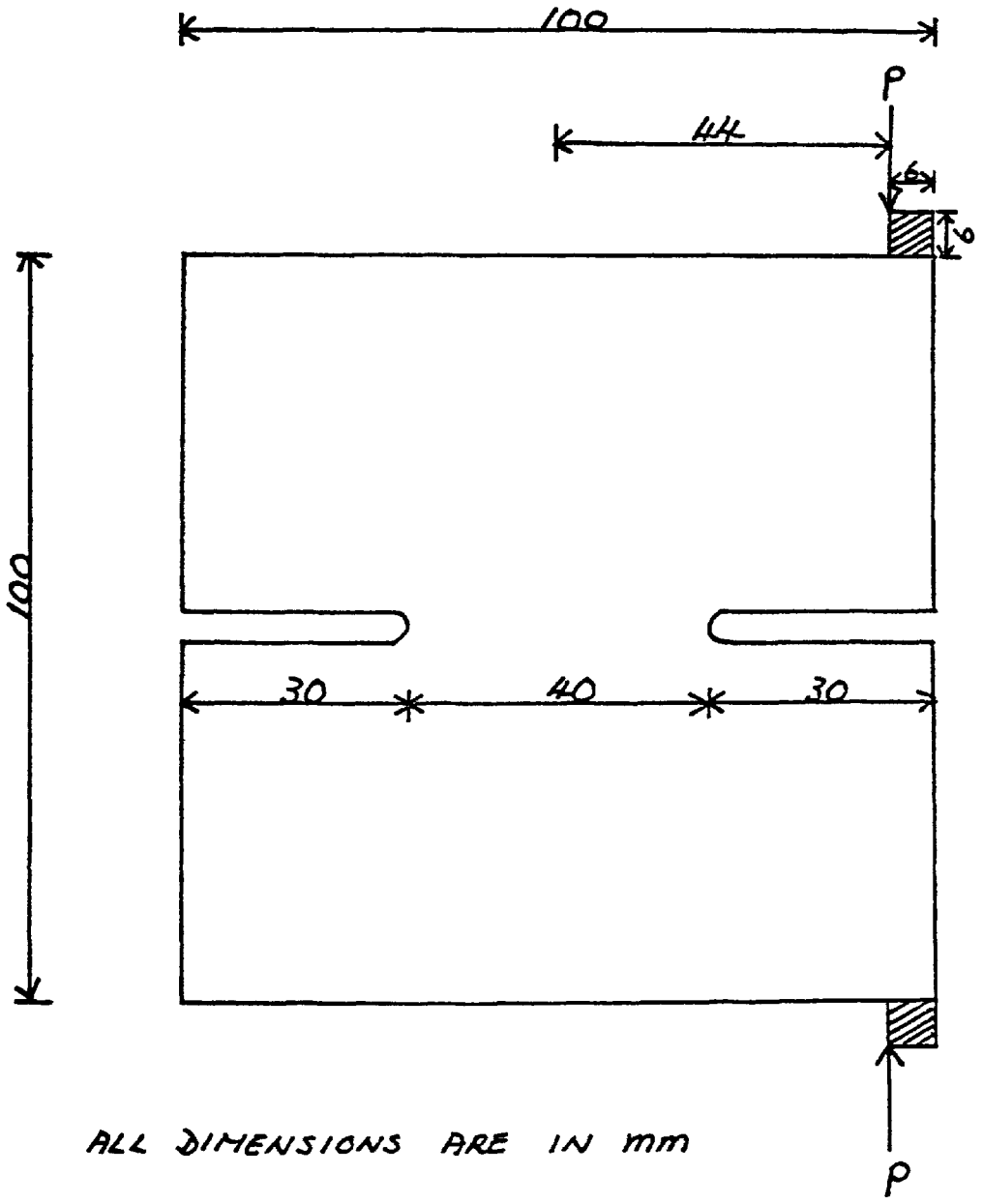

Fig. (3.1) Split cube specimen under eccentric loading

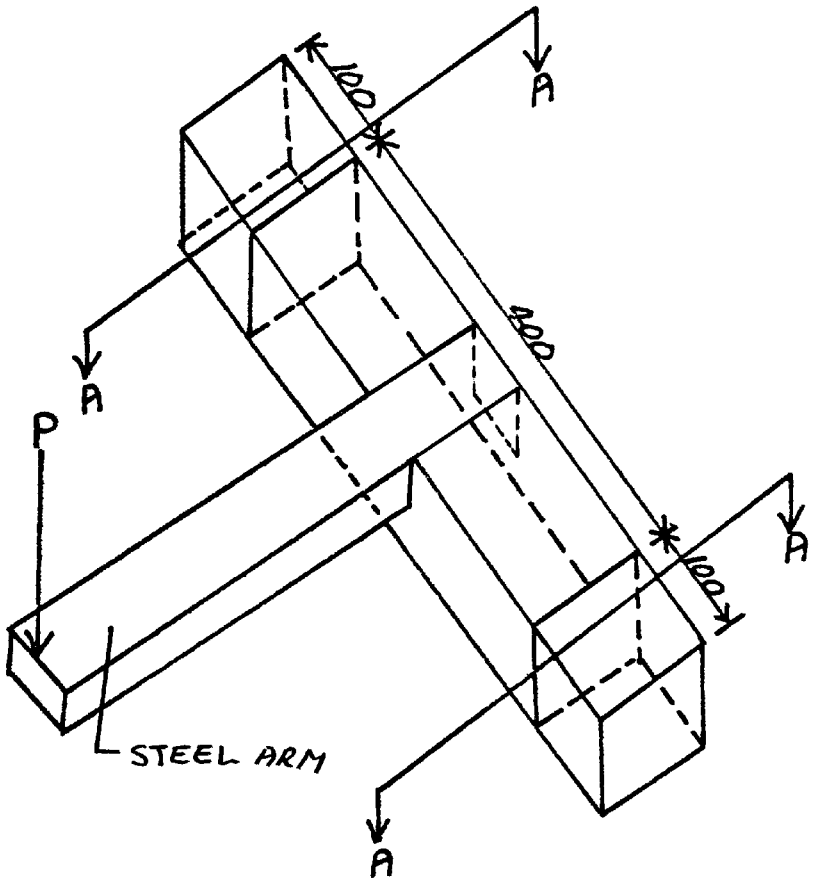

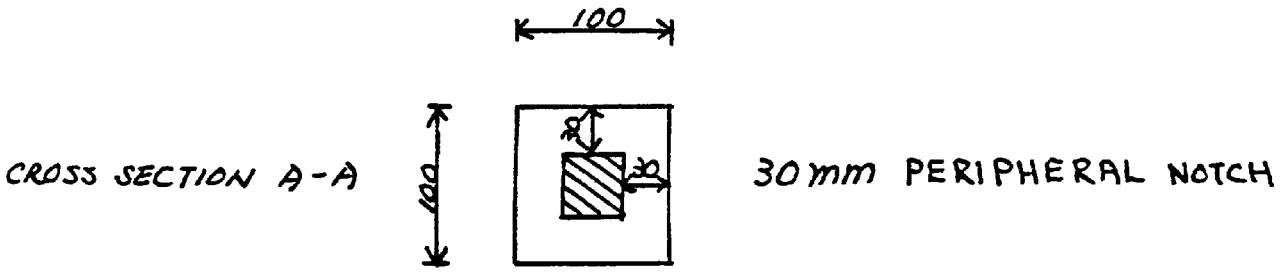

ALL DIMENSIONS ARE IN mm

Fig. (3.2) Torsion specimen

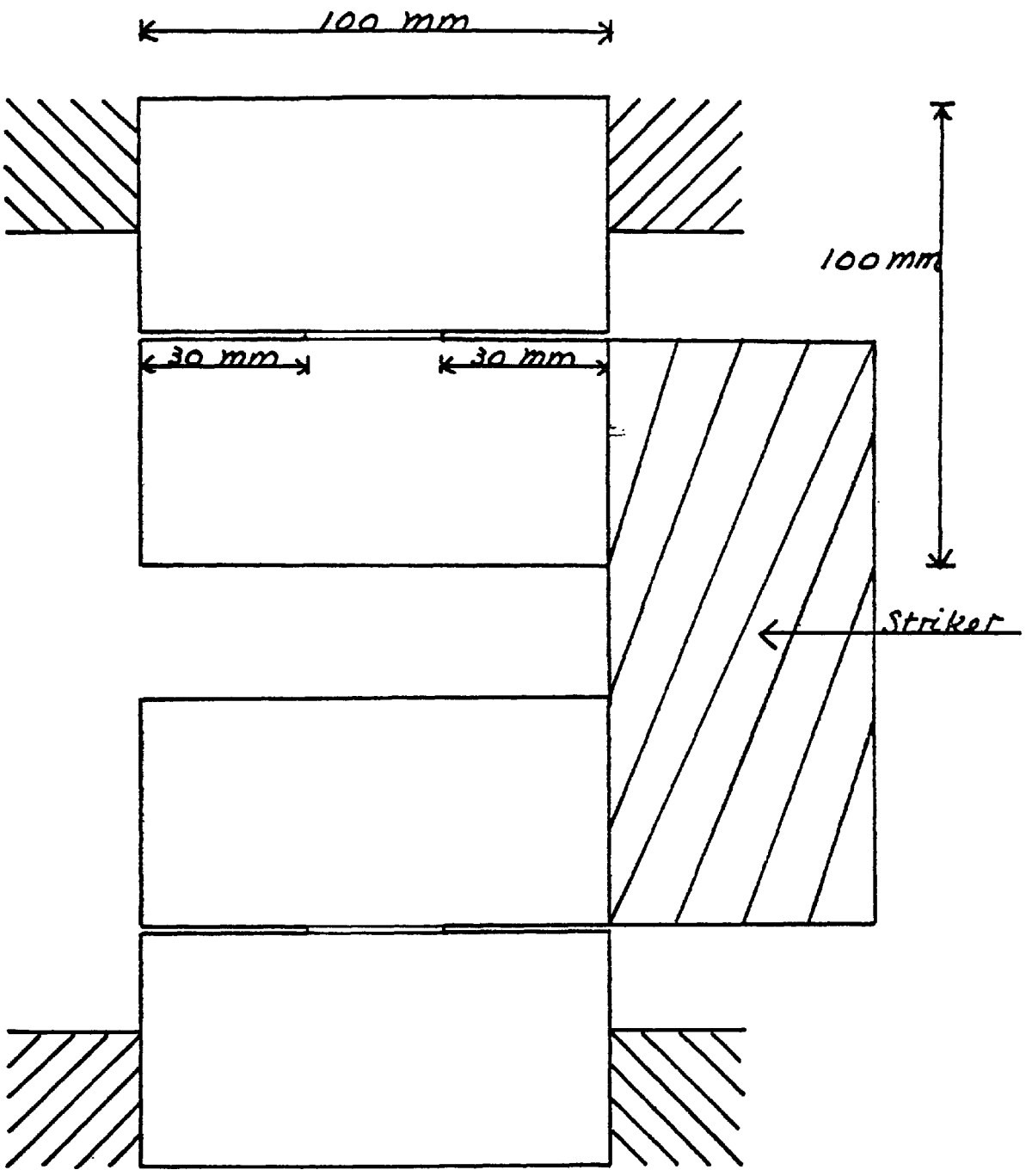

Fig. (3.3) Impact specimen

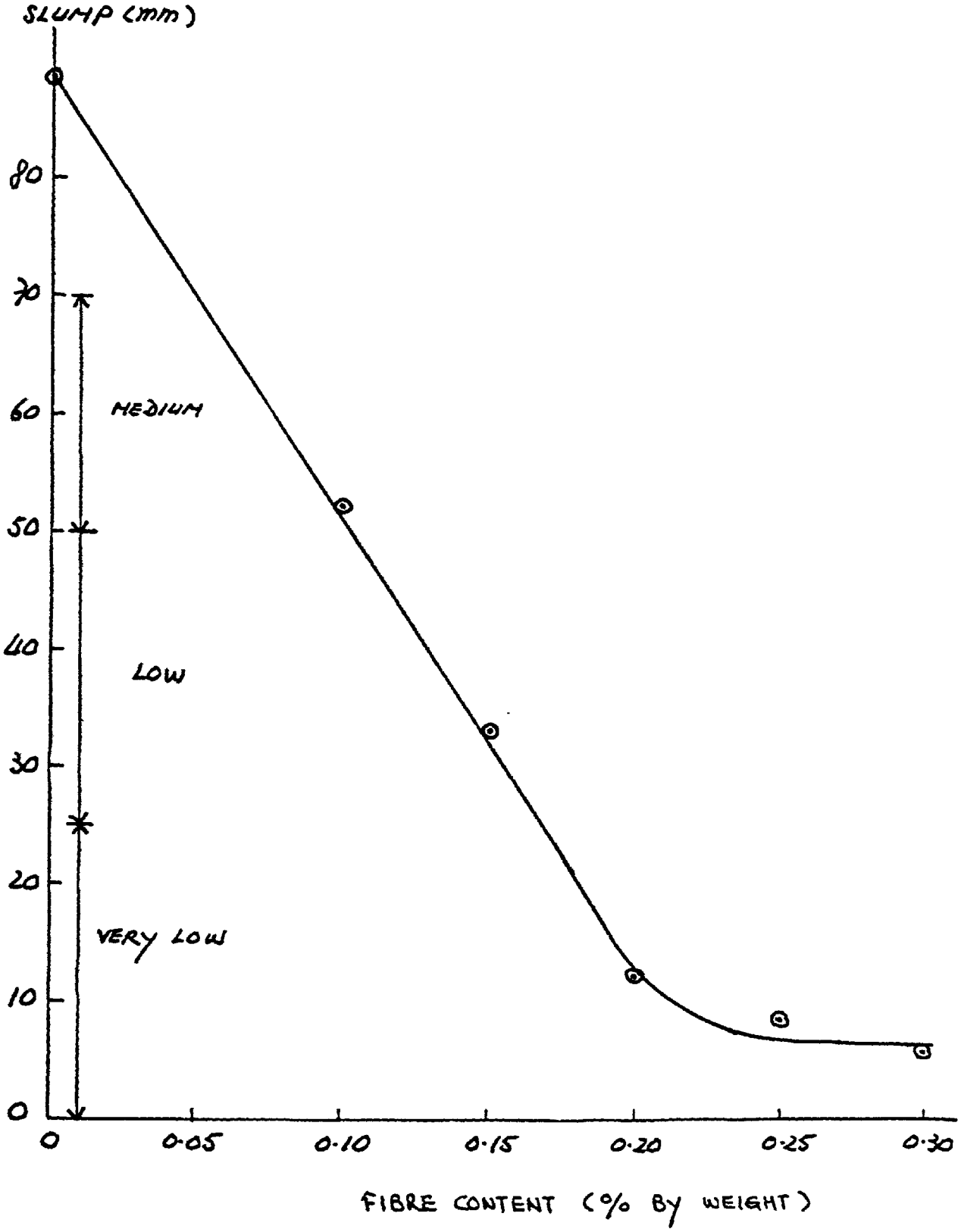

Fig. (3.4) Slump results for varying fibre content

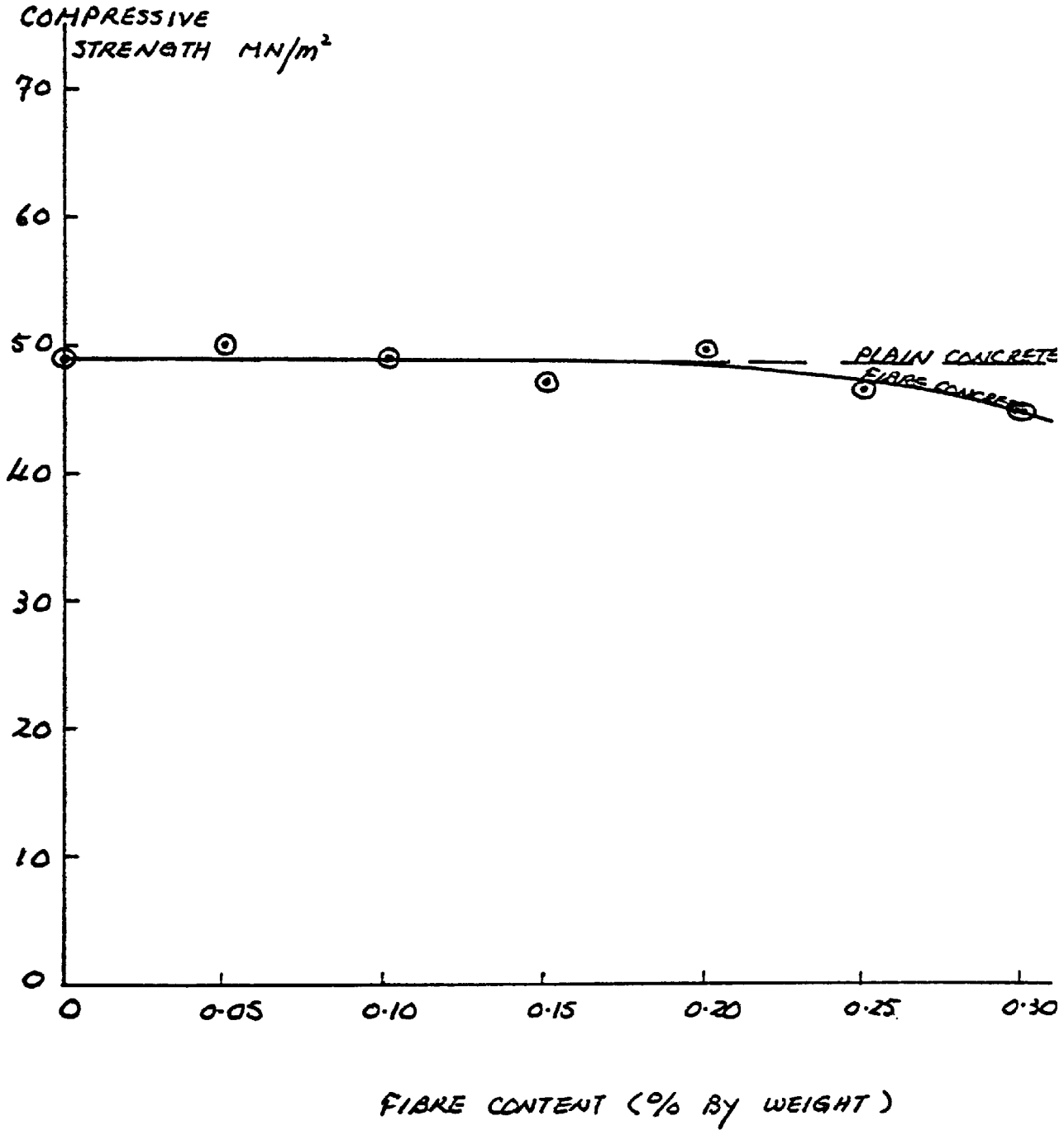

Fig. (3.5) Compressive strength results for varying fibre content

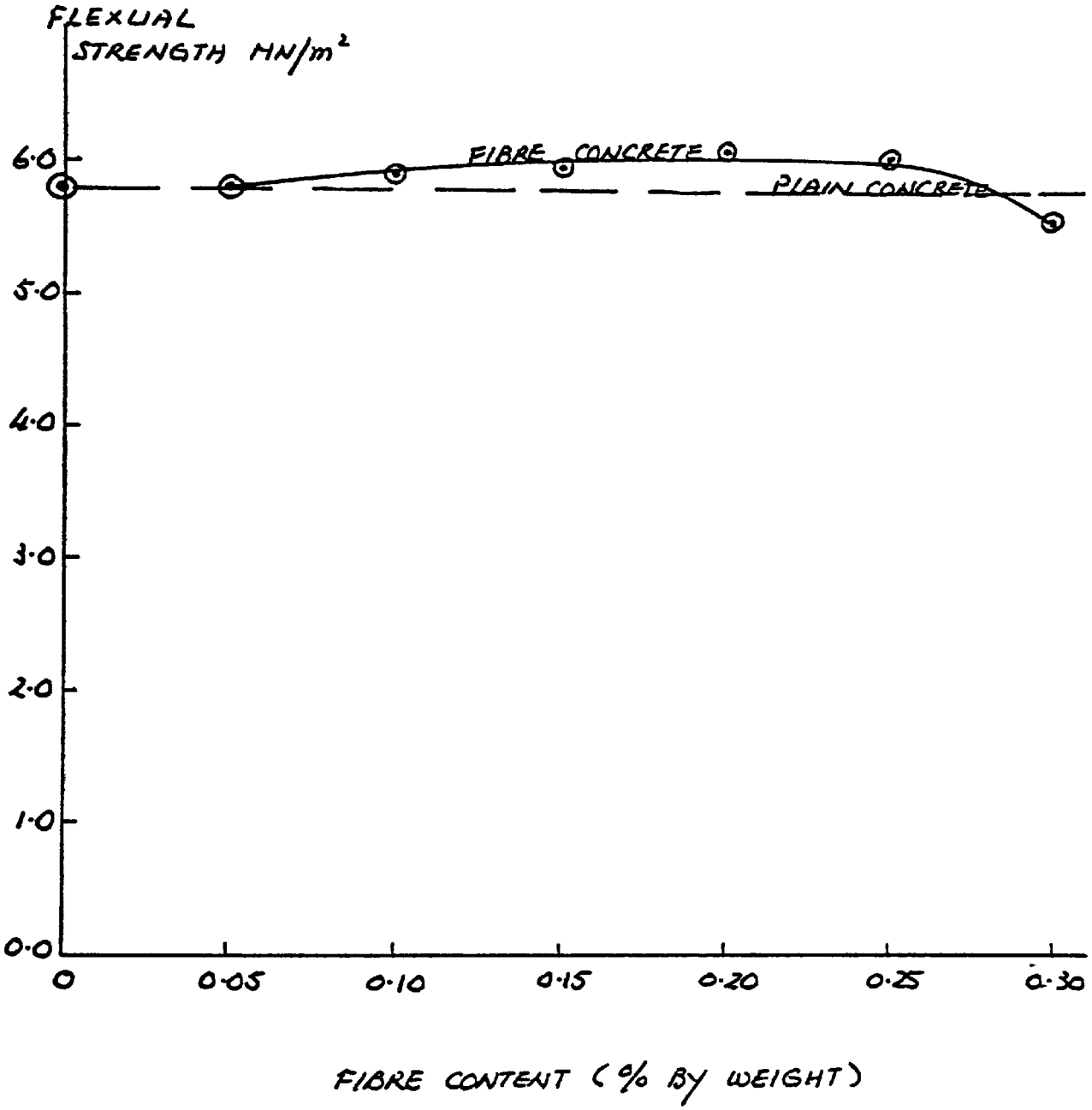

Fig. (3.6) Flexural strength results for varying fibre content

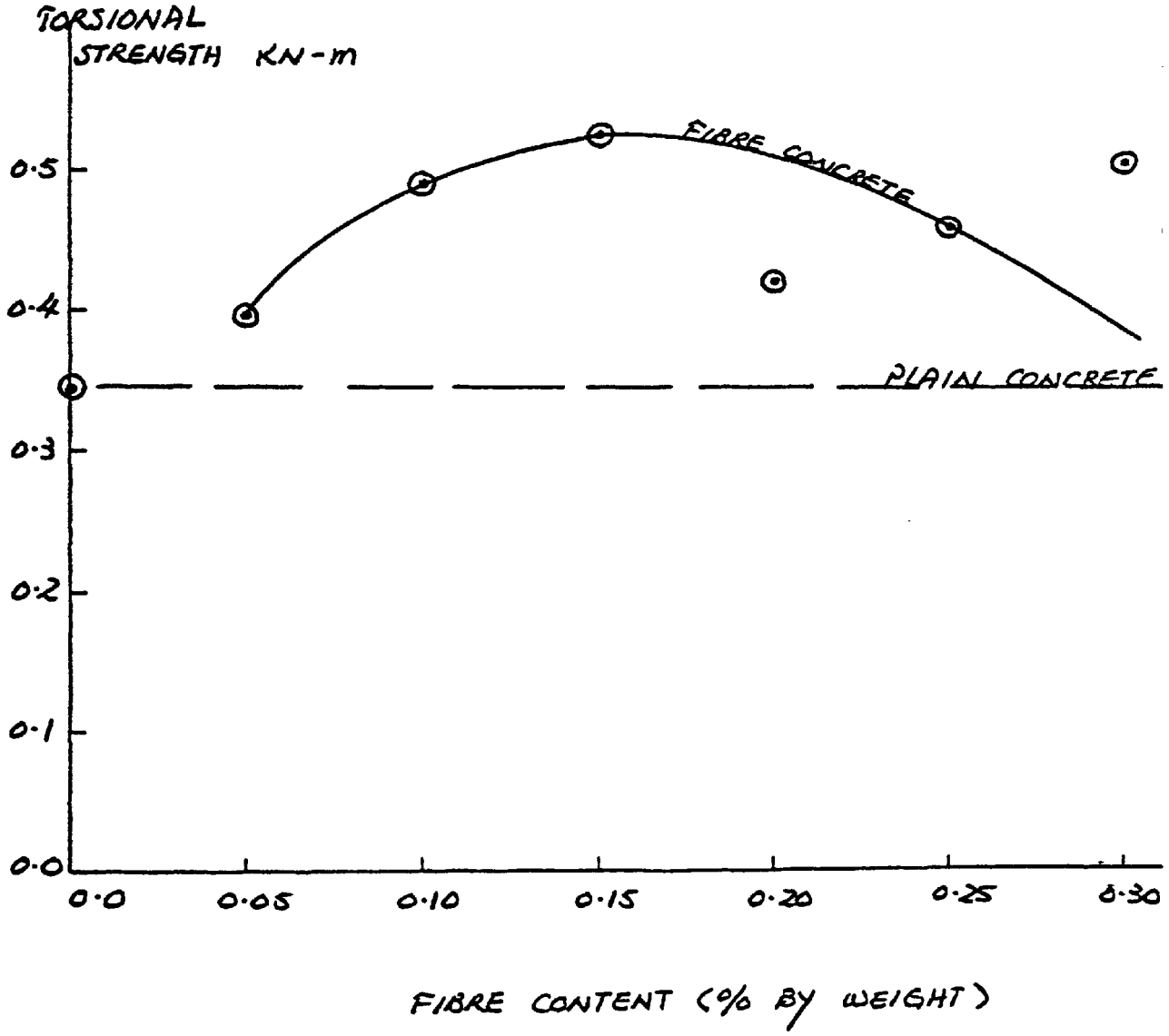

Fig. (3.7) Torsional strength result for varying fibre content

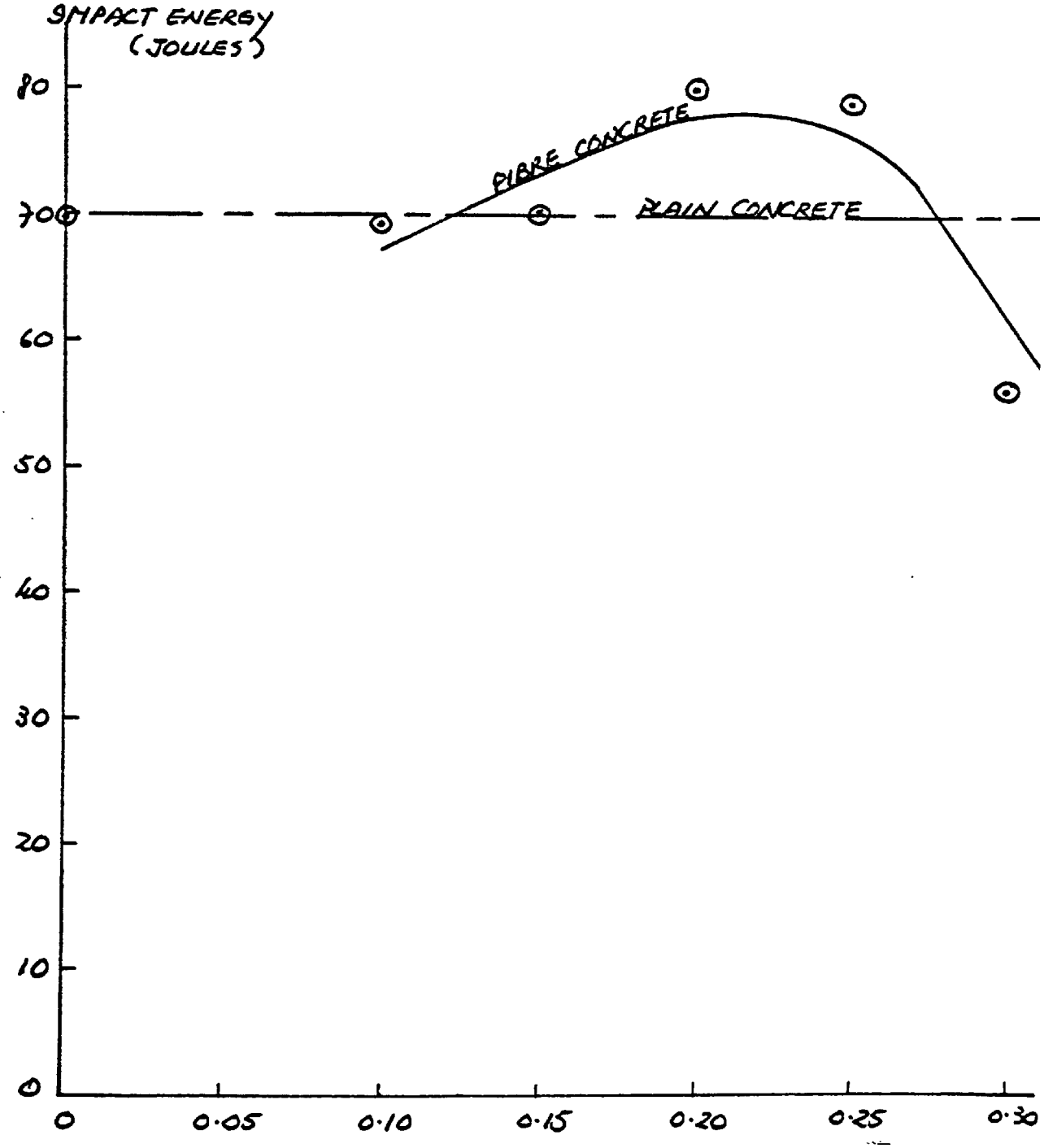

Fig. (3.8) Impact energy results for varying fibre content

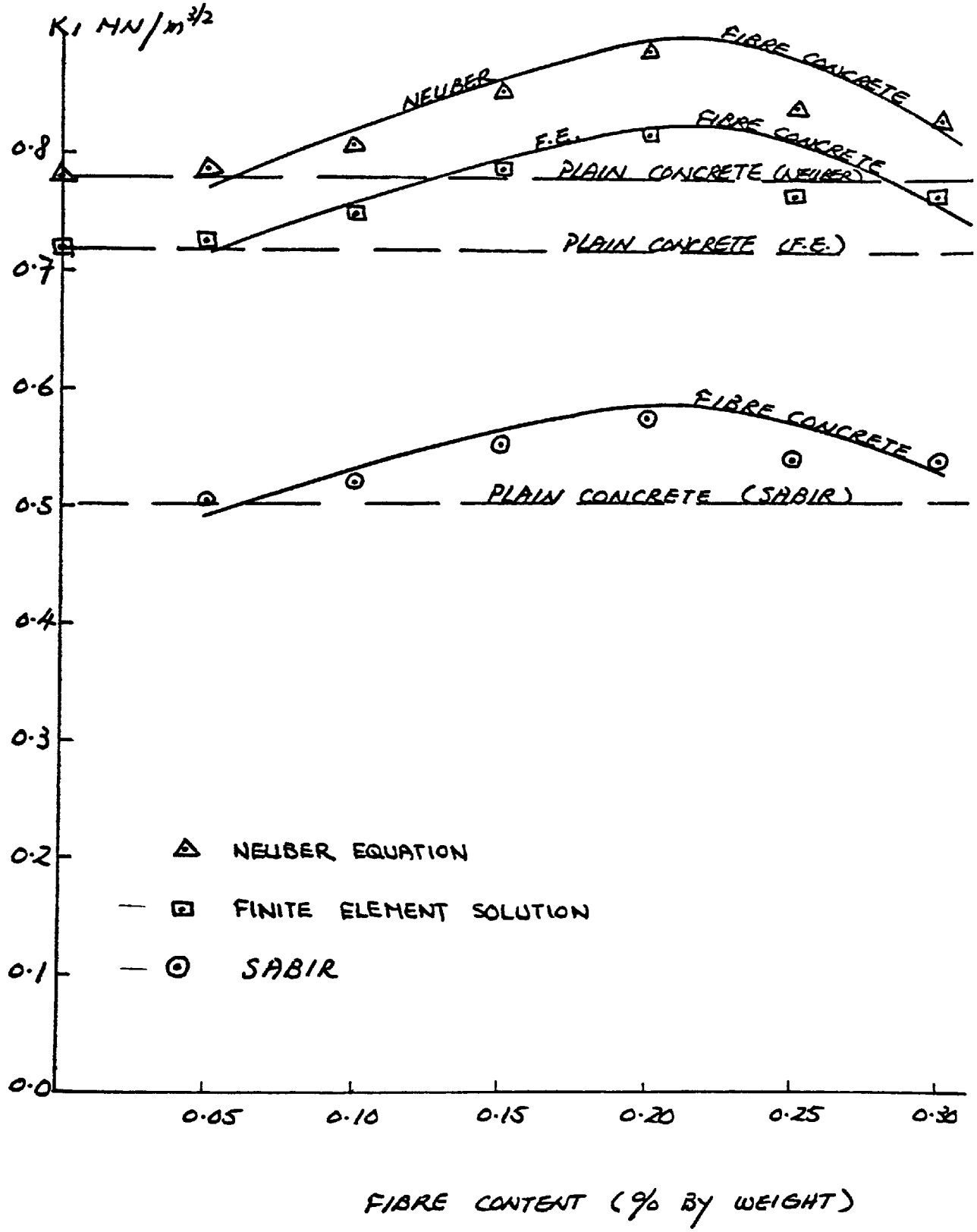

Fig. (3.9) Stress intensity factor results for varying fibre content

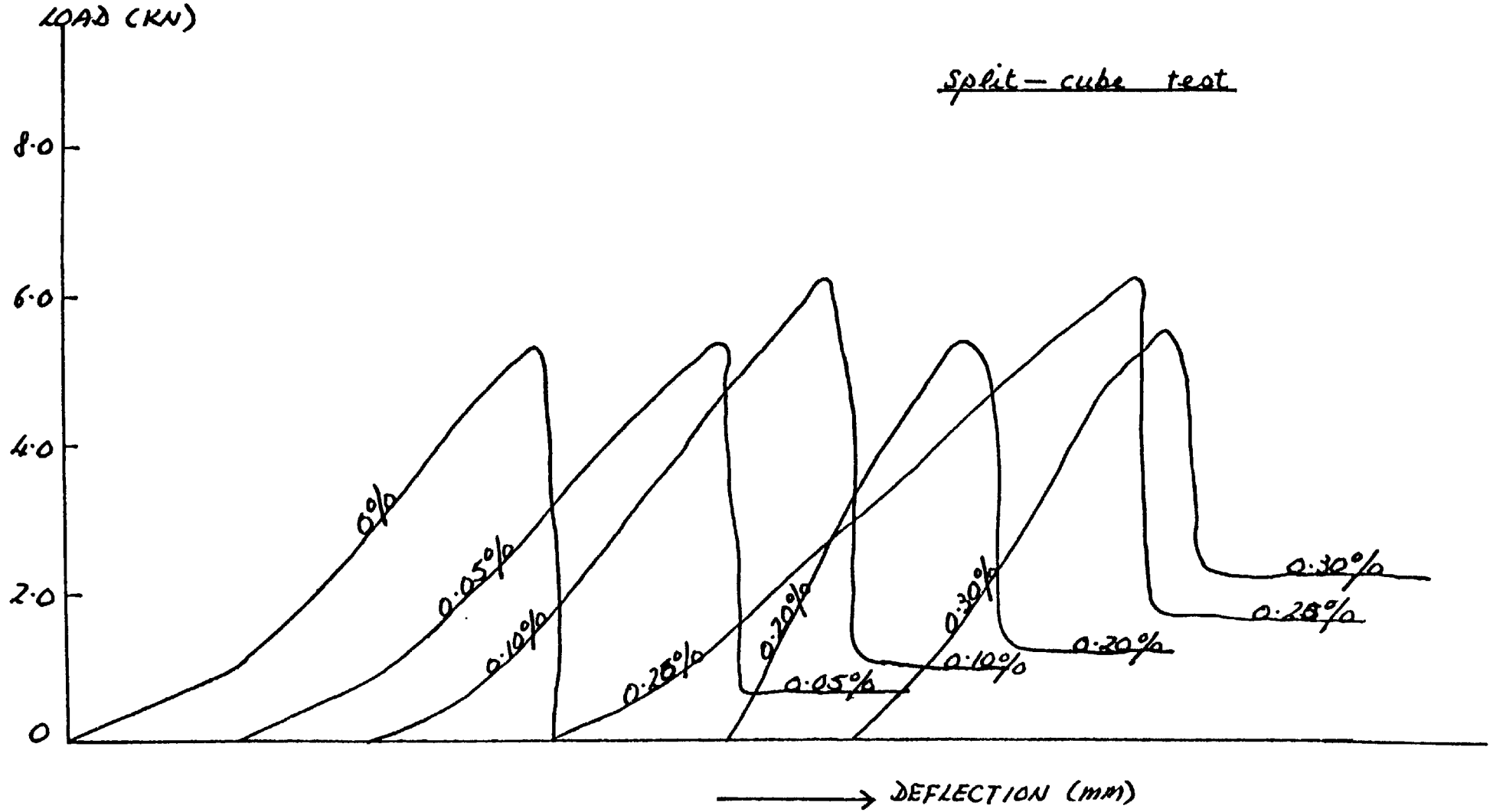

Fig. (3.10) Typical load / deflection graphs for varying fibre content

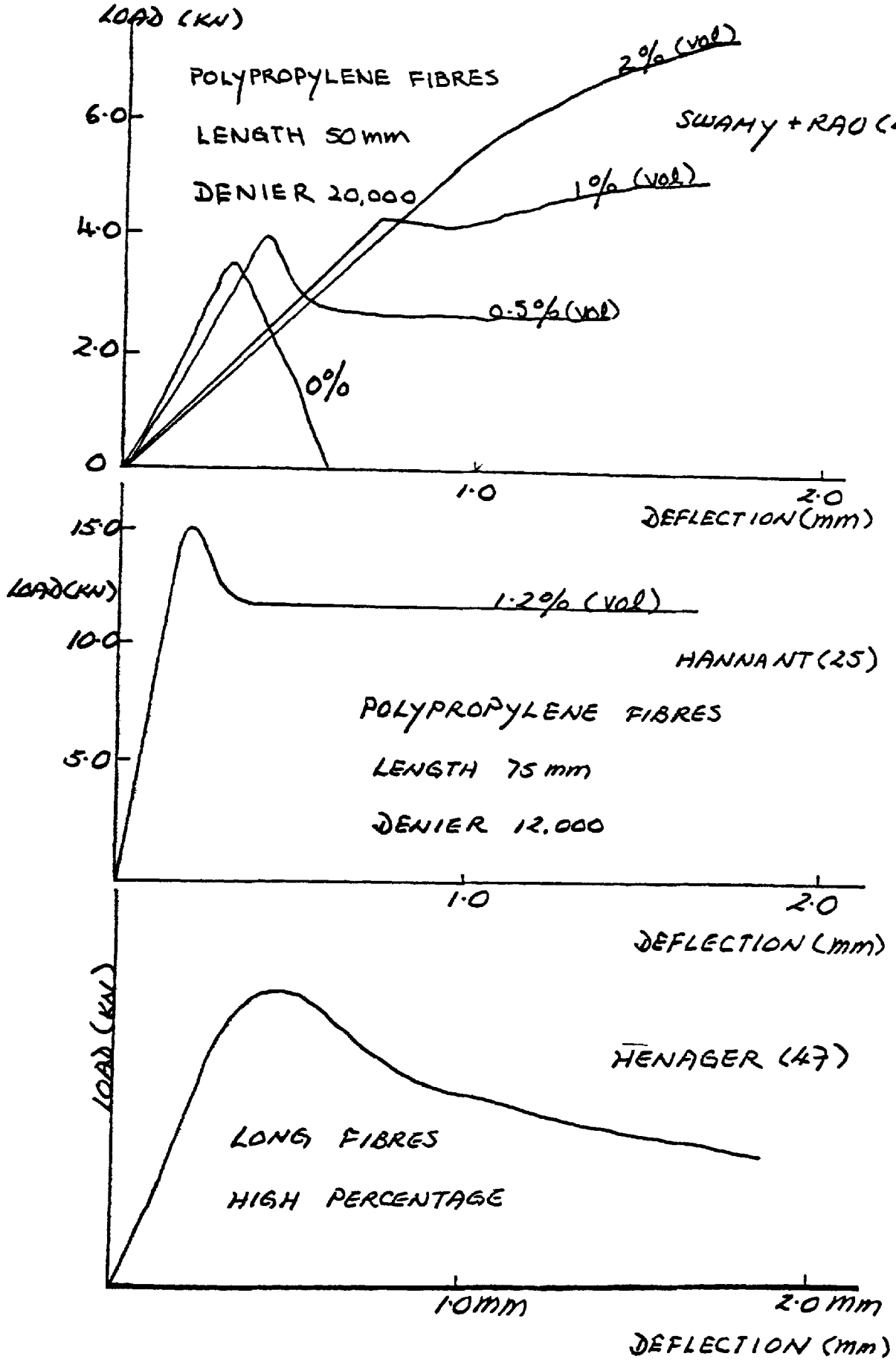

Fig. (3.11) Load / deflection graphs obtained by previous researchers (flexural tests)

Table(3.1) Compressive strength results for varying fibre content.

Fibre Content By Weight (%)	Compressive Strength MN/M^2		
0.0	49.25	44.70	51.25
	48.00	42.00	52.75
	47.50	53.00	50.03
	48.75	53.00	49.50
	42.75	52.50	48.38
	44.60	52.50	52.75
	49.75	50.40	47.00
	51.00	43.50	53.50
	49.75	44.50	44.50
0.05	52.00	52.73	49.25
	52.00	53.50	50.40
	53.00	55.00	43.25
	45.50	54.80	42.20
	45.00	51.73	52.50
	43.00	55.00	52.25
	45.00	53.10	48.25
0.10	44.75	49.20	50.50
	45.70	50.00	50.50
	46.00	50.88	49.00
	43.25	52.75	50.00
	52.00	49.00	48.13
	52.50	53.80	51.50
	50.50	48.25	46.00
	52.00	51.00	50.75
	49.50	49.75	47.00
	47.00	48.13	49.50
	44.50	50.00	45.00
0.15	48.50	47.75	46.00
	47.00	47.25	44.00
	47.00	38.50	44.75
	37.00	39.25	40.00
	53.70	50.50	50.75
	51.75	51.80	51.00
	51.25	51.00	51.00
	50.40	49.75	

Table(3.1) cont. Compressive strength results for varying fibre content.

Fibre Content By Weight (%)	Compressive Strength MN/M^2		
0.20	44.50	51.25	47.50
	54.75	42.75	54.10
	47.50	55.25	47.75
	50.75	45.00	53.00
	49.50	50.25	45.50
	48.25	47.65	49.75
	48.10	51.00	51.00
	49.75	52.15	49.00
	52.10	47.25	55.00
	54.25	54.70	46.50
	50.00	45.50	
0.25	44.00	45.50	44.25
	45.00	42.00	43.20
	43.50	45.00	47.00
	46.75	50.00	45.75
	48.00	50.50	47.75
	43.50	45.60	50.00
	49.25	50.75	51.00
	52.00	47.00	49.00
	48.50	52.75	48.75
0.30	35.00	37.00	40.25
	39.25	40.75	40.25
	46.50	40.73	40.00
	44.50	42.50	50.20
	51.25	49.00	48.00
	49.75	49.75	49.00
	49.00	49.50	45.50
	48.50	48.00	46.00
	45.20	51.00	

Table(3.2) Summarised compressive strength results for varying fibre content.

Fibre Content By Weight (%)	Average Compressive Strength (MN/M^2)	Coeff. of Variation (%)	No. of Specimens
0.0	48.78	7.21	27
0.05	49.97	8.54	21
0.10	49.04	5.46	33
0.15	47.39	10.04	23
0.20	49.71	6.78	32
0.25	47.27	6.25	27
0.30	45.25	10.44	26

Table(3.3) Flexural strength results for varying fibre content.

Fibre Content By Weight (%)	Flexural Strength MN/M^2			
0.0	4.61	4.90	5.10	
	5.90	5.90	6.50	
	5.60	5.74	5.90	
	5.90	5.90	6.50	
	5.60	5.74	5.90	
	5.70	6.50	6.30	
	5.66	6.00	6.25	
	5.70	6.05		
0.05	6.45	6.65	6.20	
	5.65	6.05	5.35	
	5.35	5.60	5.70	
	6.00	5.60	5.60	
	5.30	5.65	6.24	
0.10	5.20	5.30	5.70	
	5.30	5.70	6.00	
	6.45	6.65	6.70	
	5.80	6.45	6.40	
	5.70	5.40		
0.15	5.10	6.24	6.70	
	6.00	5.10	5.70	
	6.00	6.20	5.20	
	5.95	6.35	5.35	
	6.35	6.50	6.20	
	6.25	6.10		
0.20	6.30	6.30	6.40	
	5.90	5.85	5.60	
	5.90	6.40	6.20	
	6.35	6.30	6.20	
	6.20	6.00		

Table(3.3) cont. Flexural strength results for varying fibre content.

Fibre Content By Weight (%)	Flexural Strength MN/M^2		
0.25	5.90	5.90	6.30
	6.80	6.40	6.70
	7.10	6.10	5.70
	5.20	5.75	6.10
	5.70	5.84	5.87
0.30	4.50	4.90	5.10
	5.70	5.50	5.65
	5.80	5.80	6.35
	5.92	5.80	5.95
	5.95	5.70	

Table(3.4) Summarised flexural strength results for varying fibre content.

Fibre Content By Weight(%)	Average Flexural Strength (MN/M^2)	Coeff. of Var. (%)	No. of Specimens
0.0	5.82	8.13	23
0.05	5.83	7.14	15
0.10	5.91	8.97	14
0.15	5.96	8.33	17
0.20	6.14	3.99	14
0.25	6.09	8.13	15
0.30	5.62	8.57	14

Table(3.5) Torsional strength results for varying fibre content.

Fibre Content By Weight (%)	Torsional Strength (KN-M)			
0.0	0.260	0.345	0.371	
	0.399	0.324	0.373	
0.05	0.407	0.357	0.409	
	0.444	0.340	0.380	
	0.397	0.368	0.458	
	0.380	0.404		
0.10	0.400	0.505	0.470	
	0.5840	0.489		
0.15	0.510	0.500	0.600	
	0.498	0.503	0.549	
0.20	0.466	0.436	0.457	
	0.320			
0.25	0.364	0.423	0.472	
	0.477	0.461	0.578	
	0.519	0.415	0.448	
0.30	0.410	0.540	0.610	
	0.482	0.515	0.477	

Table(3.6) Summarised torsional strength results for varying fibre content.

Fibre Content By Weight(%)	Average Torsional Strength (KN-m)	Coeff. of Var. (%)	No. of Specimens
0.0	0.35	14.21	6
0.05	0.40	8.93	11
0.10	0.49	13.53	5
0.15	0.53	7.71	6
0.20	0.42	16.12	4
0.25	0.46	13.38	9
0.30	0.51	13.32	6

Table(3.7) Impact test results for varying fibre content.

Fibre Content By Weight (%)	Impact Energy Absorbed Joules		
0.0	69.80	*	*
	*	*	*
0.10	64.00	64.00	70.90
	78.90	*	*
0.15	66.60	67.90	70.70
	74.70	*	*
0.20	80.30	*	*
	*	*	*
0.30	43.50	57.00	58.40
	59.80	61.10	*

* invalid test

Table(3.8) Summarised impact test results for varying fibre content.

Fibre Content By Weight (%)	0.0	0.05	0.10	0.15	0.20	0.25	0.30
Impact Energy Absorbed (Joules)	69.00	——	69.45	69.98	80.30	79.40	55.96

Table(3.9) Stress intensity factor determined by Compliance method (Chapter 6).

Fibre Content By Weight (%)	Stress Intensity Factor $MN/M^{3/2}$		
0.0	0.675	0.748	0.702
	0.728	0.755	0.569
	0.730	0.682	0.685
	0.673	0.752	0.715
	0.751	0.727	0.767
	0.703	0.625	0.794
	0.715	0.704	0.847
	0.769	0.821	0.636
	0.768	0.702	0.765

Table(3.9) cont. Stress intensity factor determined by Compliance method (Chapter 6).

Fibre Content By Weight (%)	Stress Intensity Factor $MN/M^{3/2}$		
0.05	0.686	0.765	0.688
	0.741	0.768	0.736
	0.740	0.834	0.682
	0.718	0.723	0.716
	0.716	0.699	0.781
	0.690	0.755	0.647
0.10	0.768	0.741	0.609
	0.583	0.662	0.794
	0.646	0.715	0.808
	0.663	0.847	0.701
	0.576	0.730	0.822
	0.834	0.781	0.743
	0.715	0.900	0.741
	0.804	0.818	0.715
	0.887	0.733	0.818
0.15	0.821	0.675	0.688
	0.808	0.636	0.821
	0.817	0.861	0.785
	0.880	0.882	0.682
	0.748	0.782	0.743
	0.730	0.814	0.747
	0.822	0.837	0.824
	0.824	0.751	0.914
	0.739	0.861	0.813
0.20	0.821	0.900	0.741
	1.006	0.927	1.006
	0.768	0.779	0.825
	0.824	0.808	0.755
	0.785	0.808	0.781
	0.785	0.768	0.781
	0.857	0.835	0.756
	0.788	0.821	0.858
0.25	0.715	0.688	0.847
	0.715	0.702	0.741
	0.841	0.757	0.841
	0.849	0.718	0.730
	0.796	0.728	0.796
	0.814	0.749	0.782
	0.723	0.716	0.776
	0.748	0.817	0.848
	0.888		

Table(3.9) cont. Stress intensity factor determined by Compliance method (Chapter 6).

Fibre Content By Weight (%)	Stress Intensity Factor $MN/M^{3/2}$		
0.30	0.463	0.622	0.642
	0.821	0.834	0.748
	0.775	0.862	0.834
	0.801	0.737	0.808
	0.821	0.806	0.789
	0.792	0.764	0.771
	0.821	0.788	0.781
	0.794	0.841	0.751
	0.861	0.715	

Table(3.9) cont. Stress intensity factor determined by Displacement method, equation(3.1).

Fibre Content By Weight (%)	Stress Intensity Factor K_I $MN/M^{3/2}$		
0.0	0.473	0.491	0.524
	0.510	0.528	0.399
	0.511	0.477	0.479
	0.471	0.527	0.501
	0.526	0.509	0.537
	0.492	0.438	0.556
	0.501	0.493	0.593
	0.539	0.575	0.445
	0.538	0.491	0.536
0.05	0.480	0.515	0.536
	0.518	0.482	0.584
	0.519	0.477	0.538
	0.502	0.505	0.501
	0.501	0.489	0.547
	0.483	0.528	0.453
0.10	0.426	0.538	0.519
	0.408	0.463	0.556
	0.452	0.501	0.465
	0.464	0.593	0.491
	0.403	0.511	0.576
	0.584	0.547	0.520
	0.501	0.630	0.519
	0.563	0.573	0.501
	0.621	0.514	0.573

Table(3.9) cont. Stress intensity factor determined by Displacement method, equation(3.1).

Fibre Content By Weight (%)	Stress Intensity Factor K_I $MN/M^{3/2}$		
0.15	0.575	0.473	0.482
	0.565	0.445	0.575
	0.572	0.603	0.550
	0.616	0.617	0.477
	0.524	0.548	0.520
	0.511	0.570	0.523
	0.576	0.586	0.577
	0.577	0.526	0.640
	0.517	0.603	0.569
0.20	0.575	0.519	0.630
	0.704	0.649	0.704
	0.538	0.545	0.577
	0.578	0.565	0.528
	0.550	0.565	0.547
	0.550	0.538	0.547
	0.600	0.585	0.529
	0.552	0.575	0.601
0.25	0.501	0.482	0.593
	0.501	0.491	0.519
	0.589	0.530	0.589
	0.594	0.502	0.511
	0.557	0.510	0.557
	0.570	0.525	0.547
	0.506	0.501	0.543
	0.524	0.572	0.594
	0.622		
0.30	0.324	0.436	0.450
	0.475	0.584	0.524
	0.542	0.603	0.584
	0.561	0.516	0.565
	0.575	0.565	0.552
	0.554	0.535	0.539
	0.575	0.552	0.547
	0.556	0.589	0.526
	0.603	0.501	

Table(3.9) cont. Stress intensity factor results determined by using Neuber equation(2.40).

Fibre Content By Weight (%)	Stress Intensity Factor K_I $MN/M^{3/2}$		
0.0	0.674	0.727	0.747
	0.753	0.700	0.568
	0.791	0.739	0.742
	0.729	0.815	0.775
	0.813	0.788	0.831
	0.762	0.677	0.861
	0.775	0.763	0.918
	0.834	0.890	0.689
	0.832	0.760	0.829
0.05	0.743	0.832	0.829
	0.798	0.746	0.802
	0.804	0.904	0.739
	0.778	0.782	0.776
	0.776	0.757	0.847
	0.748	0.819	0.701
0.10	0.608	0.767	0.740
	0.582	0.661	0.793
	0.700	0.775	0.875
	0.719	0.918	0.760
	0.624	0.791	0.891
	0.904	0.847	0.805
	0.775	0.976	0.804
	0.871	0.887	0.775
	0.961	0.795	0.887
0.15	0.819	0.674	0.687
	0.806	0.634	0.819
	0.885	0.933	0.851
	0.954	0.955	0.739
	0.811	0.848	0.805
	0.791	0.882	0.809
	0.891	0.907	0.892
	0.892	0.813	0.990
	0.801	0.933	0.881
0.20	0.819	0.899	0.740
	1.004	0.894	1.004
	0.832	0.844	0.894
	0.892	0.875	0.818
	0.851	0.875	0.847
	0.851	0.832	0.847
	0.928	0.905	0.819
	0.854	0.890	0.930

Table(3.9) cont. Stress intensity factor results determined by using Neuber equation(2.40).

Fibre Content By Weight (%)	Stress Intensity Factor K_I $MN/M^{3/2}$		
0.25	0.714	0.687	0.846
	0.714	0.700	0.740
	0.911	0.820	0.911
	0.920	0.778	0.791
	0.862	0.789	0.862
	0.882	0.812	0.847
	0.783	0.776	0.841
	0.811	0.885	0.919
	0.962		
0.30	0.463	0.621	0.641
	0.819	0.833	0.811
	0.839	0.934	0.904
	0.868	0.799	0.875
	0.890	0.874	0.855
	0.858	0.828	0.835
	0.890	0.854	0.847
	0.861	0.911	0.813
	0.933	0.775	

Table(3.10) Summarised stress intensity results determined by various methods.

Fibre Content By Weight (%)	0.0	0.05	0.10	0.15	0.20	0.25	0.30
Stress Int. Factor(*1) $_{3/2}$ "k_I" MN/M	0.51	0.51	0.52	0.55	0.58	0.54	0.54
Stress Int. Factor(*2) $_{3/2}$ "K_I" MN/M	0.78	0.79	0.81	0.86	0.89	0.84	0.84
Stress Int. Factor(*3) $_{3/2}$ "K_I" MN/M	0.72	0.73	0.75	0.79	0.82	0.77	0.77
Coeff. of Variation	8.23	6.05	11.53	8.77	8.70	7.38	11.02
No. of Specimens	27	18	27	27	24	25	26

*1 = Displacement method.
*2 = Neuber equation.
*3 = Compliance method.

Table(3.11) Optimum values of compressive, flexural, torsional, impact and fracture toughness strengths.

	Maximum Gain in Strength (%)	Fibre Content By Weight (%)
Compressive Strength MN/M^2	NIL	UNAFFECTED
Flexural Strength MN/M^2	5.40	0.20
Torsional Strength KN-m	52.50	0.15
Impact Strength Joules	15.04	0.20
Fracture Strength $MN/M^{3/2}$	14.09	0.20

PLATE. 3.1

PLATE. 3.2

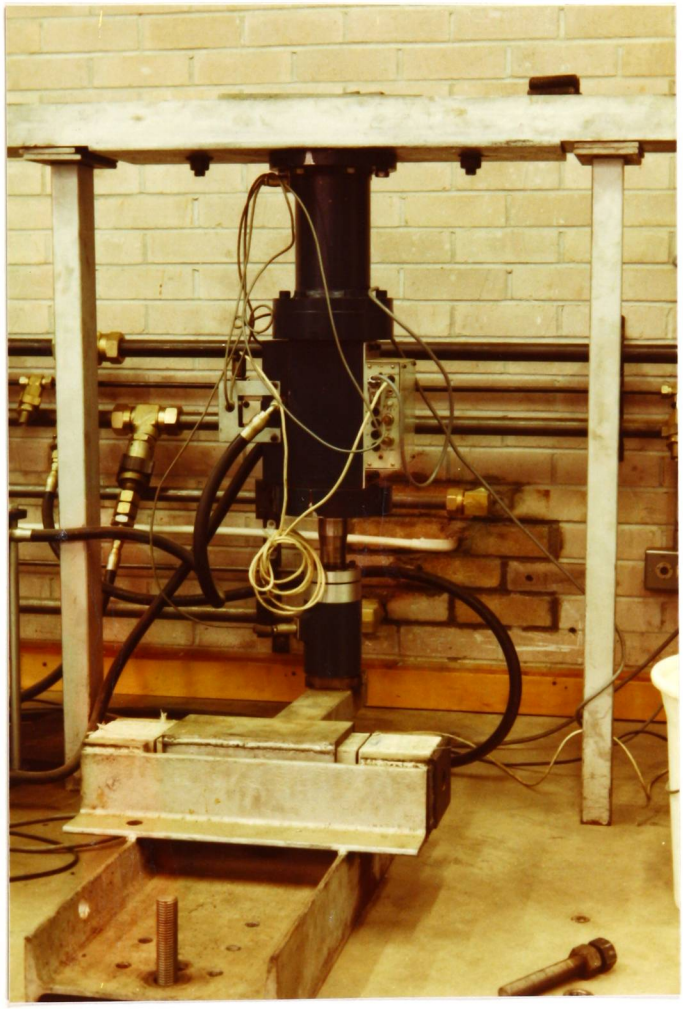

PLATE. 3.3

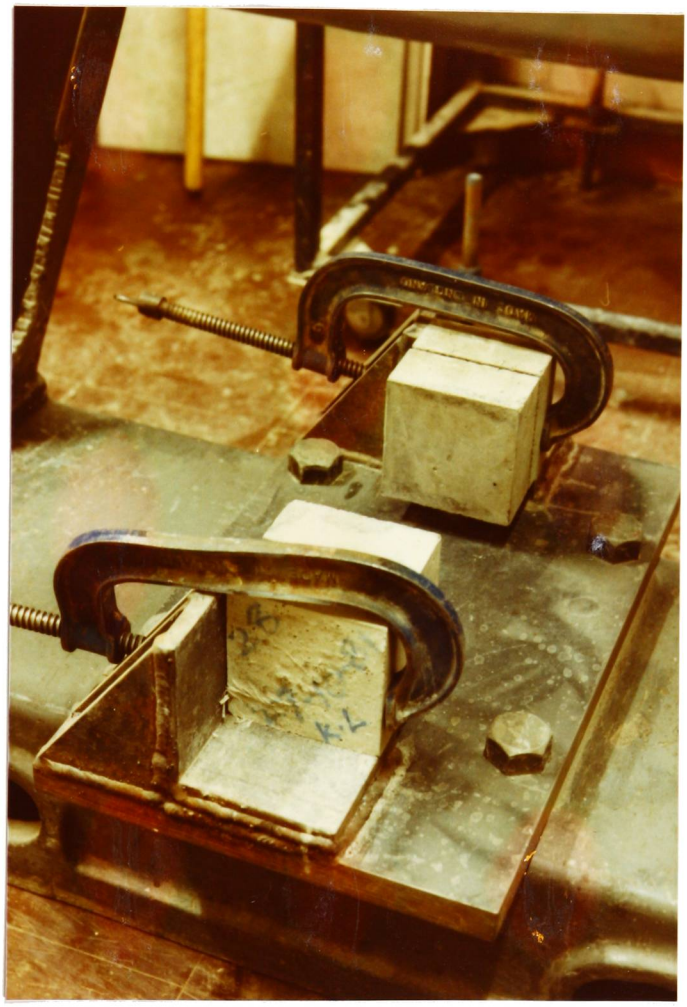

PLATE. 3.4

CHAPTER FOUR

FRACTURE TOUGHNESS OF GLASS-REINFORCED CEMENT COMPOSITE MATERIALS

4.1 INTRODUCTION

The initial application of dispersed glass fibres as reinforcement for cement was carried out in the USSR. Biryukovich et al, in their book(published in 1964) on the properties and basic methods of fabrication of the material, describe the early development work in this field. The Russian work was mainly concerned with binders of low alkali or high alumina cement and this stimulated the work at the Building Research Establishment in the United Kingdom which was directed towards the development of a glass fibre which would resist attack by the highly alkaline ordinary Portland cements commonly used in Europe and America.

The identification of alkali-resistant glasses by the Building Research Establishment and their subsequent development and commerical production in the United Kingdom by Pilkington Brothers Ltd. lead to major research efforts by both the B.R.E. and Pilkington in the early 1970s. The research at that time was directed towards understanding the physical properties of the composite materials, in particular, to impact and fracture properties. In recent years, most of the effort has been directed towards developing testing methods which could be used to determine the fracture toughness and impact properties of fibre reinforced composites. Three-point or four-point flexural

loading systems are commonly used. Patterson and Chan(33) concluded that crack-line loaded single-edge crack specimens in tension could be used to determine the fracture toughness of glass fibre-reinforced cement composite materials. Mindess et al(34) and Velazco(37) used J-integral and R-curves analysis respectively to determine the toughness of cement based composite materials. More recently, Barr et al(40) modified the standard cube, which was then subjected to eccentric loading, to evaluate the fracture toughness of polypropylene fibre-reinforced concrete.

In this Chapter, the modified compact tension specimen was used to evaluate the toughness of glass fibre reinforced cement composite materials. The sizes of the specimens, the notch-depth ratios and variation of the glass fibre content were investigated. In addition to the above study, a fracture toughness index, determined from the load-deflection results, is proposed.

4.2 TEST SPECIMEN GEOMETRIES

The general configuration of the compact tension specimen is shown in Fig.(4.1). The sizes of the specimens were 50 X 50mm and 150 X 150mm. The crack length/width ratios were 0.40, 0.50 and 0.60 and the diameter of the "loading" holes was kept constant at 13mm. The glass fibre

reinforced cement composite materials were supplied by E.H.Bradley and Sons Ltd., Swindon. The specimens were cut from large panels into their required dimensions by means of a Clipper masonry saw. The "loading" holes were introduced by means of a 13mm diameter masonry drill bit which was fitted in the R3 Radial Drill machine. The required notch depth was introduced into the specimen after the "loading" holes were completely drilled so that the specimen would not be damaged during the drilling process—especially near the notch-root region. The required notch depth was initially introduced by means of a Clipper diamond saw and then a Hack saw blade(with 24 teeth per inch) was then used for the final 10mm notch depth. This was done to ensure that a reasonable sharp notch at the crack tip was obtained.

4.3 EXPERIMENTAL DETAILS

Four different types of mixes were used throughout the experimental work. The mix details were as follows:

Cement (Kg.)	90	90	90	90
Sand (Kg.)	30	30	18	18
Glass fibre content(%) by weight of dry solids	3	5	3	5

The initial panels supplied showed some variation of thickness and, futhermore, some of the panels were a little too thin. Some additional panels were supplied which were of a more uniform thickness and of a stronger mix.

The glass fibre-reinforced composite panels were made using the spray and roll technique. This technique has been developed from the glass-reinforced plastics industry and consists of leading a continuous roving up to a compressed air operated gun which chops the roving into lengths of 50mm and blows the cut lengths at high speed simultaneously with a cement paste spray onto a forming surface. One man operates the spray gun while another follows the sprayed materials with a hand roller. The fibre-cement sheet can be bulit up to the required thickness and then demoulded.

The compact tension specimens were tested in a dry

condition. The tests were carried out at nominal room temperature. All the compact tension tests were carried out by means of a 1026 Model Instron machine. The experimental arrangements were set up as shown in Plate(4.1). A small tensile load was initially applied to the test specimen. This was done to ensure that the jaws and the specimen were aligned in the correct position. The cross head speed was kept constant at 0.5mm per minute throughout the testing programme. The load-deflection curves were obtained from the plotter automatically during testing. The fracture toughness is calculated from the limit of proportionality of the peak load achieved.

4.4 THEORIES OF COMPACT TENSION SPECIMEN AND FRACTURE TOUGHNESS INDEX

4.4.1 COMPACT TENSION SPECIMEN

The compact tension specimen is currently recommended in A.S.T.M.(14). The specimen is subjected to point loading through pins above and below the crack surfaces. The method of producing K-calibration is to make use of the compliance technique either by measuring the compliance experimentally or by calculating the overall elastic response in various regions of the specimen. The stress intensity factor is calculated from the following equation which has been established on the basis of elastic stress analysis.

$$K = P/BW^{1/2}\left[29.6(a/w)^{1/2} - 185.5(a/w)^{3/2} + 655.7(a/w)^{5/2} - 1017(a/w)^{7/2} + 638.9(a/w)^{9/2}\right] \qquad (4.1)$$

Hence $$K = \frac{P}{BW^{1/2}} \cdot Y \qquad (4.2)$$

where $$Y = f(a/w)$$

From equation(4.1) shown, it is seen that any error in the thickness, B, will give a corresponding error in the value of K. Therefore the thickness of each specimen near the crack tip was measured before the test was carried out and the peak load obtained from the limit of proportionality of

the load-deflection curve. The stress intensity factor was then determined using equation(4.1).

4.4.2 FRACTURE TOUGHNESS INDEX

Henager(48) proposed a fracture toughness index to measure the energy absorption capability of fibre concrete. Using the area under the load-deflection curve from the modulus of rupture flexural specimens, the energy absorbed up to the point of first crack was divided into the total energy absorbed up to a centre deflection of 1.9mm. The typical load-deflection curves are shown in Fig.(4.2). The fracture toughness index is dimensionless and is normally equal to 1.0 for plain concrete. Thus the addition of fibres in concrete will lead the toughness index numerically greater than unity because the fibre concrete is a great deal tougher than plain concrete. The energy absorbed (area under the curve) for fibre concrete specimens depends upon the amount, length, configuration, strength and ductility of the fibres and other factors such as cement content, aggregate amounts and sizes, water/cement ratio, age and curing conditions. Henager(48) concluded that the toughness index could be easily obtained from the modulus of rupture test and a detailed study of the index would show a relationship between the index and the length, ductility and amount of fibres in concrete.

The fracture toughness index of glass

fibre-reinforced cement composite materials obtained in this study was based on the load-deflection curve. The compact tension specimen is loaded until the load-deflection graph covers twice the deflection at initial cracking. Typical load-deflection curves are illustrated in Fig.(4.3). In Fig.(4.3a), the curve shows a linear response up to the point where the plain concrete fails and then the load reduces to zero. Thus the toughness index for plain concrete is as follows:

$$\text{Toughness index(T.I.)} = \frac{\text{Shaded area}}{\text{Total area to } 2\delta} \quad (4.3)$$

(plain concrete)

$$= 0.25 \quad \text{or} \quad 25\%$$

Fig.(4.3b) describes the typical load-deflection graph of fibre concrete. The curve exhibits a linear response up to the peak load achieved and then the load reduces to a constant value (residual load). The fracture toughness index value in this case is normally within the range $0.25<T.I.<1.0$. The maxim um toughness index value is equal to unity or 100 percent as shown in Fig.(4.3c). Thus the fracture toughness index is greatly influenced by the pattern of the load-deflection curve. Provided the load-deflection curves are obtained in the experiments the fracture toughness index can be determined using equation(4.3).

4.5 DISCUSSION OF THE TEST RESULTS

4.5.1 COMPACT TENSION SPECIMEN

The experimental fracture toughness results (for specimens 50 X 50mm and 100 X 100 mm) with varying glass fibre content are shown in Table(4.1-4.2) respectively. The relationship between the fracture toughness values and the notch depth/width ratios are illustrated graphically in Figs.(4.4-4.7) in each case. It is seen that the fracture toughness values are independent of the notch depth/width ratios. Thus the compact tension specimen can be used to evaluate the fracture toughness of the fibre-reinforced cement composite materials. The coefficient of variation of the experimental toughness results vary from 4.3 percent to 38.9 percent. However, in general, the coefficient of variation was in the range of 10 percent to 20 percent and for some series of specimen within 10 percent. Larger coefficient of variation of the test is most likely due to the small number of tests carried out and the non-uniform thickness of the specimen may have influencedthe results.

The effect of variation of glass fibre content on fracture toughness was investigated. The results are summarised in Tables(4.3-4.4). The glass fibre content of 3.0 percent and 5.0 percent (of the total dry solids) were carried out in the experimental work for each mix. The relationship between fracture toughness values and varying glass fibre content is illustrated in Fig.(4.8). From the

results shown, the addition of glass fibre increases the toughness of the composite materials. The maxim um gain in toughness is approximately 50 percent when the fibre content is increased from 3.0 percent to 5.0 percent.

The minim um and maxim um coefficient of variation(50 X 50mm) were 11.5 percent and 19.4 percent respectively while 3.6 percent and 16.4 percent were determined for the 100 X 100mm specimens as shown in Table(4.3-4.4). It is seen that the larger specimen size gives more consistent results than the smaller specimen size. The error may also be partly due to the size effect of the specimen and the 'loading' holes which were 13mm diameter. The holes were positioned comparatively closer to the crack tip which might have affected the tests results.

Due to the wide range of coefficient of variation obtained in the experimental work, it was necessary to carry out more tests to verify the validity of the compact tension specimen which could be used to determine the toughness of glass fibre-reinforced cement composite materials. Larger specimens(100 X 100mm and 150 X 150mm) were investigated. The experimental results are shown in Tables(4.5-4.6). The fracture toughness values are summarised in Table(4.7-4.8). The relationship between the toughness and the notch depth/width ratios are illustrated graphically in Fig.(4.9). The stress intensity factor was

shown to be independent of the notch depth/width ratios in both cases. There was a little drop off in toughness for a notch depth/width ratio of 0.6 probably due to the insufficient uncracked length of the specimen. When the uncracked length becomes small the stress-free boundary significantly affected the crack tip stress field.

The typical crack path of the compact tension specimen is shown in Plate(4.2). The crack propagated approximately perpendicular to the applied load and then deviated as shown. This phenomenon does not affect the calculated results because all the peak loads used to calculate the fracture toughness were obtained from the limit of proportionality of the corresponding load-deflection curves.

As the resluts shown, larger specimens give more consistent values for the stress intensity factor in the compact tension tests. The maximum and minimum coefficient of variation are 11.4 percent and 8.4 percent respectively in both cases (100 X 100mm and 150 X 150mm). Thus the compact tension specimen can be used to evaluate the toughness of fibre-reinforced cement composite materials. The most consistent results can be obtained within $0.4 \leq a/w \leq 0.5$ limits provided the compact tension specimen is sufficiently large for the tests.

4.5.2 FRACTURE TOUGHNESS INDEX

Typical load-deflection curves of glass fibre-reinforced cement composite materials are shown in Fig.(4.12). The corresponding curves with varying glass fibre content are of similar shape. The graph is initially linear up to the limit of proportionality. Beyond this limit, the slope begins to decrease and the materials become pseudo-ductile due to the effect of the glass fibre in 'pulling out' condition in the composite material.

The results showed that addition of glass fibre content improves the limit of proportionality in the composite materials. The lower sand content in the mix gave higher strength than the richer sand content. Majumdar et al(49) and Singh et al(50) used the flexural test to obtain the load-deflection curves with varying glass fibre content. The results are illustrated graphically in Fig.(4.13). It is seen that the load-deflection curves obtained in this study are similar with those of Majumdar et al(49) and of Singh et al(50).

The fracture toughness index results were determined using equation(4.3) and based on the load-deflection curves which were carried out during the tests. The detailed toughness results are shown in Tables(4.9-4.10). The fracture toughness index values for varying specimen sizes

and notch depth/width ratios are summarised in Tables(4.11-4.12). The relationship between the toughness index and notch depth/width ratios is illustrated graphically in Figs.(4.10-4.11) for each specimen size. The results show that the fracture toughness index was independent of the notch depth/width ratios in both specimen sizes. The average toughness index values were 0.91 in the case of 100 X 100mm and 0.94 in the case of 150 X 150mm. Thus the toughness index is also independent of the specimen sizes. The difference between these two values was approximately 3.3 percent which was quite acceptable in the experimental work.

The coefficient of variation for the fracture toughness index is shown in Tables(4.11-4.12). It is seen that a good correlation of results was obtained with the coefficient of variation generally within 2 percent and the fracture toughness index was independent of the notch depth/width ratios and the specimen sizes. The fracture toughness index may be used for compact compression as well as compact tension specimens provided the load-deflection curves can be obtained in the experiments; the toughness index may be used for all fibre reinforced materials so that a comparison can be made between various materials(steel, glass and polymers). The addition of fibre in concrete increases the toughness, or ductility in the material. Thus the toughness index results may be compared for varying fibre content. The test is not limited by any

artificial restriction regarding defined deflections etc. Since the index is expressed in percentage form there is no limitation regarding units.

Further investigation of fracture toughness index is necessary. Further work may show that the index may be used to characterise material performance. Furthermore, in certain design situations a minim um toughness may be specified. An index above 75 percent would yield a load-deflection curve with a positive slope at all times. Such a material could be tested in load control machin es.

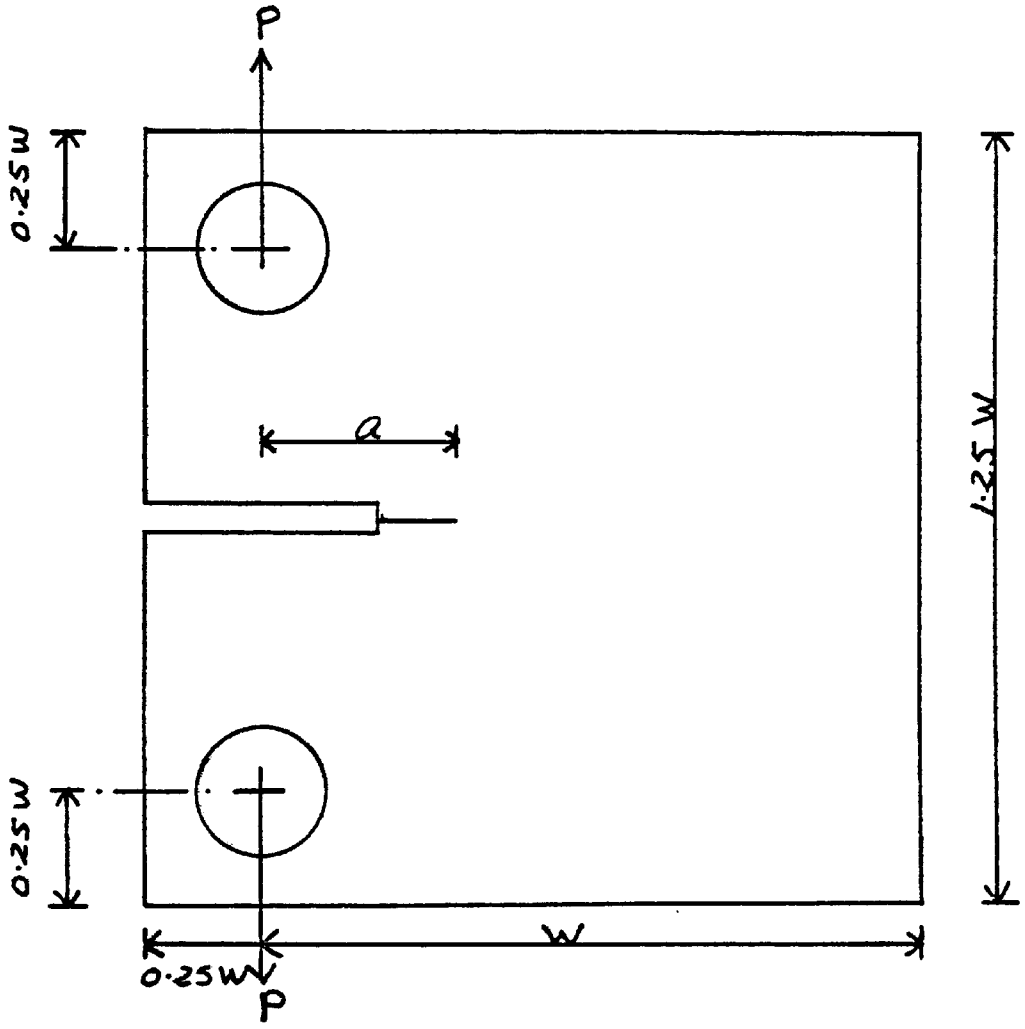

Fig. (4.1) General configuration of the compact tension specimen

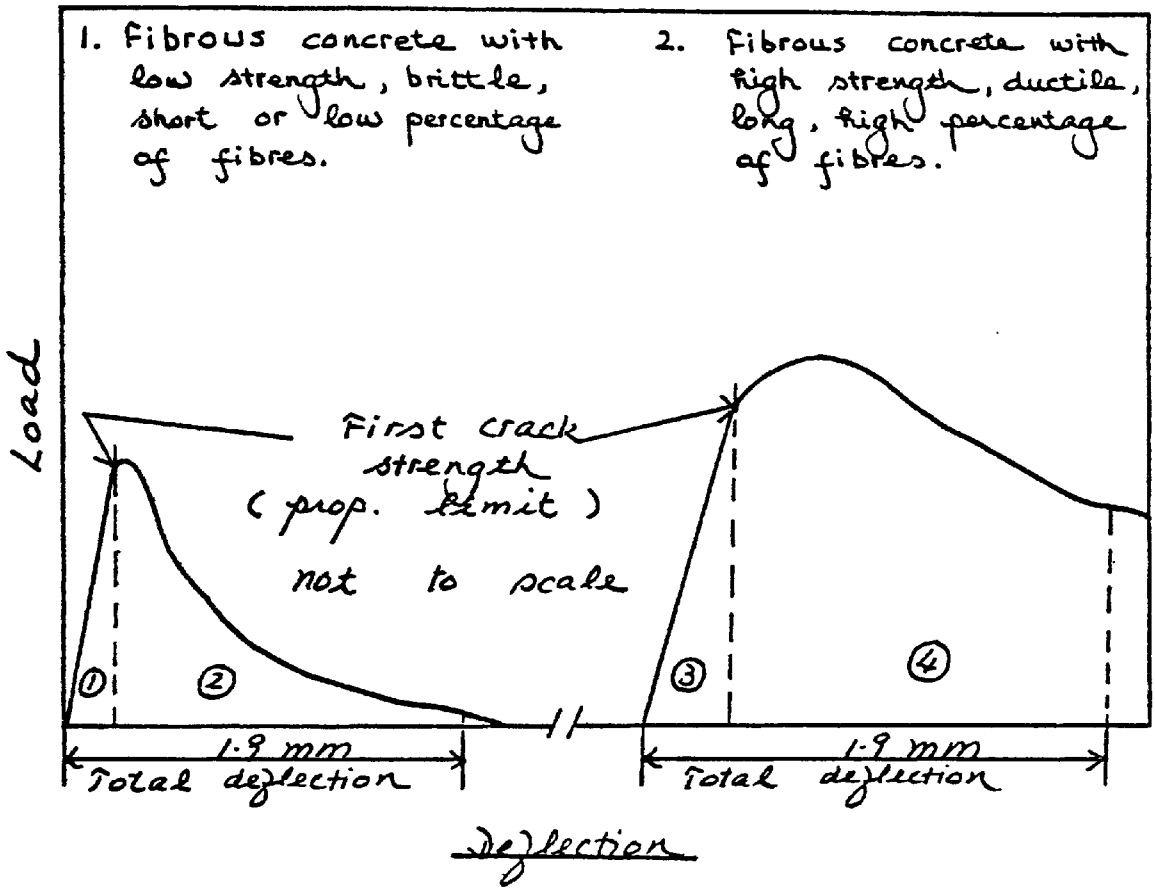

Fig. (4.2) Typical load / deflection curves obtained by Henager (48)

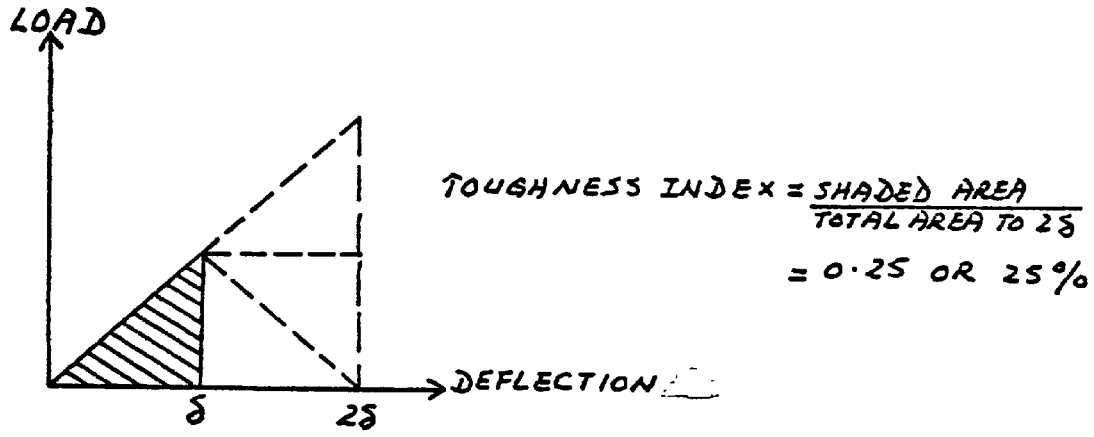

Fig. (4.3 a) Typical load / deflection curve for plain concrete

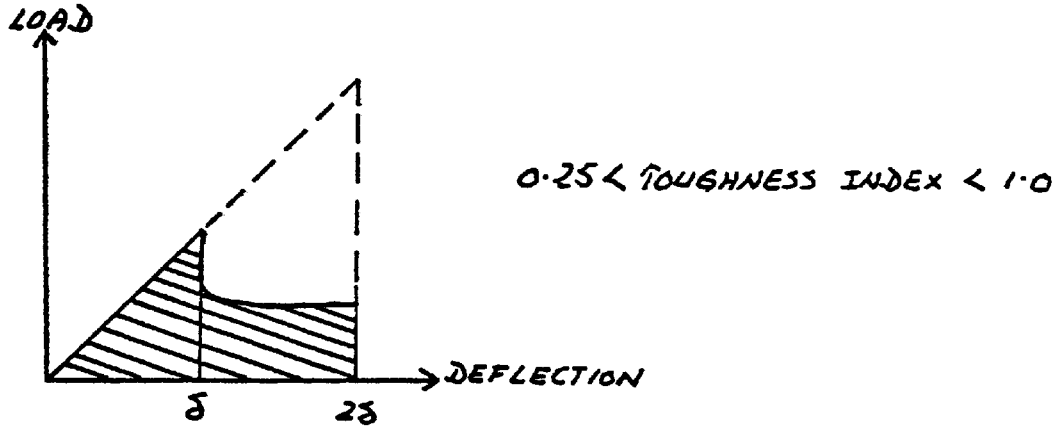

Fig. (4.3 b) Typical load / deflection curve for fibre-reinforced concrete

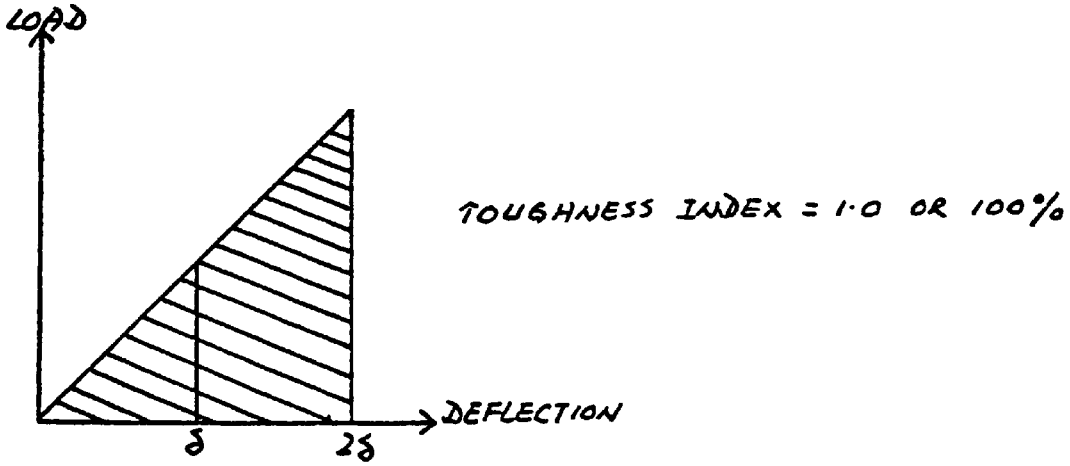

Fig. (4.3 c) Maximum (possible) toughness

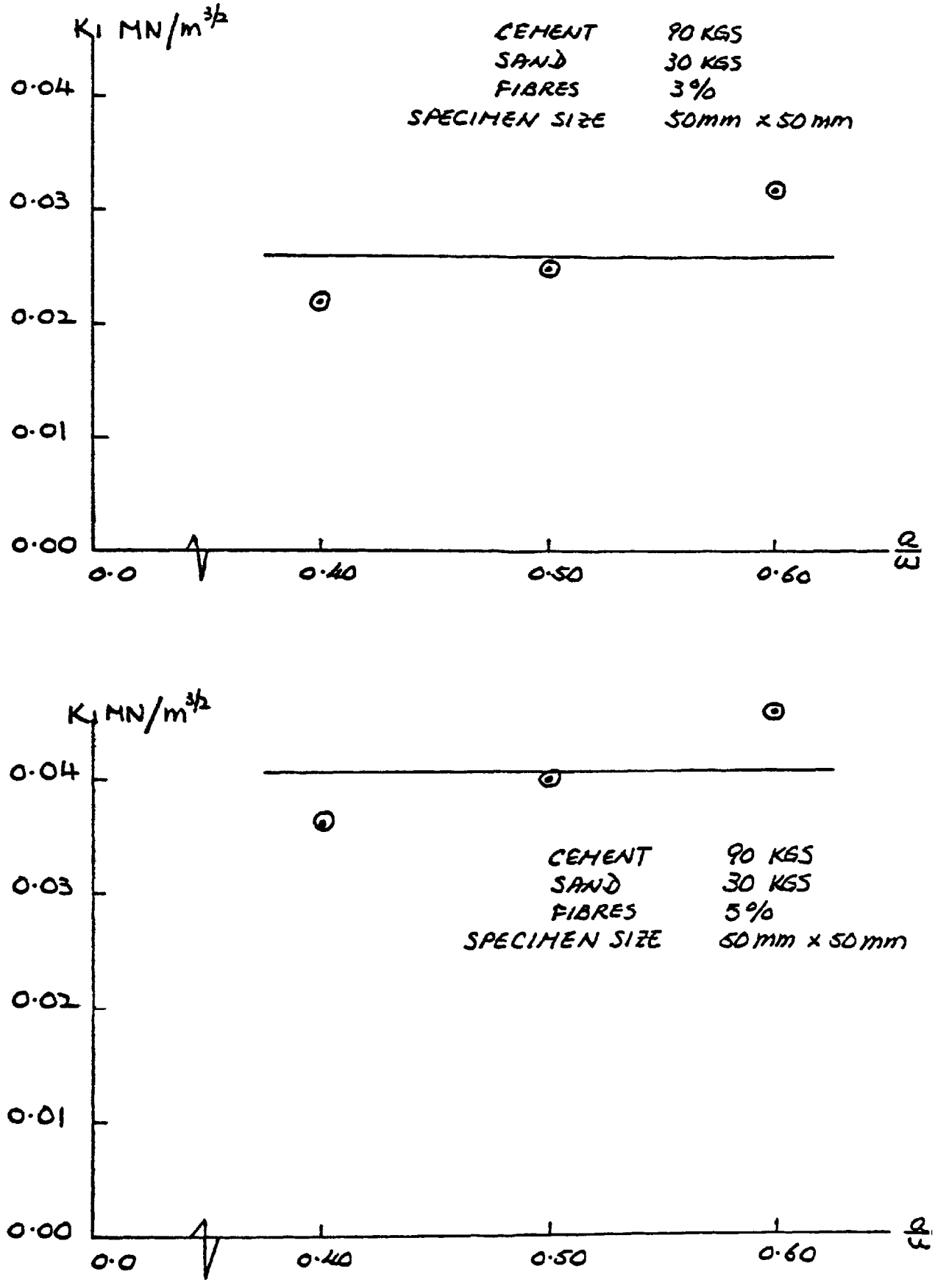

Fig. (4.4) Fracture toughness results for varying notch / depth ratio

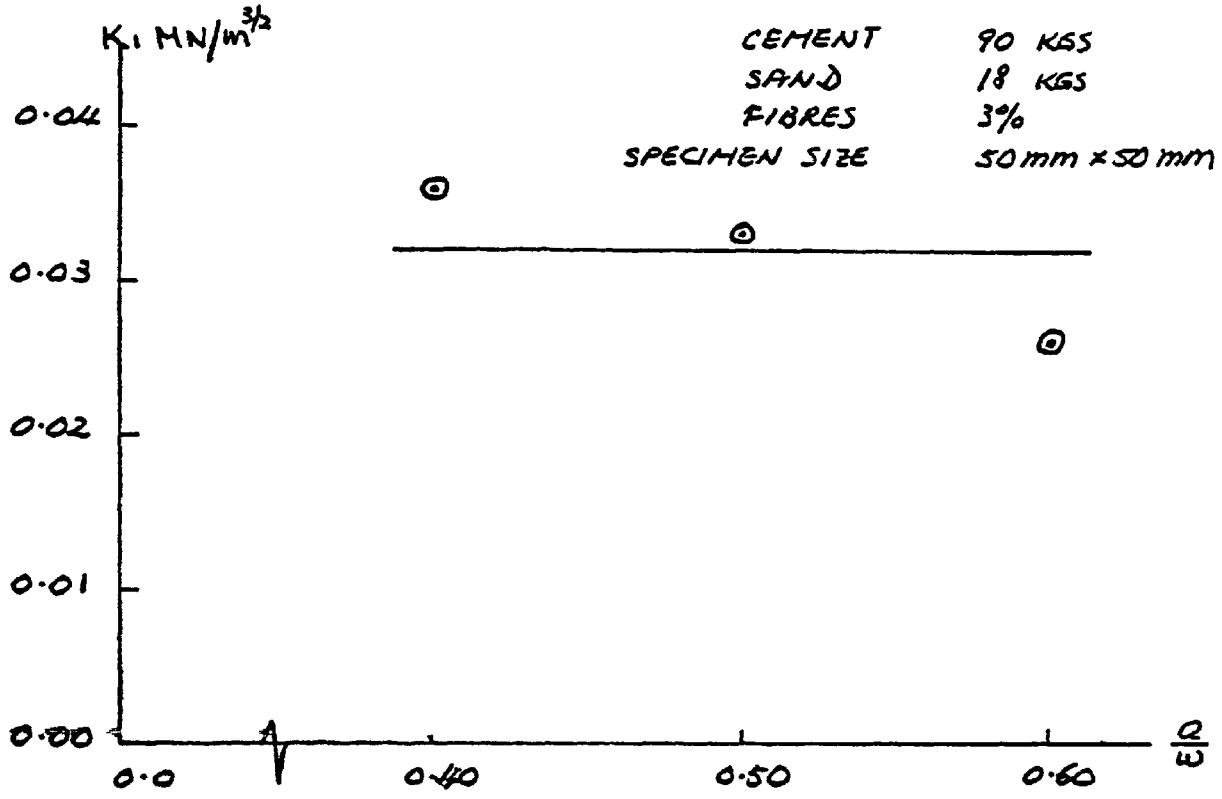

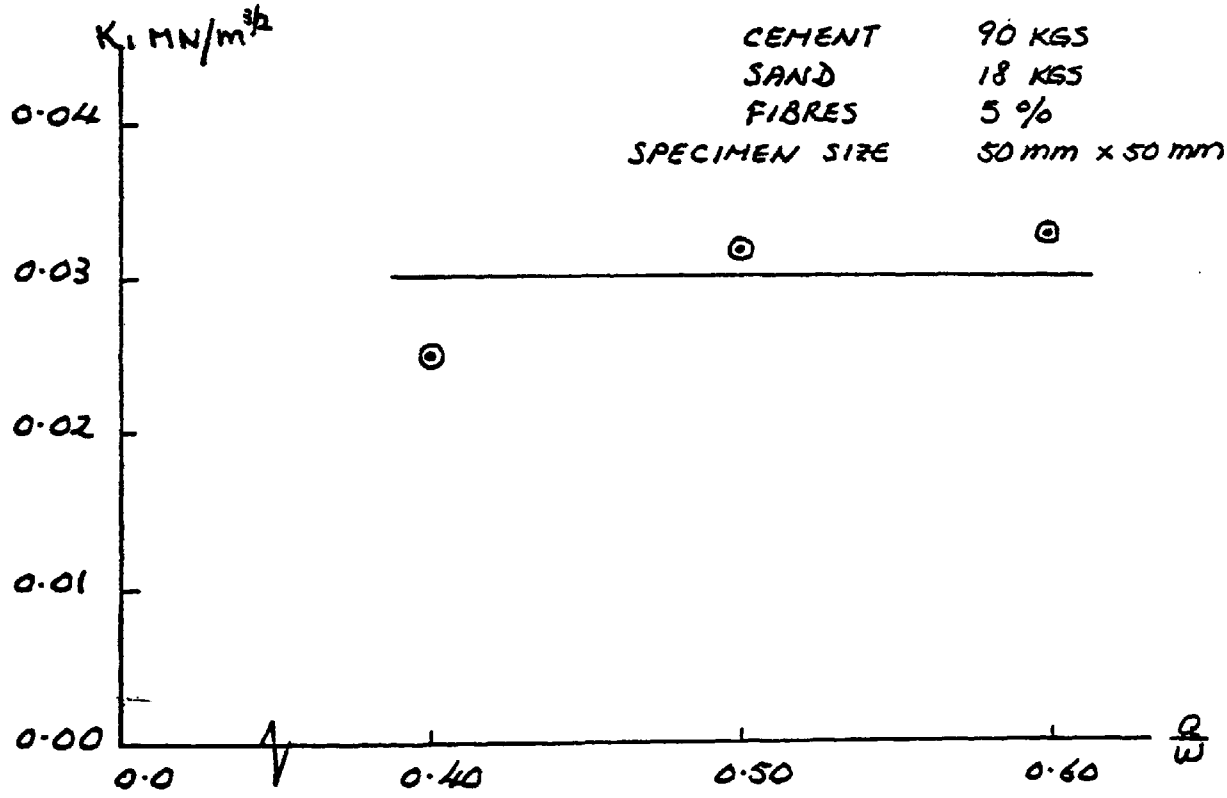

Fig. (4.5) Fracture toughness results for varying notch / depth ratio

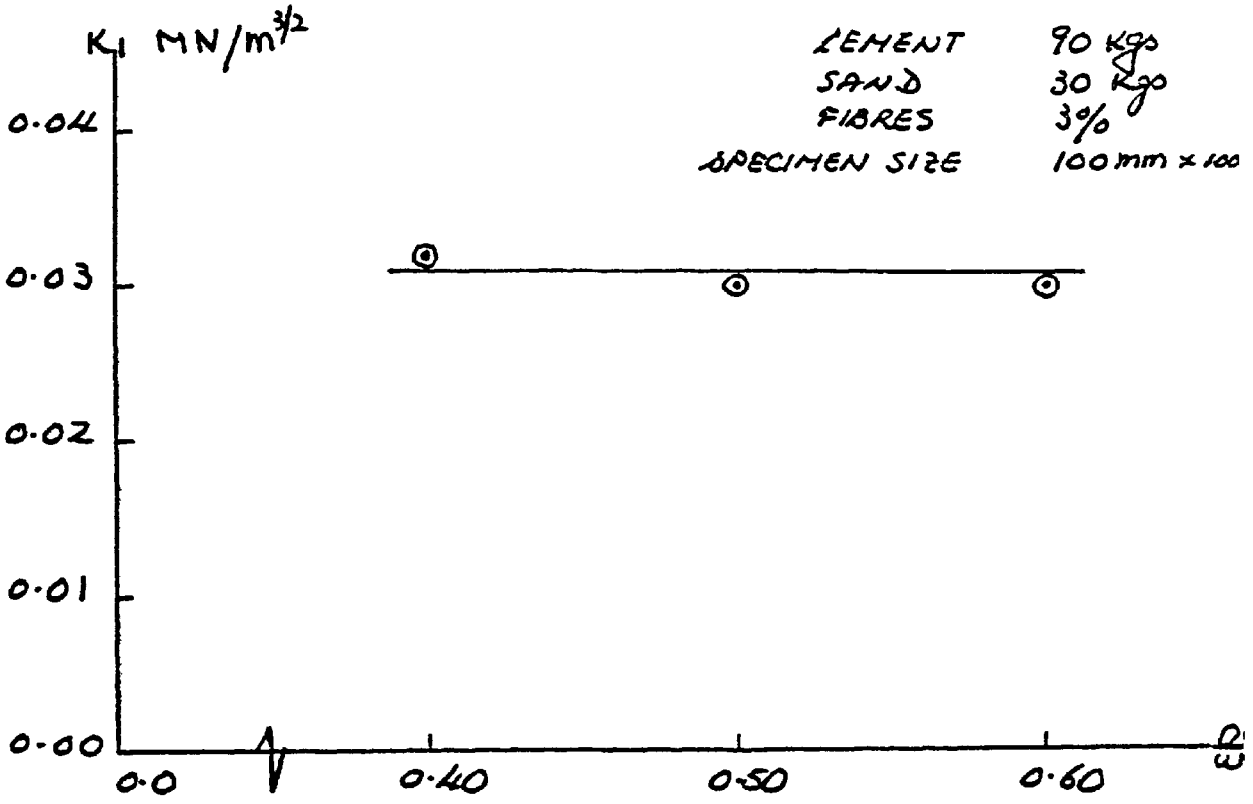

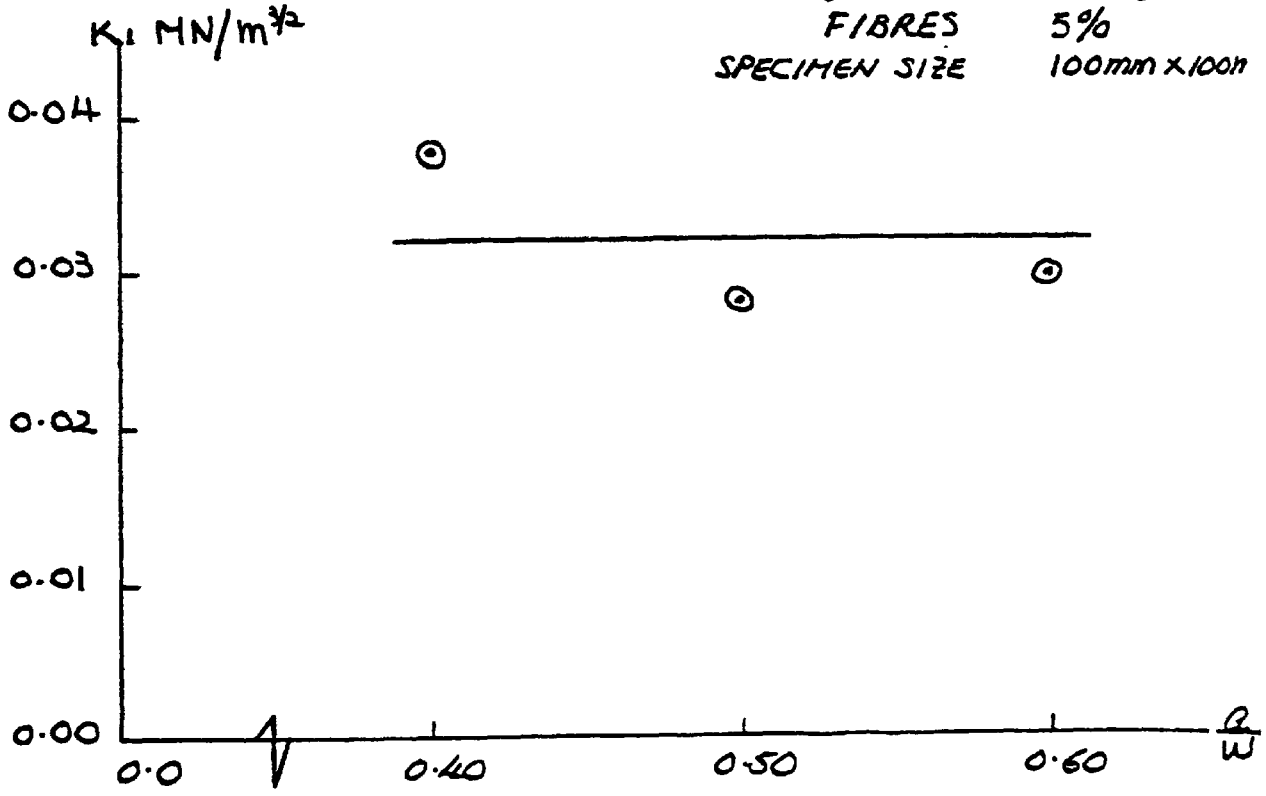

Fig. (4.6) Fracture toughness results for varying notch / depth ratio

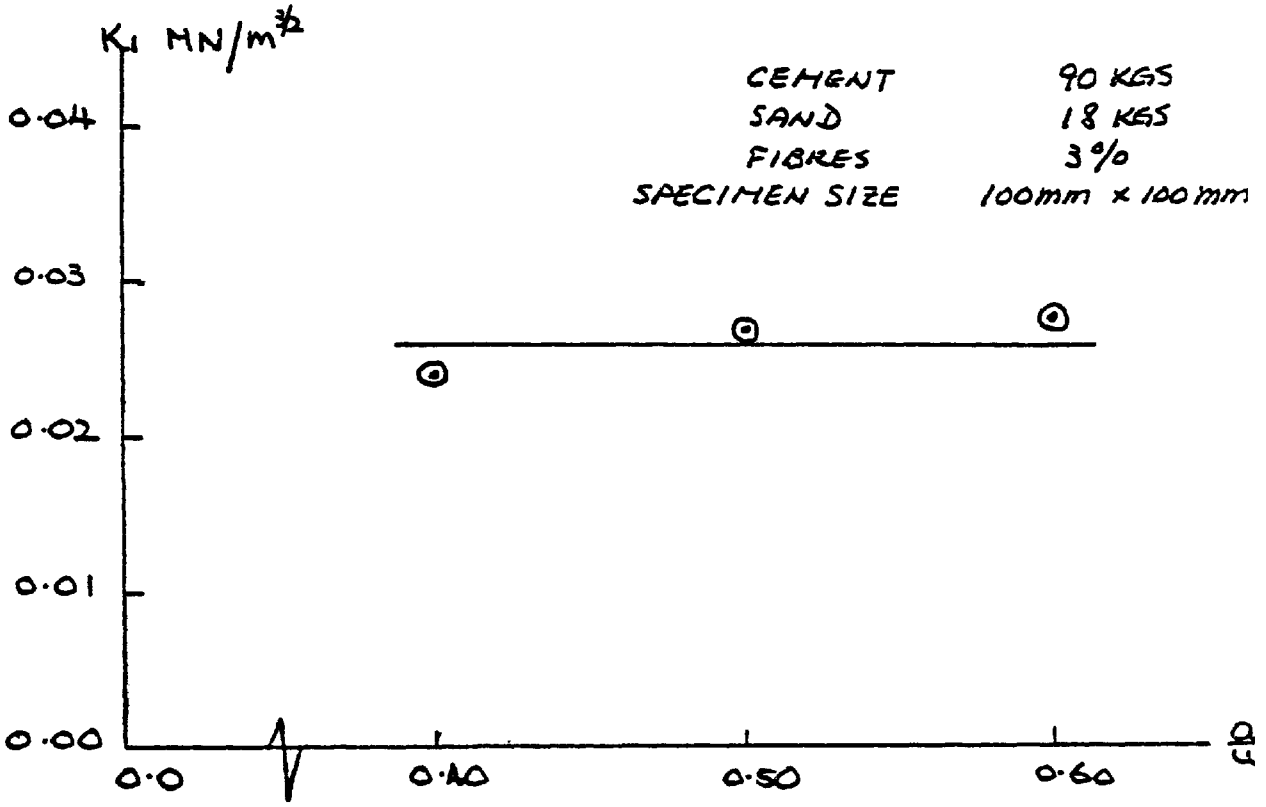

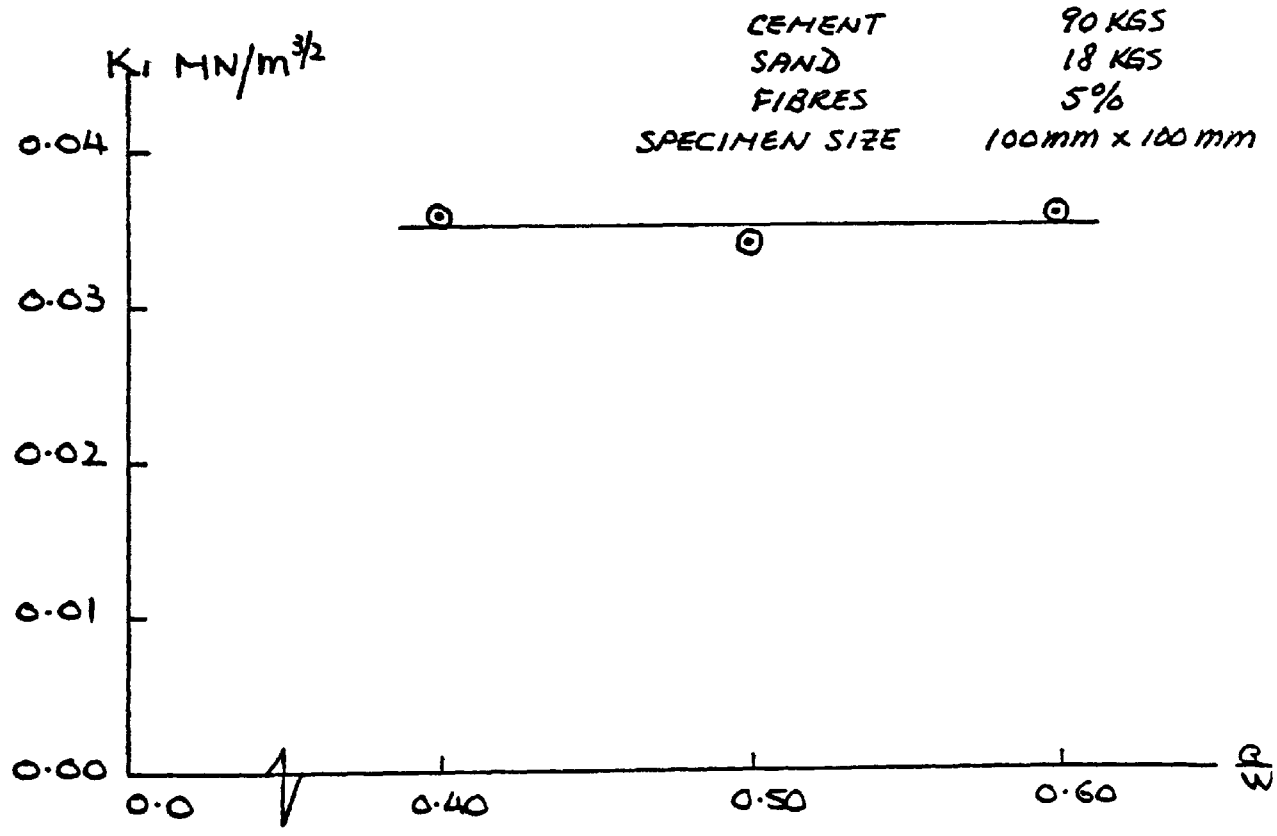

Fig. (4.7) Fracture toughness results for varying notch / depth ratio

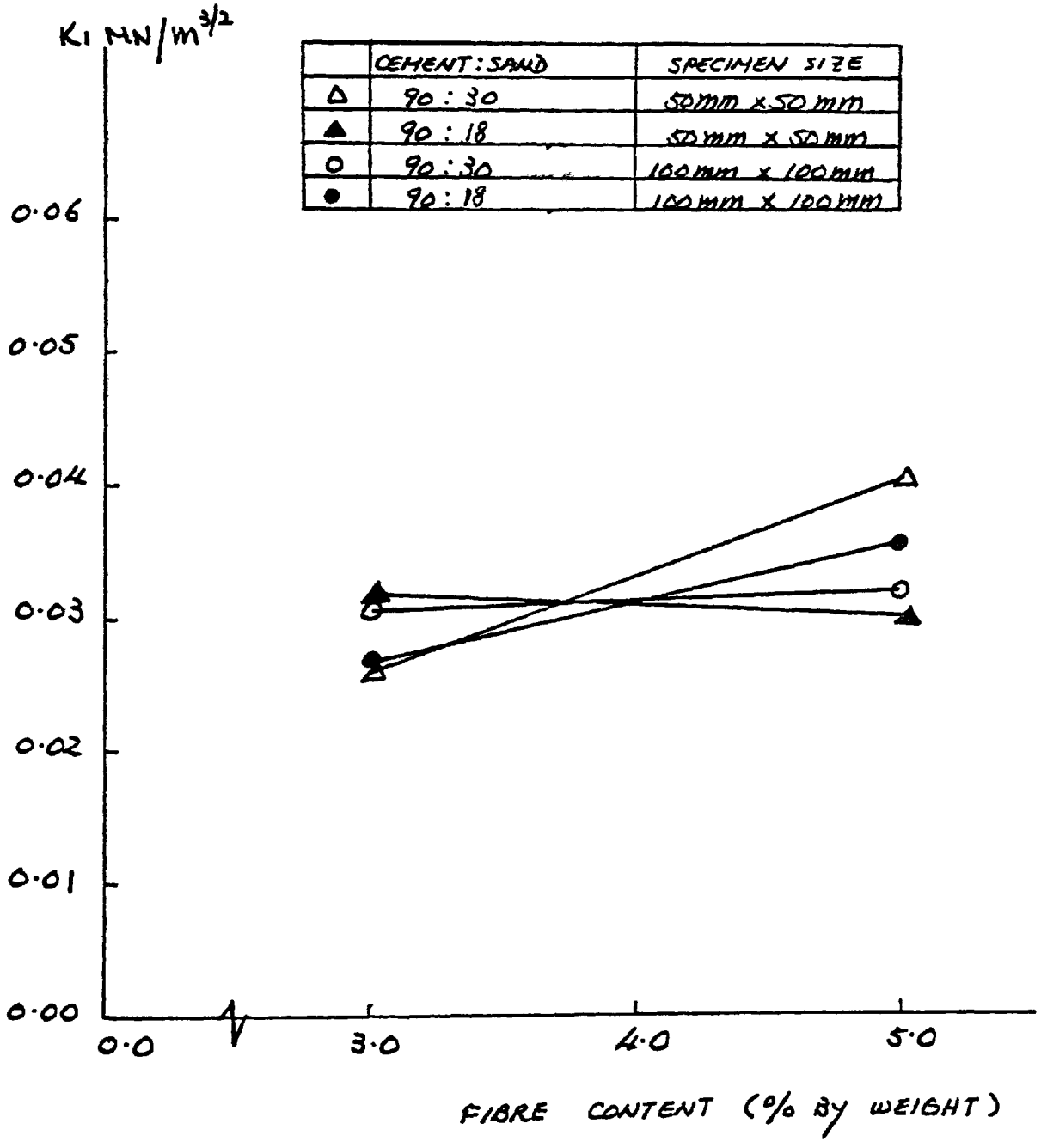

Fig. (4.8) Fracture toughness results for varying glass fibre content

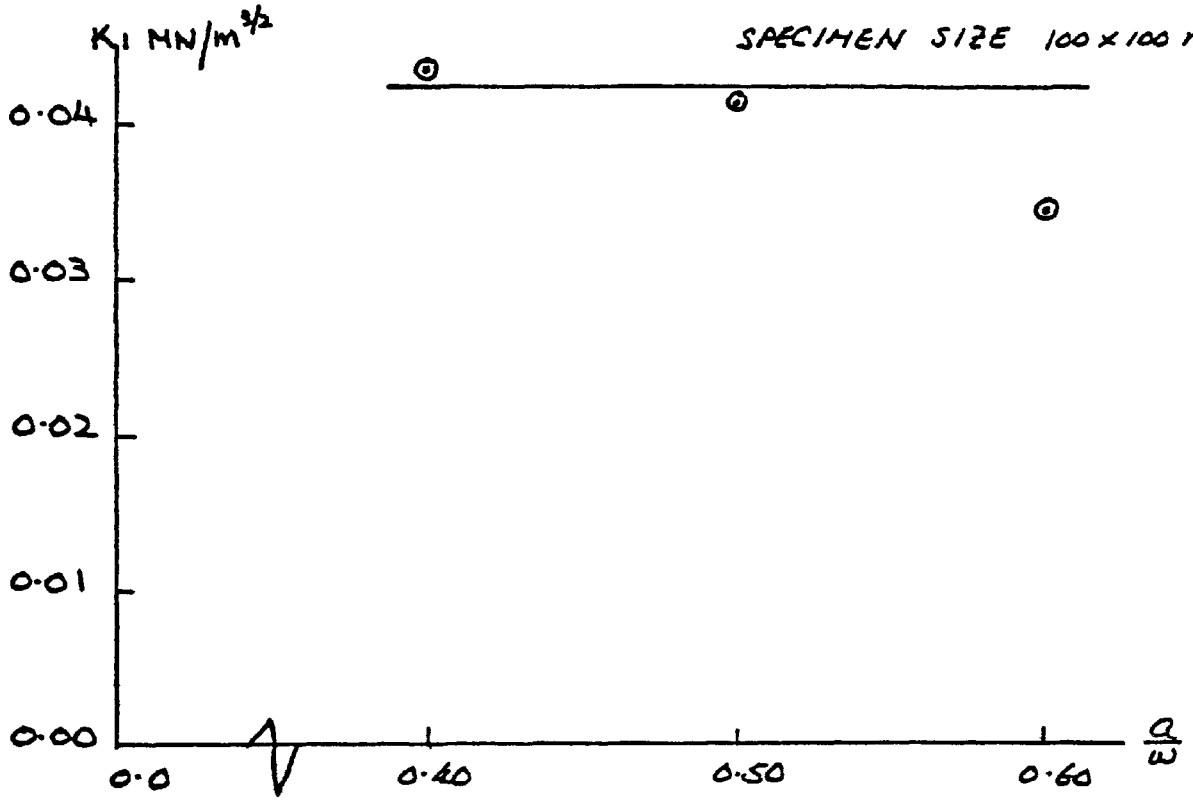

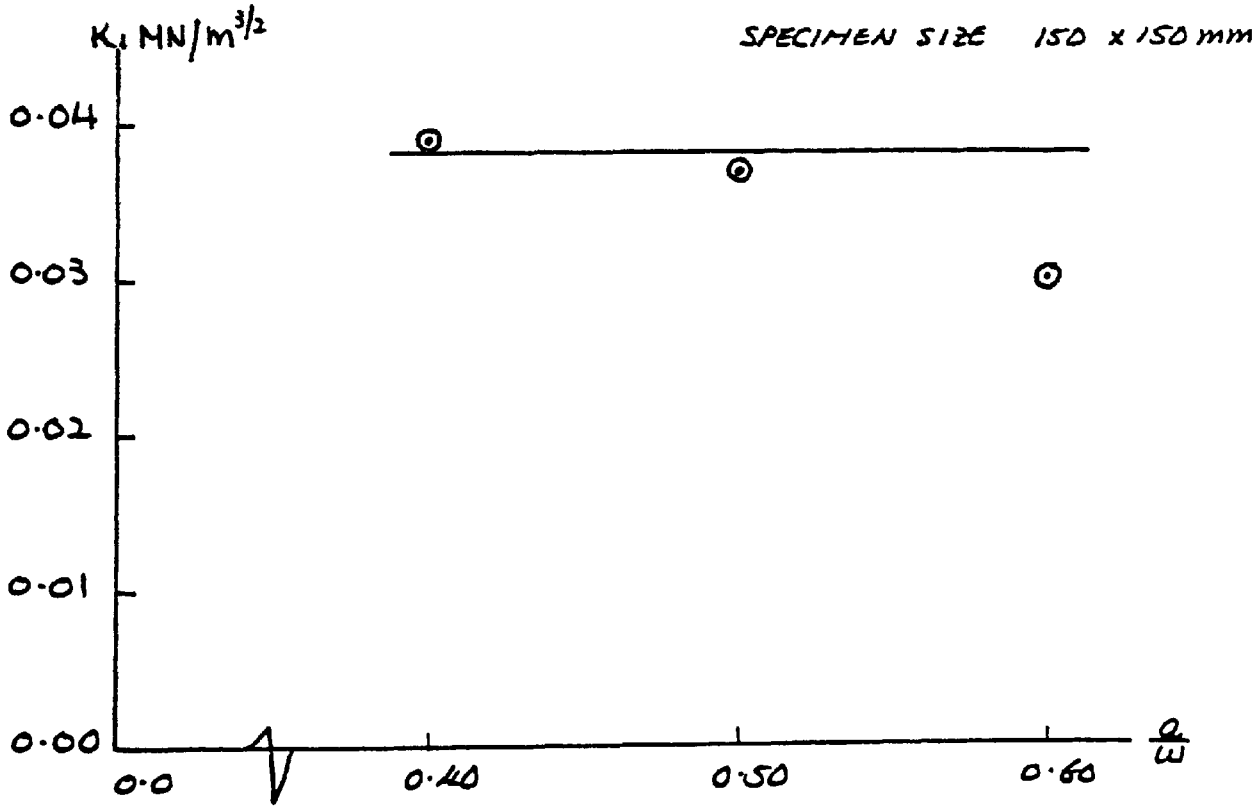

Fig. (4.9) Fracture toughness results for varying notch / depth ratio

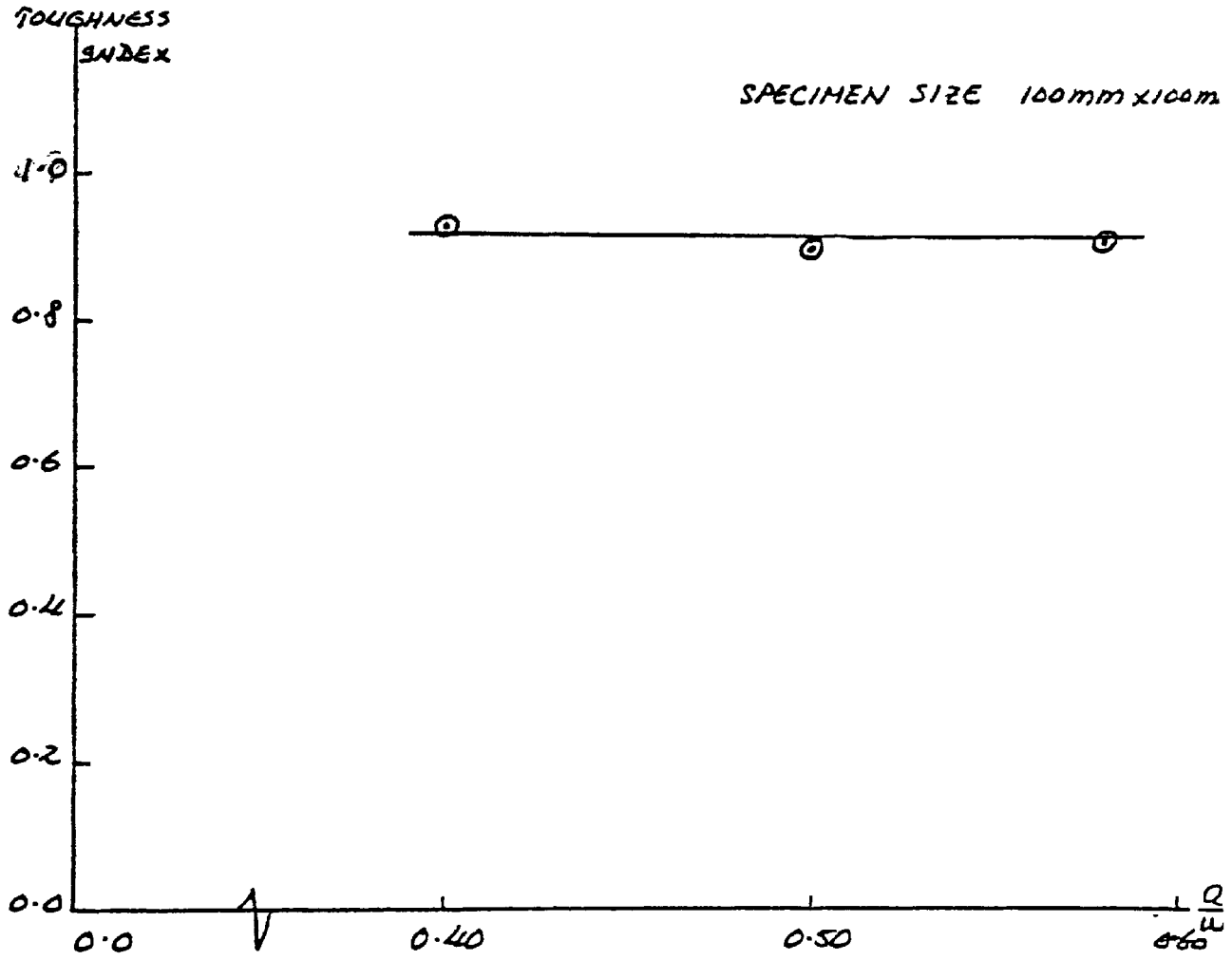

Fig. (4.10) Fracture toughness index results for varying notch / depth ratio

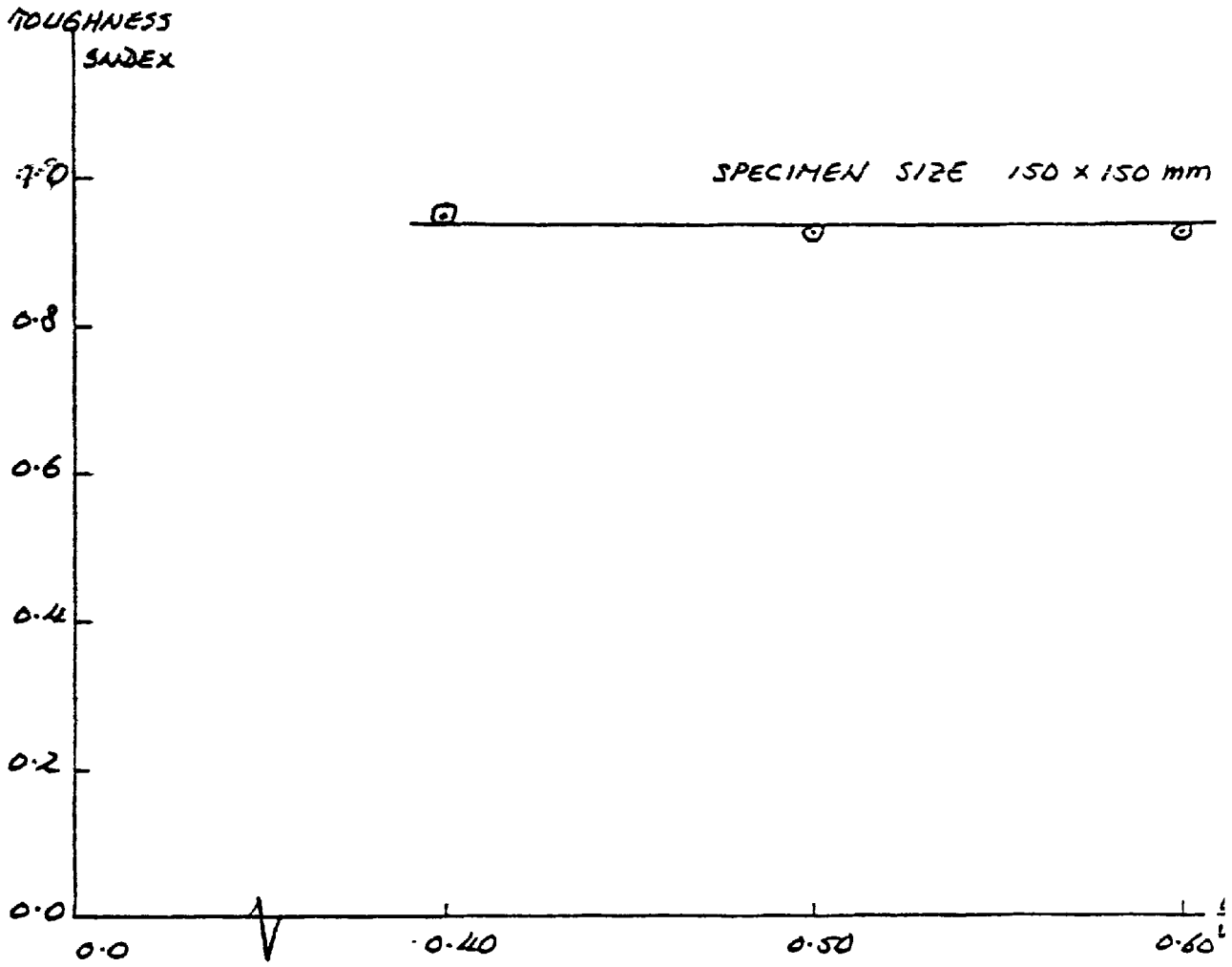

Fig. (4.11) Fracture toughness index results for varying notch / depth ratio

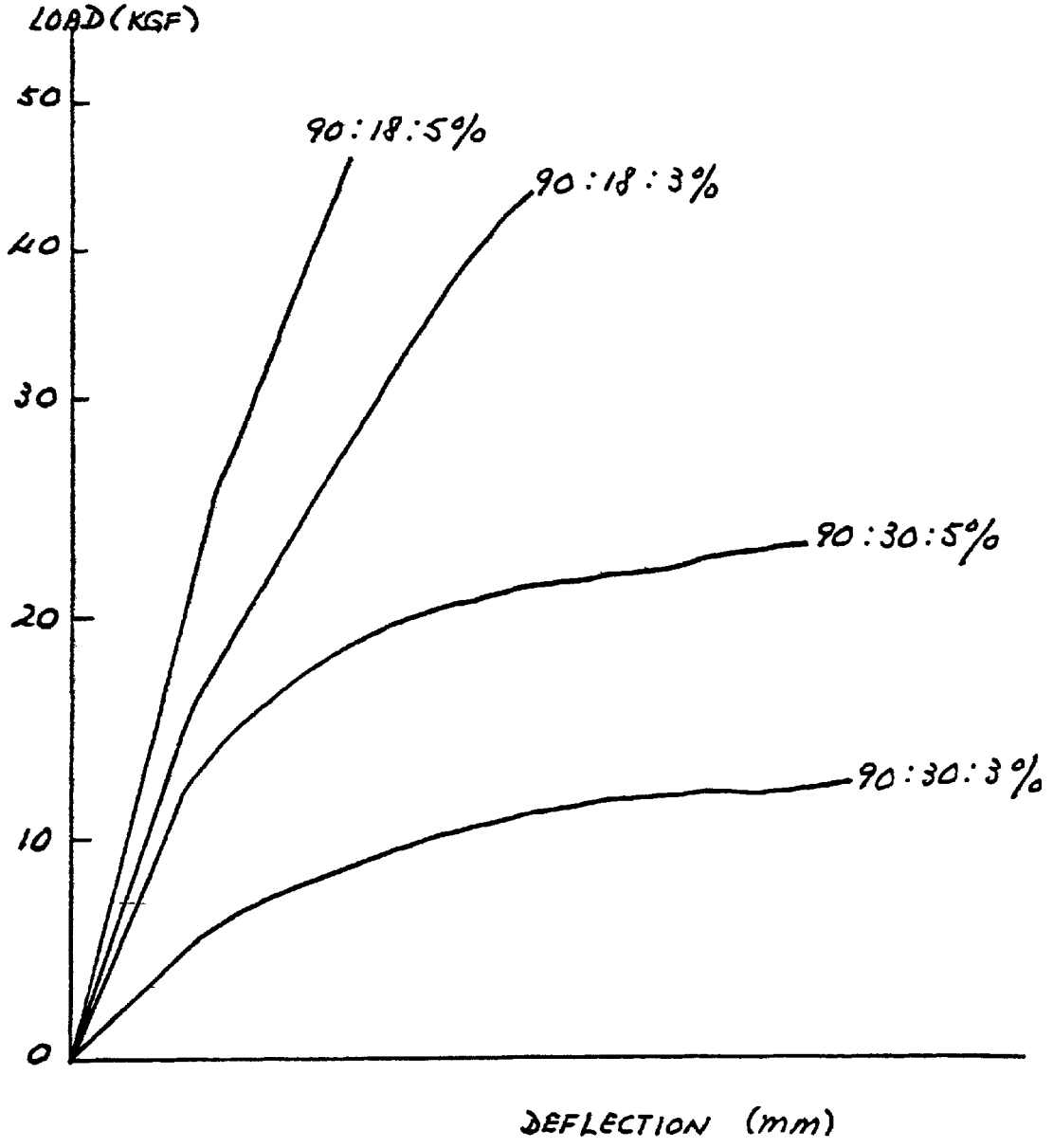

Fig. (4.12) Typical load / deflection graphs for varying glass fibre content

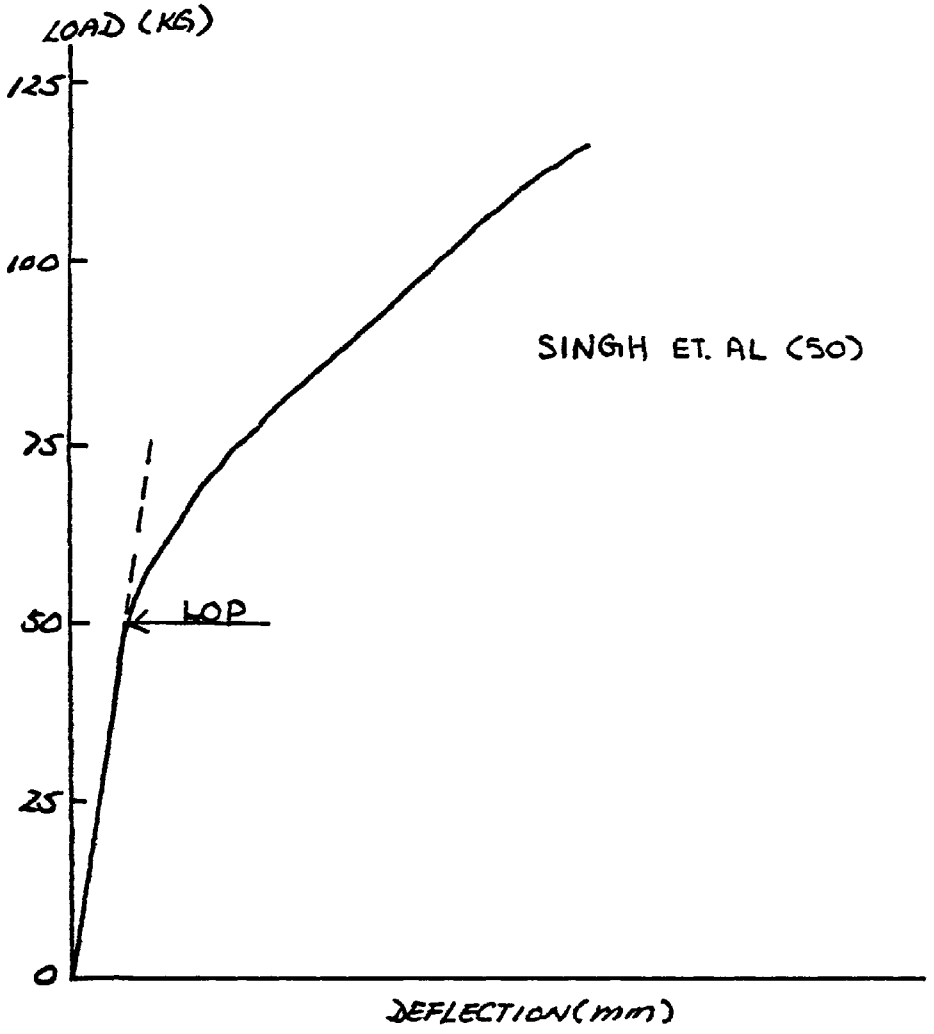

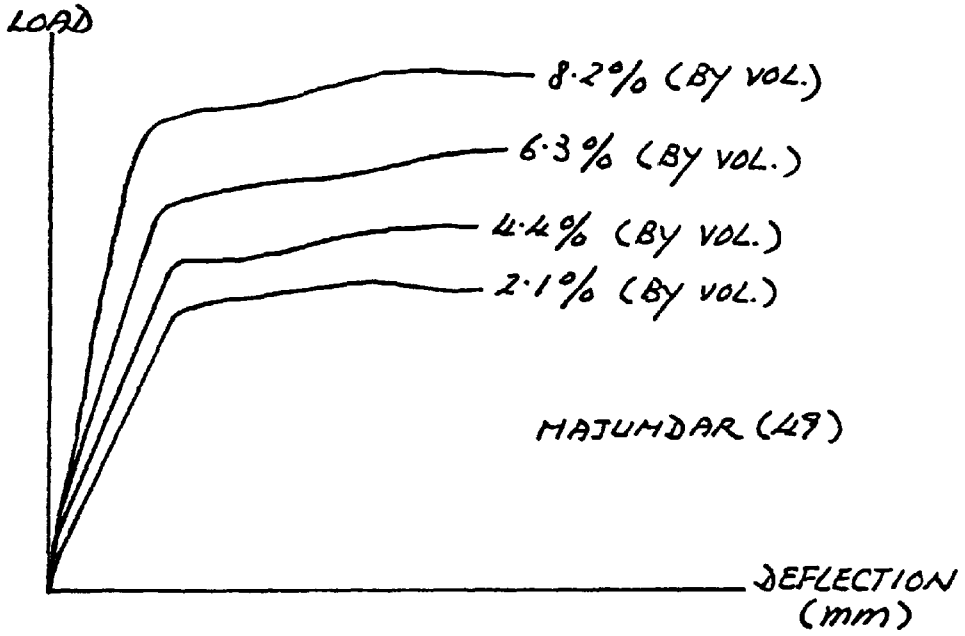

Fig. (4.13) Typical load / deflection graphs for varying glass fibre content obtained by previous researchers

Table(4.1) Fracture toughness for varying glass fibre content and notch-depth/width ratio. (50 X 50mm)

	Fracture Toughness, K_I, $MN/M^{3/2}$			
a / w	90 30 3%	90 30 5%	90 18 3%	90 18 5%
0.40	0.0197	0.0293	0.0424	0.0229
	0.0191	0.0316	0.0375	0.0259
	0.0255	0.0430	0.0306	0.0247
	0.0241	0.0407	0.0341	0.0247
Mean	0.0221	0.0362	0.0362	0.0246
Coeff. of Var.	14.385	18.574	13.913	5.038
0.50	0.0268	0.0325	0.0384	0.0334
	0.0204	0.0325	0.0384	0.0321
	0.0278	0.0362	0.0234	0.0327
	0.0247	0.0541	0.0354	0.0293
Mean	0.0249	0.0402	0.0333	0.0319
Coeff. of Var.	13.166	23.711	20.198	5.638
0.60	0.0326	0.0495	0.0216	0.0323
	0.0306	0.0317	0.0223	0.0272
	0.0341	0.0491	0.0282	0.0395
	0.0308	0.0518	0.0320	0.0313
Mean	0.0320	0.0455	0.0260	0.0326
Coeff. of Var.	5.152	20.413	19.069	15.708

Table(4.2) Fracture toughness for varying glass fibre content and notch-depth/width ratio. (100 X 100mm)

	Fracture Toughness, K_I, $MN/M^{3/2}$			
a/w	90 30 3%	90 30 5%	90 18 3%	90 18 5%
0.40	0.029	0.038	0.025	0.034
	0.026	0.036	0.024	0.025
	0.040	0.040	0.018	0.041
	0.033	0.039	0.030	0.046
Mean	0.032	0.038	0.024	0.036
Coeff. of Var.	17.968	4.324	20.129	25.695
0.50	0.037	0.042	0.026	0.020
	0.029	0.019	0.030	0.033
	0.029	0.032	0.026	0.051
	0.0257	0.0201	0.025	0.034
Mean	0.030	0.028	0.027	0.034
Coeff. of Var.	16.549	38.869	7.487	37.170
0.60	0.027	0.030	0.033	0.032
	0.029	0.036	0.034	0.022
	0.037	0.026	0.017	0.039
	0.026	0.026	0.028	0.051
Mean	0.030	0.030	0.028	0.036
Coeff. of Var.	16.874	16.075	27.096	33.648

Table(4.3) Summarised fracture toughness results for varying fibre content (50 X 50mm).

	Mix Details			
	90 30 3%	90 30 5%	90 18 3%	90 18 5%
Fracture Toughness ($MN/M^{3/2}$)	0.026	0.041	0.032	0.030
Coeff. of Variation	19.38	11.48	16.51	14.92

Table(4.4) Summarised fracture toughness results for varying glass fibre content (100 X 100mm).

	Mix Details			
	90 30 3%	90 30 5%	90 18 3%	90 18 5%
Fracture Toughness ($MN/m^{3/2}$)	0.031	0.032	0.026	0.036
Coeff. of Variation	3.64	16.44	7.69	3.35

Table(4.5) Fracture toughness for varying notch-depth/ width ratio (100 X 100mm)

a/w	Fracture Toughness, K_I, $MN/M^{3/2}$			
0.40	0.045	0.047	0.044	0.047
	0.048	0.036	0.048	0.037
	0.047	0.055	0.045	0.050
	0.046	0.060	0.054	0.051
	0.033	0.041	0.034	0.046
	0.047	0.051	0.042	0.038
	0.045	0.046	0.039	0.044
	0.041	0.046	0.040	0.041
	0.036	0.032	0.037	0.041
	0.044	0.034	0.042	0.043
0.50	0.041	0.056	0.041	0.043
	0.048	0.038	0.047	0.046
	0.045	0.037	0.047	0.049
	0.041	0.041	0.047	0.052
	0.042	0.027	0.044	0.037
	0.038	0.038	0.038	0.034
	0.043	0.043	0.049	0.035
	0.033	0.040	0.043	0.031
	0.049	0.039	0.040	0.038
	0.035	0.043	0.039	0.044
0.60	0.033	0.037	0.033	0.034
	0.041	0.036	0.034	0.033
	0.046	0.043	0.033	0.043
	0.039	0.041	0.037	0.033
	0.031	0.028	0.032	0.032
	0.033	0.041	0.031	0.027
	0.028	0.032	0.034	0.037
	0.037	0.032	0.031	0.033
	0.028	0.038	0.030	0.026
	0.041	0.037	0.035	0.035

Table(4.6) Fracture toughness for varying notch-depth/ width ratio (150 X 150mm)

a/w	Fracture Toughness, K_I, $MN/M^{3/2}$			
0.40	0.035	0.040	0.048	0.042
	0.040	0.043	0.049	0.039
	0.049	0.038	0.036	0.046
	0.048	0.045	0.041	0.040
	0.041	0.048	0.028	0.032
	0.036	0.037	0.036	0.034
	0.039	0.041	0.027	0.037
	0.035	0.035		
0.50	0.035	0.043	0.049	0.037
	0.035	0.034	0.039	0.039
	0.035	0.036	0.040	0.033
	0.024	0.034	0.030	0.034
	0.028	0.035	0.032	0.040
	0.046	0.041	0.042	0.049
	0.035	0.031	0.033	0.033
	0.037	0.038		
0.60	0.027	0.027	0.030	0.034
	0.031	0.033	0.035	0.030
	0.027	0.027	0.027	0.037
	0.021	0.022	0.027	0.028
	0.031	0.030	0.029	0.029
	0.032	0.029	0.030	0.029
	0.035	0.037	0.036	0.032
	0.034	0.029		

Table(4.7) Summarised fracture toughness values for varying notch-depth/width ratio (100 X 100mm).

$\frac{a}{w}$	0.40	0.50	0.60
Fracture Toughness K_I $MN/M^{3/2}$	0.044	0.042	0.035
Coeff. of Variation	10.58	8.407	8.779

Table(4.8) Summarised fracture toughness values for varying notch-depth/width ratio (150 X 150mm)

$\frac{a}{w}$	0.40	0.50	0.60
Fracture Toughness K_I, $MN/M^{3/2}$	0.039	0.037	0.030
Coeff. of Variation	11.40	11.41	8.83

Table(4.9) Fracture Toughness index for varying notch-depth/width ratios (100 X 100mm).

a/w	Fracture Toughness Index		
0.40	0.911	0.919	0.958
	0.946	0.949	0.927
	0.953	0.941	0.969
	0.971	0.956	0.931
	0.932	0.904	0.930
	0.935	0.940	0.927
	0.919	0.958	0.913
	0.922	0.894	0.901
	0.882	0.925	0.902
	0.901	0.899	0.930
	0.906	0.956	
0.50	0.909	0.931	0.887
	0.915	0.926	0.919
	0.860	0.935	0.918
	0.899	0.893	0.913
	0.887	0.929	0.879
	0.940	0.894	0.894
	0.914	0.903	0.890
	0.906	0.880	0.898
	0.924	0.875	0.917
	0.895	0.899	0.873
	0.885	0.862	0.905
	0.875		
0.60	0.963	0.966	0.915
	0.945	0.925	0.921
	0.928	0.854	0.898
	0.901	0.910	0.918
	0.899	0.909	0.901
	0.899	0.884	0.907
	0.892	0.946	0.905
	0.927	0.902	0.895
	0.894	0.904	0.901
	0.887	0.926	0.891
	0.884	0.896	0.894
	0.892	0.904	0.895
	0.879		

Table(4.10) Fracture Toughness index for varying notch-depth/width ratios (150 X 150mm).

a/w	Fracture Toughness Index		
0.40	0.949	0.929	0.951
	0.951	0.967	0.966
	0.974	0.953	0.936
	0.950	0.951	0.961
	0.942	0.942	0.967
	0.957	0.928	0.962
	0.937	0.943	0.946
	0.932	0.911	0.942
	0.920	0.946	0.932
	0.937	0.966	
0.50	0.939	0.912	0.915
	0.915	0.946	0.939
	0.924	0.895	0.955
	0.935	0.921	0.929
	0.948	0.941	0.963
	0.917	0.940	0.930
	0.959	0.878	0.913
	0.920	0.875	0.913
	0.915	0.942	0.931
	0.904	0.920	0.951
0.60	0.953	0.921	0.952
	0.941	0.947	0.922
	0.907	0.924	0.941
	0.961	0.953	0.924
	0.929	0.943	0.941
	0.907	0.946	0.930
	0.921	0.892	0.934
	0.916	0.946	0.912
	0.912	0.939	0.930
	0.894	0.914	0.920

Table(4.11) Summarised fracture toughness index for varying notch-depth/width ratio (100 X 100mm).

	a/w		
	0.40	0.50	0.60
Mean Fracture Toughness Index	0.926	0.900	0.907
Coeff. of Variation (%)	2.00	1.10	1.90
No. of Specimen	32	34	37

Table(4.12) Summarised fracture toughness index for varying notch-depth/width ratio (150 X 150mm).

	a/w		
	0.40	0.50	0.60
Mean Fracture Toughness Index	0.946	0.927	0.929
Coeff. of Variation	0.80	1.40	1.00
No. of Specimen	29	30	30

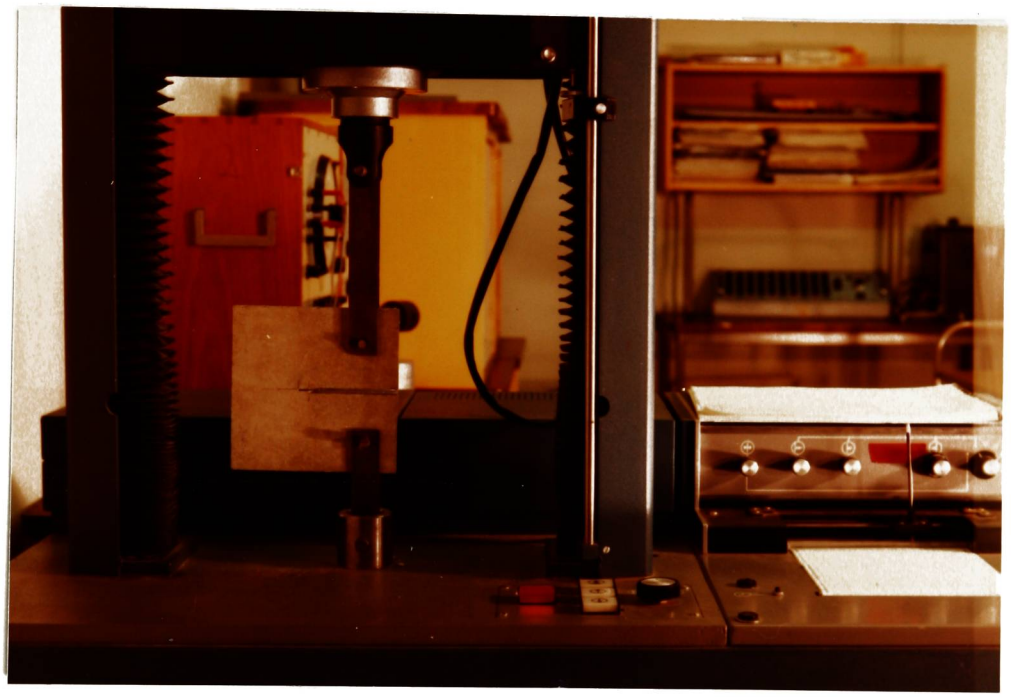

PLATE. 4.1

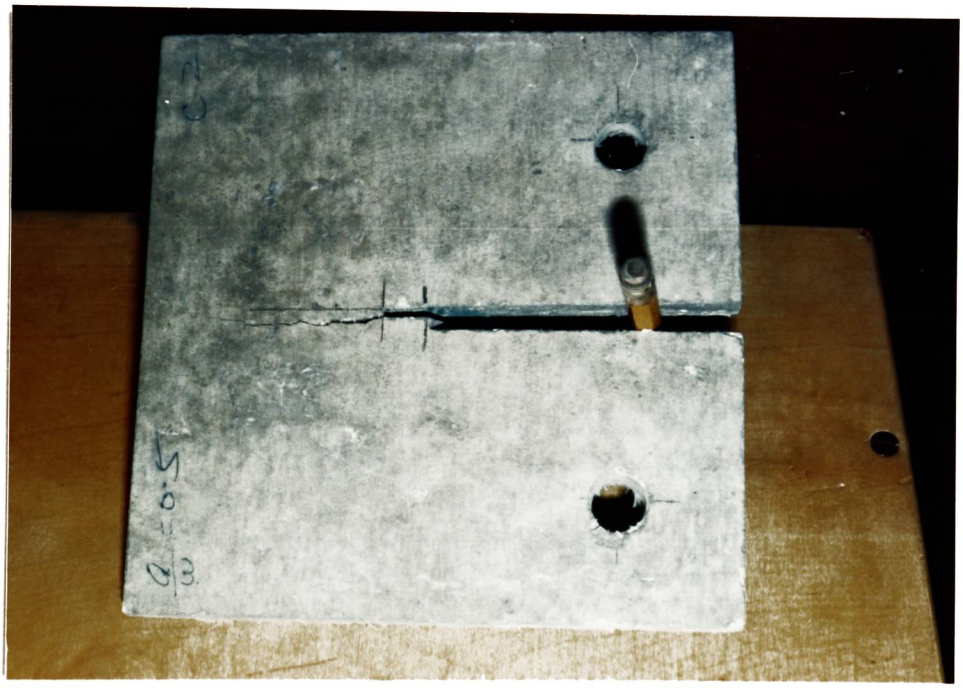

PLATE. 4.2

CHAPTER FIVE

IN-PLANE SHEAR STRENGTH OF POLYPROPYLENE FIBRE-REINFORCED CONCRETE

5.1 INTRODUCTION

Many attempts have been made to investigate the general properties of fibre-reinforced cementitious materials. These included the use of tests to determine the tensile, flexural and toughness strengths etc.. The shear strength of fibre-reinforced cementitious materials has received very little attention. The test methods for shear strength are less well developed than those for other properties. Even for materials where shear testing is well established the results are subjected to considerable variation.

Oakley and Unsworth(51) described three test methods to determine the shear strength of glass fibre-reinforced cement composite materials. These methods included the determination of interlaminar shear strength, in plane shear strength and the punch through shear strength. The definitions of the shear strengths and their corresponding specimen geometries are shown in Fig.(5.1). Oakley and Unsworth(51) concluded that shear strengths were more difficult to determine experimentally than other material properties. The simple "opposed notch" method that has been used to measure the interlaminar shear strength underestimated the true value. The experimentally simpler short beam shear method was complicated by the difficultly of ensuring that the span/thickness ratio produced the

correct failure mode. Tests for in-plane and punch through shear strengths were more successful; they could be carried out on most types of glass fibre-reinforced cements and the values obtained in these experiments were always higher than those for interlaminar shear strength.

The experimental work described in this chapter was to investigate the in-plane shear strength of plain concrete and polypropylene fibre-reinforced concrete. Addition of polypropylene fibre content in concrete was studied. The effect of the specimen geometry on the in-plane shear strength was also carried out in the experimental work.

5.2 TEST SPECIMEN GEOMETRIES

The general configuration of in-plane shear strength specimen(100 X 100 X 200mm) is shown in Fig.(5.2). The specimen size was kept constant throughout the tests. The slot separation between the opposite double notches of the specimen was ranging from 20mm to 50mm. The opposite double notches were of 50mm depth and were kept constant throughout the tests.

The in-plane shear strength test is carried out using modified concrete beams(100 X 100 X 200mm). The beams were notched by means of a clipper masonry saw which was fitted

with a 14 inches(355.6mm) diameter carborundum blade along two opposite faces as shown in Fig.(5.2). The load was applied by means of two 11mm square, 100mm long steel bars, as shown in Plate(5.1). The point of application of the load was assumed to be at the middle of the steel bars.

5.3 EXPERIMENTAL DETAILS

A standard concrete mix was used throughout the experimental work. The mix details were the same as in the split-cube tests. The water/cement ratio was kept constant at 0.5 but with an allowance made for absorption of moisture by the aggregates. The constituents were mixed in a 2 cubic foot pan mixer and the specimens compacted on a vibrating table.

The polypropylene fibre used was of 12,000 denier (700m/kg.) in 50mm single size strand. The fibres were added in percentages by weight (of the total wet solids) in multiples of 0.05 up to a maximum of 0.3 percent. The specimens were cured under water and tested at 28 days.

All the in-plane shear strength tests were carried out by means of a 1251 Model Instron machine. The tests were carried out at nominal room temperature. The load-deflection curves were plotted autographically from the Instron system. The failure load achieved was taken as

the peak load obtained from the load-deflection curve.

The mixing procedure in these experiments was similar to the procedure for the split-cube tests so that 'balling' of the fibres during mixing would be avoided.

5.4 THEORY OF IN-PLANE SHEAR STRENGTH

The method chosen to measure the in-plane shear strength of polypropylene fibre-reinforced concrete was based on the double notched specimen. Oakley and Unsworth(51) concluded that this test could be carried out on most types of glass fibre-reinforced cement composite materials. The in-plane shear strength can be determined using the following expression:

$$\text{In-plane shear strength, } \tau = \frac{\text{Failure load}}{\text{Sample thickness X Slot separation}} \qquad (5.1)$$

The failure load was obtained from the load-deflection curve and the sample thickness was kept constant (100mm) throughout the tests. The slot separation between the opposite notches was measured for each test. In practice, small variation of the slot separation was introduced in the specimens. In order to improve the accuracy of the tests, these variations have been taken into account when the in-plane shear strength results were determined.

5.5 DISCUSSION OF THE TEST RESULTS

The experimental results of in-plane shear strength tests are shown in Table(5.1). The in-plane shear strength with varying slot separation/depth ratios and polypropylene fibre contents are summarised in Table(5.2). The relationship between shear strengths and slot separation/depth ratios are illustrated graphically in Fig.(5.3-5.9). It is seen that the varying slot separation/depth ratio does not affect the in-plane shear strength either in the plain concrete or polypropylene fibre-reinforced concrete. Oakley and Unsworth(51) stressed that the in-plane shear strength was likely to be slit separation dependent. This difference is probably due to the effect of the thickness of the specimen employed. The stress in the thinner specimen tends to zero in the thickness direction and the specimen can be considered as having two free surfaces.Thus the in-plane shear strength is varying with the slit separation/depth ratio. In this study, adequate thickness (100mm) of the specimen was employed in all tests and the experimental results showed that the in-plane shear strength was independent of the slot separation/depth ratio.

The in-plane shear strengths with varying polypropylene fibre content results are illustrated

graphically in Figs.(5.10-5.13). Addition of polypropylene fibre in concrete has little effect on the in-plane shear strength. The results are summarised in Table(5.3). The comparison of the in-plane shear strength between the plain concrete and varying polypropylene fibre-reinforced concrete is illustrated in Fig.(5.14). The results show that the in-plane shear strength increases with the addition of the fibre up to the optimum fibre content of 0.15 percent. Beyond the optimum fibre content the in-plane shear strength reduces with further increasing fibre content. This is most likely due to insufficient compaction of the excess polypropylene fibre in concrete which leads to the shear strength being reduced beyond the optimum fibre content.

The coefficient of variation for the in-plane shear strength results are shown in Table(5.2). The correlation of the results rangesfrom 7.6 percent to 28.9 percent in all cases. In general, the coefficient of variation decreases with the slot separation/depth ratio increases. From the experimental results shown, the slot separation/depth ratios of 0.20 and 0.25 give the more consistent values of shear strength. This is due to the problem encountered as the aggregate size becomes a great percentage of the area when failure occurs. This provides a more uniform matrix between the opposite notches than the other slot separation (20mm and 30mm) in the in-plane shear strength specimen.

Most of the specimens developed side cracking during the loading process as shown in Plate(5.2). The crack has a meandering path and tends to go around the aggregates rather than through them because of the crack arresting action of the aggragates. The side cracks and the meandering path of the main crack cause the energy demand for crack progagation to be increased, since the area of the new crack surfaces formed is greater than of a main crack which travels in a straight line. Moavenzadeh and Kuguel(16) measured the side cracks using quantitative microscopy in concrete and concluded that the total area of the side cracking could be as high as 20 times the nominal cross-sectional area of the beam; the crack area increased significantly even after the maxim um load was reached. The side crack effect does not influence the in-plane shear strength results in this study. This is due to the fact that the shear strength was determined from the "initial cracking" of the concrete specimen. The phenomenon of side cracking in concrete is similar to metals which exhibit plasticity near the crack tips. In both cases, side cracking in concretes and plasticity in metals demand more energy for failure.

Typical load-deflection graphs for varying fibre content are illustrated in Fig.(5.15). The curves show a linear response up to the point where the concrete fails and then the load reduces to a constant strength. In the

early stages of loading, the applied load is largely carried by the matrix alone. The initial cracking of the matrix results in the fibres controlling the crack behaviour until it is completed. The ultimate strength of the composite material is then dependent on the strength of the fibres, the degree of pullout and their orientation in the specimen. The in-plane shear strength is calculated from the ultimate load achieved. It is seen that the residual load increases with polypropylene fibre content. The pattern of the load-deflection curves are similar to the split-cube test results as shown in Fig.(3.10). The difference in magnitude of the residual strength in this shear test and split-cube test is most likely due to the loading systems in which sliding and crack opening mechanisms were encountered respectively.

The experimental work carried out in the early stages in the split cube tests and in-plane shear strength tests was only concerned with the peak load achieved in the load-deflection curve. The stress intensity factor and the shear strength of the plain and polypropylene fibre-reinforced concrete were determinedfrom the peak load achieved and the specimen geometry. Thus the detailed load-deflection graphs were not obtained in both cases. Using the typical load-deflection curves as shown in Fig.(3.10) and Fig.(5.15), typical fracture toughness index values were determined with varying polypropylene fibre content and loading system. The fracture toughness index

results are shown in Table(5.4). It is seen that the fracture toughness index increases with the addition of fibres in the concrete. Thus the toughness index can be used as the indication of the ductility of the fibre-reinforced composite materials. From the results shown, the split-cube specimens and the in-plane shear specimens give similar fracture toughness index values with constant fibre content. Thus the two types of specimens can be used to evaluate the toughness index of the fibre-reinforced composite materials.

From the coefficient of variation results shown in Table(5.2), it is necessary to further investigate the in-plane shear strength specimen. Future work should include the use of various types and sizes of aggregates so that the shear strengths may be compared among them. In order to reduce the coefficient of variation of the in-plane shear strength results, either larger specimen size (150 X 150 X 200mm) or smaller aggregates (less than 10mm size) may be used in future development. Since it is difficult to compare the results with other research workers, a numerical analysis is employed to examine the in-plane shear specimen which will be discussed in Chapter 7.

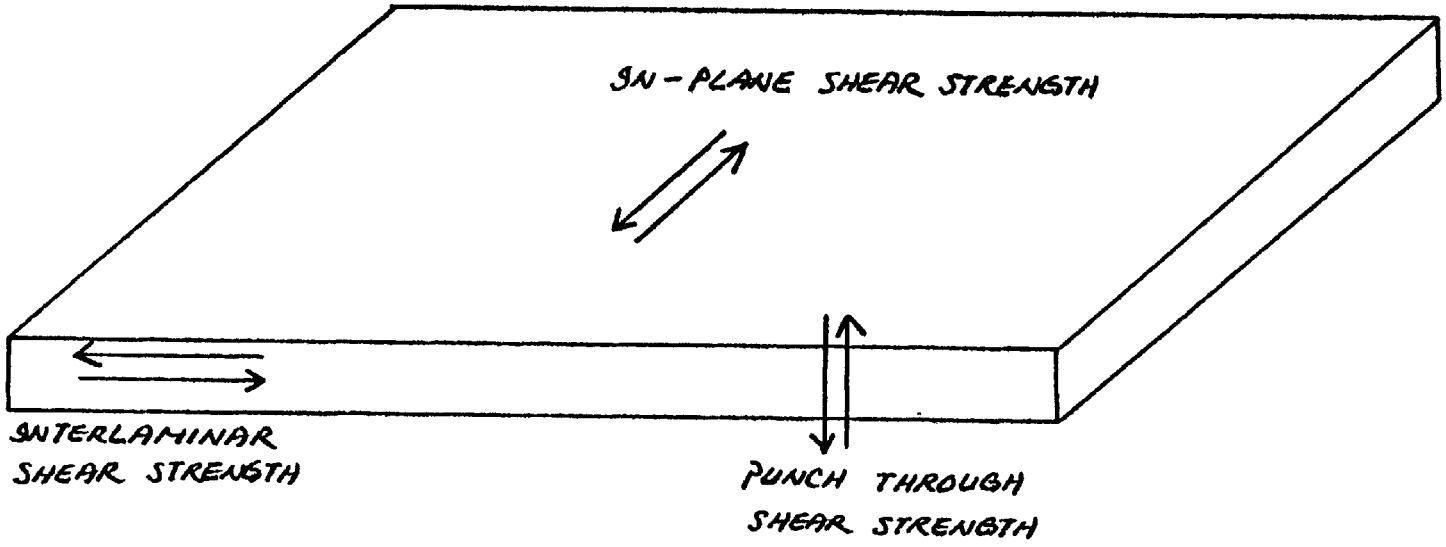

Fig. (5.1a) Definitions of shear strengths

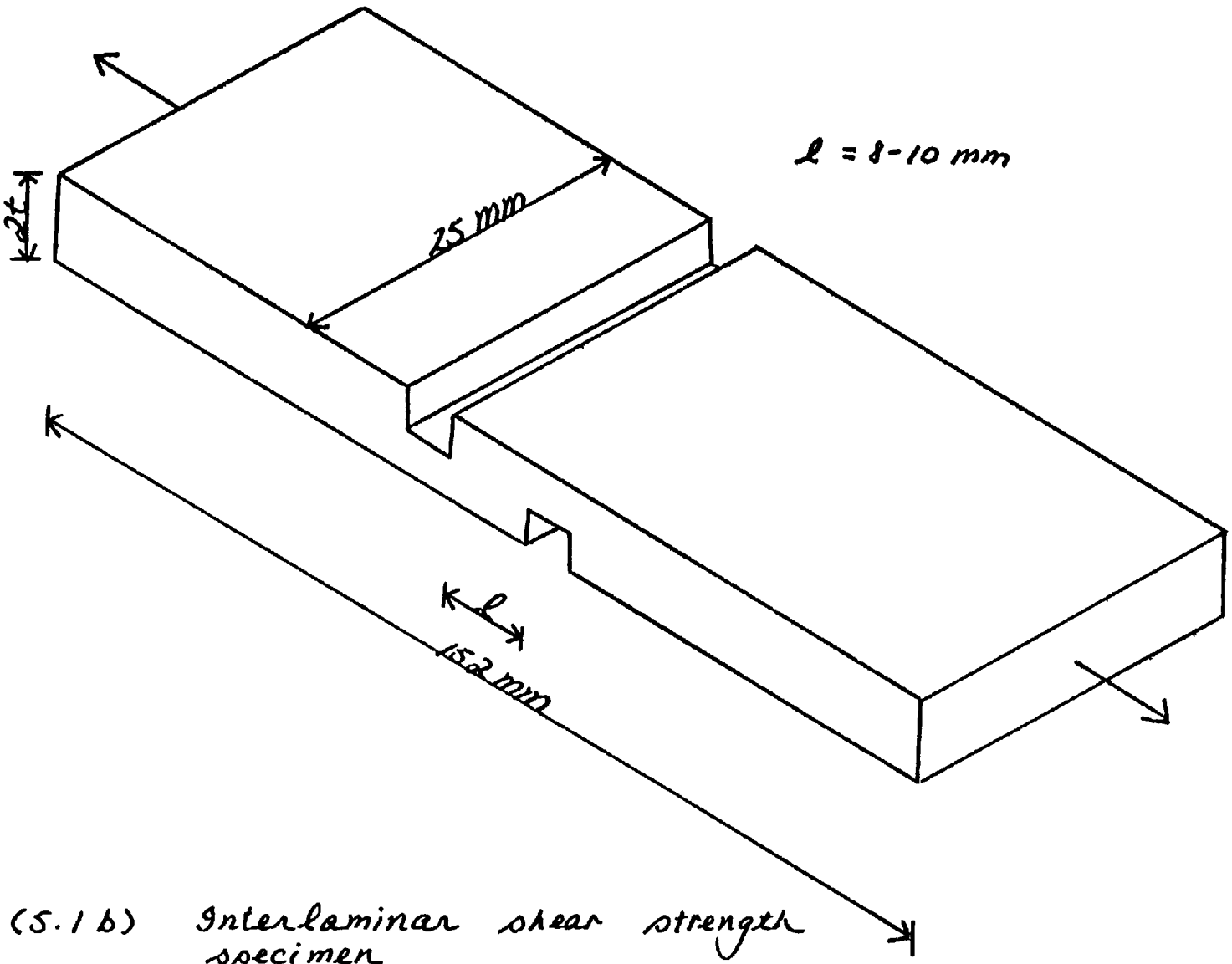

Fig. (5.1 b) Interlaminar shear strength specimen

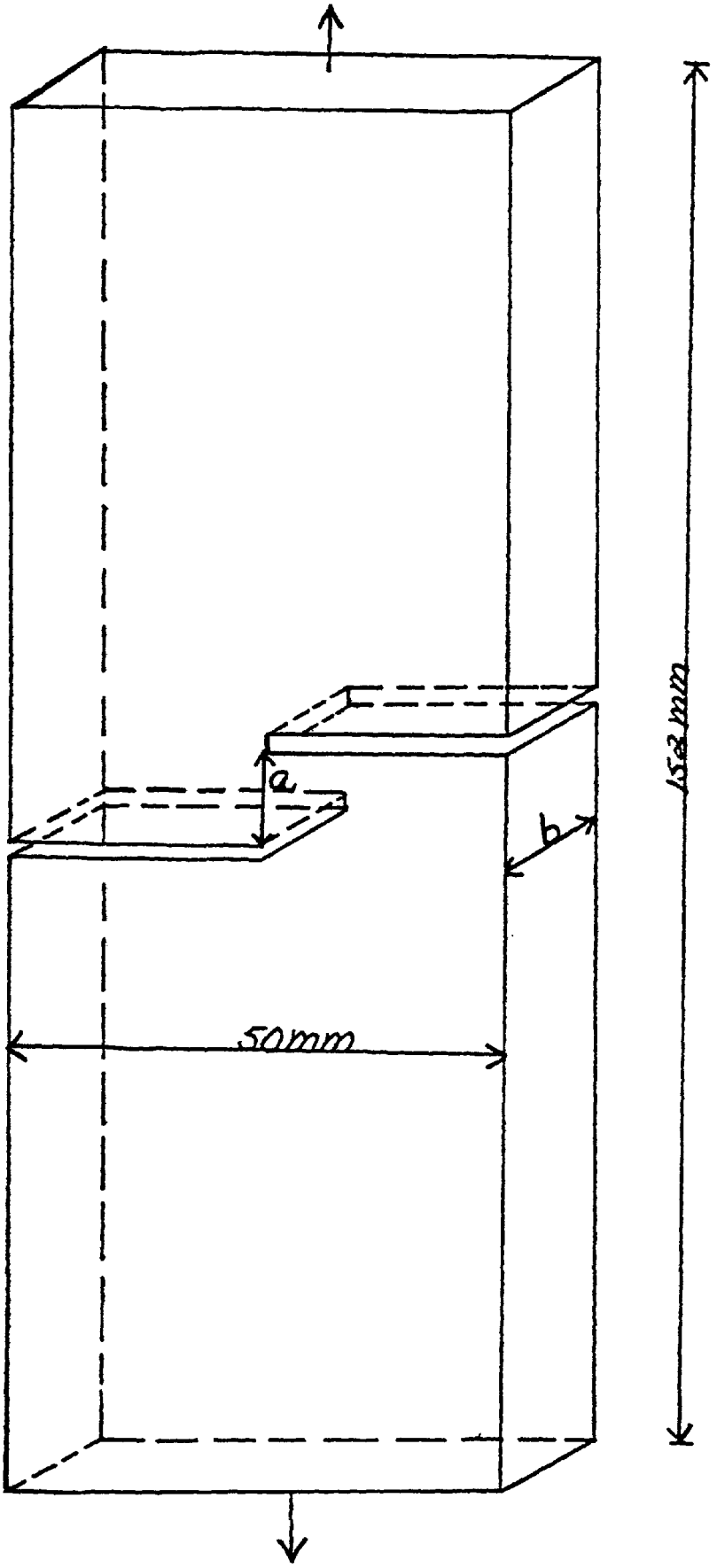

Fig. (5.1c) In plane shear strength specimen

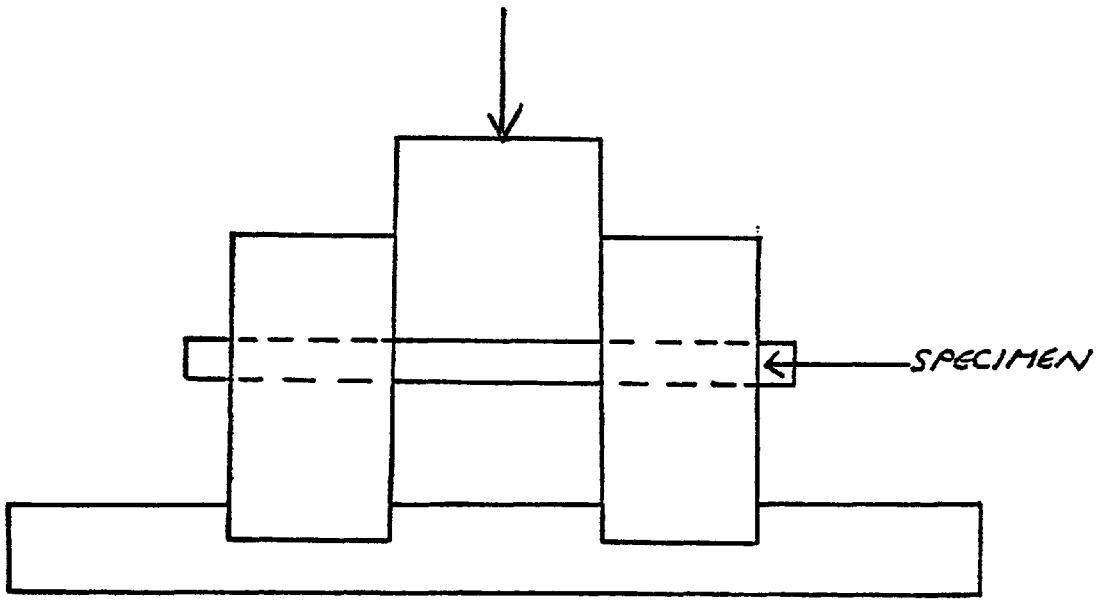

Fig. (5.1d) Punch through shear strength apparatus

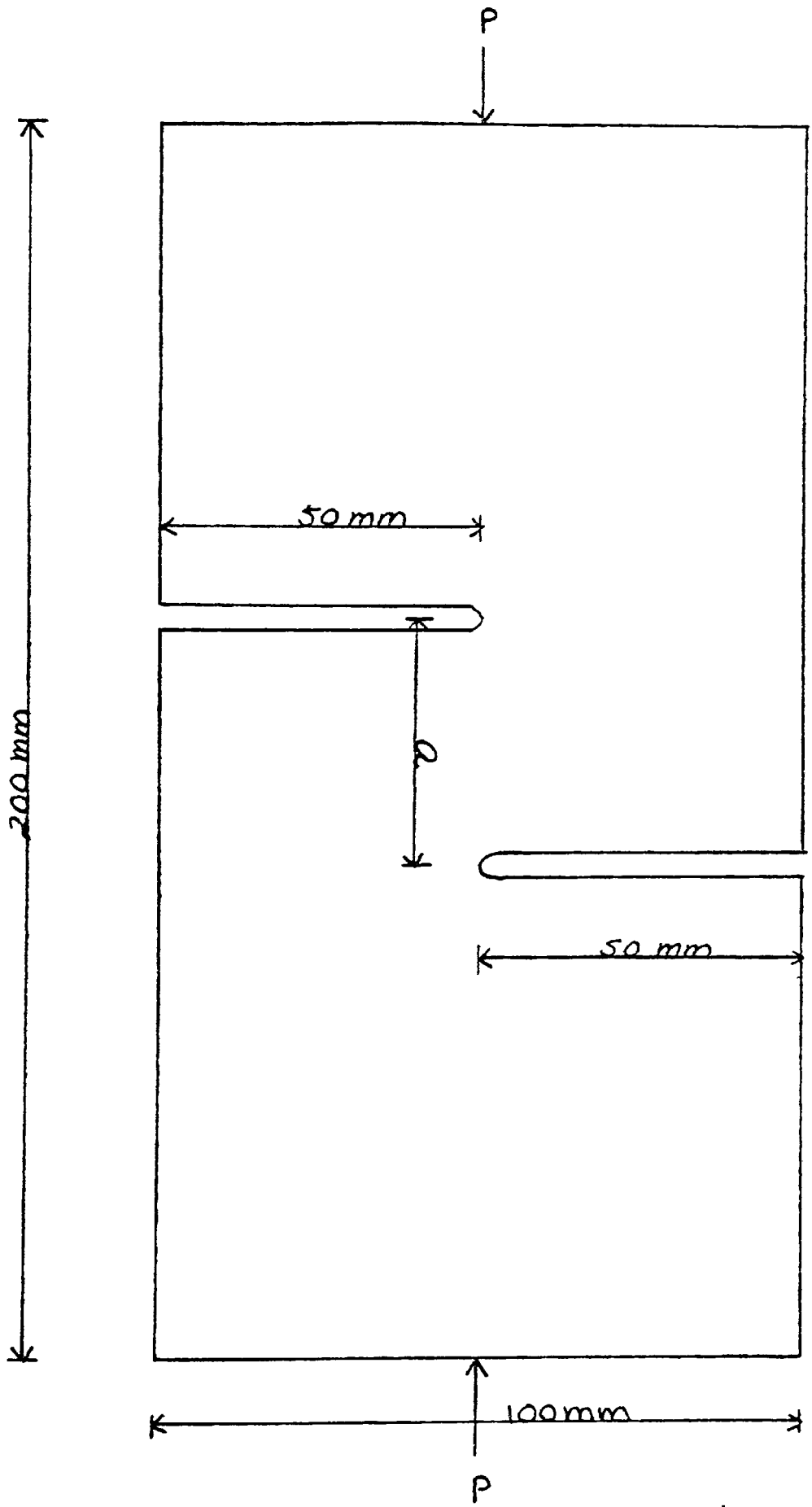

Fig. (5.2) General configuration of in plane shear specimen

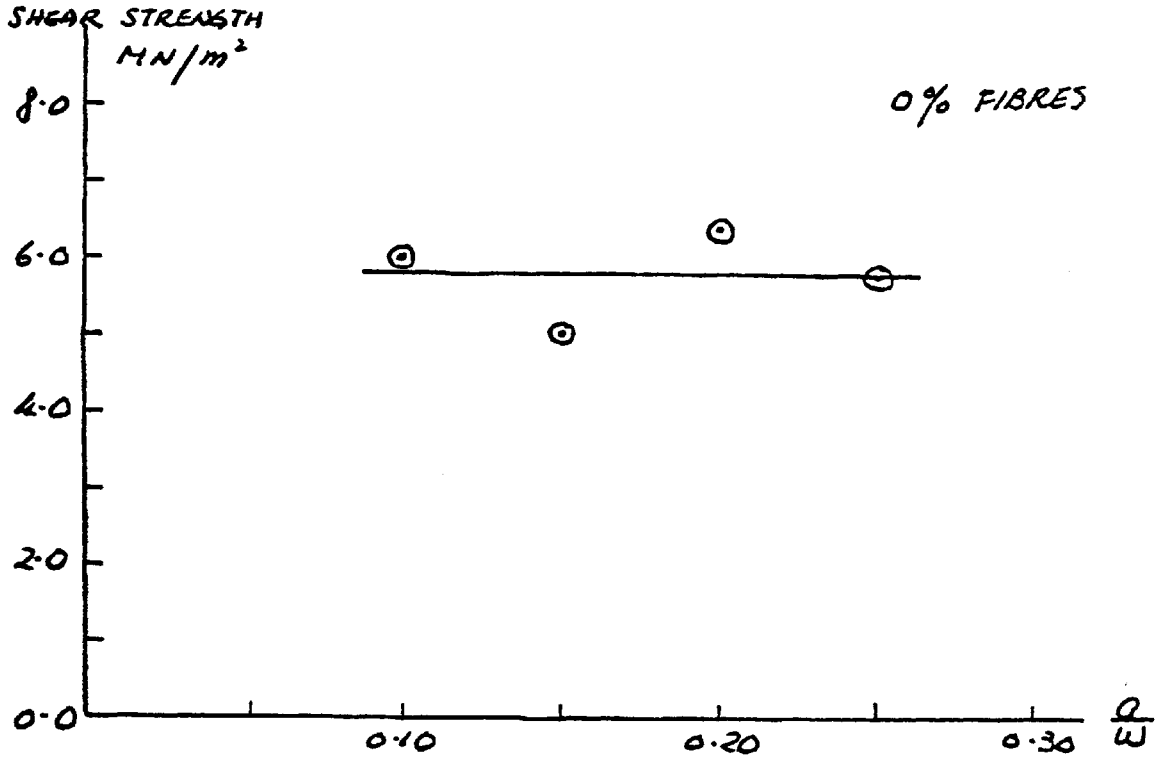

Fig. (5.3) In plane shear strength for varying slot separation ratio

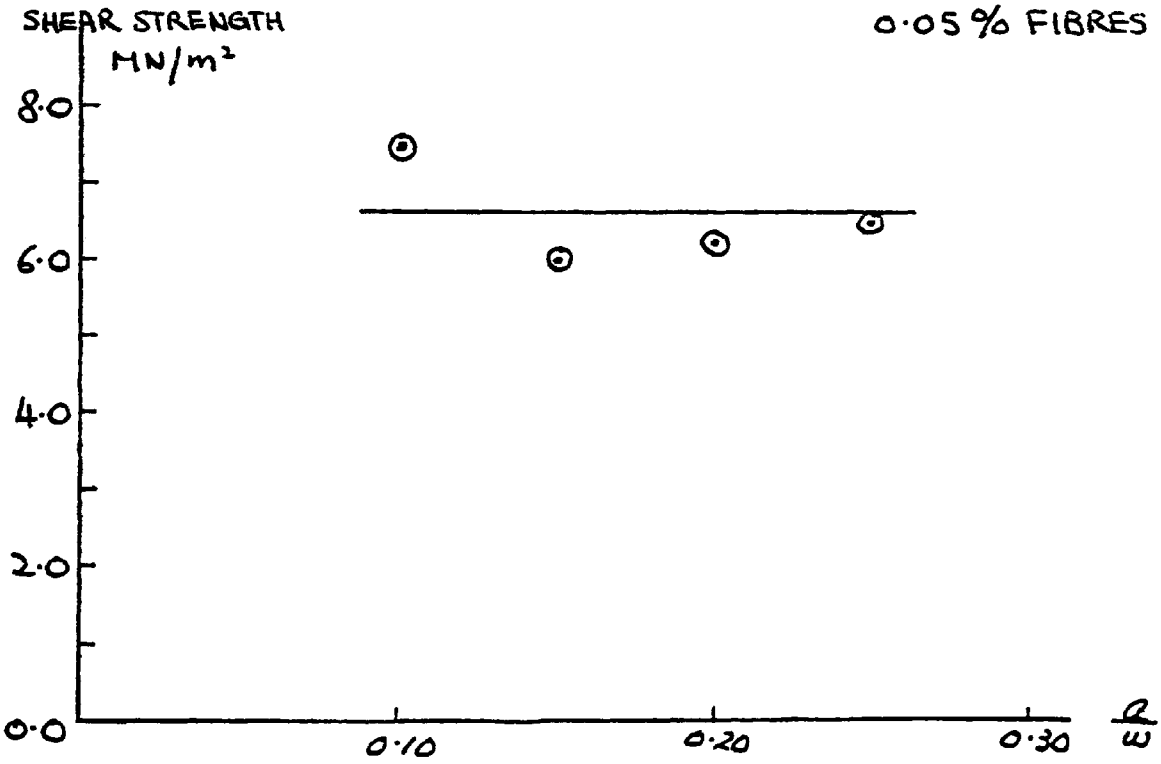

Fig. (5.4) In plane shear strength for varying slot separation ratio

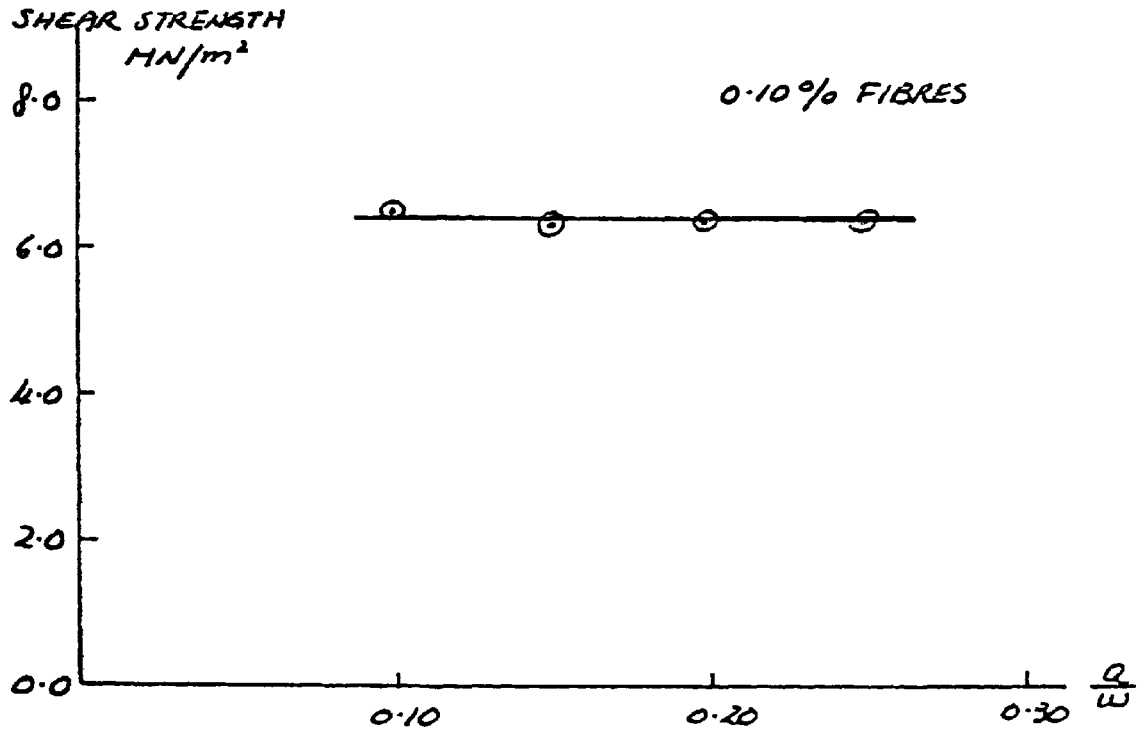

Fig. (5.5) In plane shear strength for varying slot separation ratio

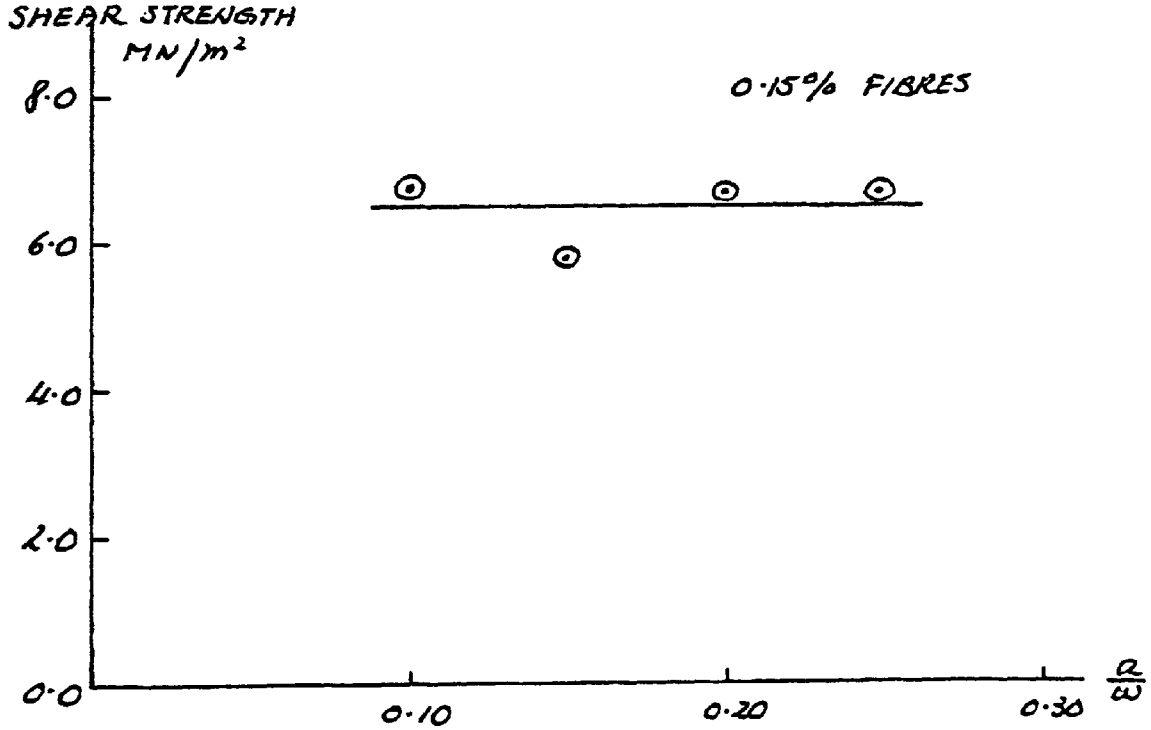

Fig. (5.6) In plane shear strength for varying slot separation ratio

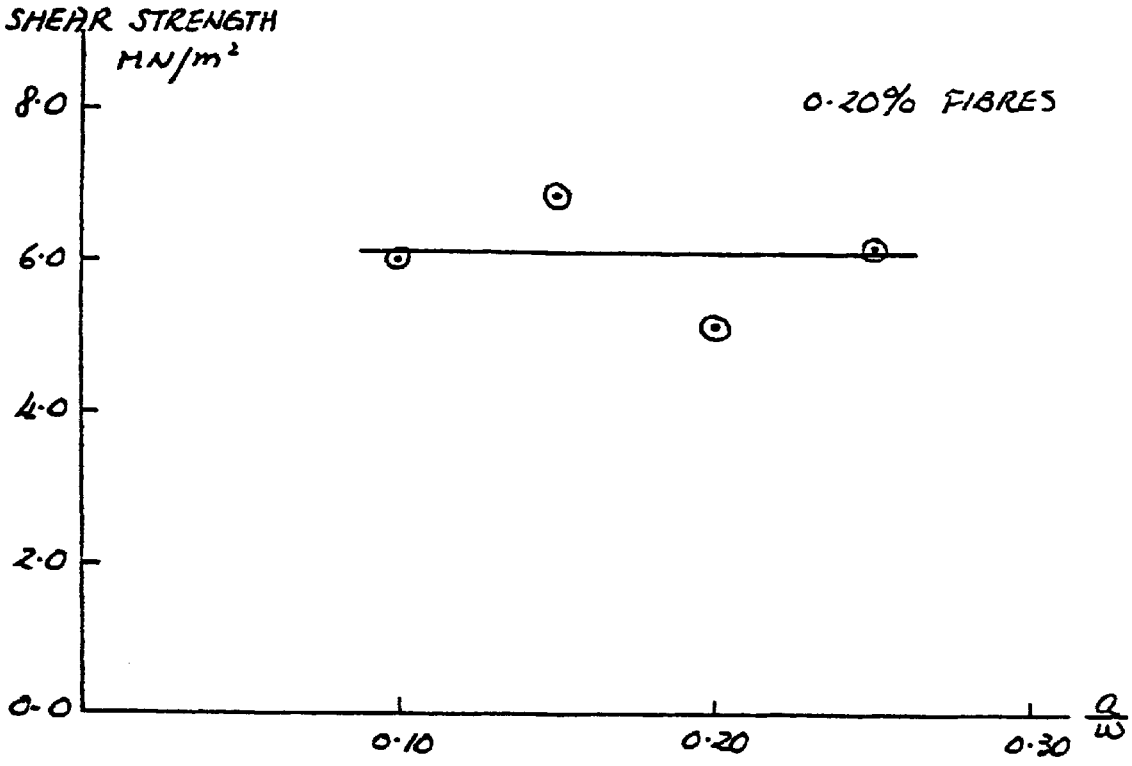

Fig. (5.7) In plane shear strength for varying slot separation ratio

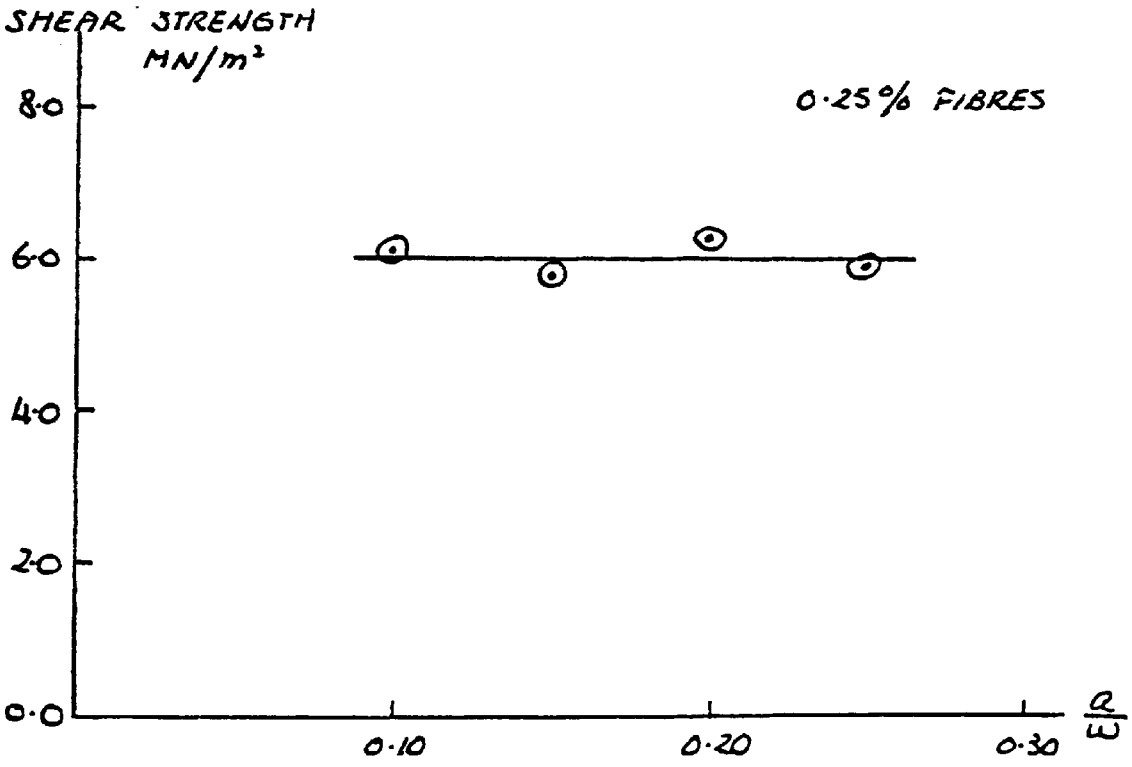

Fig. (5.8) In plane shear strength for varying slot separation ratio

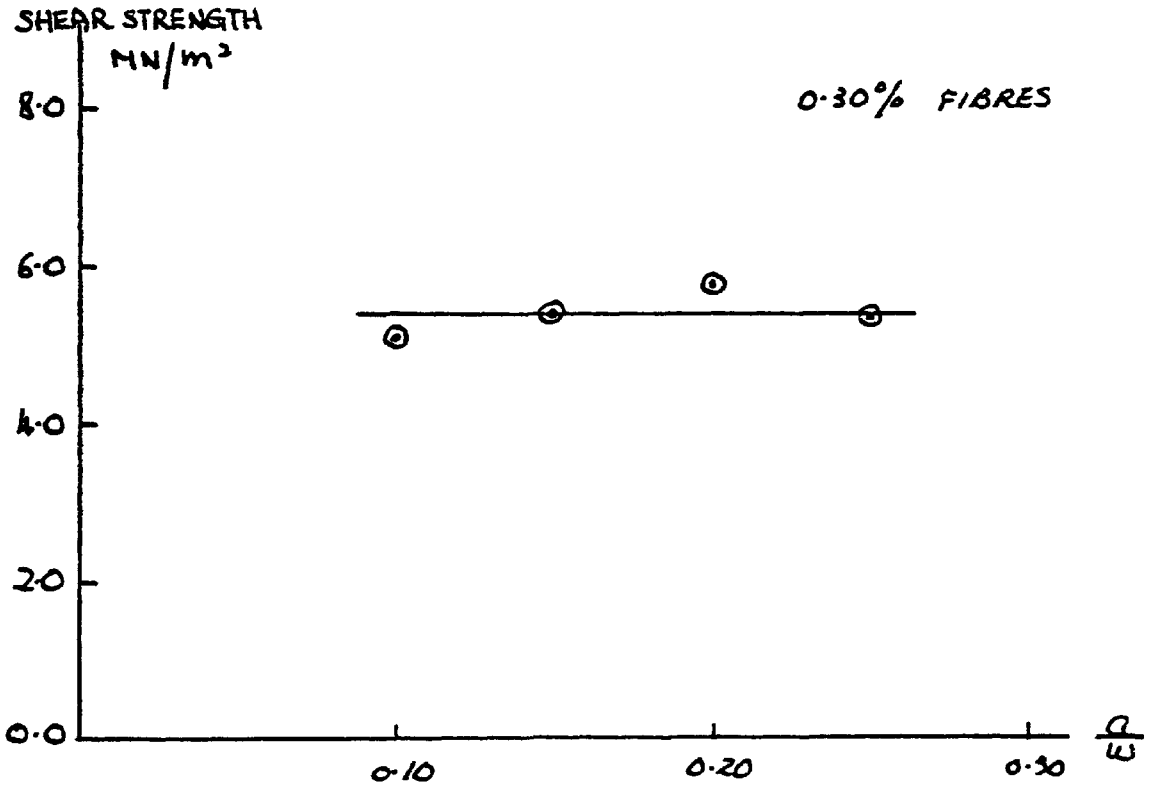

Fig. (5.9) In plane shear strength for varying slot separation ratio

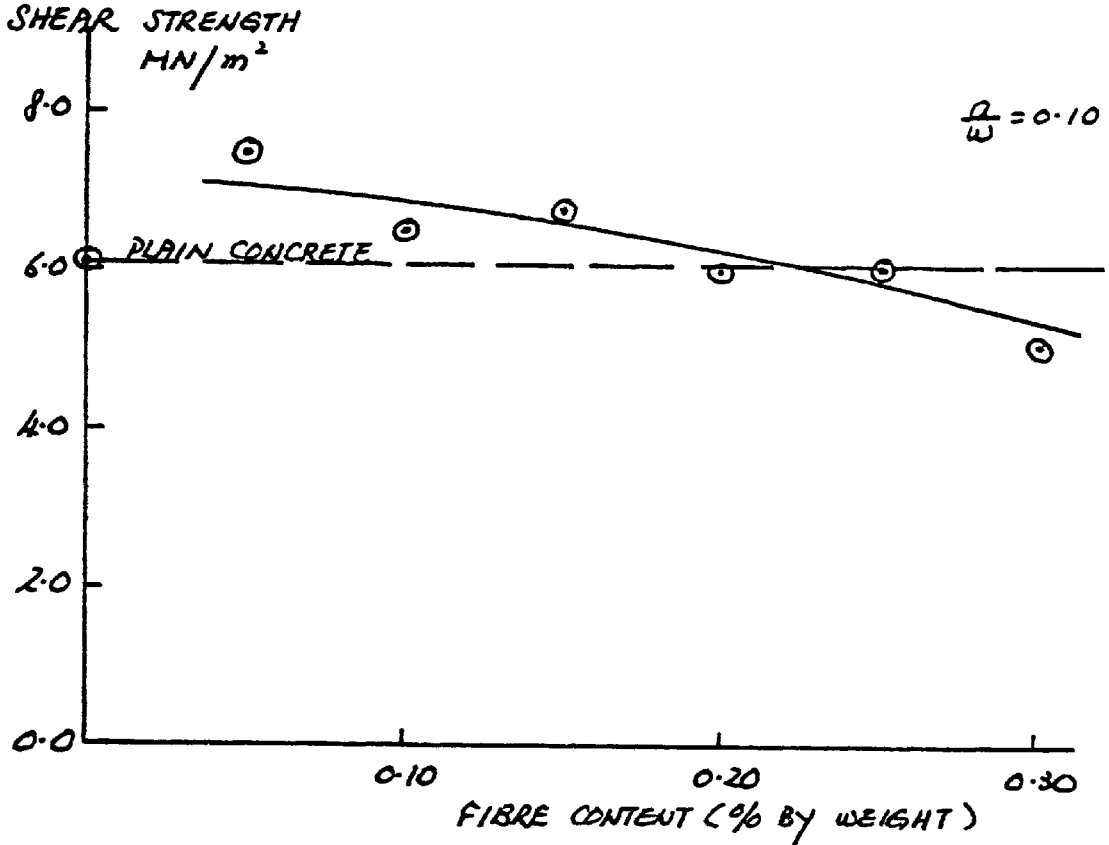

Fig. (5.10) In plane shear strength for varying fibre content

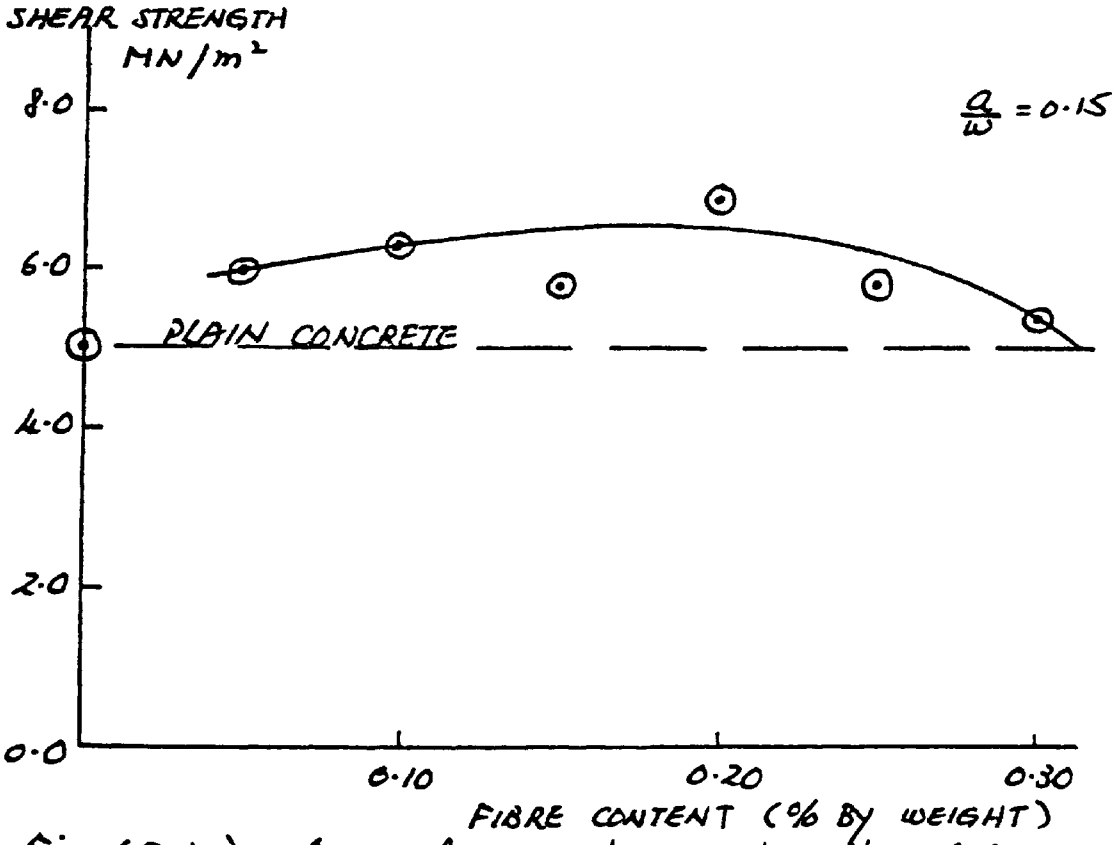

Fig. (5.11) In plane shear strength for varying fibre content

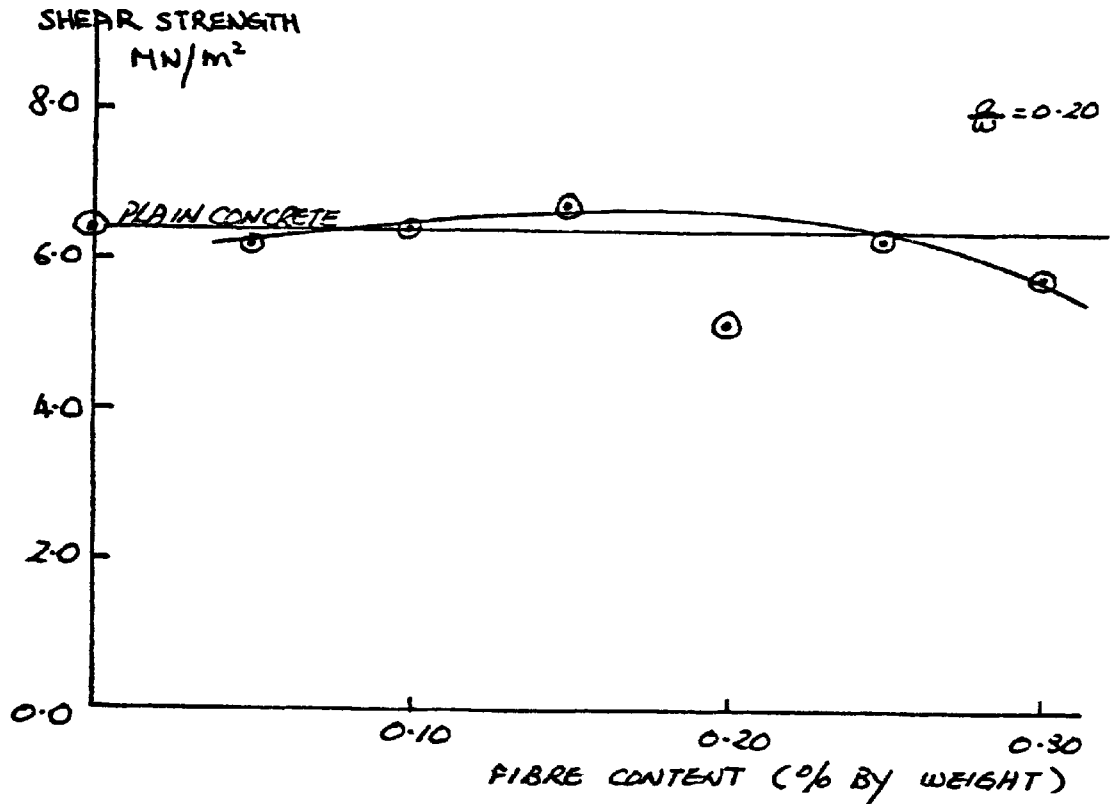

Fig. (5.12) In plane shear strength for varying fibre content

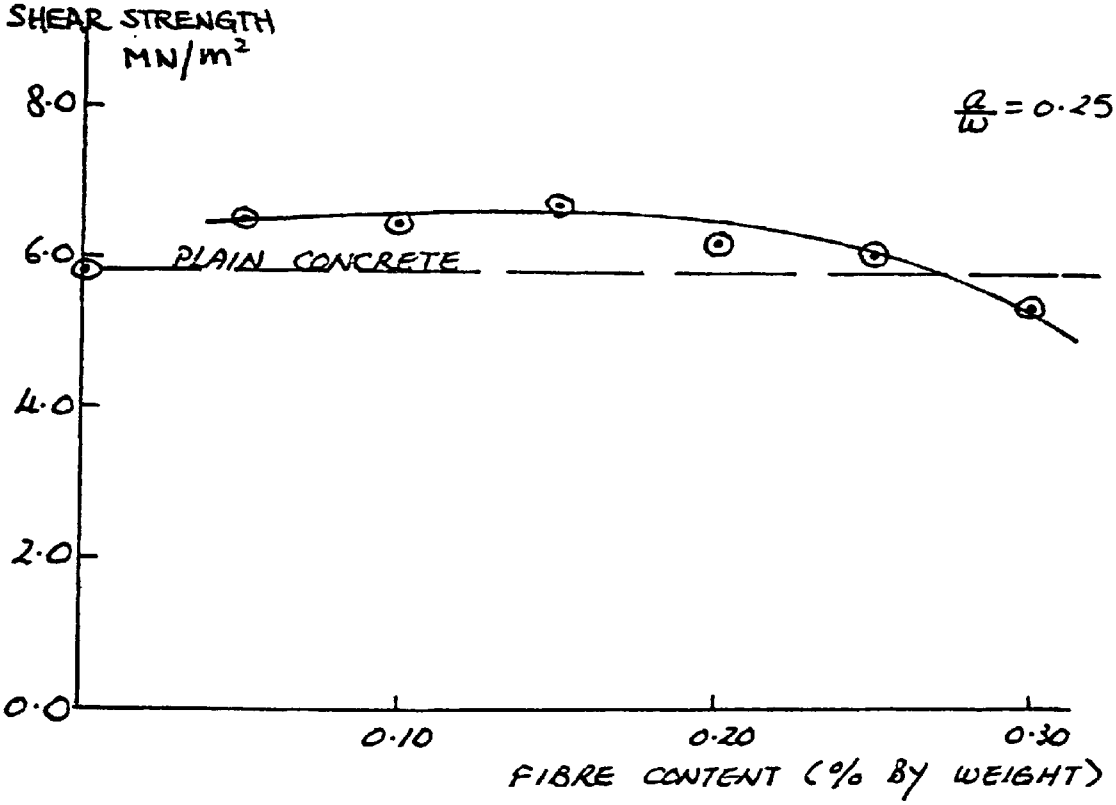

Fig. (5.13) In plane shear strength for varying fibre content

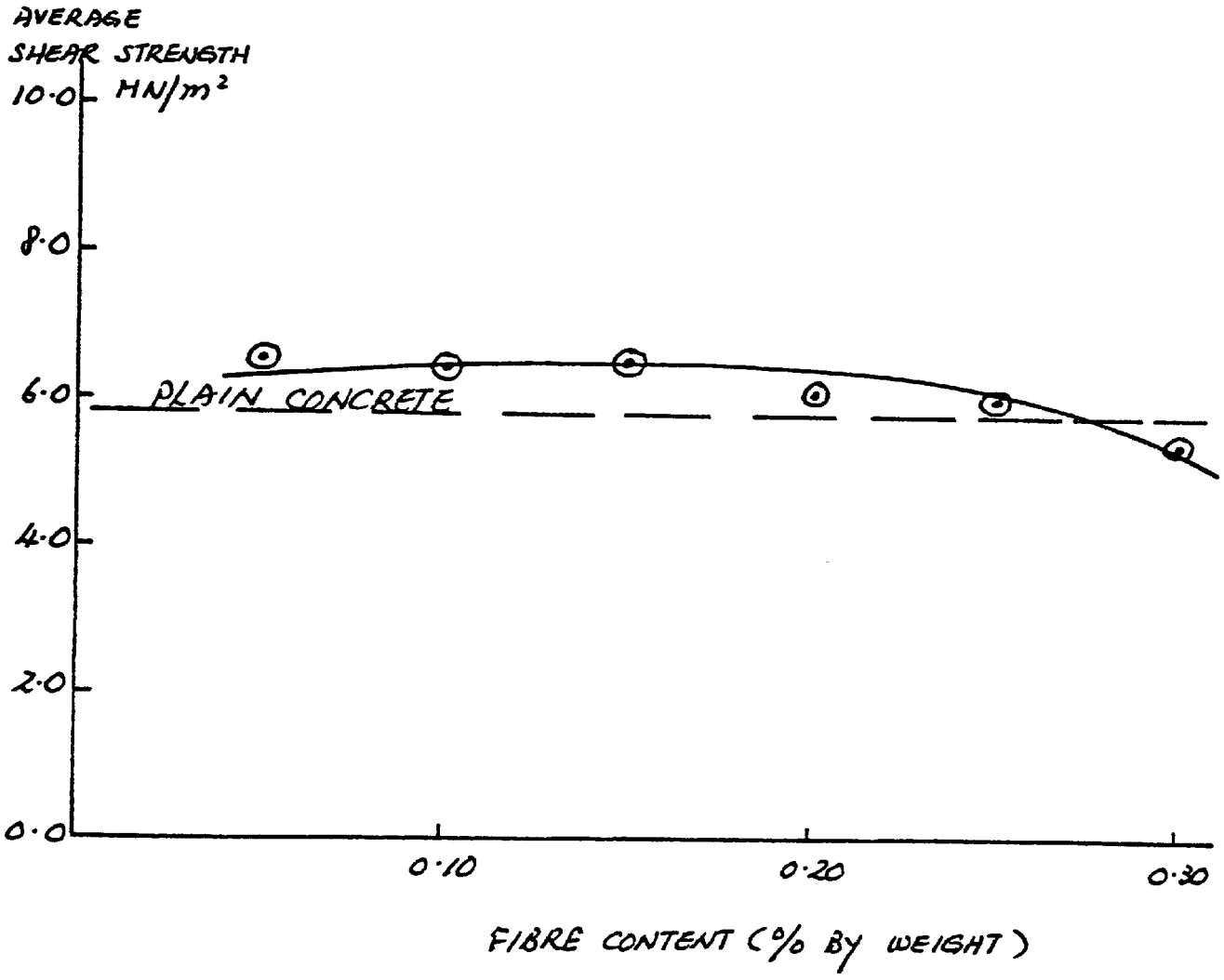

Fig. (5.14) Summarised in plane shear strength results for varying fibre content

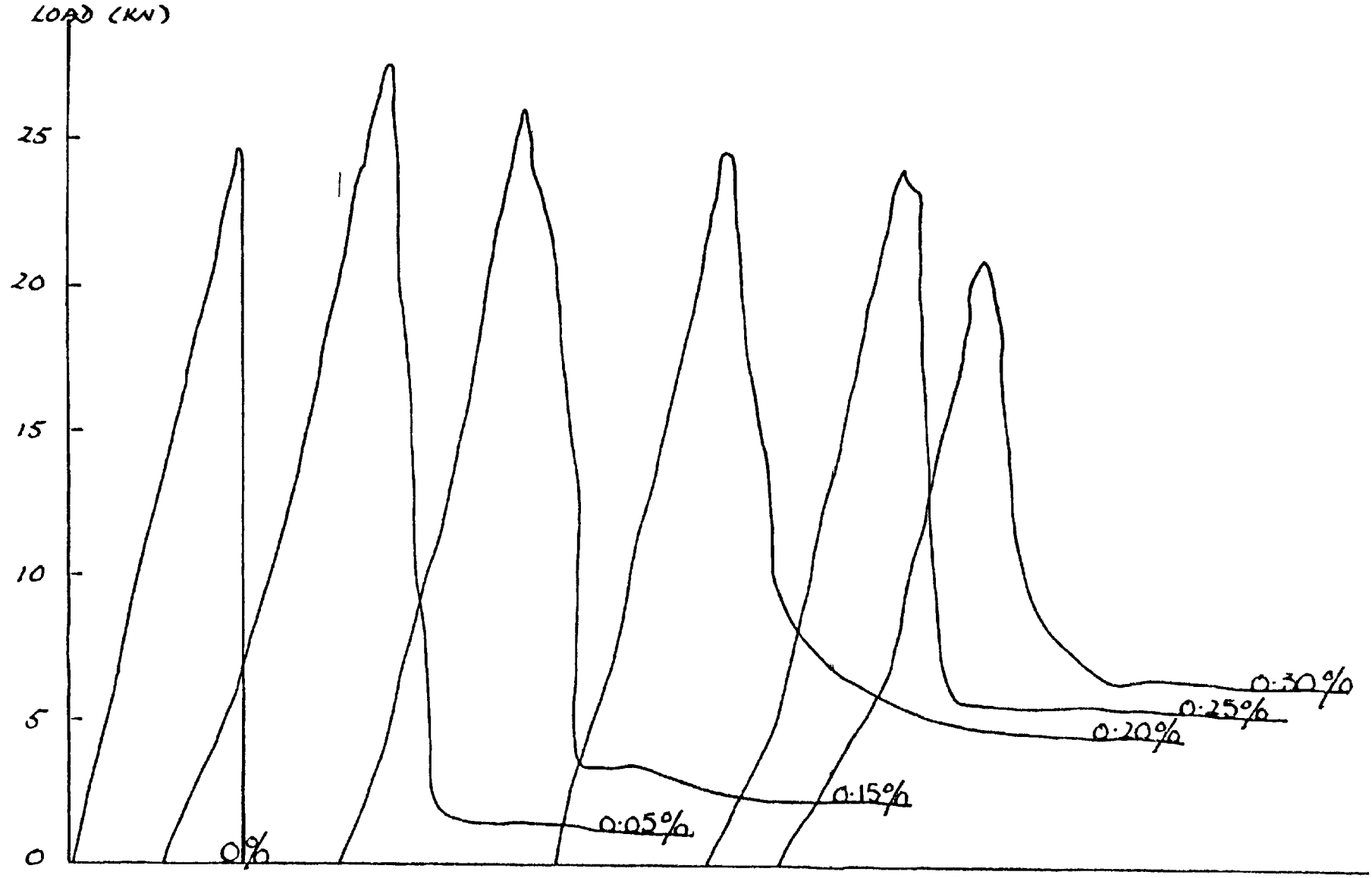

fig. (5.15) Typical load / deflection curves for varying fibre content

Table(5.1) In-plane shear strength results for varying slot-separation/specimen ratio and fibre contents.

a/w	Fibre Content By Weight (%)	Shear Strength MN/M^2				
0.10	0	4.44	7.21	6.17	3.16	7.11
		5.74	7.81	3.40	8.59	5.85
		7.25	5.53	8.21	4.10	6.82
	0.05	8.15	7.91	9.60	6.59	7.25
		9.13	8.45	9.38	6.19	8.11
		8.42	6.80	5.06	6.40	6.35
		6.91				
	0.10	6.16	7.18	6.73	4.54	7.65
		6.55	5.53	4.85	6.05	8.10
		5.57	7.71	5.50	6.85	6.55
		8.95				
	0.15	8.85	5.35	6.92	8.20	5.95
		6.10	7.02	7.10	4.55	7.85
		5.24	7.66	6.75	7.33	8.05
	0.20	4.44	4.43	4.68	6.37	7.15
		5.11	7.22	4.61	7.22	8.27
		10.1	6.00	4.51	3.67	5.25
		7.14				
	0.25	4.32	4.81	4.41	5.47	7.76
		6.33	5.50	7.18	6.53	6.61
		6.77	5.86	7.00	6.05	7.71
		5.28				
	0.30	4.86	4.45	4.87	6.63	7.44
		3.34	3.65	4.50	4.51	5.87
		8.10	5.10	4.35	3.40	3.74
		6.22				

Table(5.1) cont. In-plane shear strength results for varying slot-separation/specimen ratio and fibre content.

a/w	Fibre Content By Weight (%)	Shear Strength MN/M^2				
	0	4.33	3.58	5.83	5.42	7.00
		4.72	3.80	6.30	5.90	6.30
		4.27	4.96	3.48	7.25	5.19
		3.12	3.36	5.16	5.51	5.32
	0.05	4.35	5.30	5.81	3.61	6.28
		5.17	6.80	5.67	5.83	5.93
		6.25	7.08	7.43	5.83	7.48
		6.38	6.31			
	0.10	7.71	7.64	5.24	7.44	6.53
		7.87	6.11	5.62	6.58	7.33
		6.72	4.63	7.74	6.37	7.15
		5.27	2.92	8.23	4.79	5.67
		4.67	5.53	5.03		
0.15	0.15	4.94	6.35	6.50	6.05	7.48
		3.86	7.12	3.92	5.34	4.87
		4.08	6.69	6.53	8.00	5.77
		6.20	7.09	6.67	4.86	3.68
	0.20	8.43	5.43	7.70	8.90	6.86
		7.58	9.12	6.42	7.81	3.39
		5.08	5.89	8.52	4.99	6.36
		8.30	7.73	9.48	5.57	7.77
		5.42	4.32			
	0.25	6.78	6.00	6.86	7.89	6.51
		6.75	6.85	6.73	5.95	3.98
		7.17	4.87	4.84	7.87	4.45
		5.78	6.63	4.43	3.50	4.71
		6.45	3.48			
	0.30	4.75	4.50	4.50	4.50	5.62
		5.00	9.33	5.56	5.67	3.92
		5.28	4.80	5.95	6.22	4.37
		6.26	4.78	4.78	5.39	

Table(5.1) cont. In-plane shear strength results for varying slot-separation/specimen ratio and fibre content.

a/w	Fibre Content By Weight (%)	Shear Strength MN/M^2				
0.20	0	5.92	7.55	5.63	6.42	7.15
		6.69	5.00	6.67	7.14	4.43
		8.14	6.03	7.43	6.19	7.11
		4.69				
	0.05	5.57	5.70	6.28	5.99	5.50
		6.10	6.01	6.80	6.68	6.65
		5.56	5.94	6.39	6.22	6.97
	0.10	7.61	5.66	7.11	4.74	6.02
		6.13	6.04	6.98	6.17	7.44
		5.38	5.98	6.44	7.45	6.06
		7.45				
	0.15	7.47	5.98	6.97	7.05	6.44
		6.20	6.65	7.28	5.39	5.10
		7.40	7.32	6.58	5.33	8.35
		7.14				
	0.20	6.20	6.47	5.43	4.83	6.27
		6.93	4.63	6.06	5.29	6.45
		4.10	3.92	5.88	5.95	5.76
		4.01				
	0.25	6.00	5.60	6.93	7.12	6.15
		6.72	5.16	5.48	6.28	7.30
		5.41	6.29	5.43	5.48	7.50
		7.44				
	0.30	7.12	6.17	4.74	6.67	4.34
		4.82	7.60	6.00	5.05	5.26
		5.65	5.25	5.28	5.73	5.33
		7.05				

Table(5.1) cont. In-plane shear strength results for varying slot-separation/specimen ratio and fibre content.

a/w	Fibre Content By Weight (%)	Shear Strength MN/m²				
0.25	0	4.21	6.24	6.93	5.85	5.57
		6.96	7.02	6.37	4.56	4.27
		3.77	5.15	5.28	5.66	6.28
		5.49	5.87	6.91	7.47	5.23
	0.05	5.86	7.65	7.24	6.03	7.23
		6.28	6.10	7.34	7.96	5.60
		7.01	6.65	5.22	5.71	6.61
		6.22				
	0.10	6.00	6.83	6.32	7.02	6.28
		6.90	5.73	6.52	6.21	7.08
		6.85	5.99	6.63	6.94	5.31
		5.71				
	0.15	6.94	6.40	7.11	5.28	7.55
		5.88	6.36	6.25	7.15	6.87
		7.76	7.08	7.13	7.39	6.39
		5.76				
	0.20	6.75	5.89	5.91	4.00	4.76
		6.75	6.65	6.97	7.05	6.31
		5.33	6.86	6.69	6.75	6.85
	0.25	5.77	5.88	5.58	6.47	5.83
		5.37	6.68	6.41	4.83	6.04
		6.27	7.13	5.59	6.19	6.53
		5.60	5.38	5.00	7.18	
	0.30	6.24	5.85	5.53	7.19	6.81
		5.10	3.63	4.12	5.40	4.88
		4.46	5.11	3.92	6.00	5.32
		6.28	5.95	5.77	3.80	6.11
		3.02				

Table(5.2) Summarised in-plane shear strength results for varying slot-separation/specimen ratio and fibre content.

Fibre Content By Weight (%)	Coeff. of Var.	Shear Strength MN/M^2	Number of Specimens	a / w
0	28.05	6.09	15	0.10
0.05	17.18	7.54	16	
0.10	18.41	6.53	16	
0.15	17.36	6.84	15	
0.20	28.91	6.01	16	
0.25	17.69	6.10	16	
0.30	28.11	5.06	16	
0	24.59	5.03	20	0.15
0.05	16.87	5.97	17	
0.10	17.98	6.34	23	
0.15	22.24	5.80	20	
0.20	24.51	6.87	22	
0.25	22.96	5.84	22	
0.30	21.98	5.35	19	
0	16.65	6.39	16	0.20
0.05	7.64	6.16	15	
0.10	13.12	6.42	16	
0.15	13.38	6.67	16	
0.20	17.29	5.12	16	
0.25	12.86	6.27	16	
0.30	16.39	5.75	16	
0	18.08	5.75	20	0.25
0.05	12.17	6.55	16	
0.10	8.39	6.39	16	
0.15	10.33	6.71	19	
0.20	14.43	6.23	15	
0.25	10.91	5.99	19	
0.30	20.96	5.26	21	

Table(5.3) Summarised in-plane shear strength results for varying polypropylene fibre content.

Fibre Content By Weight (%)	0.0	0.05	0.10	0.15	0.20	0.25	0.30
In-plane Shear Strength MN/M^2	5.81	6.55	6.42	6.50	6.06	6.05	5.36

Table(5.4) Typical fracture toughness index results for varying polypropylene fibre content and loading system.

Polypropylene Fibre Content (%)	0.05	0.20	0.30
Split-cube Specimen	0.33	0.41	0.50
In-plane Shear Specimen	0.38	0.49	0.53

PLATE. 5.1

PLATE. 5.2

CHAPTER SIX

APPLICATION OF THE FINITE ELEMENT METHOD TO MODE I FRACTURE MECHANICS (SPLIT-CUBE)

6.1 INTRODUCTION

Bear and Barr(21) described two tests which could be used to evaluate the fracture toughness of both rock and fine-grained concrete as shown in Fig.(2.16). Dowers(39) further developed one of the tests by replacing the round specimen by an ordinary concrete cube (with two opposite notches). The notched cube was then subjected to an eccentric load as illustrated in Fig.(2.25). The stress intensity factor was calculated from the peak load achieved together with the Nueber solution given by equation(2.40). It was reported by Dowers(39), that the toughness value thus determined varied with the crack length/specimen ratio. Thus the measured toughness did not reflect a true definition of fracture toughness as a material constant.

More recently, Sabir(52) employed the finite element technique to analyse the split cube specimen geometry and made a comparative study in his results with the Nueber equation(2.40). Both 100mm and 150mm cubes were analysed and plane strain conditions were assumed. The modulus of elasticity (13.33 KN/mm^2) and the Poisson ratio(0.2) of the material were kept constant throughout the finite element analysis. Several notch depths were considered giving a range of crack length/specimen(a/d) ratios. The details of the mesh employed in the upper half of the cube are given in Fig.(6.1) for the case of 100mm cube with notch depth

a=25mm. The mesh contained 373 elements and 219 nodal points. Roller supports were employed at the nodal points along the uncracked part of the notch plane. The loads at fracture obtained experimentally were applied at a distance of 6mm from the edges of the cubes. The finite element analysis was carried out using the displacement method around the tip of the notch. The expressions for the stress intensity factors were as follows:

For 100mm cube

$$K_I = P/Bd^{1/2}\left[18.3(a/d)^{1/2} - 430.0(a/d)^{3/2} + 3445.2(a/d)^{5/2} - 11075.8(a/d)^{7/2} + 12966.8(a/d)^{9/2}\right] \qquad (6.1)$$

For 150mm cube

$$K_I = P/Bd^{1/2}\left[30.5(a/d)^{1/2} - 612.0(a/d)^{3/2} + 4441.5(a/d)^{5/2} - 13404.8(a/d)^{7/2} + 14930.0(a/d)^{9/2}\right] \qquad (6.2)$$

Dowers(39) concluded that the load-deflection graphs of the split-cube specimens obtained from the loading system showed a linear response up to the point where the concrete failed as shown in Fig.(6.2). This phenomenon indicated that linear elastic fracture mechanics can be applied in concretes. Due to the fact that the Nueber results (obtained from equation(2.40)) are influenced by the notch depth effect, the finite element method was used by Sabir(52) to evaluate the fracture toughness of the

split cube specimen. The effect of the notch depth was eliminated in the numerical results.

Sabir(52) compared the finite element results with the Nueber equation(2.40). The comparison is illustrated graphically in Fig.(6.3). From the graphs shown, Sabir(52) concluded that equation(2.40) results in considerable variation in fracture toughness, while those obtained from the finite element analysis gave more consistent values. For the 100mm cubes, the coefficient of variation calculated by finite element method was 10 percent while that obtained from Nueber equation(2.40) was 29 percent as shown in Table(6.1). If the finite element results could be trusted, Nueber equation(2.40) gave considerable overestimated values for fracture toughness.

In this chapter, experimental and numerical work were carried out to investigate the effect of eccentricity of loading in the split-cube test. Since the compliance determination was used in the finite element method, thus the effect of varying the modulus of elasticity of concrete in fracture toughness, was also investigated in the numerical analysis.

6.2 TEST SPECIMEN GEOMETRIES AND EXPERIMENTAL DETAILS

The experimental work was carried out using 100mm cubes throughout the tests. The split-cube specimen geometry, loading conditions and the mix details were similar to the work described in chapter 3. A major feature of the study describd in this chapter is the further investigation of geometrical variations. If the test is a valid test, then the fracture toughness values should be independent of all geometrical variations including the eccentricity of loading. The point of application of the load was assumed to be at the edge of the steel bars nearest the notch-root since, as deformation took place, the load was concentrated to these edges. The specimens were made of plain concrete and were cured under water and tested at 28 days. All the tests were carried out at nominal room temperature.

6.3 EXPERIMENTAL AND FINITE ELEMENT RESULTS

The experimental results for the split-cube tests are shown in Table(6.2). It is seen that the failure load decreases as the notch depth increases. A number of specimens with shallow notch depth(25mm) and eccentricity(44mm) could not be used in the determination of the stress intensity factor. This is because smaller

notch depths often result in shear failure of the specimen near the point of loading. In order to obtain a valid result, notch depth should be equal or greater than 25mm in the 100mm split-cube specimens so that shear failure would not occur in the zone adjacent to the point of application of the load.

The computer program used for the finite element analysis was developed by Coughlan(53). The program is in two-dimensional form and then can be used for either plane strain or plane stress conditions. A typical finite element mesh used in the split-cube specimen is illustrated in Fig.(6.4). Plane strain conditions were assumed throughout for all cases considered. The modulus of elasticity ($40KN/MM^2$) and Poisson ratio(0.20) were kept constant throughout the study. Several notch depths and eccentricities were investigated in the numerical work. The details of the typical mesh used in the upper half of the specimen is given. This is shown in Fig.(6.4) for 100mm cube with the notch depth of 30mm. The mesh consists of 186 triangular elements and 117 nodal points. Roller supports were used at the nodal points along the uncrack part of the notch plane as shown. The size of the element around the crack tip was not necessarily more refined than the other elements because the strain energy release rate method of the entire body through the compliance determinations was used throughout the analysis.

The finite element results are shown in Table(6.3). The typical compliance curve is illustrated graphically in Fig.(6.5). The stress intensity factor is determined as follows:

$$G_1 = \frac{P^2}{2B}\left(\frac{\partial C}{\partial a}\right) \tag{6.3}$$

and

$$K_1 = -\left(\frac{GE}{1-\nu^2}\right)^{1/2} \tag{6.4}$$

Using the least-square technique, the best curve is determined and the most accurate polynomial in powers of (2a/w) is obtained. This is denoted the calibration coefficient Y(2a/w). The general stress intensity factor equation in the split-cube test can be expressed as follows:

$$\frac{K_1}{K_\infty} = Y(2a/w) \tag{6.5}$$

and

$$K_\infty = \sigma_\infty \sqrt{a} \tag{6.6}$$

The combined stress at infinity ($\sigma_{c\infty}$) consists of two

components: direct stress $\sigma_{d\infty}$ and bending stress $\sigma_{b\infty}$ at infinity. Thus

$$\sigma_{c\infty} = \sigma_{b\infty} - \sigma_{d\infty} \qquad (6.7)$$

where

$$\sigma_{b\infty} = \frac{6Pe}{BW^2} \qquad (6.8)$$

and

$$\sigma_{d\infty} = \frac{P}{BW} \qquad (6.9)$$

Therefore, from equation(6.7),

$$\sigma_{c\infty} = \frac{6Pe}{BW^2} - \frac{P}{BW}$$

$$= \frac{P}{BW}\left(\frac{6e}{W} - 1\right) \qquad (6.10)$$

Thus, equation(6.6) becomes

$$K_\infty = \frac{P\sqrt{a}}{BW}\left(\frac{6e}{W} - 1\right) \qquad (6.11)$$

and

$$K_I = K_\infty \cdot Y(2a/w)$$
$$= \frac{P\sqrt{a}}{BW}\left(\frac{6e}{w} - 1\right) Y(2a/w) \qquad (6.12)$$

or

$$K_I = \frac{P\sqrt{a}}{BW}(6e/w - 1)\left[A + B(2a/w) + C(2a/w)^2 + D(2a/w)^3 + E(2a/w)^4 + F(2a/w)^5 + \ldots\right] \qquad (6.13)$$

where A, B, C, D, E and F are coefficients.

The calibration coefficient obtained by Sabir(52) consisted of five notch depth/specimen ratios. Due to the accuracy of the expression obtained in this study, an extra term of notch depth/specimen ratio was introduced in the calibration coefficient. From the compliance curve shown in Fig.(6.5), it is necessary to obtain two extra points (2a=45mm and 85mm) so that the slopes of the compliance curve could be accurately determined at 2a=50mm amd 80mm. The calibration coefficient obtained in this Chapter will not be reduced to its simplest form. Since the eccentricity, e, is variable in this case, the powers of notch depth/specimen ratios are easier to determine with the calculators for equation(6.13) than the square root of notch depth/specimen ratios obtained in equation(6.1).

The finite element solution for varying eccentricity is shown in Table(6.4). The calculated stress intensity factors using the equations shown in Table(6.4) are summarised in Table(6.5). It is seen that within a certain range, the stress intensity factor is independent of the notch depth/specimen ratio and the eccentricity. The results are illustrated graphically in Fig.(6.6). The fracture toughness value at 2a/w=0.80 is about half of that when the aspect ratio is less than 0.70. This is most probably due to the steep slope of the compliance curve within the range of 75mm to 85mm notch depths. Therefore, small error in determination of the slope will lead to error in the stress intensity factor; a small resisting area of uncut concrete (total notch depth=80mm) may also introduce problems related to the aggregrate size used in the concrete. Thus the notch depth/specimen ratio of 0.80, if taken as a valid one, would lead to a considerable underestimation of the toughness. In practical terms, this apparent toughness value is clearly undesirable. It directly follows that if a flaw of such magnitude developed in the structure, the catastrophic failure would occur under very low loads.

The eccentricity has very little effect on the measured fracture toughness. The results are illustrated graphically in Fig.(6.7). It is seen that the fracture toughness values are quite consistent with varying eccentricities and notch depth/specimen ratios. Although

the fracture toughness at 2a/w=0.80 is nearly constant with varying eccentricity, the toughness values are underestimated due to the small areas of uncut concrete specimens so that these values should not be taken as valid results. In order to improve this specimen geometry effect, larger specimen(150mm) should be investigated in future work.

The coefficients of variation for the fracture toughness results are shown in Table(6.5). The most consistent fracture toughness values have been calculated when the eccentricity, e=41mm. A good correlation of the results was obtained with the coefficient of variation generally within 8.0 percent. If the varying eccentricity and notch depth have no effect on fracture toughness were assumed except in the case of 2a=80mm, the overall average fracture toughness value was given by $0.7077 MN/m^{3/2}$ and the corresponding coefficient of variation was reduced to 5.8 percent — the results are given in Table(6.6). Thus it may be concluded that varying eccentricity and notch depth have no effect on the fracture toughness values obtained in the split-cube specimen.

Typical stress distributions along the uncracked length of the split-cube specimen were obtained from the numerical work. The results are illustrated graphically in Fig.(6.8). When the eccentric load is applied at the edge of the specimen, both compressive stress and tensile stress

are set up at the vicinity of the crack tips. This is the tensile stress which initiates the crack opening along the defined crack pattern. The tensile stress, σ_y, decreases very rapidly to the compressive region and leads to failure of the specimen. The tensile stresses and shear stresses are obtained from the centroids of the triangular elements slightly above the uncracked length of the specimen. Thus shear stress, τ_{xy}, exists in the specimen during fracture. It is the tensile stress, which is many times higher than the shear stress, which dominate the crack opening process. Thus the specimens were fractured by the Mode I mechanism.

Neuber equation(2.40) gives an approximation for the fracture toughness values; the finite element method should give results in the same range. The finite element results are compared with the toughness values determined using Nueber equation(2.40). The eccentricity of 44mm was employed in this case. The results are shown in Table(6.7). It is seen that the toughness values obtained from the Neuber equation(2.40) are higher than the values obtained from the numerical analysis. The average fracture toughness values determined are generally within 9.2 percent correlation. The results are illustrated graphically in Fig.(6.9). Dowers(39) used the finite element equation(6.1) which was developed by Sabir(52) to evaluate the fracture toughness of concrete. Dowers(39) compared his results with the Neuber equation(2.40) values and concluded that the Neuber equation(2.40) overestimated the fracture toughness

value by 24 percent. Similar conclusions were drawn by Sabir(52).

The experimental and numerical results give more consistent fracture toughness values in the split-cube specimens. From the results shown, the varying eccentricity and notch depth have no effect on the fracture toughness values. It may be concluded that the most consistent results have been obtained within $0.50 \leqslant 2a/w \leqslant 0.70$ limits and the eccentricity, e=4lmm.

6.4 THE EFFECT OF VARYING THE MODULUS OF ELASTICITY IN CONCRETE IN THE SPLIT-CUBE TEST

Dowers(39) and Sabir(52) concluded that the Neuber equation(2.40) overestimated the fracture toughness value by 24 percent when compared with the value obtained from equation(6.1). The overestimated value between Neuber equation(2.40) and the finite element solution obtained in this study was 9.2 percent. Thus the two finite element approaches (displacement method and compliance method) are not in agreement with each other. It is seen that the Neuber equation(2.40) is independent on the modulus of elasticity obtained from the material while the numerical solutions obtained from the displacement method and compliance method are largely depended on that property of the material. Different values of the modulus of elasticity were used (13.33KN/mm^2 and 40 KN/mm^2) in the two finite element approaches. Thus it is seen that equation(6.1) can only be applied to mortar or low strength concretes.

The numerical results obtained in this study have been compared with the Sabir work(52). The fracture toughness values were determined using equation(6.1) and the expression shown in Table(6.11). The modulus of elasticity and eccentricity were 13.33KN/mm^2 and 44mm respectively. The results are shown in Table(6.12) and illustrated graphically in Fig.(6.11). It is seen that a

good correlation of the fracture toughness values is generally within 10 percent. The overall average stress intensity factor values are $0.5589 MN/m^{3/2}$ and $0.5598 MN/m^{3/2}$. Therefore, it can be concluded that the two computer programs and finite element approaches used (displacement method and compliance method) give similar results on the fracture toughness values.

Sabir(52) employed two types of triangular elements in the numerical work to determine the fracture toughness of concrete. The mesh consists of 373 elements and 219 nodal points as shown in Fig.(6.1). A more simpler mesh which consists of 187 elements and 118 nodal points were used in this study. From the results determined in both methods (displacement and compliance), it is found that the element sizes have no effect on the fracture toughness values if the compliance method is used in the numerical work. Nowbray(46) using the compliance method in the finite element analysis to evaluate the fracture toughness of the single-edge-crack specimen. He concluded that good results could be obtained with the compliance method without excessive grid size refinement in the vicinity of the crack tip. Although the displacement method which was used by Sabir(52) gave similar results, it is seen that the compliance method is simpler than the displacement method in the finite element analysis.

In the finite element analysis, stress method can be

used to evaluate the stress intensity factor without the knowledge of modulus of elasticity of the material as indicated in the review of literature(42). From the results showed in this study, the modulus of elasticity greatly influenced the fracture toughness value if the displacement method or compliance method was employed in the finite element analysis. Thus it is necessary to investigate the effect of varying the modulus of elasticity of concrete on fracture toughness. Similar numerical procedures were carried out in the analysis. Several values of the modulus of elasticity (1, 10, 20 and 30 KN/mm^2) were investigated so that a wide range of materials such as soil-cement, mortars, low-strength and high-strength concretes can be applied in the split-cube tests. The numerical results are shown in Table(6.8). The calibration coefficient Y(2a/w) with varying the modulus of elasticity is summarised in Tables(6.9-6.10). The polynomial equations obtained from the numerical results are shown in Table(6.11). It is seen that the calibration coefficient increases with the notch depth. The varying value of the modulus of elasticity has influenced the calibration coefficient results. This phenomenon indicates that the modulus of elasticity has effected the fracture toughness value. The results are illustrated graphically in Fig.(6.10). From the graphs shown, the calibration coefficient curves do not significantly change within the range of the modulus of elasticity values between $10KN/mm^2$ to $20KN/mm^2$. Thus the modulus of elasticity values between these limits

(10-20KN/mm^2) have little effect on the fracture toughness results.

The numerical expressions have been developed with varying modulus of elasticity as shown in Table(6.11). The stress intensity factors of the materials such as soil-cement, mortars and concretes can be determined using those expressions provided the failure loads are obtained from the split-cube specimens. In future work, other materials such as soil-cement and mortars should be used in the split-cube tests to evaluate the fracture toughness values and compare the results with other research workers.

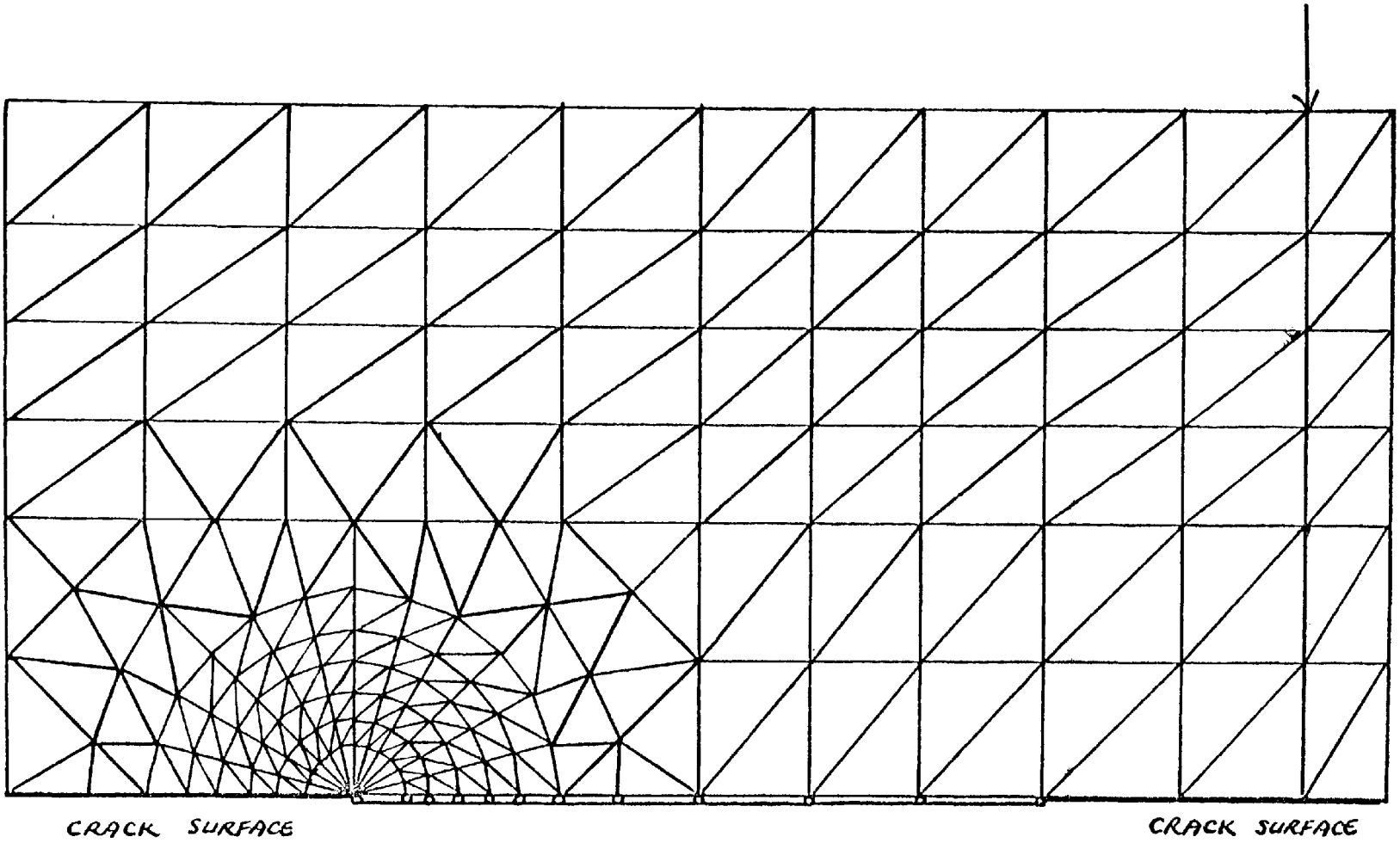

Fig. (6.1) Finite element representation — split cube (Sabir[52])

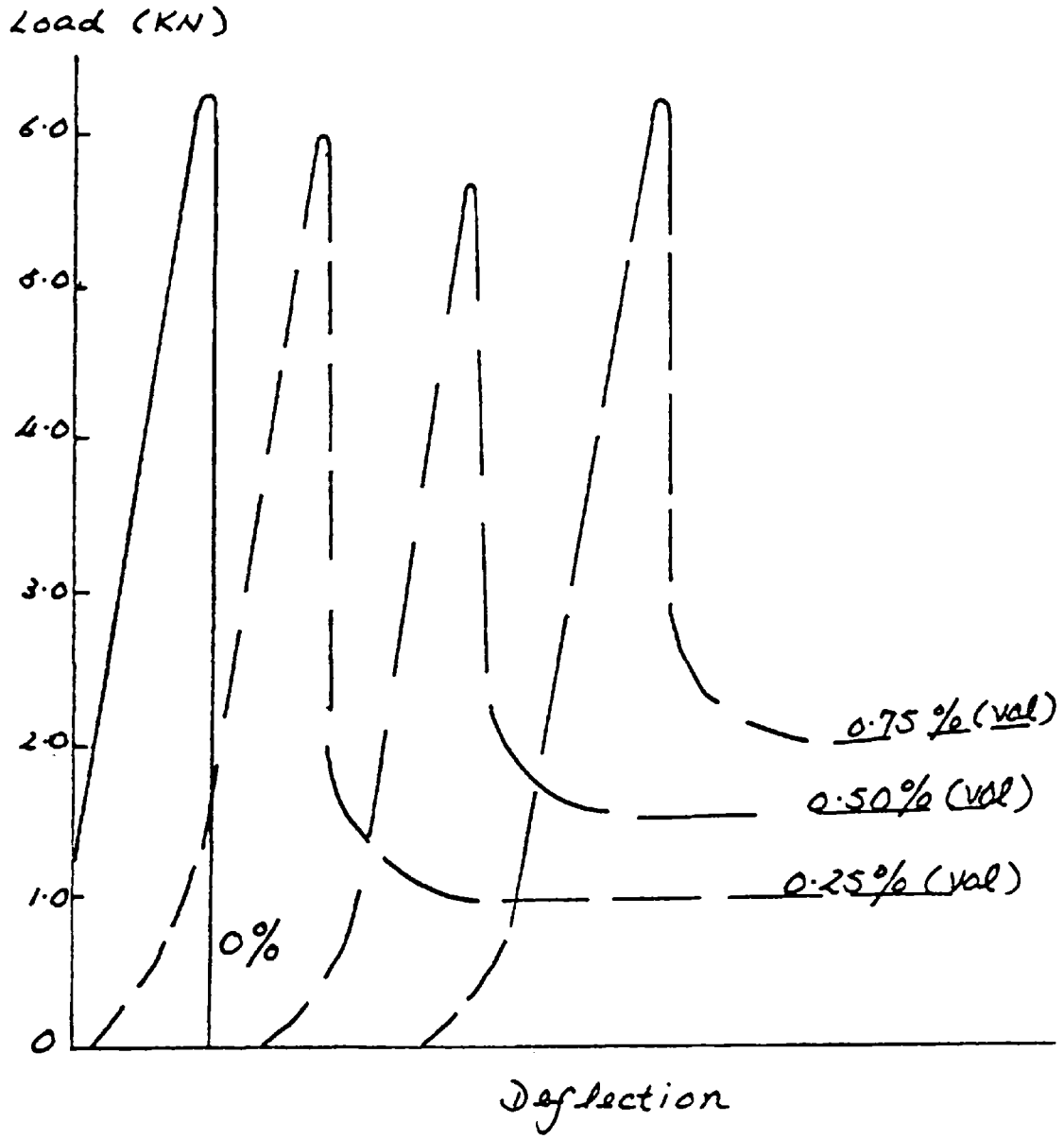

Fig. (6.2) Typical load / deflection curves for split cube specimen (Dowers[39])

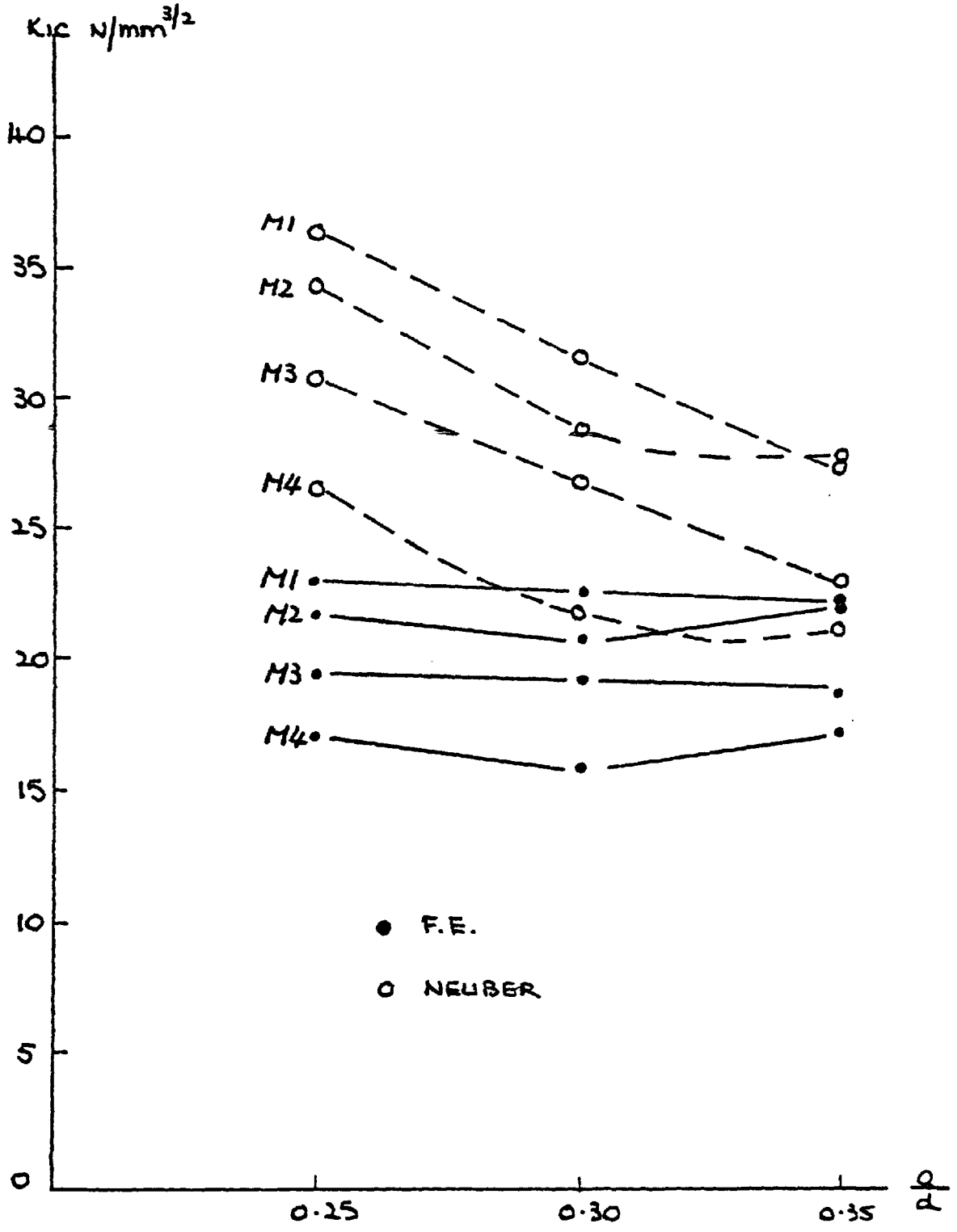

Fig. (6.3) Variation of fracture toughness with notch depth ratio for 100 mm split cube (Sabir [52])

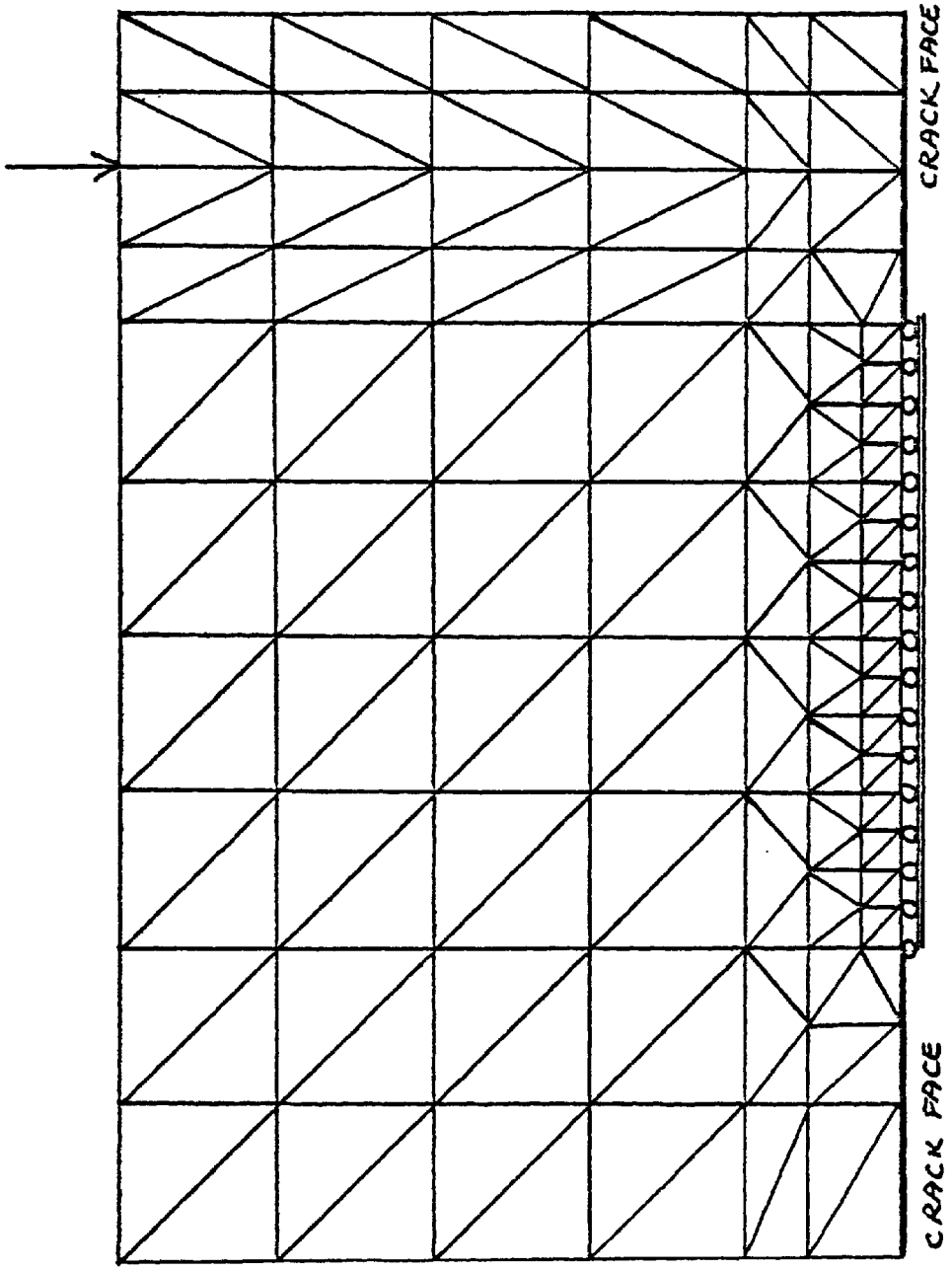

Fig. (6.4) Finite element representation — split cube

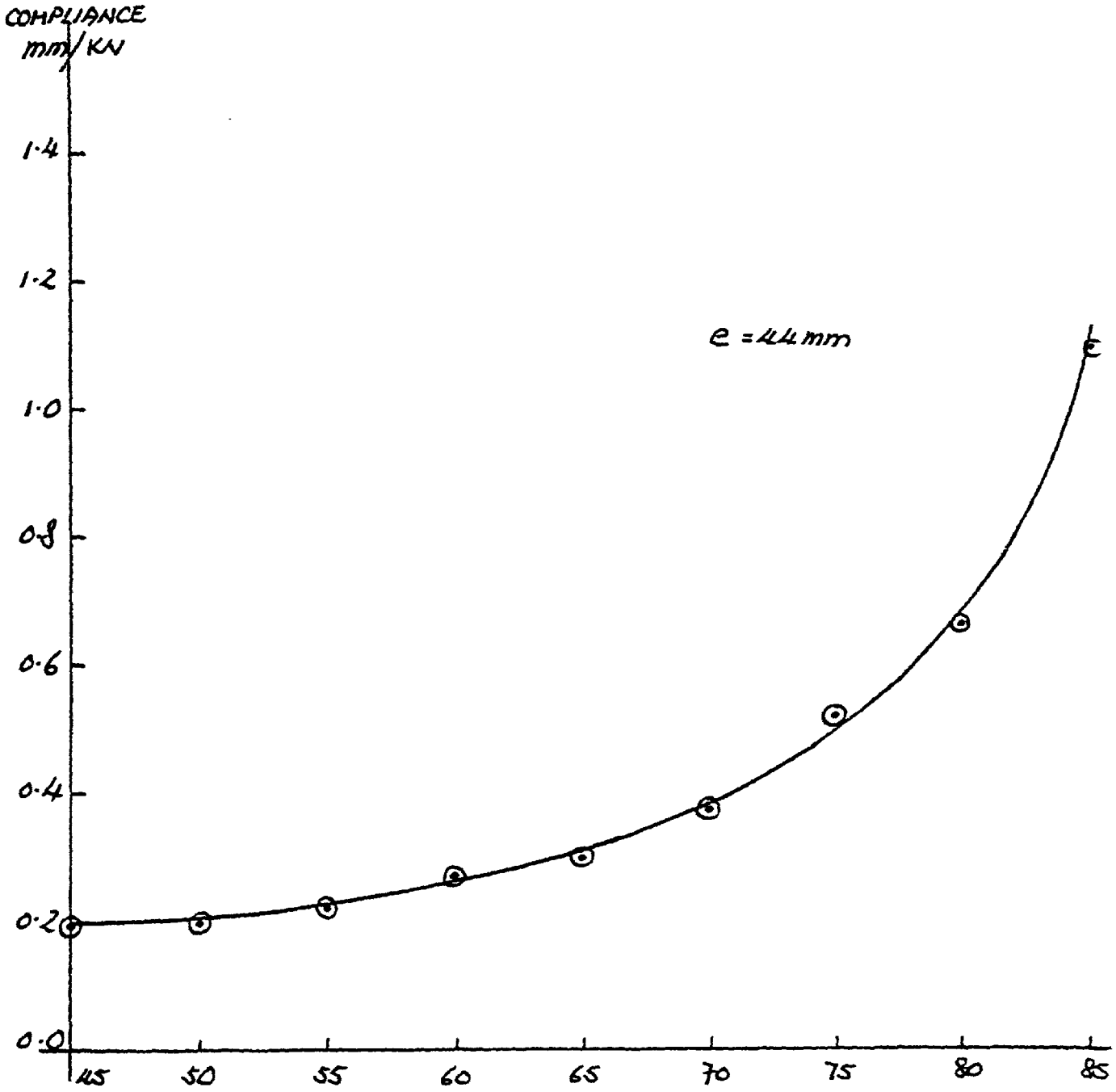

2a

Fig. (6.5) Typical compliance curve for split cube specimen

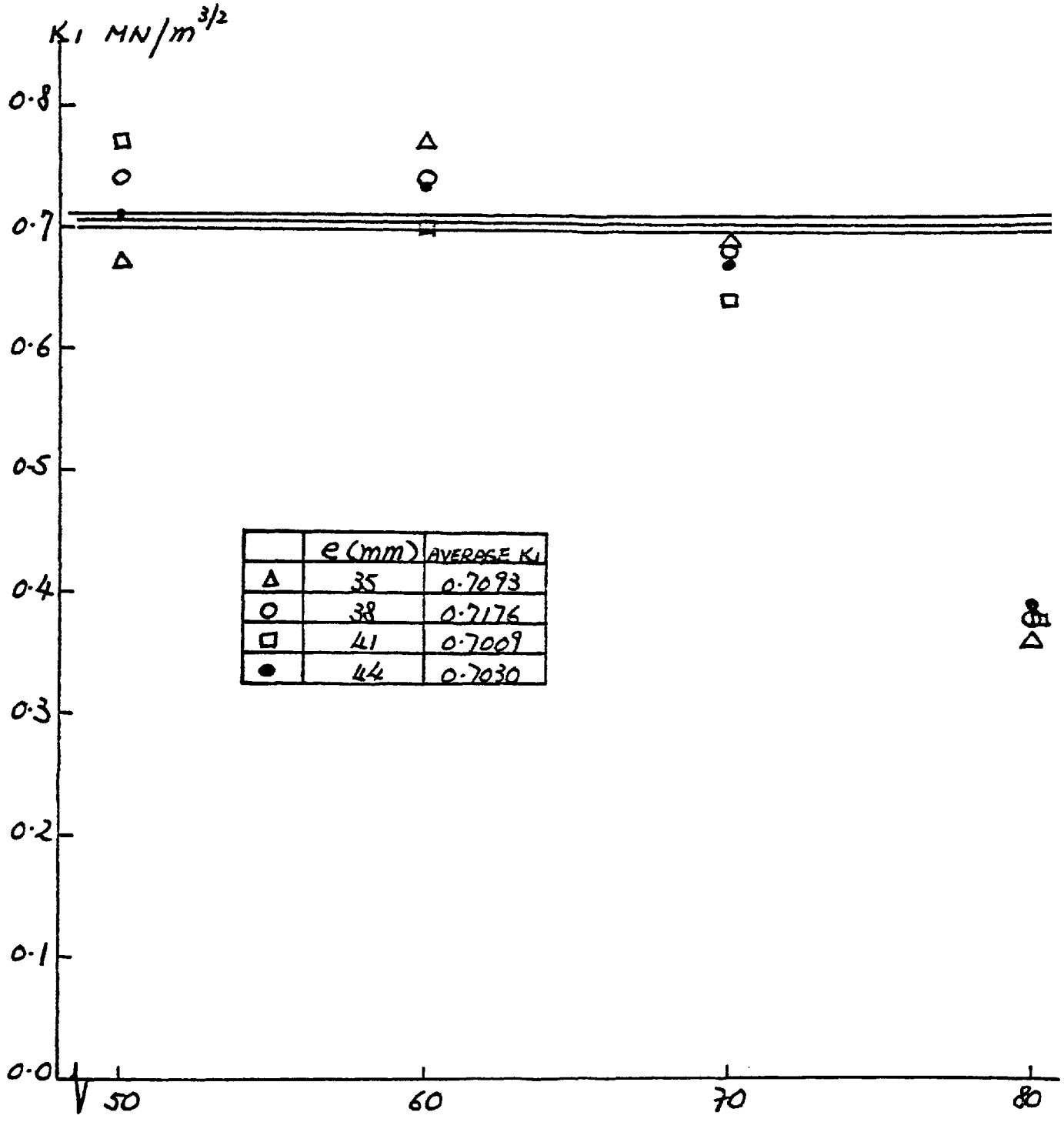

	e (mm)	AVERAGE K1
△	35	0·7093
○	38	0·7176
□	41	0·7009
●	44	0·7030

Fig. (6.6) Fracture toughness results for varying crack length

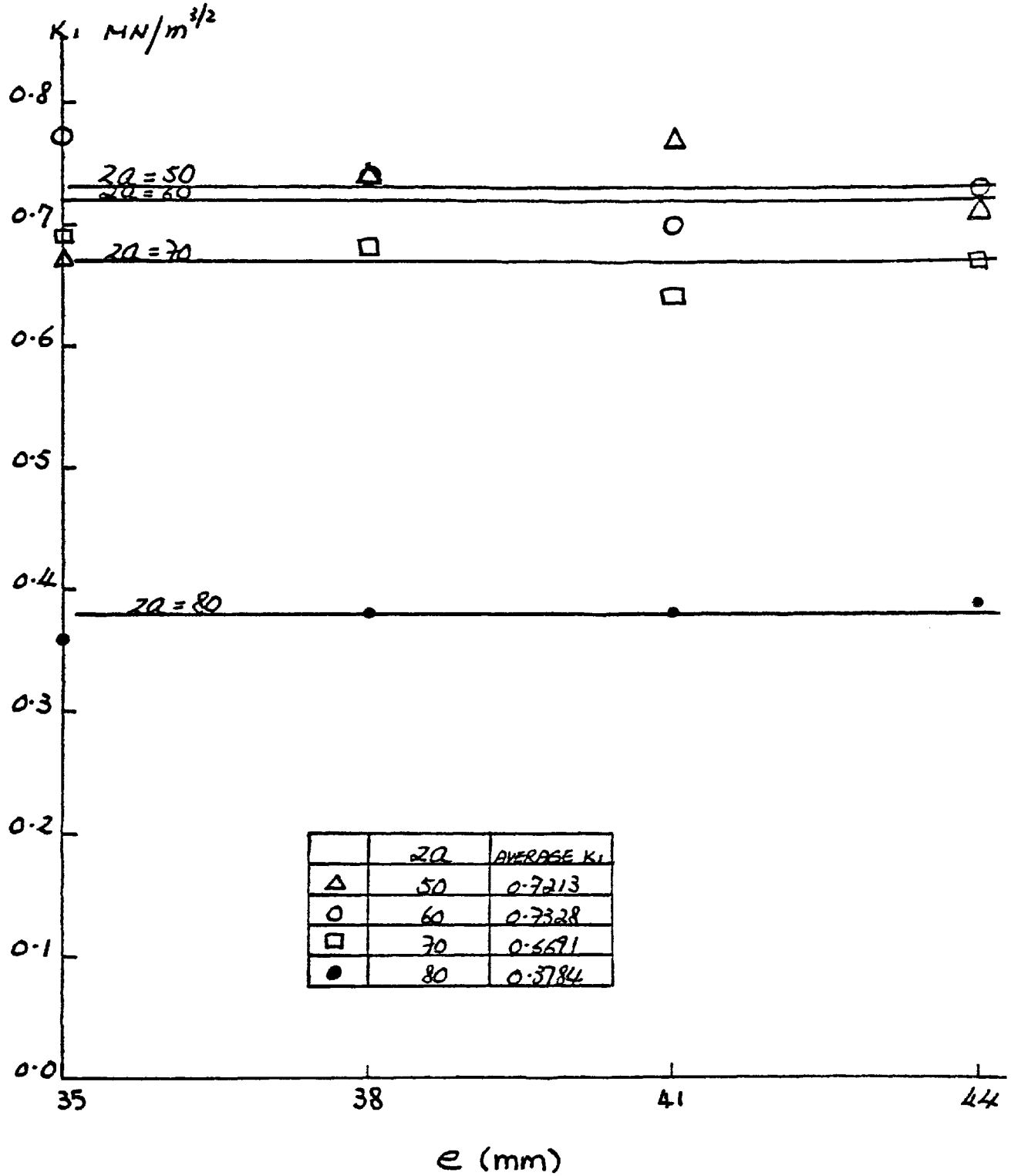

	2α	AVERAGE K1
△	50	0·7213
○	60	0·7328
□	70	0·5691
●	80	0·3784

Fig. (6.7) Fracture toughness results for varying eccentricity

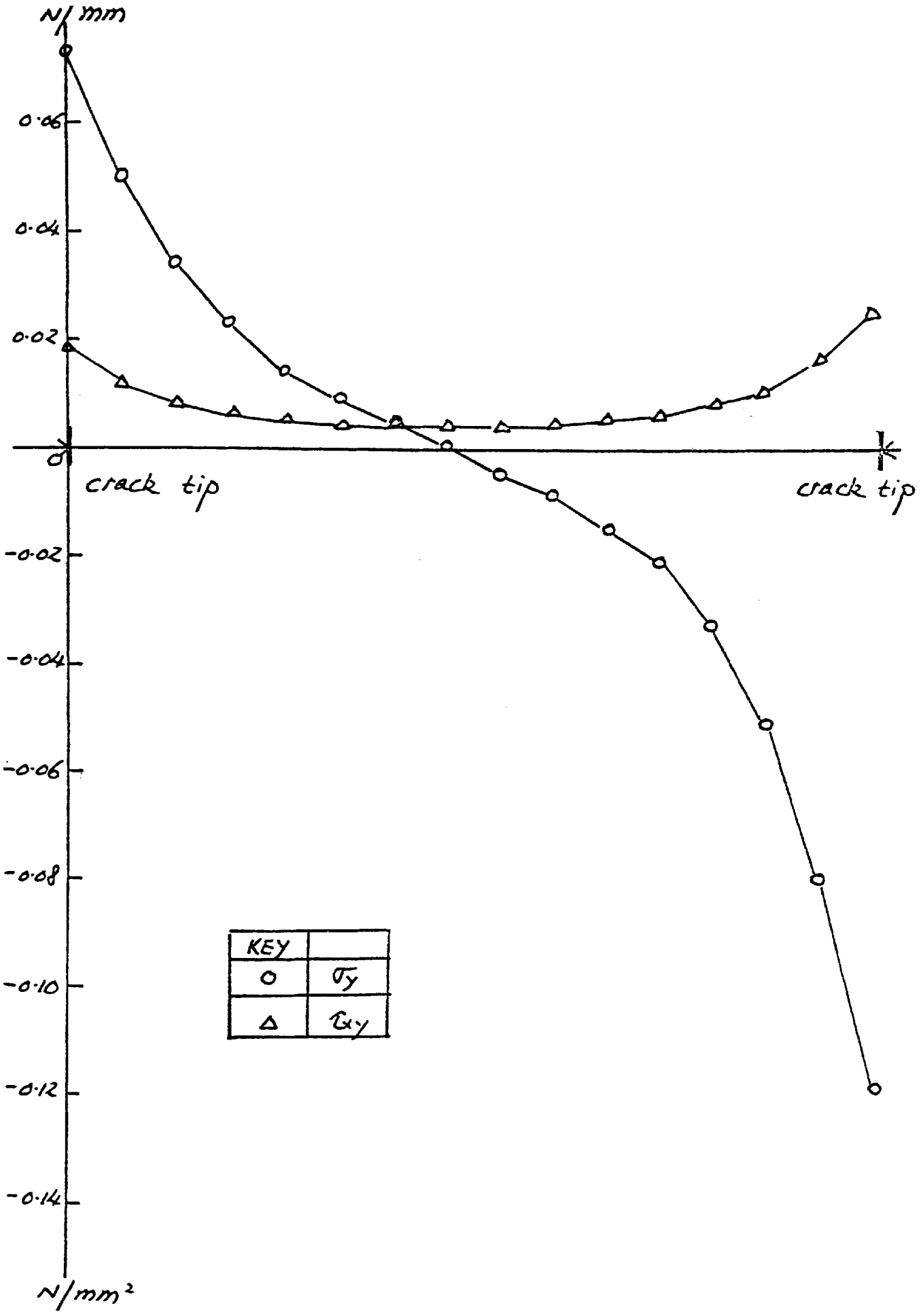

Fig. (6.8) Typical stress distributions for split cube specimen

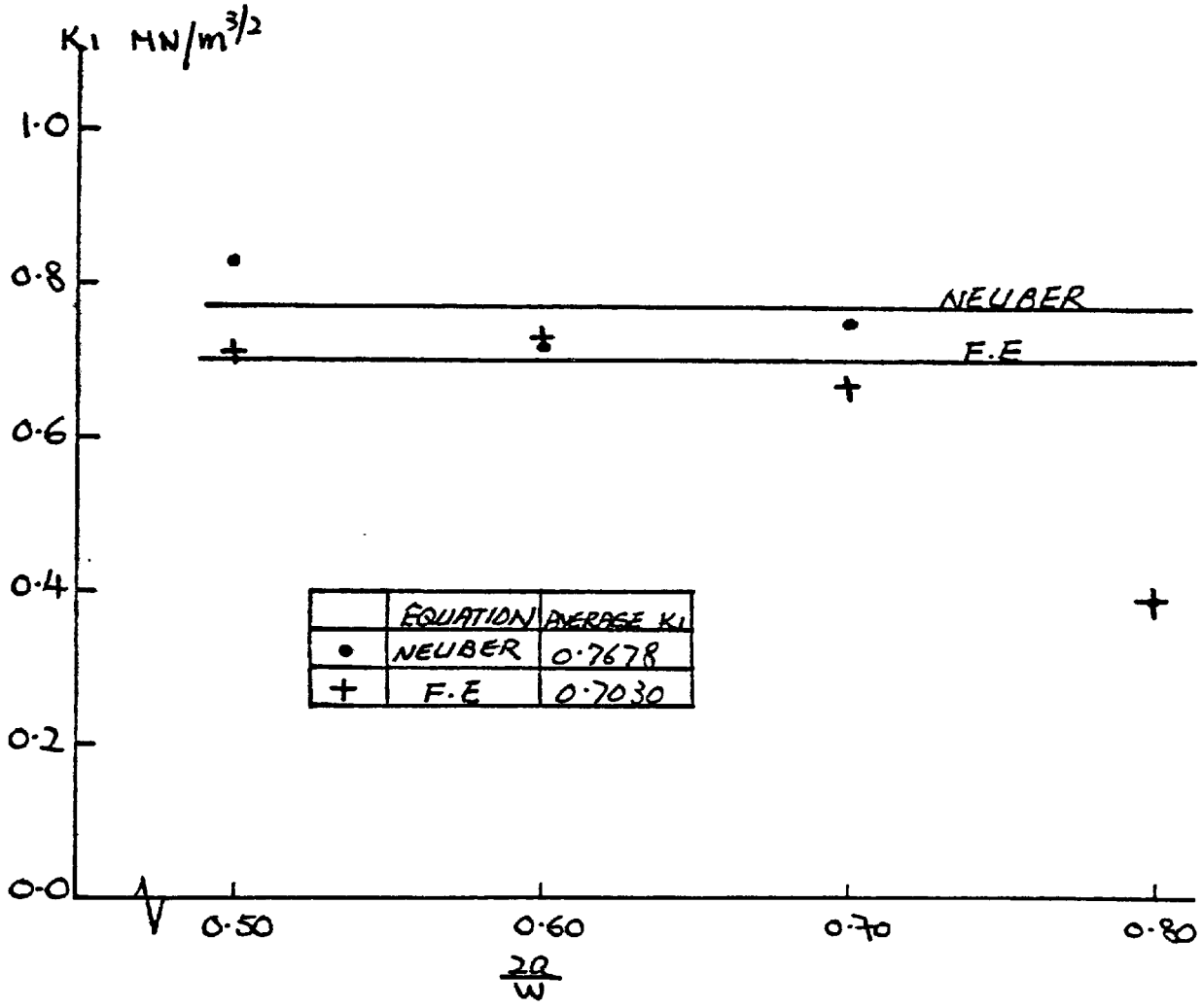

Fig. (6.9) Fracture toughness results for varying notch / depth ratio

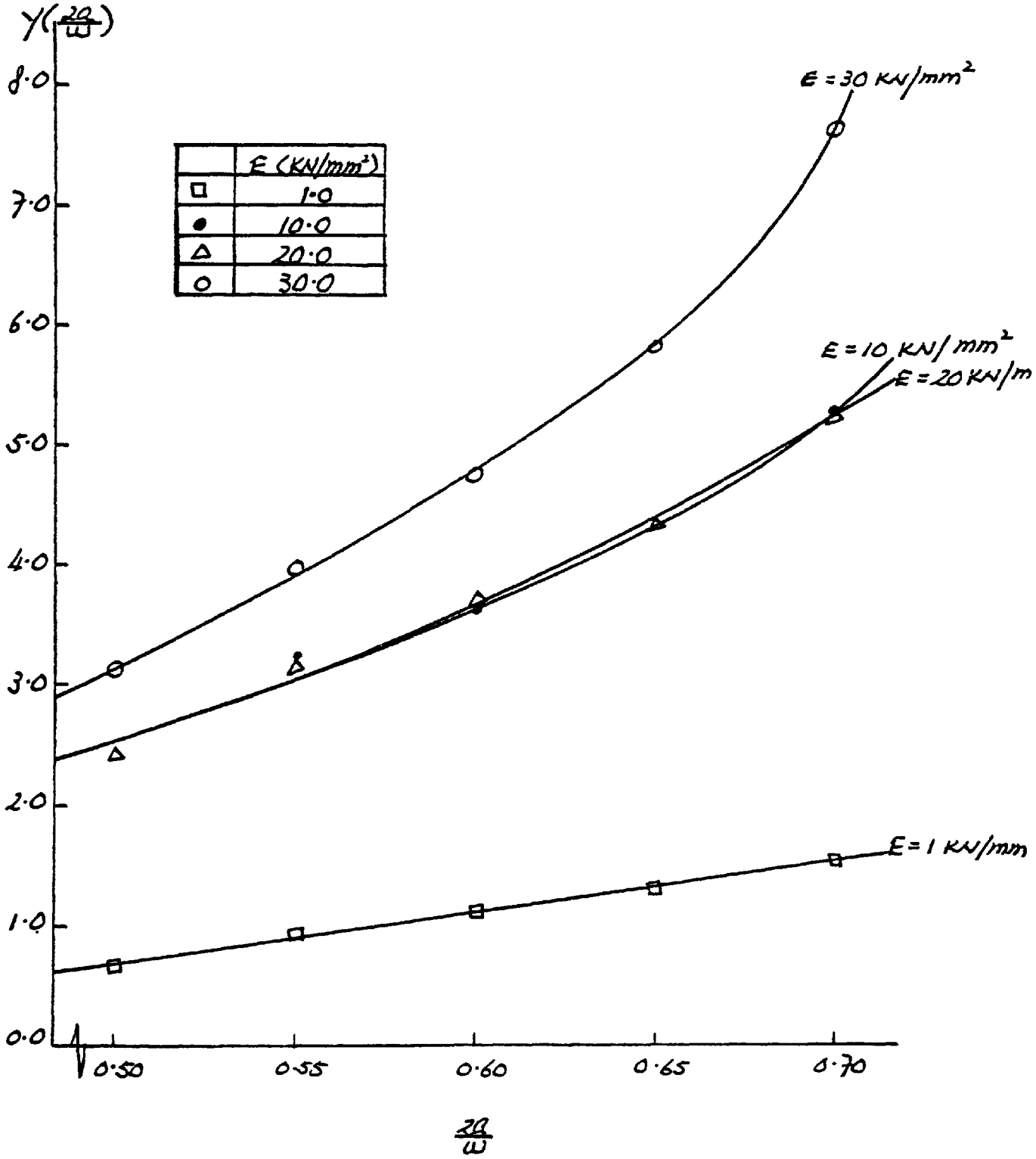

Fig. (6.10) Calibration factor results for varying notch / depth ratio

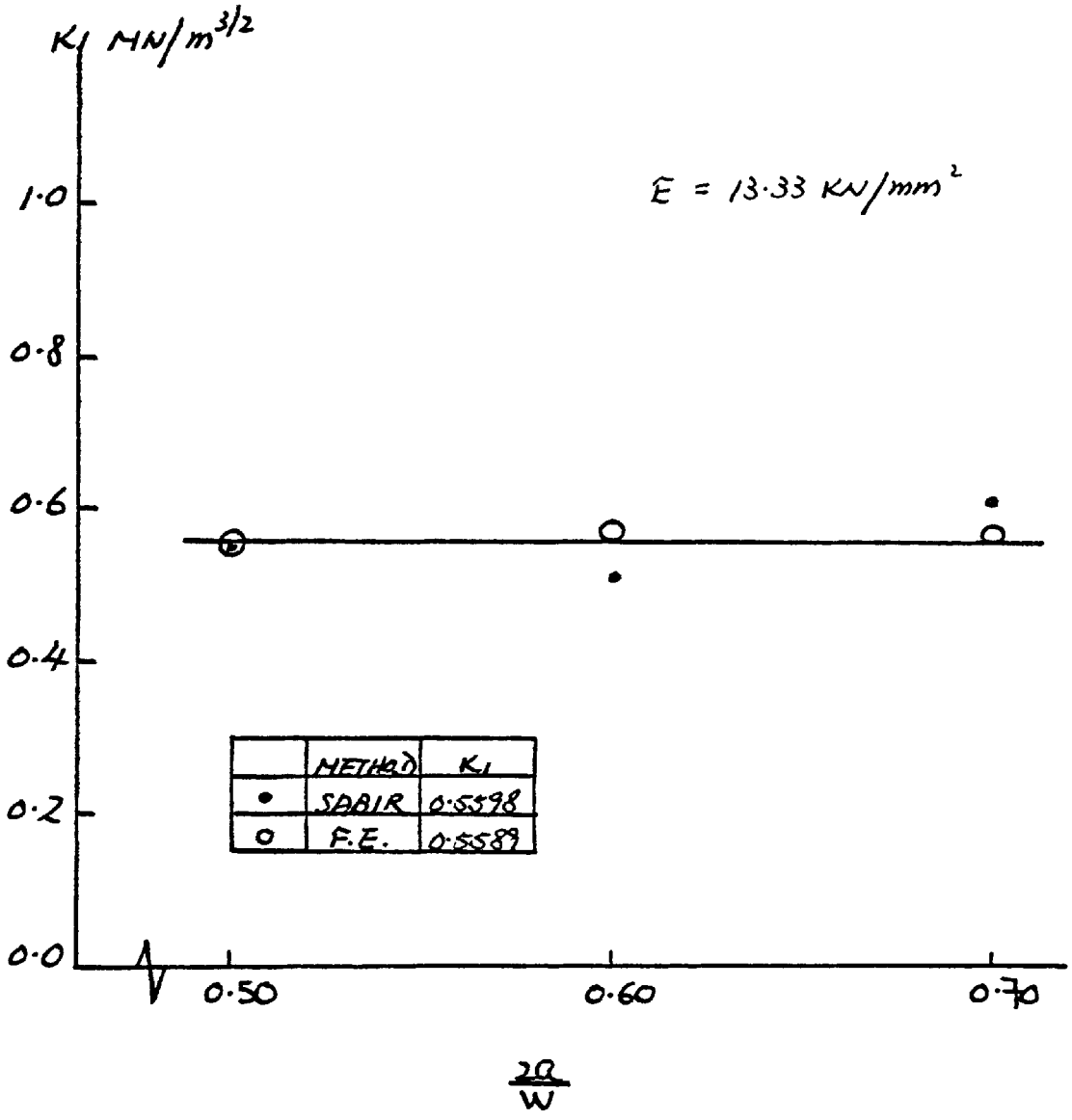

Fig. (6.11) Fracture toughness results for varying notch / depth ratio

Table(6.1) Variation in fracture toughness values($N/mm^{3/2}$) by Sabir(52). (100mm cubes).

Mix	Neuber Eqn.(2.40)		Finite Element	
	Average	Coeff. of Var.	Average	Coeff. of Var.
M1	32.0	28	22.8	4
M2	31.2	20	21.8	9
M3	26.9	29	19.2	5
M4	24.1	22	16.6	10

Table(6.2) Failure load results for varying eccentricity and notch-depth ratio.

Eccentricity (mm)	2a/w	Failure Load KN				
35	0.50	13.90	12.75	13.60	14.60	13.00
	0.60	5.60	6.80	9.00	7.60	8.55
	0.70	4.15	4.30	4.05	3.75	4.10
	0.80	1.85	1.15	1.50	1.21	1.45
38	0.50	11.50	12.10	11.00	11.30	11.30
	0.60	6.70	6.30	7.40	6.30	6.65
	0.70	4.10	3.43	3.90	3.20	3.80
	0.80	1.32	1.62	1.50	1.52	1.25
41	0.50	10.70	10.50	11.10	11.90	11.60
	0.60	5.60	6.60	6.20	6.40	6.20
	0.70	3.20	3.10	3.10	3.20	3.50
	0.80	1.30	1.20	1.40	1.15	1.25
44	0.50	9.70	9.60	9.80	9.60	9.00
	0.60	5.25	5.20	5.90	5.75	5.30
	0.70	3.70	3.90	3.00	3.60	2.90
	0.80	1.20	1.25	1.20	1.05	1.38

Table(6.3) Displacement results for varying eccentricity and notch-depth ratio.

2a (mm) \ Eccentricity (mm)	35	38	41	44
45	0.189	0.155	0.126	0.105
50	0.196	0.167	0.140	0.121
55	0.221	0.189	0.159	0.132
60	0.274	0.225	0.192	0.162
65	0.300	0.260	0.222	0.189
70	0.375	0.324	0.277	0.234
75	0.527	0.455	0.389	0.327
80	0.666	0.577	0.495	0.421
85	1.099	0.954	0.820	0.696

* Displacements are in mm.

Table(6.4) Finite element solution for varying eccentricity.

Coefficients (mm)	Eccentricity (mm)			
	35	38	41	44
A	-2508.7	-2407.6	357.7	-1505.1
B	19901.7	19089.4	-2172.9	11748.9
C	-62831.8	-60088.3	4892.6	-36573.3
D	98681.6	93900.8	-4818.8	56839.2
E	-77017.2	-72797.7	1774.6	-44077.2
F	23902.6	22410.8	-----	13656.5

$$K_I = \frac{P\sqrt{a}}{BW}(6e/w - 1)\left[A + B(2a/w) + C(2a/w)^2 + D(2a/w)^3 + E(2a/w)^4 + F(2a/w)^5\right]$$

$$K_I = \frac{P\sqrt{a}}{BW}(6e/w - 1) \cdot Y(2a/w)$$

Table(6.5) Stress intensity factor results for varying eccentricity and notch-depth ratio.

Eccentricity (mm)	2a/w	Stress Intensity Factor, Kic MN/M$^{3/2}$					Mean Kic	Coeff. of Var.
	0.50	0.67	0.63	0.67	0.72	0.64	0.67	5.2
35	0.60	0.58	0.70	0.92	0.78	0.88	0.77	18.2
	0.70	0.70	0.73	0.69	0.64	0.70	0.69	5.0
	0.80	0.47	0.29	0.38	0.37	0.31	0.36	19.4
	0.50	0.74	0.78	0.71	0.73	0.73	0.74	3.6
38	0.60	0.74	0.70	0.70	0.82	0.74	0.74	6.7
	0.70	0.70	0.75	0.63	0.71	0.59	0.68	9.9
	0.80	0.35	0.43	0.40	0.40	0.33	0.38	10.6
	0.50	0.74	0.72	0.76	0.82	0.80	0.77	5.3
41	0.60	0.63	0.74	0.70	0.72	0.70	0.70	6.0
	0.70	0.64	0.62	0.62	0.64	0.70	0.64	5.1
	0.80	0.39	0.36	0.42	0.35	0.38	0.38	7.6
	0.50	0.73	0.72	0.73	0.72	0.67	0.71	3.3
44	0.60	0.70	0.69	0.78	0.76	0.70	0.73	5.9
	0.70	0.73	0.77	0.59	0.71	0.57	0.67	13.0
	0.80	0.38	0.40	0.38	0.34	0.44	0.39	9.7

Table(6.6) Summarised stress intensity factor results for varying eccentricity and notch-depth ratio.

2a/W \ e (mm)	35	38	41	44
0.50	0.67	0.74	0.77	0.71
0.60	0.77	0.74	0.70	0.73
0.70	0.69	0.68	0.64	0.67
0.80	0.36	0.38	0.38	0.39

* Stress intensity factors are in MN/M$^{3/2}$.

Table(6.7) Stress intensity factor results obtained by finite element (compliance method) and Neuber equation(2.40).

a/w	0.50	0.60	0.70	0.80
F. E.	0.71	0.73	0.67	0.39
Neuber	0.83	0.72	0.75	0.53

* Stress intensity factors are in $MN/M^{3/2}$.
* Eccentricity = 44mm.

Table(6.8) Displacement results for varying the modulus of elasticity and notch-depth ratio.

E N/mm^2 \ 2a/W	0.45	0.50	0.55	0.60	0.65	0.70	0.75	0.80
1,000	3.40	5.40	6.00	7.40	8.20	10.00	14.40	17.80
10,000	0.34	0.54	0.60	0.74	0.82	1.00	1.44	1.78
20,000	0.17	0.27	0.30	0.37	0.41	0.50	0.72	0.89
30,000	0.23	0.38	0.44	0.55	0.58	0.75	1.02	1.31

* Displacements are in mm.
* Eccentricity = 44mm.

Table(6.9) Calibration coefficient Y(2a/w) for varying the modulus of elastricity and notch-depth ratio.

E = 1 KN/mm^2		E = 10 KN/mm^2	
$\frac{2a}{w}$	Y(2a/w)	$\frac{2a}{w}$	Y(2a/w)
0.50	0.65	0.50	2.23
0.55	0.92	0.55	3.25
0.60	1.11	0.60	3.64
0.65	1.29	0.65	4.11
0.70	1.53	0.70	5.31

Table(6.10) Calibration coefficient Y(2a/w) for varying the modulus of elastricity and notch-depth ratio.

E = 20 KN/mm^2		E = 30 KN/mm^2	
$\frac{2a}{w}$	Y(2a/w)	$\frac{2a}{w}$	Y(2a/w)
0.50	2.40	0.50	3.14
0.55	3.16	0.55	3.98
0.60	3.72	0.60	4.75
0.65	4.33	0.65	5.84
0.70	5.24	0.70	7.66

Table(6.11) Polynomial equations for varying the modulus of elasticity.

E KN/mm^2	A	B	C	D
1	-20.21	98.09	-155.27	85.00
10	-190.04	963.27	-1607.48	900.07
20	-71.71	361.91	-595.88	337.00
30	-95.37	504.67	-876.90	523.13

$$Y(2a/w) = A + B(2a/w) + C(2a/w)^2 + D(2a/w)^3$$

Table(6.12) Stress intensity factor results obtained by displacement method and compliance method.

2a / w	0.50	0.60	0.70	Mean
Displacement Method Eqn. (6.1)	0.56	0.51	0.61	0.56
* Compliance Method	0.55	0.57	0.56	0.56

$$* K_I = \frac{P\sqrt{a}}{BW}(6e/w - 1)\left[-190.0 + 963.27(2a/w) - 1607.5(2a/w)^2 + 900.1(2a/w)^3\right]$$

CHAPTER SEVEN

APPLICATION OF THE FINITE ELEMENT METHOD TO MODE II FRACTURE MECHANICS (IN-PLANE SHEAR)

7.1 INTRODUCTION

Most of the research work in fracture mechanics has dealt with Mode I(crack opening) failure. Mode II(shear) failure has received very little attention for homogeneous and isotropic materials such as metals, because Mode I has been considered to be the most severe loading condition for crack propagation in these materials. In recent years, fracture mechanics has been applied to cement-based composite materials such as mortars, plain concretes and fibre-reforced concretes. However, these composite materials are generally weak in shear. Thus it is necessary to investigate the Mode II fracture toughness especially in concrete materials.

Chisholm and Jones(54) presented a boundary collocation solution for determining the Mode II stress intensity factor for a pair of edge cracks in a finite isotopic plate. The configuration of the compact shear specimen used in the analysis is shown in Fig.(7.1). Since no independent analysis of the compact shear specimen was available, it was necessary to verify the validity of the numerical solution by using photoelastic analysis. The photoelastic compact shear specimen was fabricated with dimensions identical to those chosen in the numerical solution. The specimen was notched by first hand sawing to within 0.25inch (6.35mm) of the desired crack length and

then filing with a screw-head file produced a crack tip radius of 0.004inch (0.1mm). Finally, a razor blade was used with a special striking fixture to crack the specimen to the desired depth. The specimen was loaded in tension in a Dillon universal test machine. The photoelastic results were used to evaluate the shear stress distribution in the vicinity of the tip of the cracks. The maximum in-plane shear stress may be written as:

$$\tau_m = \left[\left(\frac{\sigma_y - \sigma_x}{2}\right)^2 + \tau_{xy}\right]^{1/2} \qquad (7.1)$$

By substituting for σ_x, σ_y and τ_{xy} from the Westergaard stress equations(2.8-2.9), τ_m can be expressed in terms of K_I and K_{II} as follows:

$$\tau_m = \frac{1}{2(2\pi r)^{1/2}}\left\{\left[K_I \sin\theta + 2K_{II}\cos\theta\right]^2 + \left[K_{II}\sin\theta\right]^2\right\}^{1/2} \qquad (7.2)$$

For the case of pure Mode II, ($\theta = 0^\circ$) and equation(7.2) reduces to

$$K_{II} = \tau_m (2\pi r)^{1/2} \qquad (7.3)$$

The photoelastic data and fringe pattern were used to evaluate maximum shear stress values at points at small distances, r, ahead of the crack. A plot of K_{II} against r could then be made by the use of equation(7.3). Thus crack

tip stress intensity factors were then obtained by extrapolation to r=0. The results of the photoelastic experiments were compared with the numerical solution obtained for the same specimen by the boundary collocation method. The comparison of collocation results with photoelastic data is shown in Fig.(7.2). Chisholm and Jones (54) concluded that the K_{II} values obtained from the boundary collocation method and photoelastic studies were in good agreement and the photoelastic experiments also verified that a pure Mode II condition existed at the crack tips.

Sabir(52) investigated two new crack tip elements. These elements could be used for both Mode I and Mode II conditions. Sabir(52) used his elements to evaluate the stress intensity factor for Mode II problems under plane strain conditions. The dimensions of the specimen, which were approximately the same as those of reference(54), are shown in Fig.(7.3). Several crack depths were considered giving a range of a/w ratios. Because of symmetry about the centreline only one half of the plate was considered. The pin loads were simulated by point loads as shown in Fig.(7.3). Since the loads are sufficiently far away from the crack tip, this approximation gives a similar stress distribution in the vicinity of the crack. The comparison between the results of Chisholm and Jones(53) and the finite element results is illustrated graphically in Fig.(7.4). Sabir(52) concluded that reasonable agreement

was obtained between the finite element results and those obtained by Chisholm et al(53)

Sharples(60) has used a finite element program based on the constant strain triangular element to determine the Mode II stress intensity factors. The compliance method was used to determine the values of stress intensity factor from the finite element program output data. The dimensions of the compact shear specimen which is similar to Chisholm and Jones(53) is shown in Fig.(7.5). The finite element results are illustrated graphically in Fig.(7.6). It is evident that the values of stress intensity factor obtained by the finite element method are lower than those of Chisholm et al(54). Sharples(60) concluded that the finite element analysis was a relatively simple method to use in solving fracture mechanics problems. For many cases no alternative solutions are available and the finite element results are assumed to be correct. For many practical situations approximate values of stress intensity factors only may be what is required, and the finite element is an ideal method to use in these cases.

More recently, Agarwal and Giare(61) carried out experiments to investigate the Mode II fracture toughness of short fibres composites. The work has been performed on the randomly oriented short-glass-fibre reinforced epoxy composites and an average fibre length of 50mm was used as the reinforcement. The Mode II fracture toughness test was

conducted by applying equal and opposite forces parellel to the plane of the crack and perpendicular to the crack front, as shown in Fig.(7.7). The tests were performed on 28.5mm wide specimens with the crack lengths varying from 2.0mm to 20mm. The cracks were machined using a 0.30mm thick milling cutter and the crack tip(about 0.5mm long) was finished manually using a 0.15mm thick razor blade with saw teeth cut on it. The stress intensity factor in Mode II was determined through compliance method as follows:

$$K_{II} = Y_{II}\tau\sqrt{(a)} \qquad (7.4)$$

where Y_{II} = calibration factor in Mode II

τ = nominal shear stress

a = crack length

The compliance method has been described in the review of literature (Chapter 2) and the procedure will not be repeated in this section. The calibration factor(Y_{II}) with varying notch depth/width ratio was determined from the compliance curve. The results are illustrated graphically as shown in Fig.(7.8). The best fit curve for the calibration factor could be obtained through a computer analysis. Thus

$$Y_{II} = 6.1387 - 7.6700(a/w) + 4.7912(a/w)^2 - 1.9953(a/w)^3 \qquad (7.5)$$

Agarwal and Giare(61) used equations(7.4-7.5) to evaluate the Mode II fracture toughness of the composite material. The critical strain energy release rate, G_{IIc}, was determined using the following relationship,

$$G_{IIc} = K_{II}^{2}/E \qquad (7.6)$$

The results of the critical strain energy release rate, G_{IIc}, with varying crack length are shown in Fig.(7.9). Agarwal and Giare(61) concluded that the critical strain energy release rate was independent of the crack length in Mode II failure. Thus the tested specimen could be used to determine the Mode II fracture toughness on fibrous composites.

In this Chapter, numerical work was carried out to investigate the Mode II fracture toughness of the in-plane shear specimen. Due to the compliance method which was used in the analysis as described in Chapter 6 vary with the modulus of elasticity. Several values of the modulus of elasticity were used in the investigation.

7.2 DISCUSSION OF THE IN-PLANE SHEAR SPECIMEN RESULTS

The numerical work was carried out using the modified rectangular beam specimen(100 X 100 X 200mm). The experimental results were obtained from the in-plane shear strength tests described in Chapter 5. The specimen geometries and the finite element idealization are shown in Fig.(7.10) with slot separation a = 20mm. The mesh consists of 174 triangular elements and 114 nodal points. The nodal points along the centre-line of the specimen were restrained in the horizontal direction. The modulus of elasticity and Poisson ratio were 40 KN/mm^2 and 0.20 respectively. The numerical procedures were similar to the split-cube specimen as described in Chapter 6. The energy method through compliance determinations was employed in all the numerical analysis.

The compliance results with varying modulus of elasticity and slot separation of the specimen are shown in Table(7.1). It is seen that the slot separation has no effect on the compliance — a straight horizontal line is obtained in all cases. The results are illustrated graphically in Fig.(7.11). The stress intensity factor, K_{IIC}, is determined in the form of

$$K_{IIC} = \hat{\iota} \sqrt{\pi c}\, Y(a/w) \qquad (7.7)$$

where $\tau = P/Ba$

$Y(a/w)$ = calibration coefficient

c = crack length

a = Slot Separation

Using the least-square technique, the best straight horizontal lines are determined and the most accurate polynomial in powers of (a/w) are obtained. The results are shown in Table(7.2) and Fig.(7.12). It is seen that the calibration coefficient Y(a/w) is independent of the slot separation. The calibration coefficient curves are of similar shape to the results obtained by Chisholm and Jones(54) as shown in Fig.(7.2). Sabir(52) also employed the finite element technique(displacement method) to evaluate the Mode II fracture toughness. The shape of the calibration coeficient Y(a/w) with varying notch depth, Fig.(7.4), is similar to the results obtained in this study.

Typical stress distributions along the line of action between the two slots(40mm) were obtained and are illustrated graphically in Fig.(7.13). It is seen that in the region at the crack vicinity compressive and shear stresses are initially set up as shown. When proceeding along the line of action between the slots, the compressive stress gradually changes in magnitude and nature and finally stabilises to a constant value which is almost an order of magnitude lower than the corresponding shear stress. Thus the in-plane shear specimen is fractured by

the Mode II mechanism (shear fracture). From the stress distributions shown in Fig.(7.13), tensile stress exists along the line of action between two slots. Therefore further investigation of the in-plane shear specimen is necessary. Lateral loads should be applied between the two slots together with the compressive loads so that the tensile stress would be eliminated during shear fracturing. Thus a pure shear failure mechanism may be obtained. Although tensile stress exists in the shear fracturing, it is the shear stress, which is several times higher than the tensile stress, which dominate the Mode II fracture mechanism.

The Mode II fracture toughness was determined using the numerical results as shown in Table(7.2). The stress intensity factor, K_{IIc}, calculated for: (a) varying slot separation distance and (b) varying percentage of polypropylene fibre content. The results are shown in Table(7.3) and are summarised in Table(7.4). It is seen that the slot separation has no effect on the fracture toughness (Mode II) as shown in Figs.(7.14-7.20). The addition of polypropylene fibre in concrete has little influence on the stress intensity factor K_{IIc}. The results are illustrated graphically in Figs.(7.21-7.24). The Mode II fracture toughness are dependent on the maximum load at crack initiation. The toughness, as exhibited by the post-cracking behaviour, will be discussed in detail in the conclusion.

The stress intensity factor, K_{IIc}, slightly increases with the polypropylene fibre content up to the optimum value (fibre content) and then drops off. The maximum toughness strengths obtained in this study are within the range of 0.10 percent to 0.15 percent polypropylene fibre content. Further increase of the fibre content beyond this value leads to a reduction of the toughness strength. This phenomenon is most probably due to insufficient compaction of the polypropylene fibre-reinforced concrete — this problem has already been discussed in Chapter 3.

The coefficient of variation for the fracture toughness values are shown in Table(7.4). The results show considerable variation — within the range of 7.6 percent to 28.1 percent. The best correlation of the results were determined within the slot separation/specimen ratios of 0.20 and 0.25 limits. The spread of the results are most likely due to the size of the aggregate used in the concrete which leads to the non-uniformity of the region between the opposite notches in the specimen. This phenomenon is clearly seen in the slot separation/specimen ratios of 0.10 and 0.15. The results are summarised graphically in Fig.(7.25). It may be concluded that the most consistent results have been obtained within $0.20 \leq a/w < 0 \leq 25$ limits.

The average fracture toughness (Mode II) with varying

polypropylene fibre content is shown graphically in Fig.(7.26). It can be seen that the polypropylene fibre content between 0.05 percent and 0.15 percent (by weight) increases the shear toughness by approximate 12 percent over that of plain concrete, but the polypropylene fibre content of 0.30 percent decreases the Mode II fracture toughness by about 8 percent. The compressive strength with varying polypropylene fibre content is shown in Fig.(7.26). The compressive strength up to 0.20 percent of the polypropylene fibre content is practically constant and equals that of plain concrete. The drop in compressive strength of about 10 percent can be seen when the polypropylene fibre content is 0.30 percent. It may be concluded that the fibre content up to 0.15 percent (by weight) improves the shear toughness of the concrete, but when the fibre content is greater than 0.20 percent both the compressive strength and the fracture toughness in shear decrease due to insufficient compaction of the concrete.

In recent years, a number of research workers has investigated the Mode I fracture toughess of plain and fibre-reinforced concretes as described in the review of literature. The reason for the concentration of research in Mode I is that it is an easy mode to test where all the necessary conditions are not difficult to achieve in the laboratory. In addition, the analytical approach associated with Mode I, is easier than Mode II fracture mechanism.

Mode II fracture toughness of fibre-reinforced concretes is important due to these composite materials are generally weak in shear. The in-plane shear specimen has been developed in this thesis to evaluate the Mode II fracture toughness of fibre-reinforced concrete. The test results may be used either to determine the fracture toughness or to give an indication of toughness from the load-deflection graphs of the cracked specimen. Since there is no similar work reported by other research workers, the experimental and numerical results of this study cannot be compared with others.

Although the in-plane shear specimen results are independent of the slot separation and give constant fracture toughness value, it is seen that the results show considerable variation(7.6 percent-28.1 percent). Thus the in-plane shear specimen should be further investigated to verify its validity for Mode II fracture toughness testing. From the results shown in Table(7.4), the size of the aggregate(10mm) has greatly influenced the Mode II fracture toughness value within the slot separation/specimen ratios of 0.10 to 0.15 limits. In order to reduce the variation of the results, either the aggregate size should be reduced or the specimen geometries should be increased. Thus a more uniform region between the opposite notches is obtained. Apart from the concrete specimens, materials such as mortar and soil-cement should be employed in the in-plane shear test. It is because these materials provide more uniform

homogeneous property in the matrix, they should give more consistent results than the fibre-reinforced concrete.

Since the in-plane shear specimen can be used to determine either the fracture toughness or to give the indication of toughness from the test results, various types of fibres such as steel and glass etc. can be used in concretes, so that the comparisons of the stress intensity factor values (Mode II) or toughness can be made among them. In general, the fracture toughness index of fibre-reinforced concrete gives a better indication of toughness than the load at initial cracking -- the advantages of the fracture toughness index has already been discussed in Chapter 4.

The experimental and numerical work carried out in this study was based on the maximum compressive load obtained in the experiment. The fracture toughness (Mode II) is calculated from the peak load achieved. Further experiments should be carried out with a tensile load acting at both ends of the in-plane shear specimen. The shear failure of the specimen in this case (tensile load) should be similar to those obtained in this study (compressive load). Thus the results could be compared between the two loading systems.

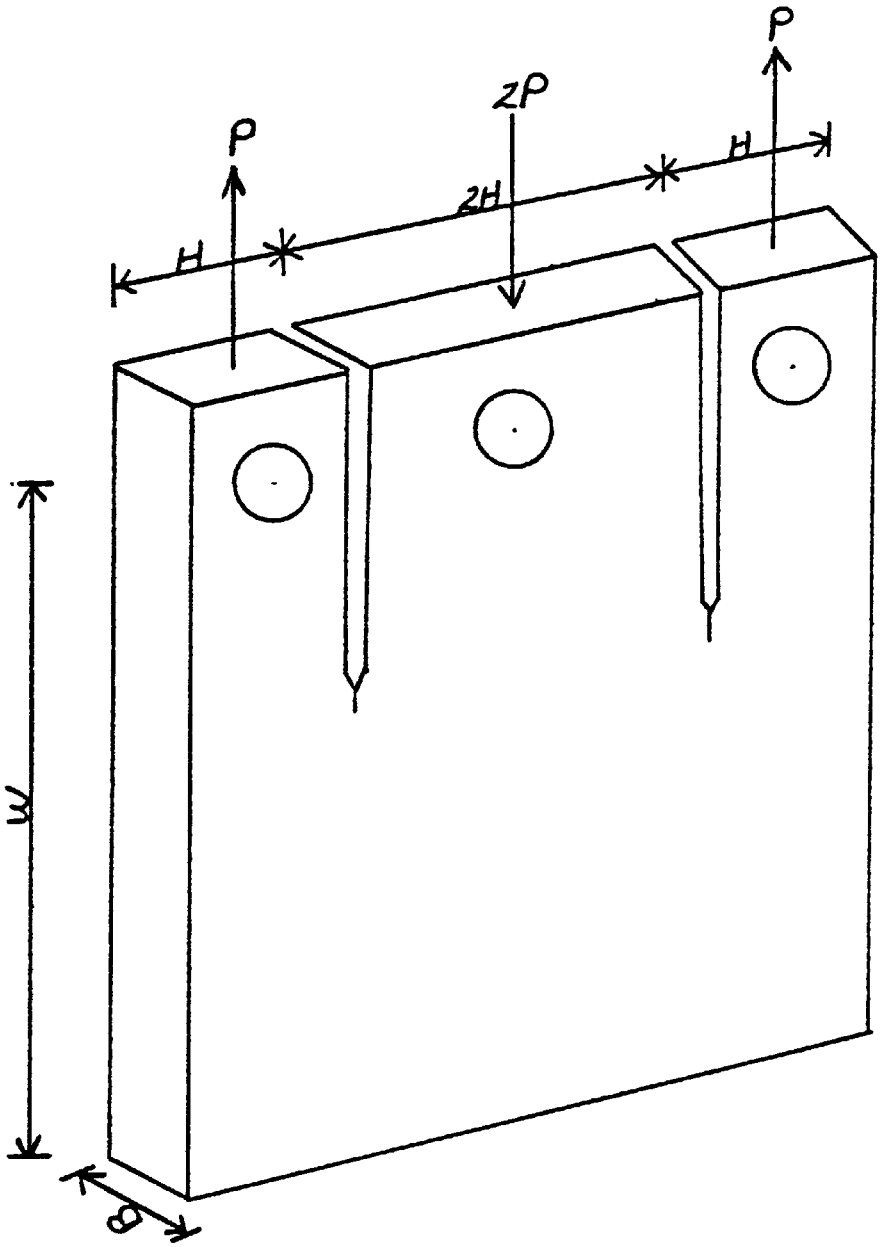

Fig. (7.1) Compact shear specimen used by Chisholm et al (54)

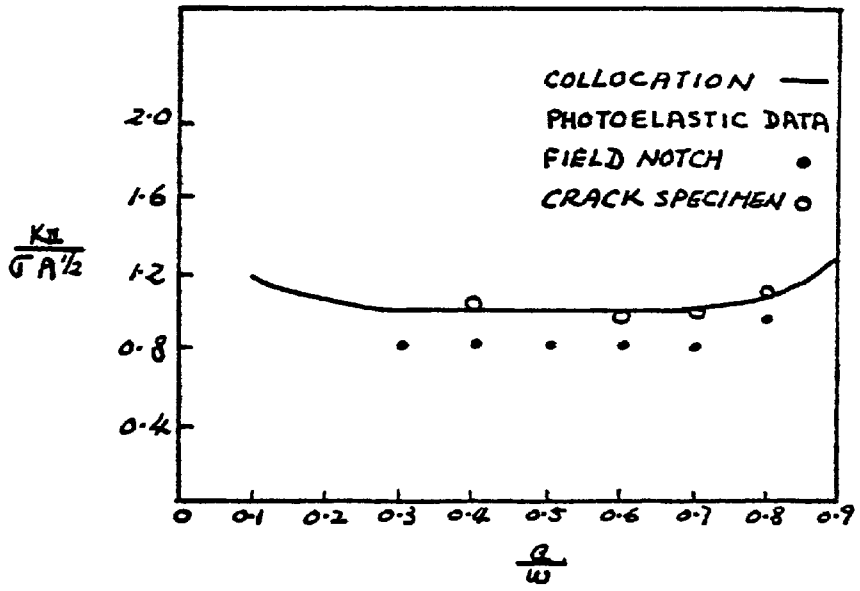

Fig. (7.2) Comparison of collocation results with photoelastic data (Chisholm et al[54])

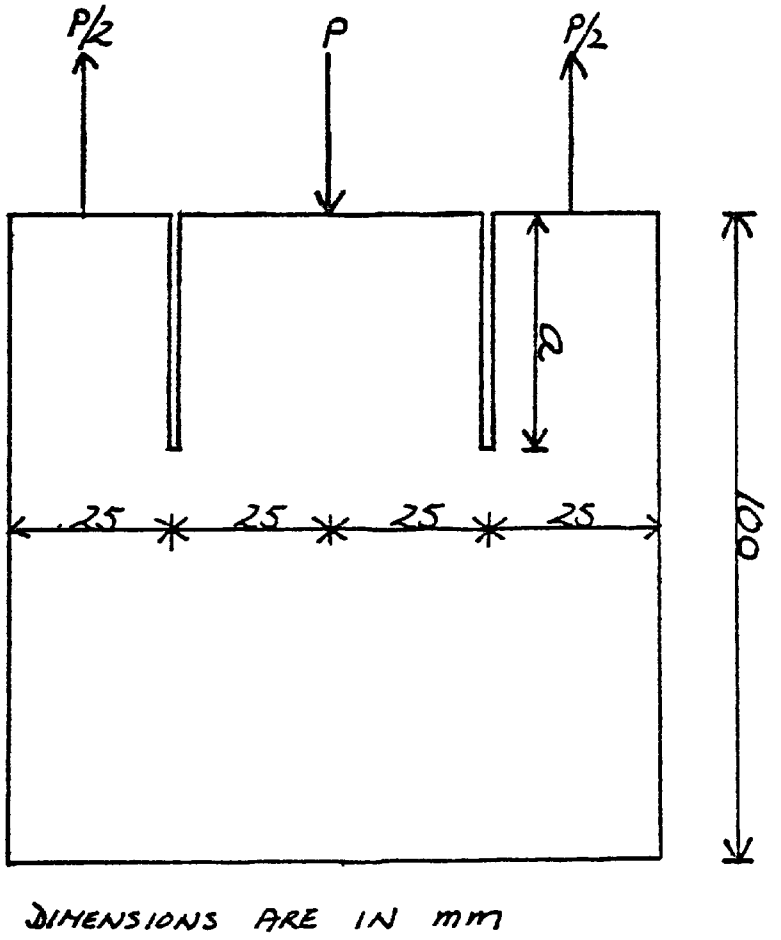

Fig. (7.3) Compact shear specimen used in the finite element analysis (Sabir [52])

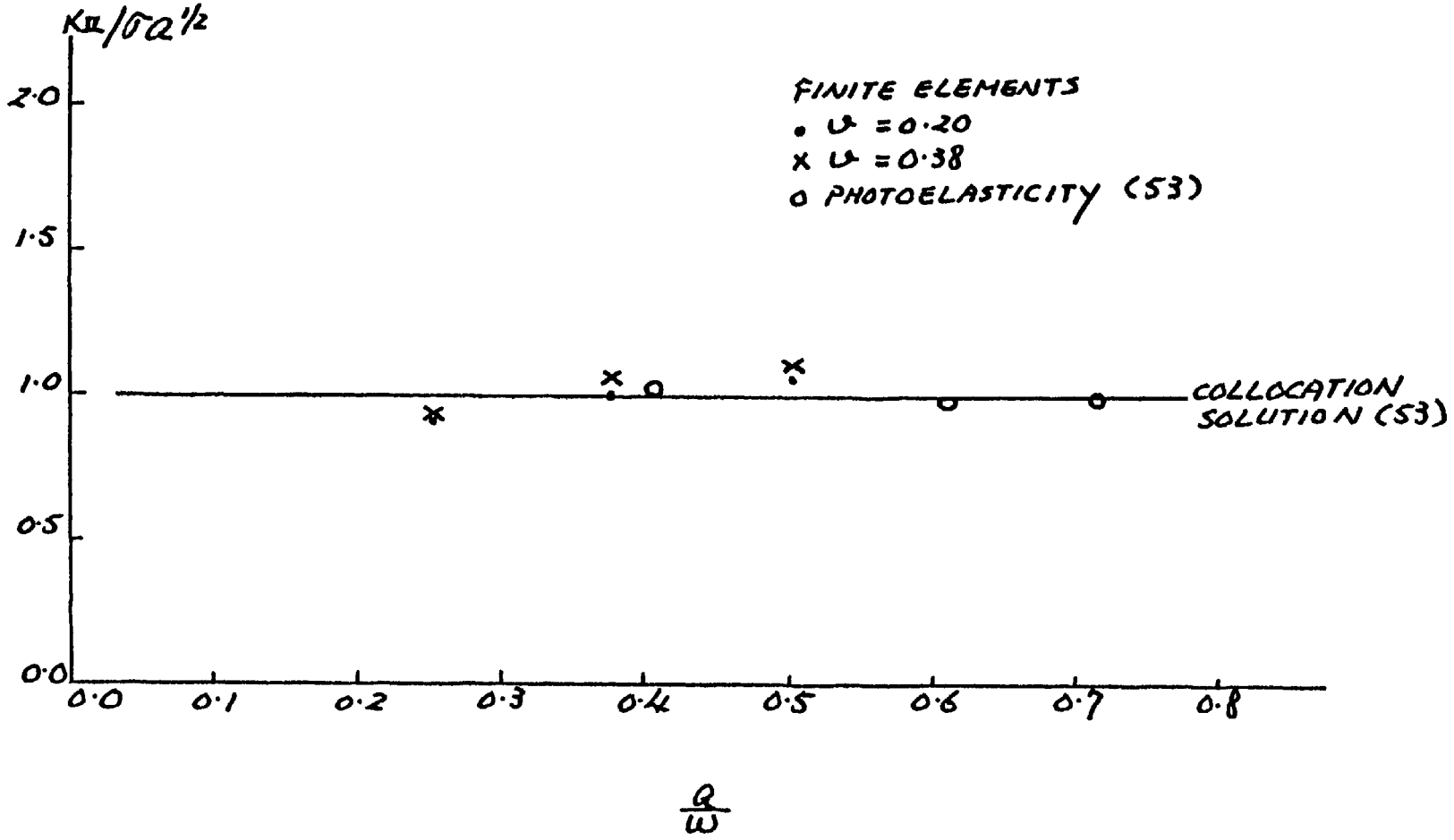

Fig. (7.4) Results for the compact shear specimen (Sabir[62])

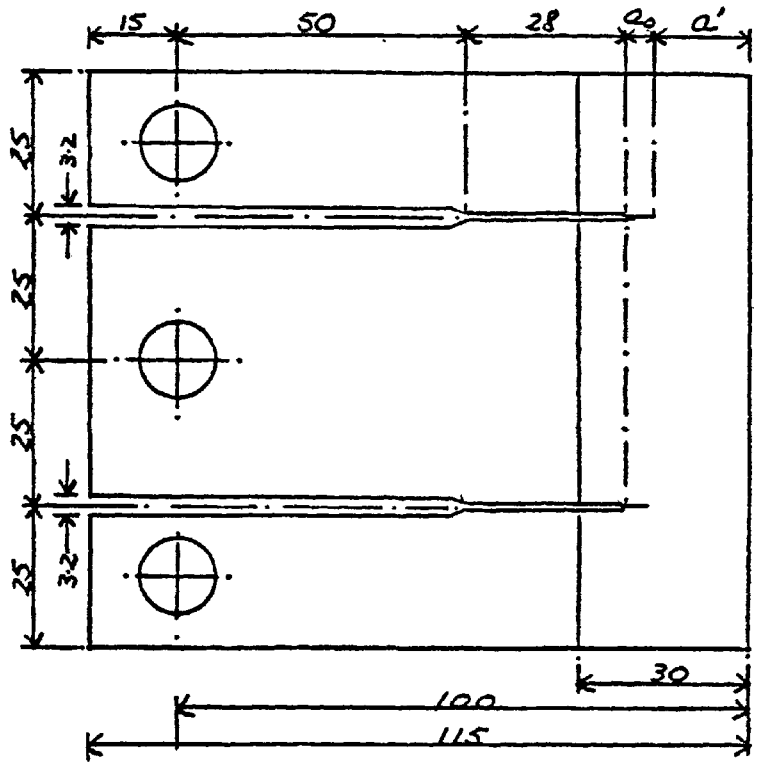

Fig. (7.5) Compact shear specimen used by Sharples (60)

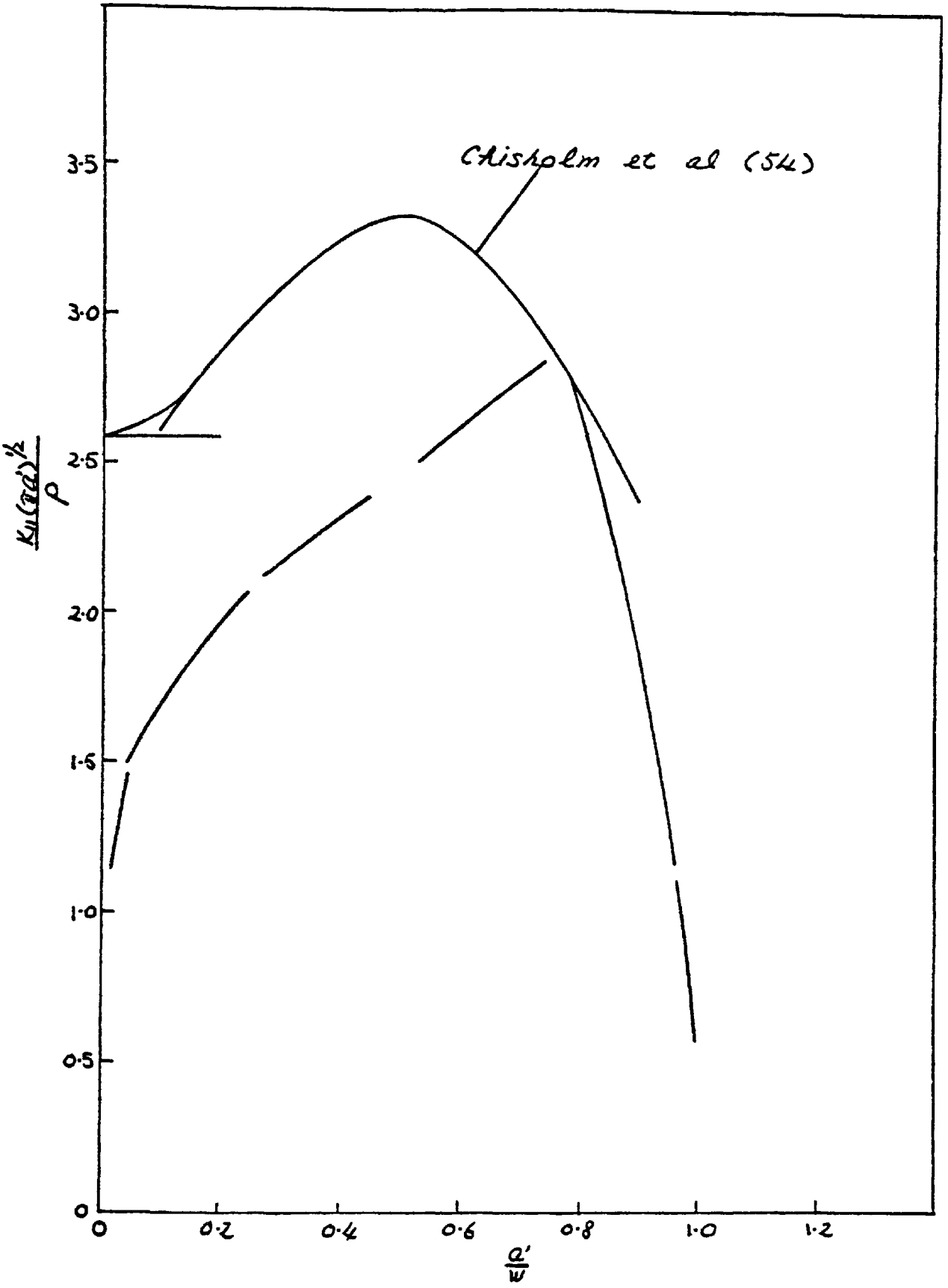

Fig. (7.6) Stress intensity factor results for Mode II (Sharples[60])

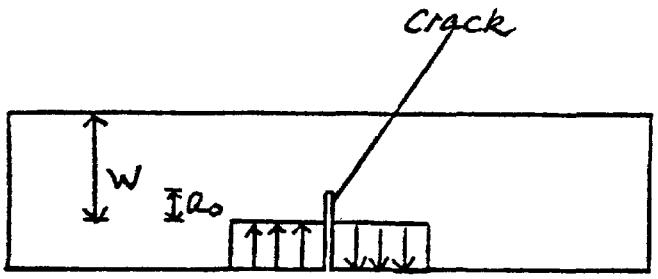

Fig. (7.7) Mode II loading of a specimen (Agarwal et al [61])

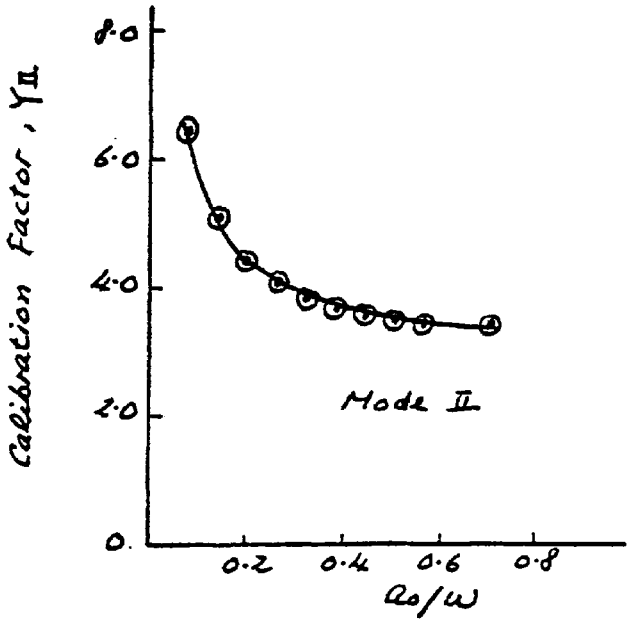

Fig. (7.8) Calibration factor in Mode II (Agarwal et al [61])

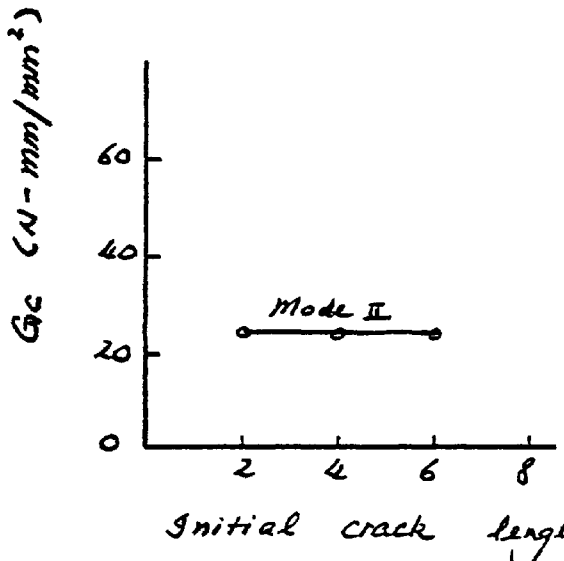

Fig. (7.9) Variation of critical strain energy release rate with initial crack length (Agarwal et al [61])

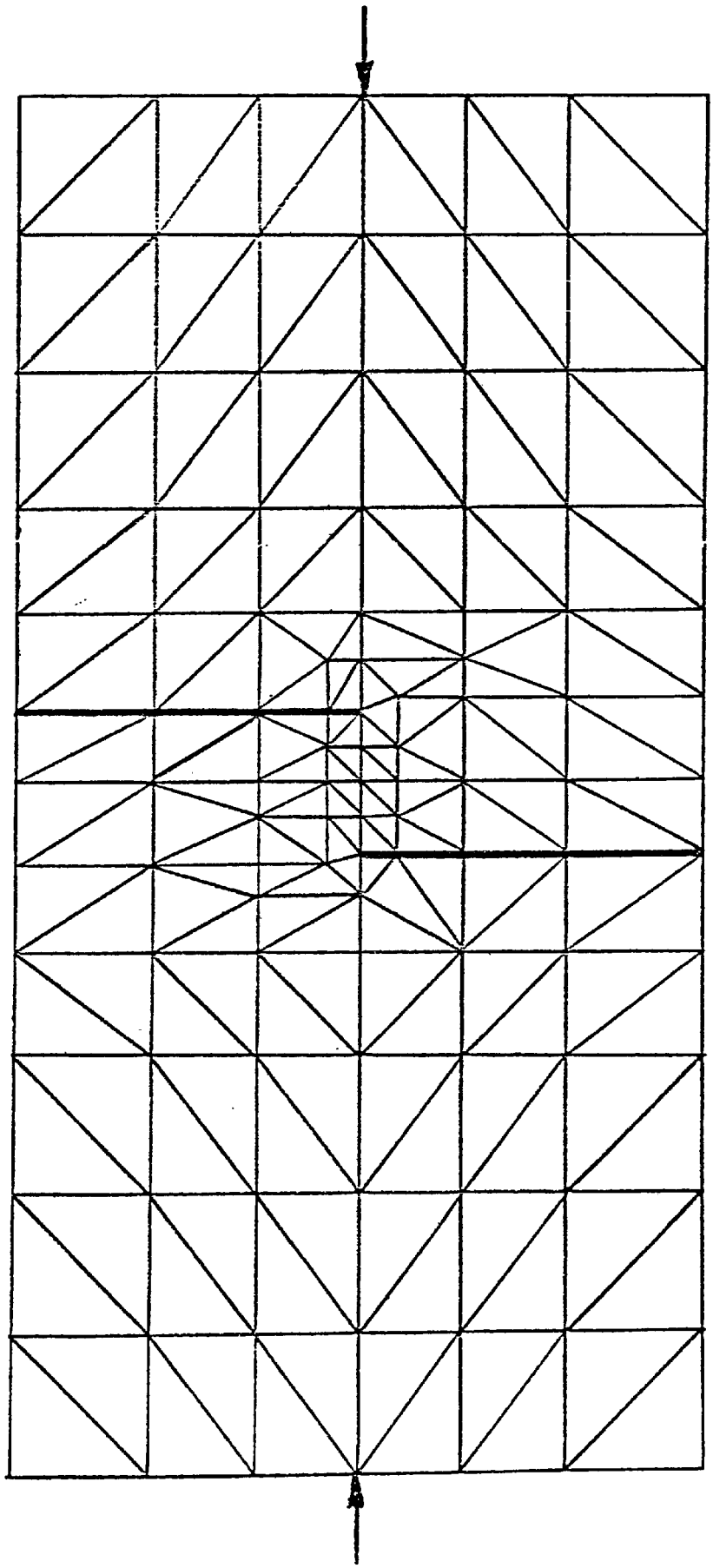

Fig. (7.10) Finite element representation (in plane shear)

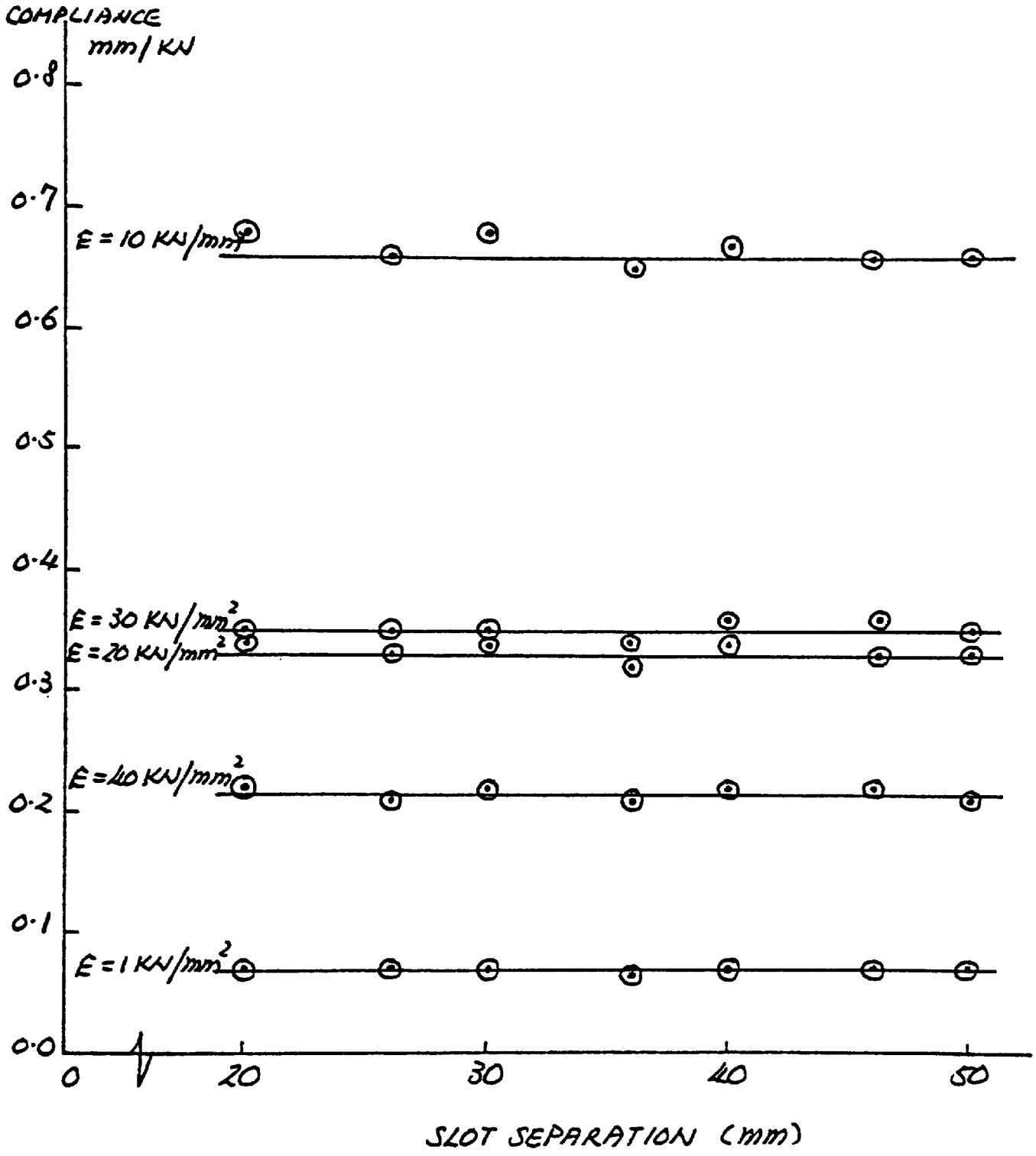

Fig. (7.11) Compliance results for varying slot separation

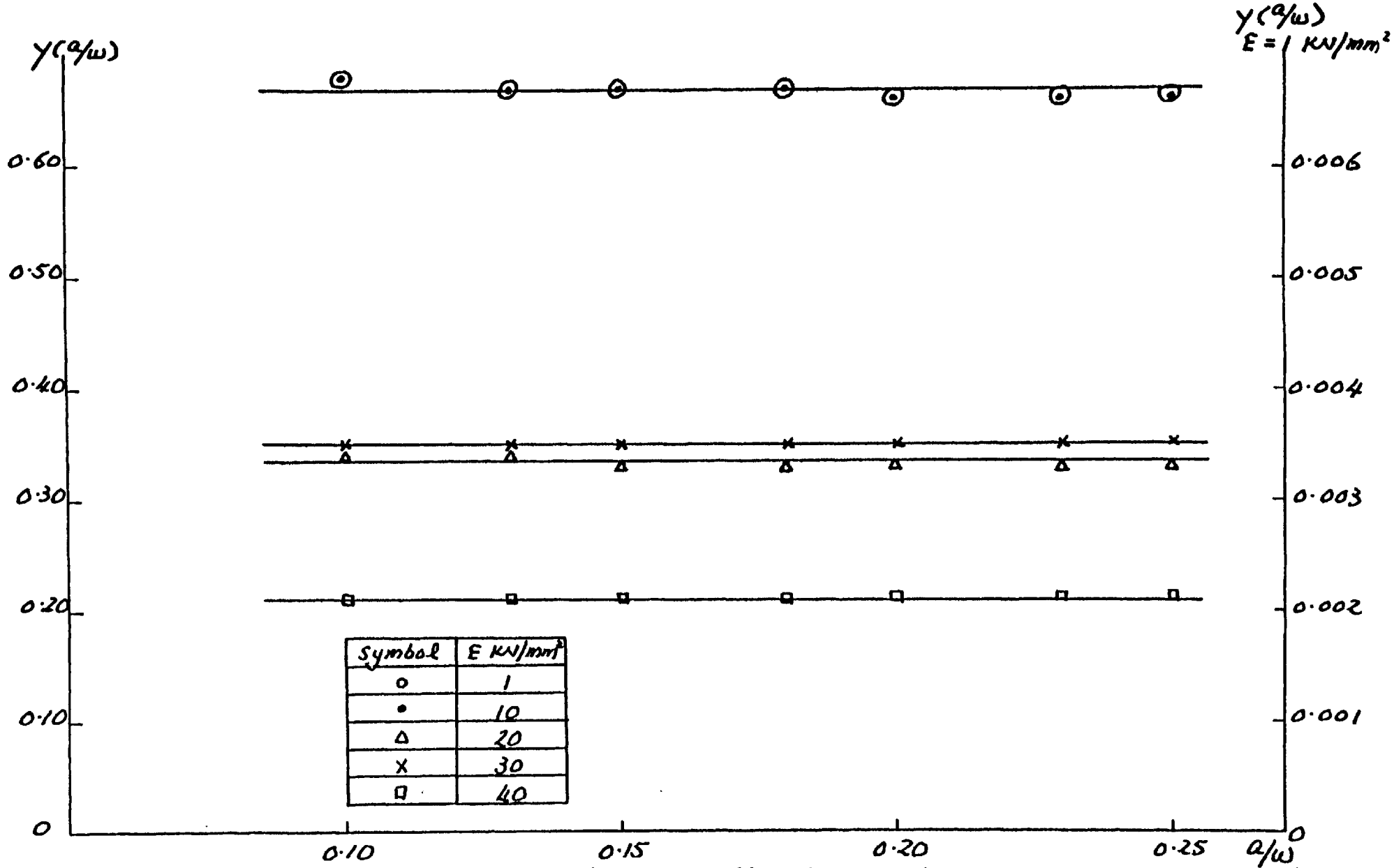

Fig. (7.12) Calibration coefficient results for varying slot separation ratio

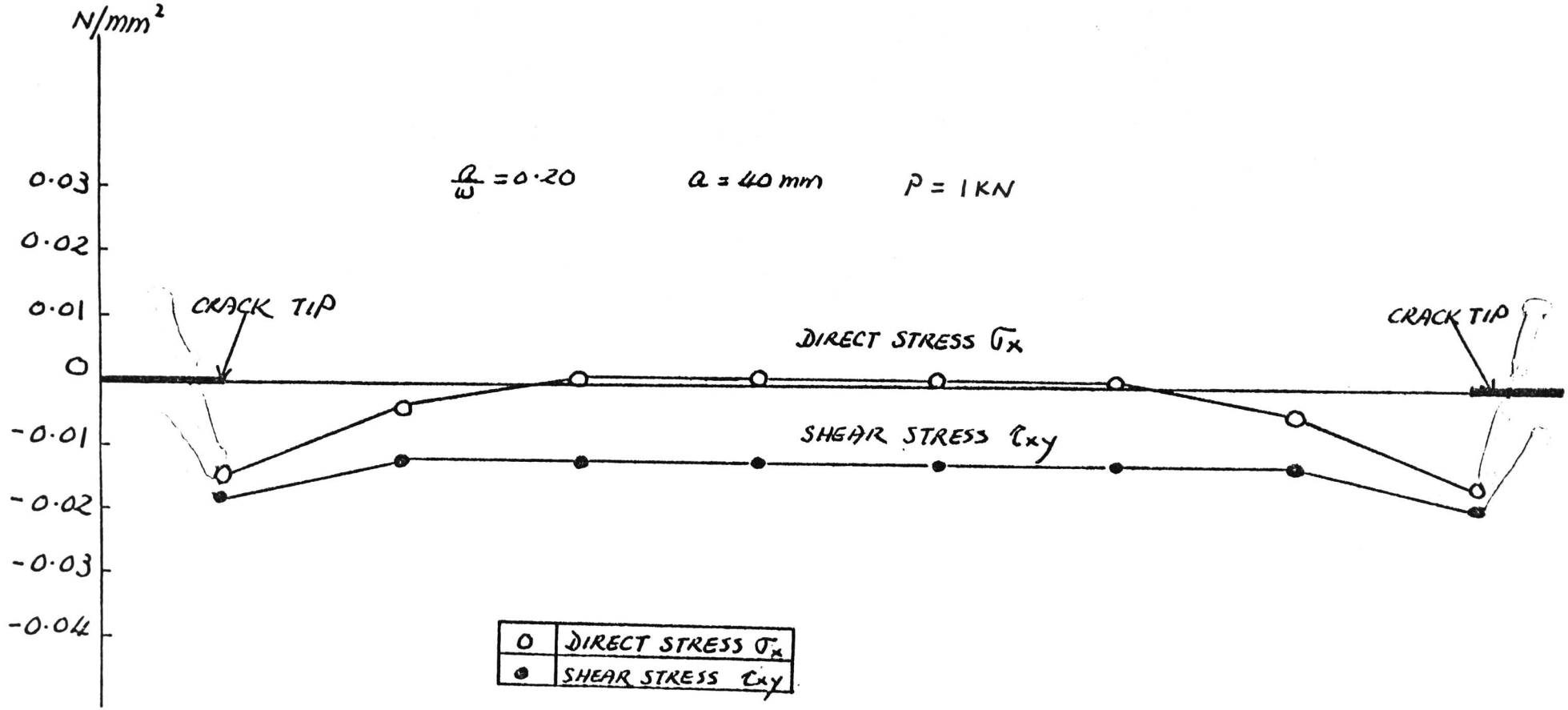

Fig. (7.13) Typical stress distributions between opposite crack tips

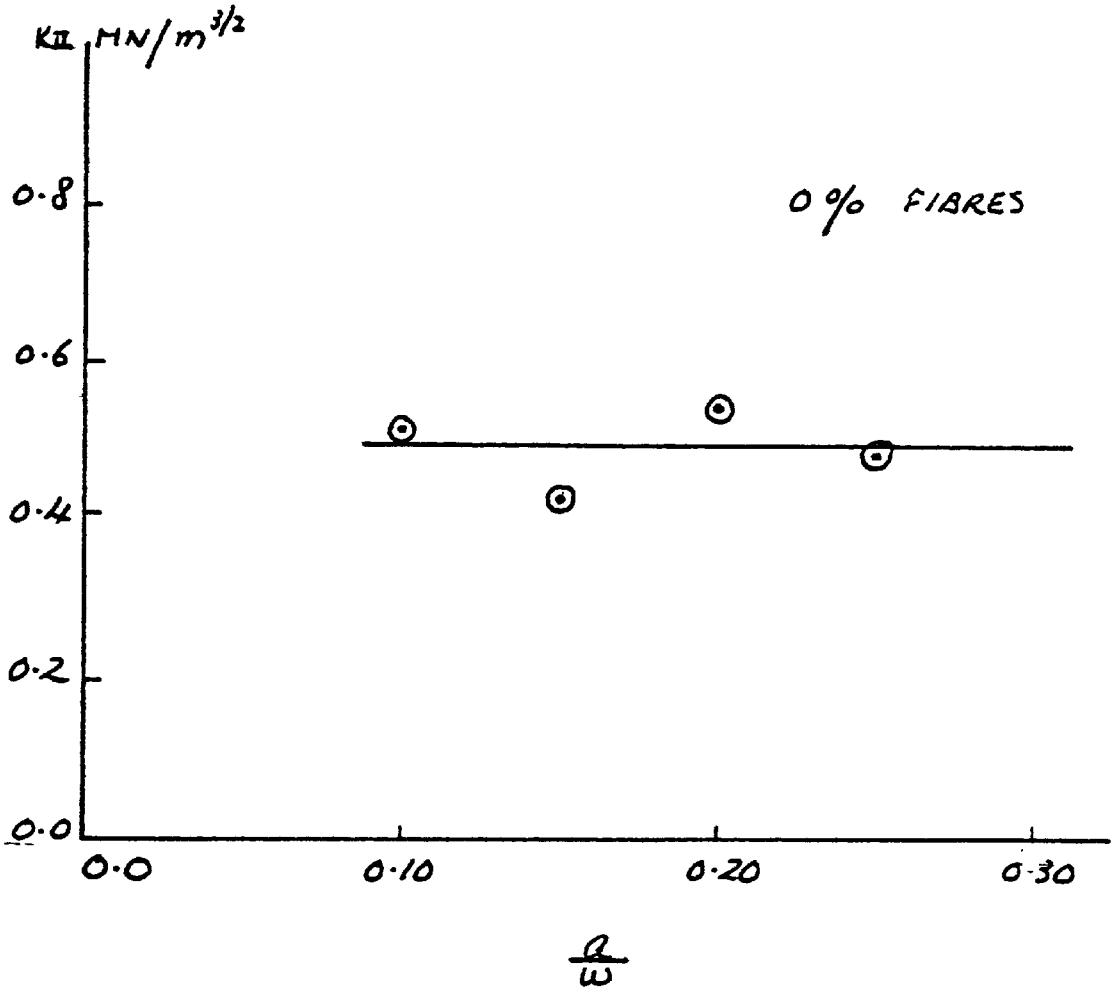

Fig. (7.14) Fracture toughness results for varying slot separation ratio

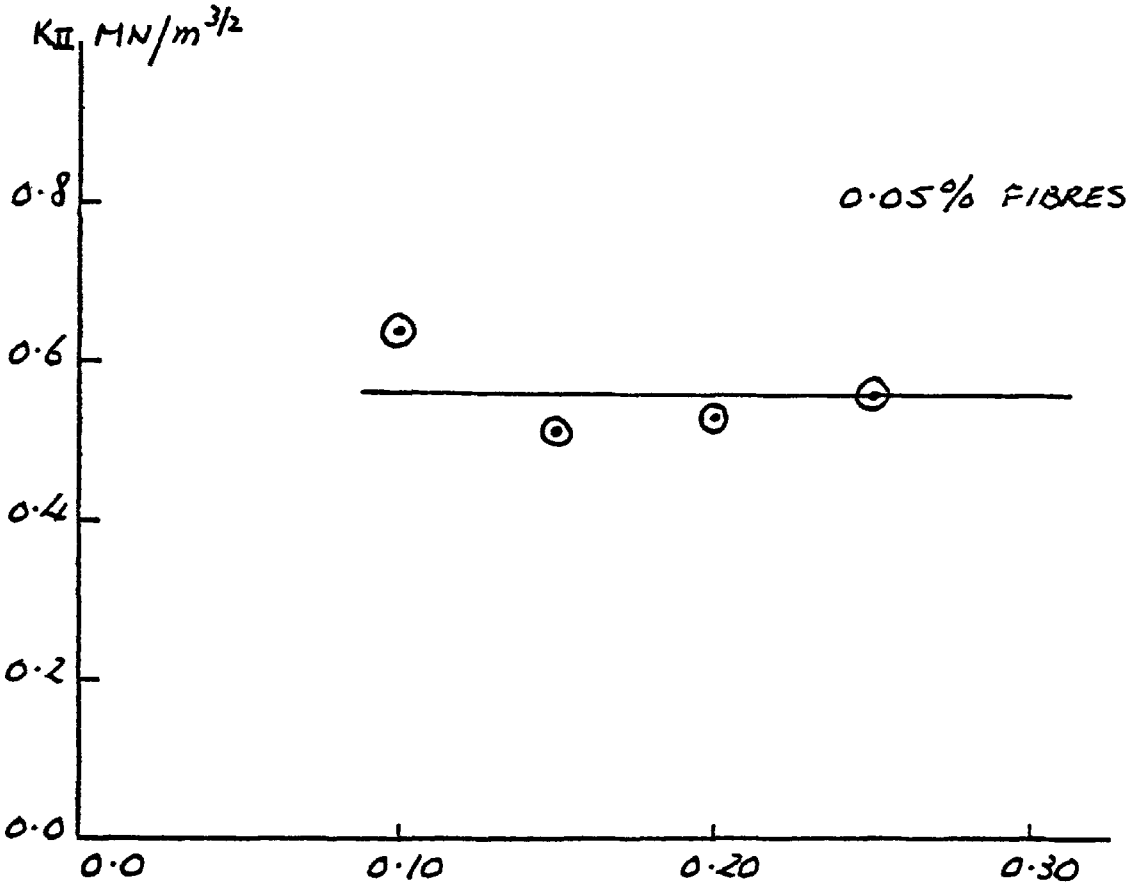

Fig. (7.15) Fracture toughness results for varying slot separation ratio

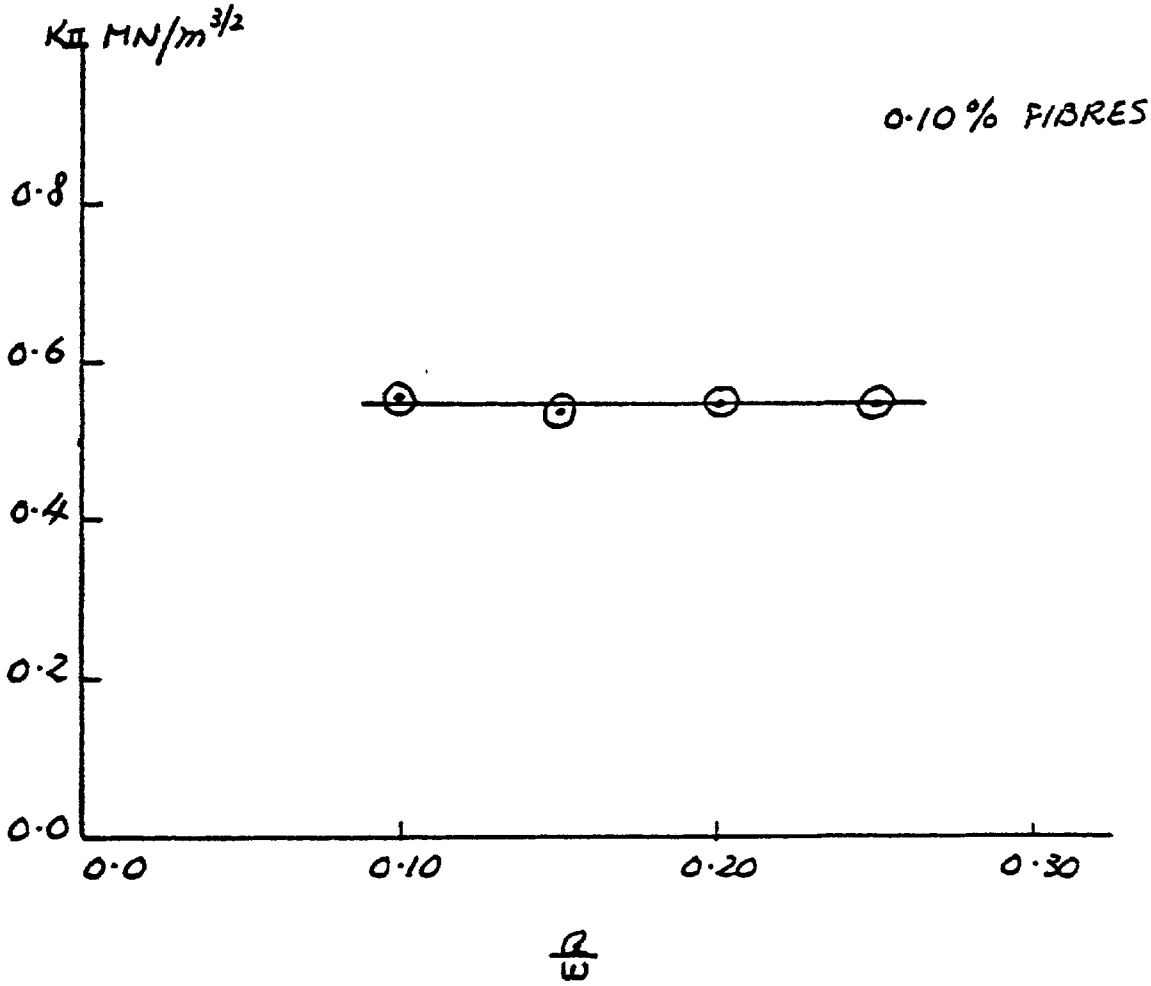

Fig. (7.16) Fracture toughness results for varying slot separation ratio

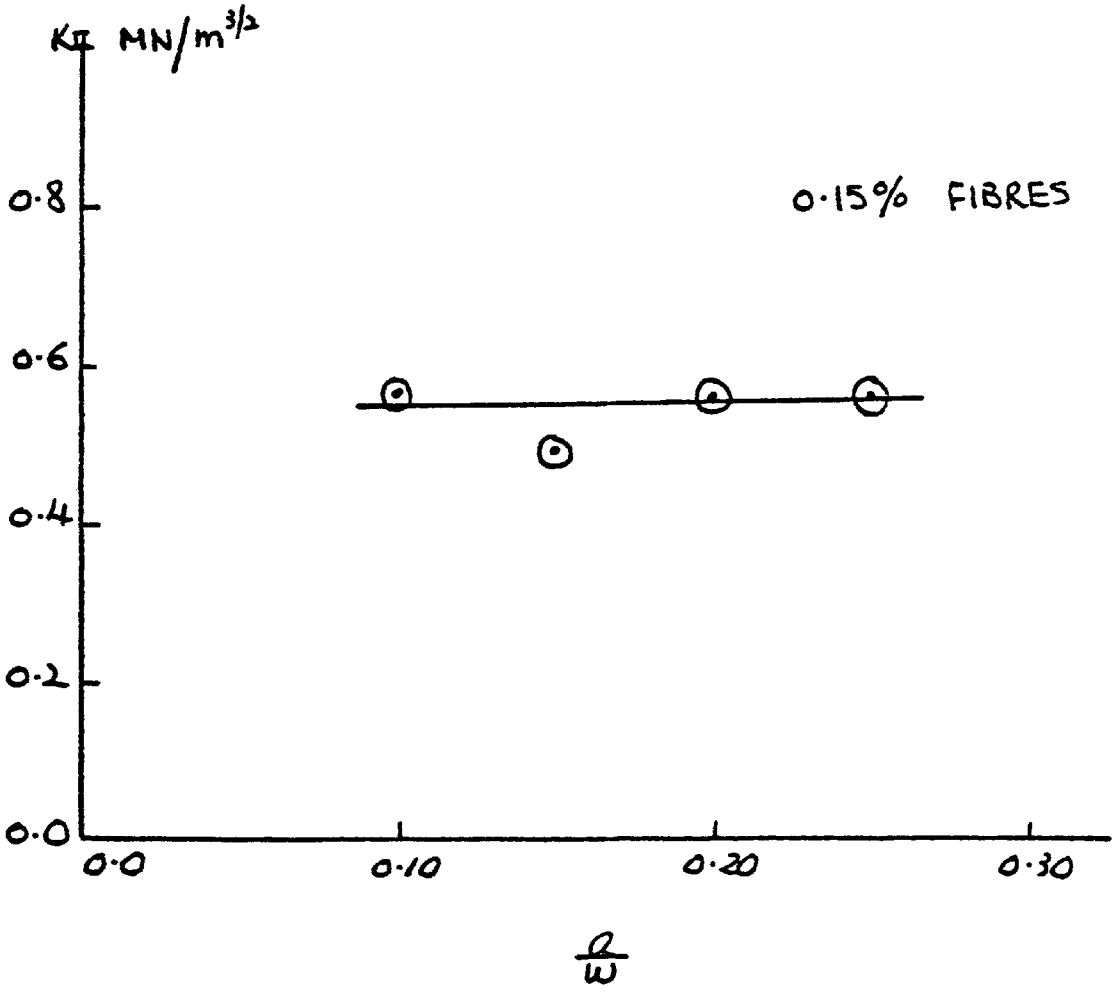

Fig. (7.17) Fracture toughness results for varying slot separation ratio

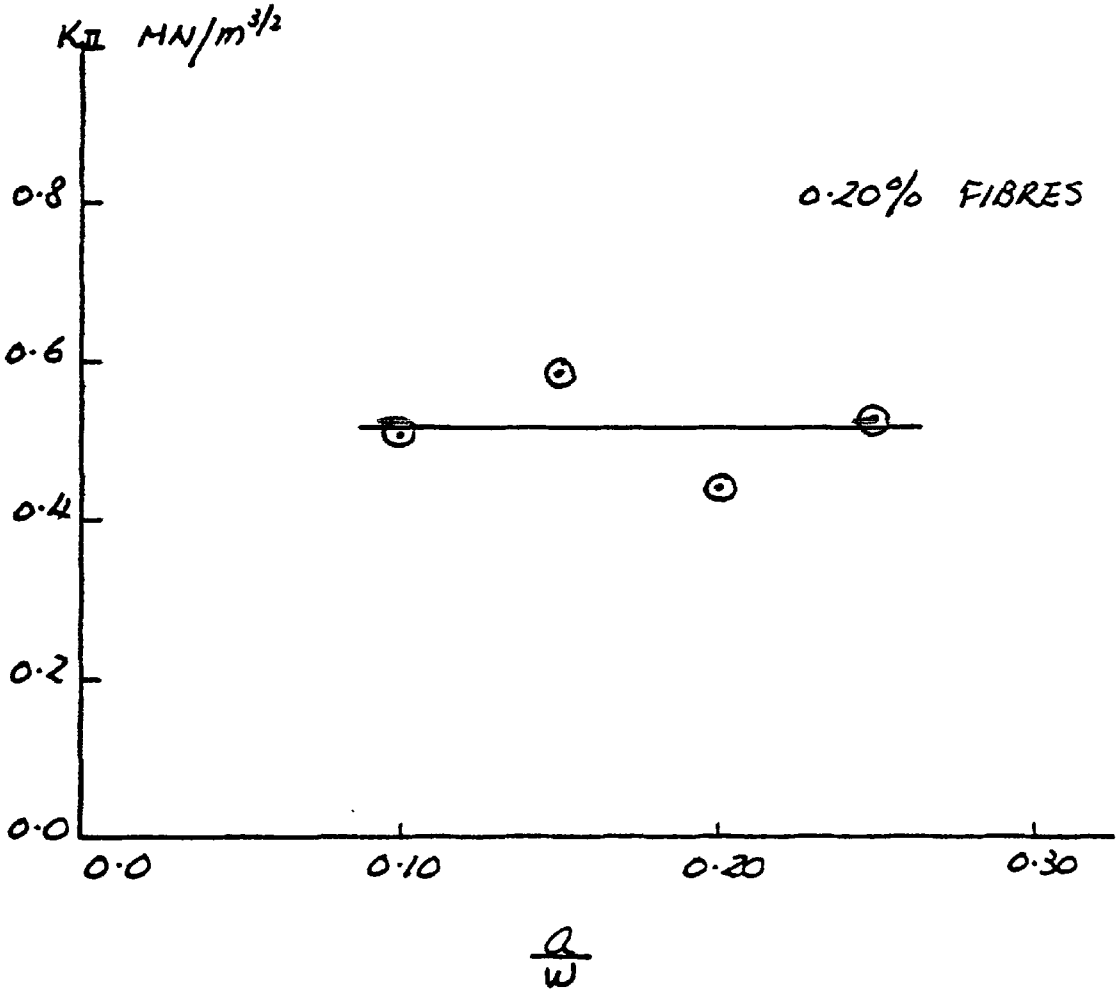

Fig. (7.18) Fracture toughness results for varying slot separation ratio

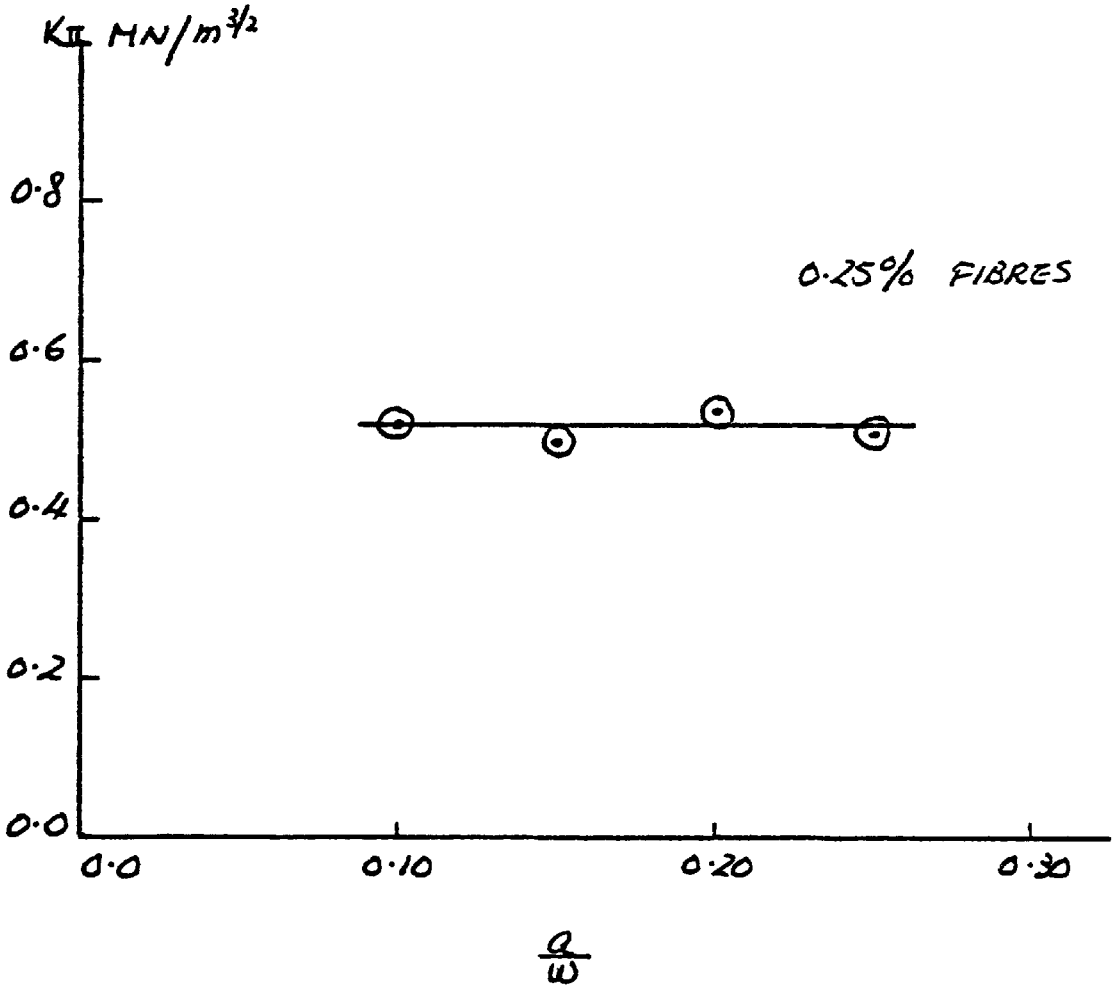

Fig. (7.19) Fracture toughness results for varying slot separation ratio

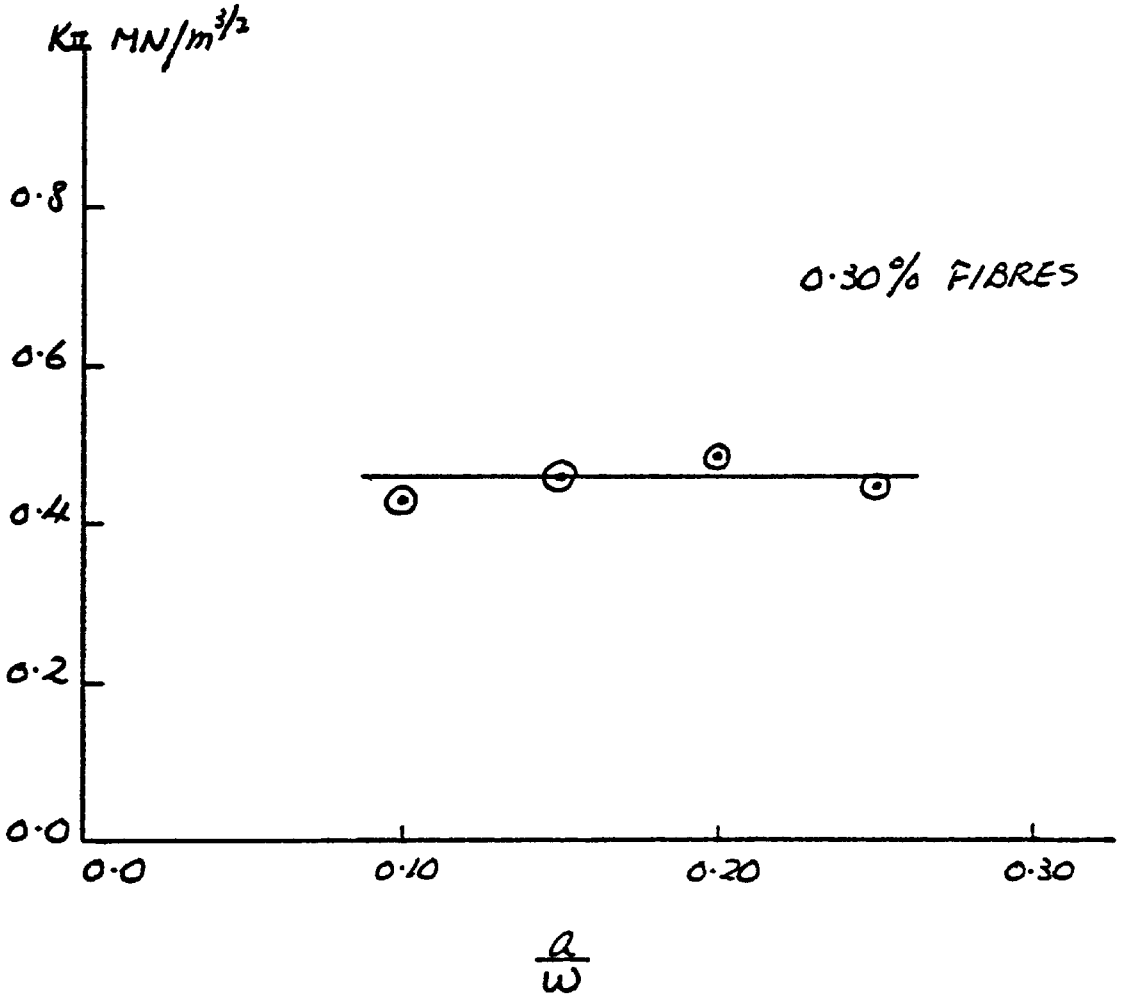

Fig. (7.20) Fracture toughness results for varying slot separation ratio

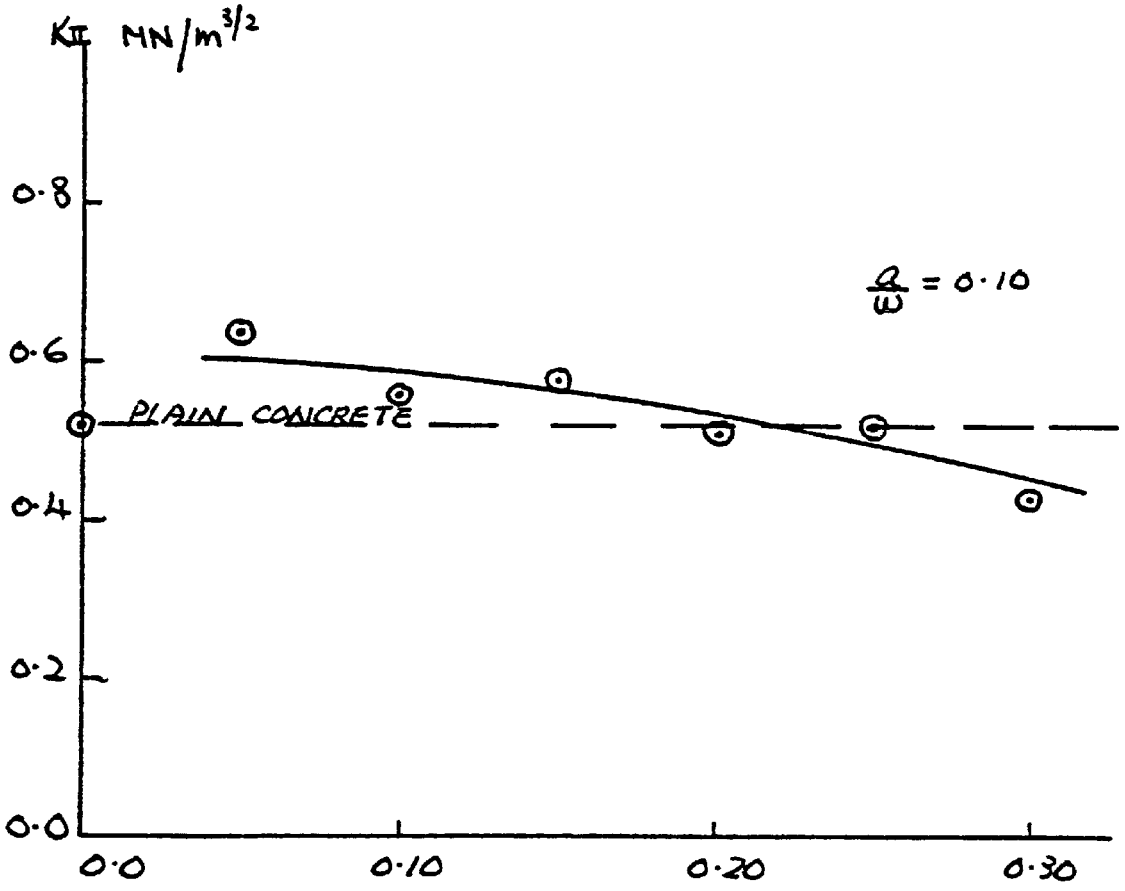

Fig. (7.21) Fracture toughness results for varying fibre content

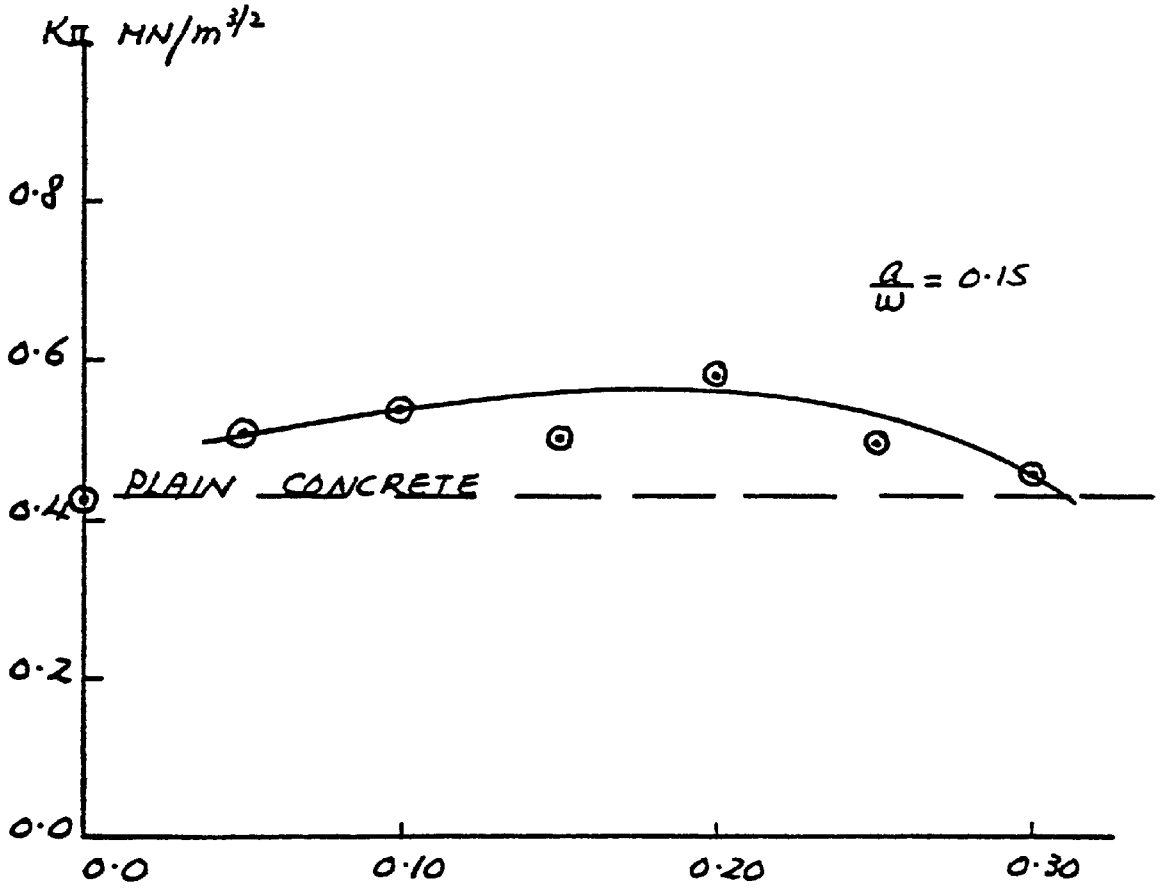

Fig. (7.22) Fracture toughness results for varying fibre content

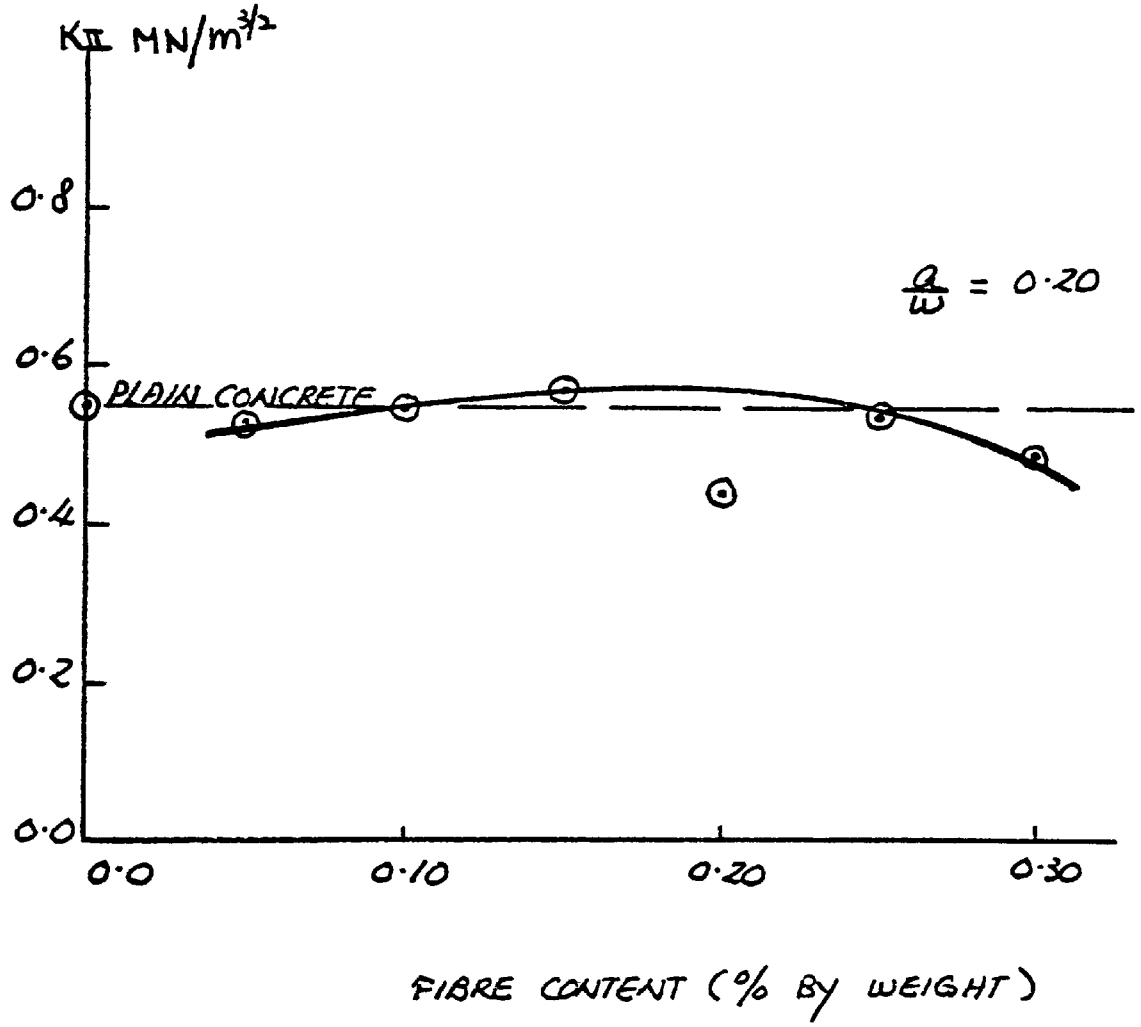

Fig. (7.23) Fracture toughness results for varying fibre content

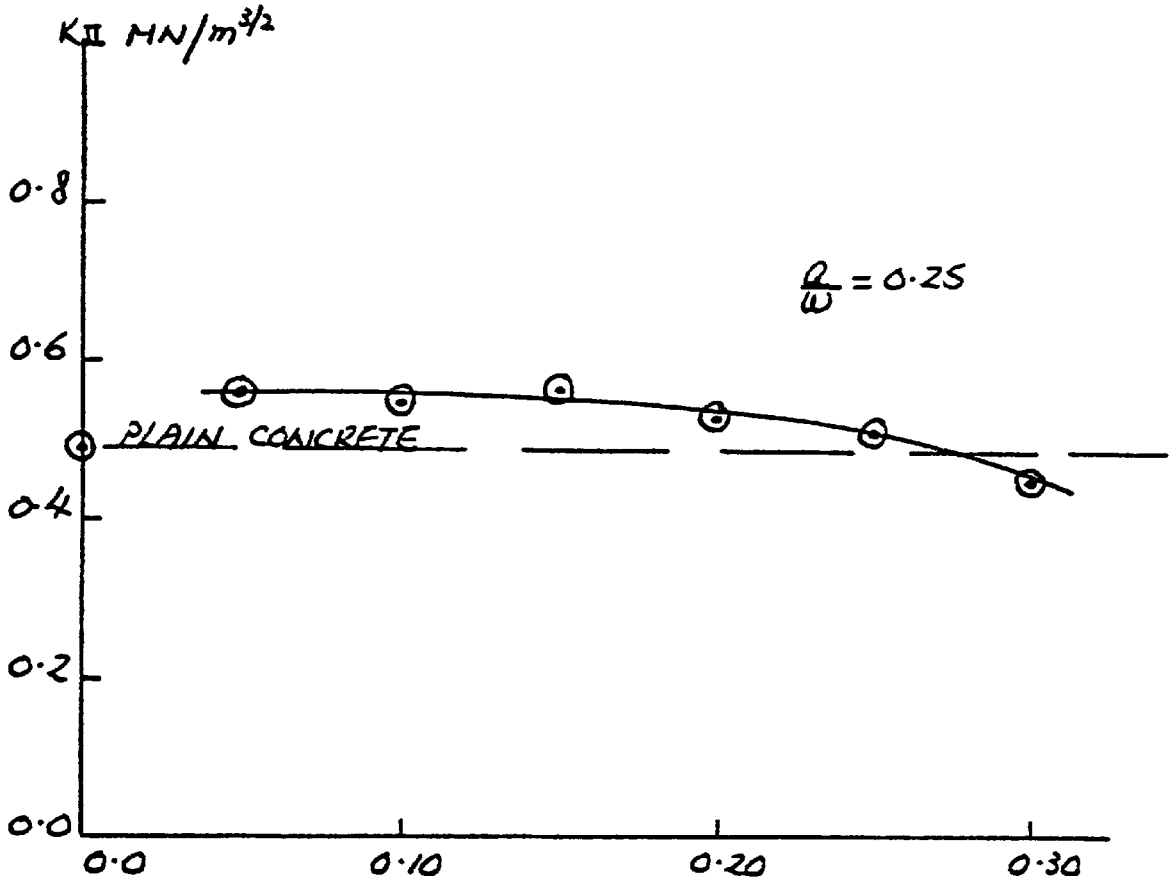

Fig. (7.24) Fracture toughness results for varying fibre content

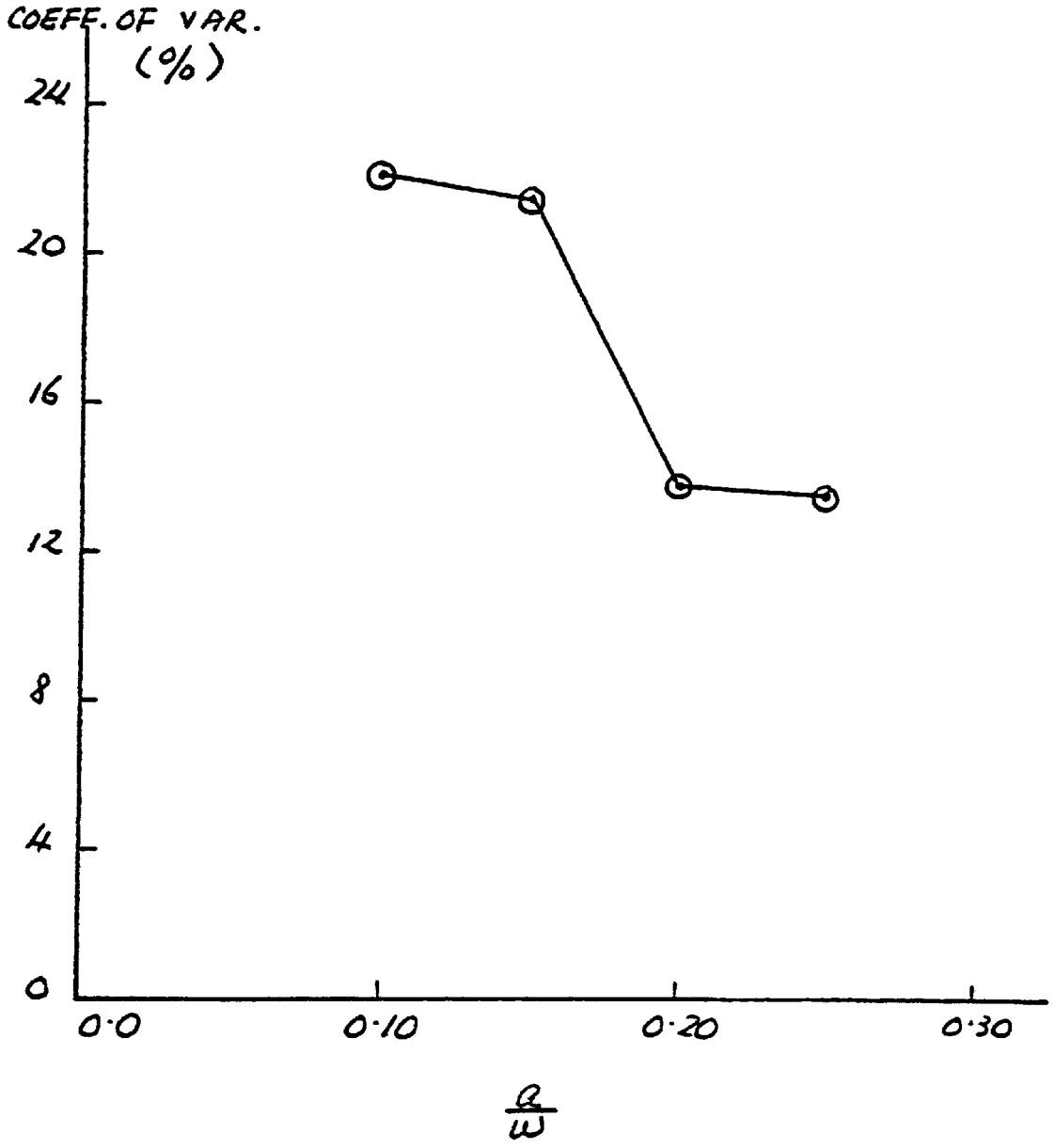

Fig. (7.25) Coefficient of variation results for varying slot separation ratio

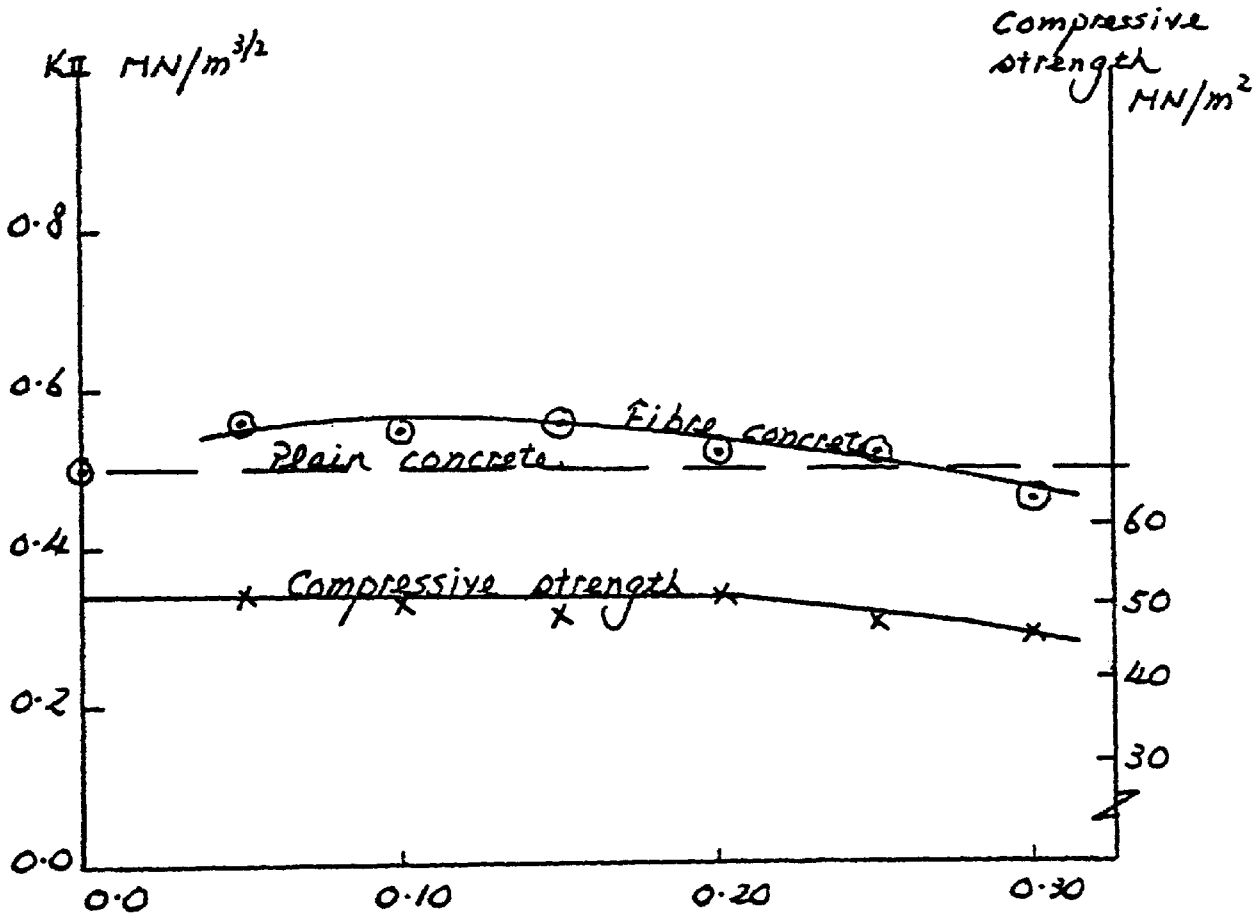

Fig. (7.26) Average fracture toughness results for varying fibre content

Table(7.1) Compliance results for varying the modulus of elasticity and slot-separation.

a (mm) \ E KN/mm²	1	10	20	30	40
20	0.0069	0.68	0.34	0.35	0.22
26	0.0066	0.66	0.33	0.35	0.21
30	0.0068	0.68	0.34	0.35	0.22
36	0.0065	0.65	0.32	0.34	0.21
40	0.0067	0.67	0.34	0.36	0.22
46	0.0067	0.66	0.33	0.36	0.22
50	0.0066	0.66	0.33	0.35	0.22

Table(7.2) Calibration coefficient results for varying the modulus of elastricity.

E KN/mm²	A	B
1	0.0069	-0.0014
10	0.6908	-0.1403
20	0.3454	-0.0704
30	0.3509	——
40	0.2155	——

$$Y(a/w) = A + B(a/w)$$

Table(7.3) Mode II fracture toughness results for varying fibre content and slot-separation ratio.

a/w	Fibre Content By Weight (%)	Stress Intensity Factor, K_{II},					
0.10	0	0.38	0.62	0.53	0.27	0.61	0.49
		0.67	0.29	0.73	0.50	0.62	0.47
		0.70	0.35	0.58			
	0.05	0.70	0.68	0.82	0.56	0.62	0.78
		0.72	0.80	0.53	0.70	0.72	0.58
		0.43	0.55	0.54	0.59		
	0.10	0.53	0.61	0.58	0.39	0.65	0.56
		0.47	0.41	0.52	0.69	0.48	0.66
		0.47	0.59	0.56	0.76		
	0.15	0.73	0.46	0.59	0.70	0.51	0.52
		0.60	0.61	0.39	0.67	0.45	0.65
		0.58	0.63	0.69			
	0.20	0.38	0.38	0.40	0.54	0.61	0.44
		0.62	0.39	0.62	0.71	0.86	0.51
		0.39	0.31	0.45	0.61		
	0.25	0.37	0.41	0.38	0.47	0.66	0.54
		0.47	0.61	0.56	0.57	0.58	0.50
		0.60	0.52	0.66	0.45		
	0.30	0.42	0.38	0.42	0.57	0.64	0.29
		0.31	0.38	0.39	0.50	0.69	0.44
		0.37	0.29	0.32	0.53		
0.15	0	0.37	0.31	0.50	0.46	0.40	0.33
		0.36	0.42	0.50	0.60	0.54	0.54
		0.30	0.62	0.44	0.27	0.29	0.44
		0.47	0.45				
	0.05	0.37	0.45	0.50	0.31	0.54	0.44
		0.58	0.48	0.50	0.51	0.53	0.61
		0.64	0.50	0.64	0.55	0.54	

Table(7.3) cont. Mode II fracture toughness results for varying fibre content and slot-separation ratio.

a/w	Fibre Content By Weight (%)	Stress Intensity Factor, K_{II},					
		0.66	0.65	0.45	0.64	0.56	0.67
	0.10	0.52	0.48	0.56	0.63	0.57	0.40
		0.66	0.54	0.61	0.45	0.51	0.70
		0.41	0.48	0.40	0.47	0.43	
		0.43	0.54	0.56	0.52	0.64	0.33
	0.15	0.61	0.34	0.46	0.42	0.35	0.57
		0.56	0.68	0.49	0.53	0.61	0.57
		0.42	0.31				
		0.72	0.46	0.66	0.76	0.59	0.65
0.15	0.20	0.78	0.55	0.67	0.29	0.43	0.50
		0.73	0.43	0.54	0.71	0.66	0.81
		0.48	0.66	0.46	0.37		
		0.58	0.51	0.59	0.67	0.56	0.58
	0.25	0.58	0.58	0.51	0.34	0.61	0.42
		0.41	0.67	0.38	0.49	0.57	0.38
		0.30	0.40	0.55	0.30		
		0.41	0.38	0.38	0.38	0.48	0.43
	0.30	0.80	0.48	0.48	0.34	0.45	0.41
		0.51	0.53	0.37	0.54	0.41	0.41
		0.51					
		0.51	0.65	0.48	0.55	0.61	0.57
	0	0.43	0.57	0.61	0.38	0.70	0.52
		0.64	0.53	0.61	0.40		
		0.48	0.49	0.54	0.51	0.47	0.52
	0.05	0.51	0.58	0.57	0.57	0.48	0.51
		0.55	0.53	0.60			
		0.65	0.48	0.61	0.41	0.52	0.52
0.20	0.10	0.52	0.52	0.60	0.53	0.64	0.46
		0.51	0.55	0.64	0.52	0.64	
		0.64	0.51	0.60	0.61	0.55	0.53
	0.15	0.57	0.62	0.56	0.44	0.63	0.63
		0.56	0.46	0.71	0.61		
		0.53	0.55	0.46	0.41	0.54	0.59
	0.20	0.40	0.52	0.45	0.55	0.35	0.34
		0.50	0.51	0.49	0.34		

Table(7.3) cont. Mode II fracture toughness results for varying fibre content and slot-separation ratio.

a/w	Fibre Content By Weight (%)	Stress Intensity Factor, K_{II},					
0.20	0.25	0.51	0.48	0.59	0.61	0.53	0.57
		0.44	0.47	0.54	0.62	0.46	0.54
		0.47	0.47	0.64	0.64		
	0.30	0.61	0.53	0.41	0.57	0.37	0.41
		0.65	0.51	0.43	0.45	0.48	0.45
		0.45	0.49	0.45	0.61		
0.25	0	0.36	0.53	0.59	0.50	0.48	0.59
		0.60	0.54	0.39	0.37	0.32	0.44
		0.45	0.48	0.54	0.47	0.50	0.59
		0.64	0.45				
	0.05	0.50	0.65	0.62	0.52	0.62	0.54
		0.52	0.63	0.68	0.48	0.60	0.57
		0.45	0.49	0.57	0.53		
	0.10	0.51	0.58	0.54	0.60	0.54	0.59
		0.49	0.56	0.53	0.61	0.59	0.51
		0.57	0.59	0.45	0.49		
	0.15	0.59	0.55	0.61	0.45	0.65	0.50
		0.54	0.53	0.61	0.59	0.66	0.61
		0.61	0.63	0.55	0.49	0.44	0.49
		0.48					
	0.20	0.58	0.50	0.51	0.34	0.41	0.58
		0.57	0.60	0.60	0.54	0.46	0.59
		0.57	0.58	0.59			
	0.25	0.49	0.50	0.48	0.55	0.50	0.46
		0.57	0.55	0.41	0.52	0.54	0.61
		0.48	0.53	0.56	0.48	0.46	0.43
		0.61					
	0.30	0.53	0.50	0.47	0.61	0.58	0.44
		0.31	0.35	0.46	0.42	0.38	0.44
		0.34	0.51	0.45	0.54	0.51	0.49
		0.33	0.52	0.26			

Table(7.4) Summarised Mode II fracture toughness results for varying slot separation ratio and fibre content.

a/w	Fibre Content By Weight (%)	K_{II} $MN/M^{3/2}$	Coeff. of Var.	No. of Samples
0.10	0.00	0.520	28.047	15
	0.05	0.644	17.181	16
	0.10	0.558	18.407	16
	0.15	0.585	17.357	15
	0.20	0.513	28.908	16
	0.25	0.521	17.688	16
	0.30	0.433	28.106	16
0.15	0.00	0.429	24.590	20
	0.05	0.510	16.867	17
	0.10	0.541	17.978	23
	0.15	0.495	22.241	20
	0.20	0.587	24.508	22
	0.25	0.499	22.964	22
	0.30	0.457	21.977	19
0.20	0.00	0.546	16.648	16
	0.05	0.526	7.639	15
	0.10	0.548	13.119	16
	0.15	0.569	13.382	16
	0.20	0.437	17.291	16
	0.25	0.535	12.857	16
	0.30	0.491	16.389	16
0.25	0.00	0.491	18.077	20
	0.05	0.559	12.165	16
	0.10	0.546	8.386	16
	0.15	0.573	10.328	19
	0.20	0.533	14.430	15
	0.25	0.511	10.910	19
	0.30	0.449	20.957	21

CHAPTER EIGHT

CONCLUSION AND FUTURE WORK

8.1 CONCLUSIONS

The principal objectives of this study can be classified into three main areas:

(a) The general behaviour of polypropylene fibre-reinforced concrete.

(b) The development of fracture toughness tests for Mode I and Mode II fracture of concrete materials.

(c) The application of the finite element method of analysis to investigate the fracture of concrete.

8.1.1 THE INFLUENCE OF POLYPROPYLENE FIBRES IN CONCRETE

The results of the tests carried out on polypropylene fibre-reinforced concrete indicate little change in flexural, compressive and fracture toughness strengths. The impact and torsional strengths seem to increase when compared with the plain concrete results. In most cases, it is seen that the strengths are increased with the addition of fibres up to the value of about 0.20 percent(by weight) and then drop off. The polypropylene fibre content within 0.05 percent to 0.20 percent by weight improve the general properties of concrete.

Polypropylene fibres have been added in quantities up to 0.30 percent by weight(0.75 percent by volume) in this study. An increase in fibre content beyond this value will

increase the problems of "balling" of the fibres during mixing and the difficulty of compaction. Inefficient compaction increases the occurrence of voids and thus reduces the strengths. Polypropylene fibres in quantities up to 0.80 percent by weight(2.0 percent by volume) have been used by previous researchers. In order to improve the polypropylene fibre content in excess of 0.30 percent (by weight), it is recommended that the possibilities of the use of admixtures and a more effective means of compaction are investigated.

Unlike steel fibres, the modulus of elasticity of polypropylene fibres is considerably lower than the cement matrix. Excess of polypropylene fibres can act as the equivalent of air voids in concrete due to their low stiffness - especially in compression. The compressive strength of fibre concrete is approximately constant and equivalent to plain concrete. Further increases of fibre content leads to reduction of the compressive strength below the value of that for plain concrete.

It is seen that the addition of polypropylene fibres in concrete has little effect on compressive and flexural strengths. Thus, there is little point of including fibres in concrete to increase the static strengths. More encouraging results were obtained from impact and torsional strengths in which the strengths were 15.0 percent and 52.0 percent higher than the plain concrete results. Thus, the

application of polypropylene fibre-reinforced concrete should be encouraged in areas where torsional and impact strengths are important factors.

The application of linear elastic fracture mechanics to fibre-reinforced concrete is not as obvious as for the case of plain concrete. The results obtained from the non-standard tests indicated that for the range of fibre contents, the evaluated fracture toughness value does not adequately reflect the useful properties of the fibres. Previous researchers also came to the same conclusions. Mindess et al(34) concluded that J-integral analysis was a much more sensitive indicator of the effectiveness of fibre addition - but this analysis was dependent on the specimen geometry.

The load-deflection curves confirmed that the polypropylene fibre-reinforced concrete behaves approximate linear elastically up to the "first crack" load at which point the matrix fails. This linear elastic response is obtained in both Mode I and Mode II tests. The fracture toughness values are then calculated from the peak load achieved. Side cracking was observed near the crack tips in plain and polypropylene fibre-reinforced concretes during shear fracturing(Mode II). The crack has a meandering path and tends to go around the aggregates rather than through them. The side crack and the meandering path of the main crack cause the energy demand for crack propagation to be

increased. This phenomenon did not affect the Mode II fracture toughness values because the corresponding fracture toughness values were determined from the "first crack" loads.

8.1.2 THE SPLIT-CUBE SPECIMEN FOR MODE I

The experimental and numerical results of the split cube tests indicate that the split-cube specimens are independent of the notch-depth ratios and the eccentricities of the applied load. It is seen that smaller notch depths(less than 25mm) often result in shear failures of the specimens near the point of loading while deeper notches(greater than 35mm) result in small areas of uncut concrete which introduce problems related to the aggregate size used in the concrete and underestimate the fracture toughness value

The computer program used for the finite element analysis(compliance method) is in two-dimensional form and can be used for either plane strain or plane stress conditions. From the typical stress distributions along the uncracked length of the split-cube specimen shown, both compressive stress and tensile stress are set up at the vicinity of the crack tips. It is the tensile stress, which is many times higher than the shear stress, which dominate the Mode I fracture process.

Unlike the stress method, the results obtained from the displacement and compliance methods are greatly influenced by the values of the modulus of elasticity. The numerical results showed that the calibration coefficient increases with the notch depth and the varying value of the modulus of elasticity has influenced the calibration coefficient. This phenomenon indicates that the modulus of elasticity has to be taken into account when evaluating on the fracture toughness value. The numerical expressions have been developed with several values of the modulus of elasticity. The fracture toughness values of the materials such as soil-cement, mortars and concretes can be evaluated using those expressions provided the failure loads are obtained from the split-cube specimens.

The compliance method and the displacement method in the numerical analysis give similar results. It is found that the element sizes have no effect on the fracture toughness values if the compliance method is used. Thus good results can be obtained with the compliance method without excessive grid size refinement in the vicinity of the crack tip. From the results obtained in this study, it is seen that the compliance method is simpler than the displacement method in the numerical analysis.

The coefficient of variation for the split-cube test results is only marginally greater than that obtained for the compression test results. The fracture toughness values

obtained in this study showed that the split-cube specimens are independent of the notch-depth ratios and the eccentricities of the applied load. It is concluded that the validity of the split-cube test can give consistent results within $0.50 \leqslant 2a/w \leqslant 0.70$ limits.

The majority of fracture toughness tests carried out on concrete have been taken the form of a notched beam subjected to three point or four point bending. The results obtained from this type of specimen geometry have been reported to give inconsistent results. The split-cube test has been shown to be a simple, reproducible test for toughness. The test results may be used either to determine the fracture toughness or to give an indication of toughness from the residual strength of the cracked specimen. The test is economic of the material used and is suitable for application on site. The main advantages of the split cube test is that specimens can be prepared readily using standard moulds and that the notches can be inserted with sufficient accuracy with a Clipper. Provided that standard notch depths are introduced into the cubes, the fracture toughness is directly proportional to the peak load achieved.

8.1.3 THE COMPACT TENSION SPECIMEN

The main objective of the work was to adopt the standard compact tension test for metallic materials for a test which can be used to evaluate the toughness of fibre-reinforced cement composite materials. The results showed that the fracture toughness values are independent of the notch-depth/width ratios. Thus the compact tension specimen can be used to evaluate the fracture toughness of the fibre-reinforced cement composite materials.

Several specimen sizes (50 X 50mm, 100 X 100mm and 150 X 150mm) were investigated in the experimental work. It is seen that the larger specimen sizes give more consistent results than the smaller specimen size. The error may be partly due to the size effect of the specimen — for the smaller specimens, the loading holes were positioned comparatively closer to the crack tip region. The small drop off in toughness value for the notch depth /width ratio of 0.60 was probably due to the insufficient uncracked length of the specimen in this case. When the uncracked length becomes small the stress-free boundary significantly affects the crack tip stress region.

The load value obtained in the test and used in the evaluation of K_{Ic} (using equation (4.1)) was obtained from the limit of proportionality of the load-deflection graph.

Therefore, linear elastic fracture mechanics theory was assumed to evaluate Mode I fracture toughness. It is important to note that misalignment of the loading straps and specimen gives unsatisfactory results. This is a well known problem in testing all materials e.g. steel, aluminium and plastic -- even small errors in alignment can cause large variations in the toughness values. A small applied load is necessary to help with the specimen alignment before loading in the test. The thickness of the specimen must be accurately measured so that it will not give incorrrect fracture toughness values.

From the results obtained in the compact tension tests, the maximum and minimum coefficient of variation are 11.4 percent and 8.4 percent respectively in the larger specimen sizes (100 X 100mm and 150 X 150mm). The fracture toughness values determined in this study are independent of the notch-depth/width ratios. Thus the compact tension specimen can be used to evaluate the toughness of fibre-reinforced cement composite materials. The most consistent results can be obtained within $0.40 \leqslant a/w \leqslant 0.50$ limits provided the compact tension specimen size is sufficiently large for the tests.

8.1.4 THE FRACTURE TOUGHNESS INDEX

The fracture toughness index of fibre-reinforced cement composite materials obtained in this study was based on the load-deflection curve. The value of the fracture toughness index was determined from the area under the 'first crack' X 4 and the area under the load-deflection curve which extends to twice the deflection at the point of 'first cracking'. Thus the value of the fracture toughness index is greatly influenced by the pattern of the load-deflection curve obtained during cracking.

The fracture toughness index results of the glass fibre-reinforced cement composite materials were obtained from the compact tension tests. The results showed that the fracture toughness index is independent of the notch-depth/width ratio and the specimen size. The average fracture toughness index values were 0.91 in the case of 100 X 100mm and 0.94 in the case of 150 X 150mm. The difference between these two values was approximately 3.3 percent. It is seen that a good correlation of the fracture toughness index results was obtained with the coefficient of variation generally within 4.0 percent. Thus the fracture toughness index can be used to measure the energy absorption capability of fibre concrete.

Typical fracture toughness index values were determined with varying polypropylene fibre content and loading system (split-cube and in-plane shear specimens). It is seen that the fracture toughness index increases with the addition of polypropylene fibres in the concrete. Thus the toughness index can be used as the indication of the performances or characteristics of the fibre-reinforced composite materials. The split-cube specimens and in-plane shear specimens give similar fracture toughness index values with constant fibre content. Thus the two types of specimens can be used to evaluate the toughness index of the fibre-reinforced composite materials. In general, the fracture toughness index of the in-plane shear specimen is slightly higher than the split-cube specimen. This phenomenon is probably due to the loading systems employed in the tests, in which the shear mode demands more energy for fracturing the specimen, due to the resistance of the matrix than in the Mode I (split-cube specimen) failure.

From the results shown in this study, the fracture toughness index may be used for all fibre-reinforced materials provided the load-deflection curves can be obtained in the experiments. Thus the toughness index results may be compared for varying types of fibre and fibre content. The main advantage of this method is that the test is not limited by any artificial restriction

regarding defined deflections. Since the index is expressed in percentage form there is no limitation regarding units.

8.1.5 THE IN-PLANE SHEAR SPECIMEN

The in-plane shear specimen for testing plain concrete and fibre-reinforced concrete was investigated in the experimental and numerical work. The varying slot separation/depth ratio does not affect the in-plane shear strength of the concrete. The coefficient of variation of the results range from 7.6 percent to 28.9 percent in all cases. In general, the coefficient of variation decreases as the slot separation /depth ratio increases. The slot separation/depth ratios of 0.20 and 0.25 give more consistent values of shear strength. This is due to the problem encountered as the aggregate size becomes an increasing percentage of the area where failure occurs. Thus increasing the slot separation/width ratio will provide a more uniform matrix between the opposite notches and give more consistent results.

Side cracking developed in the specimen during the loading process. The crack has a meandering path and tends to go around the aggregates. The side cracks and the meandering path of the main crack cause the energy demand for crack propagation to be increased. The side crack

effect does not influence the in-plane shear strength results. This is probably due to the fact that the shear strength was determined from the initial cracking of the concrete specimen. Since side cracks demand more energy for crack propagation, this phenomenon overestimates the fracture toughness index value. Side cracking in concrete is similar to metals which exhibit plasticity near the crack tips. In both cases, side cracking in concretes and plasticity in metals demand more energy for failure.

Typical stress distributions between the opposite notches were obtained from the numerical study. The compressive stress gradually changes in magnitude and nature and finally stablises to a constant value which is almost an order of magnitude lower than the corresponding shear stress. Thus the specimen is fractured by a shear mechanism. The compliance curves obtained in all cases give approximately constant values. Unlike the split-cube specimen, the calibration polynomial for Mode II fracture toughness reduces to less powers (in polynomial form) of the slot separation ratio. The results obtained in this study were similar to those obtained by Chisholm et al(53) and Sabir(52).

Agarwal et al (61) carried out experiments to determine the Mode II fracture toughness of short fibres composites and compared the results with the Mode I fracture values. They concluded that the critical strain

energy release rate in Mode II is less than that in Mode I. The results are shown in Fig.(8.1). The comparison of the Mode I and Mode II results (split-cube test and in-plane shear test) obtained in this study are illustrated graphically in Fig.(8.2). It is seen that the Mode II fracture toughness is less than that in Mode I. Thus the results obtained in this study are similar to the work obtained by Agarwal et al(61). Since fracture toughness in Mode II is less than that in Mode I, this phenomenon indicates that in the case of concrete materials, the fracture toughness tests in Mode II may be more important than the tests in Mode I.

The in-plane shear specimen results obtained in this study indicate that the test results can be used either to evaluate the fracture toughness or the toughness index. The preparation of the specimen is easy to carry out. Provided that the opposite notch depths are introduced into the specimens with a Clipper and the slot separations are within $0.20 \leqslant a/w \leqslant 0.25$ limits, the Mode II fracture toughness can be determined from the peak load achieved.

8.1.6 THE FINITE ELEMENT ANALYSIS

The load-deflection graphs obtained from the split-cube specimens and the in-plane shear specimens indicate that the curves show an approximate linear response up to the point where the concrete fails. This loading response showed that the linear elastic fracture mechanics theory may be applied for both plain and fibre-reinforced concretes. In all cases, the energy method, through compliance determinations, was used in the numerical work. The constant strain triangular element was employed in the analysis.

The numerical results obtained by means of the compliance method were compared with the results obtained by means of the displacement method which was used by Sabir(52). The results showed that the Mode I fracture toughness expressions for the split-cube test are similar for the two methods of analysis used to evaluate toughness. It is seen that the compliance method gives more consistent results with varying notch-depth ratio than the displacement method. This is probably due to the degree of refineness of the elements around the crack in the displacement method. The compliance method is simpler than the displacement method because good results can be obtained with the compliance method without excessive grid size refinement in the vicinity of the crack tip. Thus the

test results confirm the validity of using the finite element analysis (compliance method) for the determination of the fracture toughness in plain and fibre-reinforced concretes.

Unlike the stress method, the compliance method involves the use of the material's stiffness i.e. its modulus of elasticity. Thus the numerical results vary with the modulus of elasticity. In order to determine the fracture toughness of concrete, it is necessary to evaluate the corresponding value of the modulus of elasticity before using the finite element solutions obtained in this study.

From the numerical work described in this thesis, it may be concluded that the computer program employed in this study can be used to evaluate the fracture toughness in two-dimensional fracture mechanics problems. Although the compliance method and the displacement method give similar results, it is found that the compliance method is simpler than the displacement method. Finally, the numerical results obtained in both methods vary with the material's stiffness.

8.2 FUTURE WORK

In general, several methods have been investigated to determine the fracture toughness of plain concrete and fibre-reinforced concrete. Although most of the tests developed in this study give satisfactory results, it is considered that further investigations should be carried out in order to improve the results and the testing methods.

In the impact tests, the specimens should be replaced by concrete beams (100 X 100 X 500mm). This would result in easier alignment of the impacting face with the concrete specimen being tested. In the torsion tests, the torque should be applied at both ends instead of the middle part of the notched beam. This loading arrangement should reduce stresses which are locked into the test specimens before applying the torque. In general, polypropylene fibre-reinforced concrete exhibits higher strengths in torsion and impact tests than in other tests (flexural, toughness and compression). Further study of the polypropylene fibre-reinforced concrete should be applied to those areas where the impact and torsion strengths are the main problems.

In the split-cube tests, results showed that 100mm concrete cubes can be used to evaluate the fracture toughness. Larger specimen size such as 150mm cubes should

be used in future investigations and the results compared with those for the 100mm cubes. These comparisons would ensure that there is no size effect problems occur in the split-cube specimens. Alternately, other standard-concrete moulds such as cylinders could be used to carry out a parallel series of tests.

Apart from concrete materials, the split-cube specimen could be used to determine the fracture toughness of soil-cement, rock, cement paste etc.. The fracture toughness of the corresponding rock and cement paste used in this study would give an approximation of the fracture toughness value obtained in concrete.

A good quality mix was used throughout the split-cube tests investigated in this study. Dowers(39) concluded that the water-cement ratios for this mix had no effect on fracture toughness. A poor concrete mix with low cement content should be used in further tests and the effect of varying water-cement ratio on fracture toughness investigated. Finally, various types and sizes of aggregates should also be investigated.

The thickness of the compact tension specimen is an important factor which greatly influences test results. A fully investigation of fracture toughness of cement based composite materials with varying thickness should be included in any future work. The pattern of the fracture

toughness results for varying thickness could be compared with the results for metallic materials.

Other standard tests such as the bend test could be carried out to determine the fracture toughness of fibre-reinforced cement composite materials. The bend specimen should be modified -- similar to the test specimen described in reference(14). The results could then be compared with the compact tension specimen results obtained in this study.

Fracture toughness index results showed that the index may be used to characterise fibre-reinforced composite materials. Other types of fibre such as steel and polymers should be used to determine their fracture toughness index values. Thus a comparison of the index values could be made among various fibre materials. Furthermore, an index above 75 percent would yield a load-deflection curve with a positive slope at all times. Such a materials could be tested in a load control machine.

The in-plane shear specimen should be further investigated in order to reduce the variability of the test results. Larger specimen size (150 X 150 X 200mm) or smaller aggregate size (less than 10mm) may be used to reduce the coefficient of variation of the results. Future work should include the use of various types and sizes of aggragate so that the shear strengths may be compared among

them. Other materials such as mortar and soil-cement (which have a more uniform matrix) should be used in the in-plane shear test.

Since a small amount of tensile stresses exist between the opposite notches in the in-plane shear specimen, lateral load should be applied between the opposite notches together with the compressive failing load. Thus the tensile stresses would be eliminated during shear fracturing, and a pure shear failure mechanism may be obtained. Further experiments should be carried out with a tensile load acting at both ends of the in-plane shear specimen. The shear failure of the specimen (tensile load) should be similar to those obtained in this study (compressive load). Thus the results could be compared between the two loading systems. Apart from the numerical analysis, experimental analysis such as photoelasticity should be used to compare the results obtained in the numerical study. In the photoelasticity analysis, the crack tips must be very carefully notched to the required depth because small errors would lead to invalid results obtained in this experimental work.

Other research workers concluded that the in-plane shear specimen was geometry dependent. As far as the results obtained in this study are concerced, the in-plane shear specimen results were independent of the specimen geometry. The difference between the two conclusions is

most likely due to the thickness of the specimens used. Thus the in-plane shear specimen with varying thickness should be investigated in future work. The results could be used to determine the minimum thickness of the specimen which would give results independent of the thickness.

Since the compliance method and the displacement method are dependent on the modulus of elasticity of the materials, the stress method (which is independent on the modulus of elasticity) should be used to analyse the specimen geometries in both the split-cube specimen and the in-plane shear specimen. Thus the finite element results could be compared for the three methods. Furthermore, a finite element solution obtained from the stress method is more convenient than the other methods (compliance and displacement methods) because the solution could be immediately used without the knowledge of the modulus of elasticity of the materials.

The polypropylene fibre-reinforced concrete results obtained in this study indicate that the addition of fibres increases the strengths of the concrete up to an optimum fibre content. Further increase the polypropylene fibre content will reduce the strengths. In order to increase the optimum fibre content in the mix, it is recommended that the possibility of using admixtures and a more effective means of compaction should be investigated. In general, other types of fibre (steel, polymers) should be used in

the tests developed in this study.

Fracture toughness tests in Mode I and Mode II for plain concrete and fibre-reinforced concrete have been developed in this study. Further investigations should be carried out to develop a testing method for Mode III fracture toughness (torsion). The main philosophy to be applied for this fracture mode should include the use of standard geometry specimens, simple notches and testing system. Thus the Mode III fracture toughness of concrete could be determined as simply as possible.

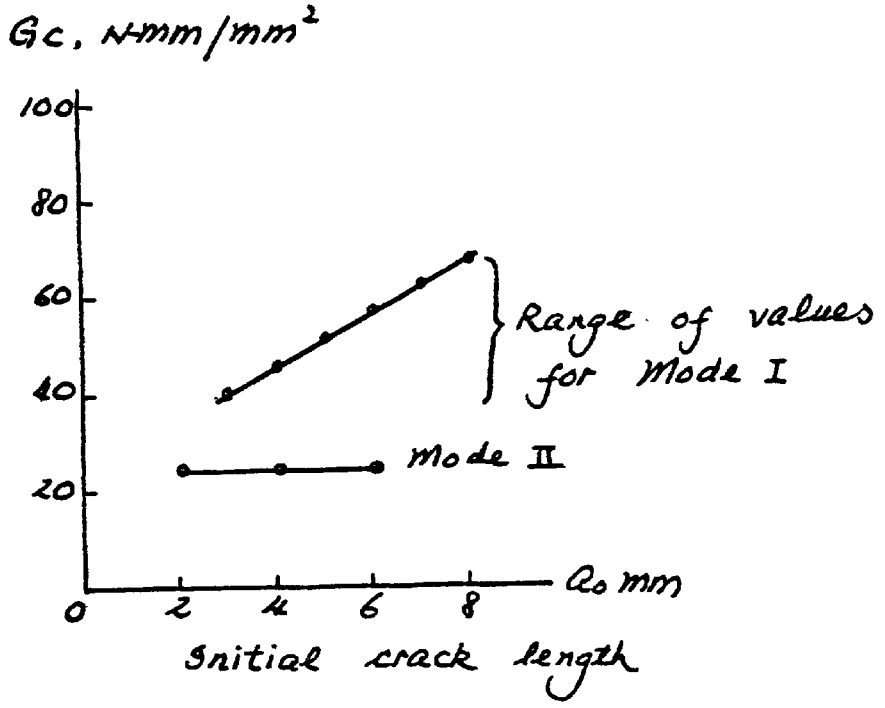

Fig. (8.1) Variation of critical strain energy release rate with initial crack length (Agarwal and Giare[61])

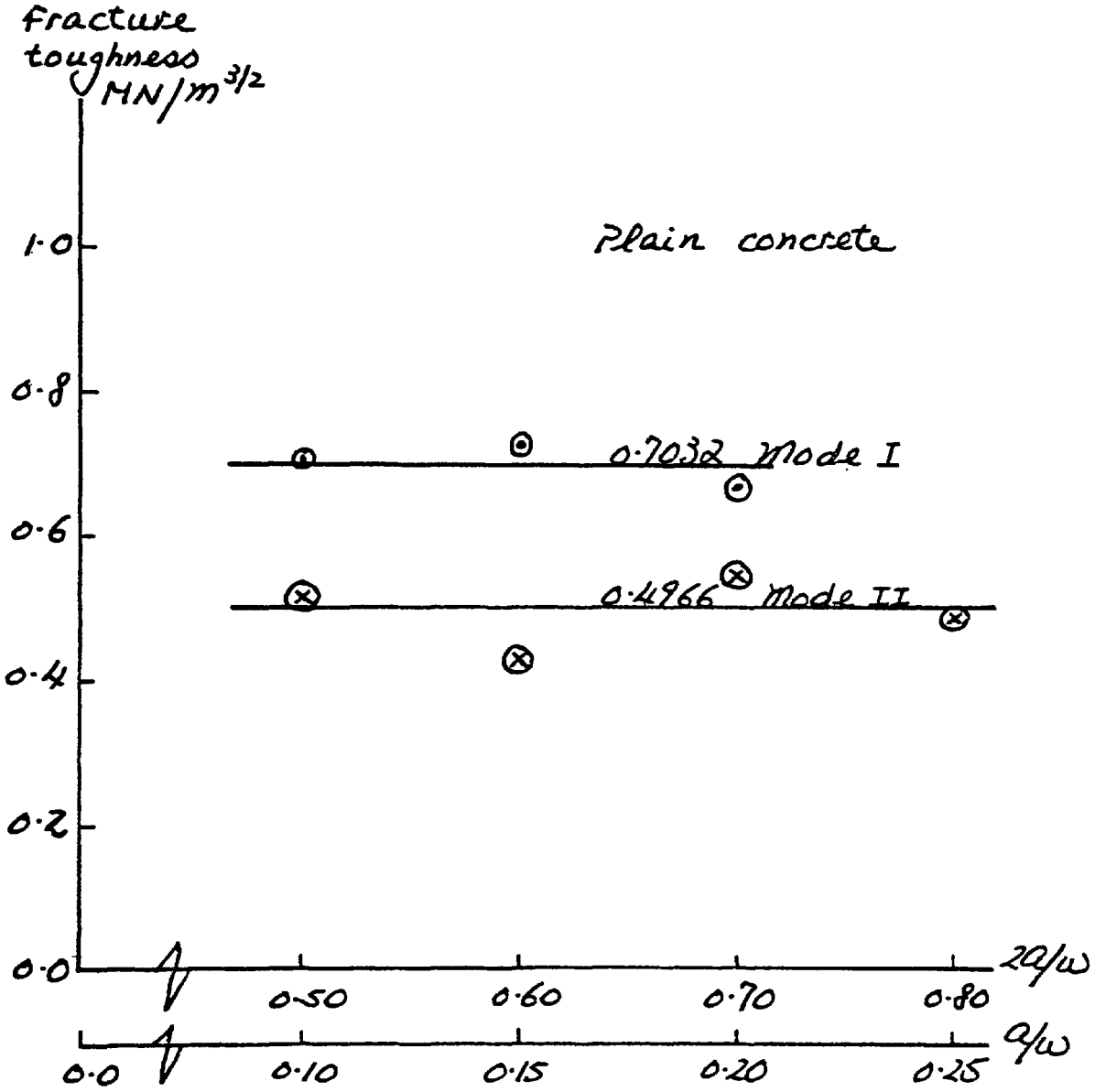

Fig. (8.2) Mode I and Mode II fracture toughness results for varying notch depth and slot separation ratios

REFERENCES

REFERENCES

1) Griffith A. A.
'The phenomena of rupture and flow in solids',
Transactions Royal Soc., London, vol.A221, pp.163-198,
1920.

2) Orowan, E.
'Fracture and strength of solids',
Prog. Phys., vol.12, pp.185-232, 1949.

3) Irwin, G. R.
'Fracture Dynamics, fracturing of metals',
Am. Soc. metals, Cleveland, pp.147-166, 1948.

4) Irwin, G. R.
'Analysis of stresses and strains near the end of a
crack transversing a plate'
Journal of Appl. Mech., 1957, 24, 361.

5) Westerg aard, H. M.
'Bearing pressures and cracks',
Journ. Applied Mech., vol.6, pp.49-53, 1939.

6) Irwin, G. R. and Kies, J. A.
'Critical energy rate analysis of fracture strength',
Welding Journal Research Supplement, vol.33, pp.193-198,

1954.

7) Tetelman, A. S. and McEvily, A. J.
'Fracture of structural materials',
John Wiley and Sons, Inc., 1967.

8) Brown, W. F. and Srawley, J. E.
'Plane strain crack toughness testing of high strength metallic materials',
ASTM Special technical publication no.410.

9) Irwin, G. R.
'Plastic zone near a crack and fracture toughness',
Proc. Seventh Sagamore Ordinance Material Research conf.,
Report No.M & TE661-611/F, Syracuse University Research Inst., August 1960

10) Dugdale, D. S.
Journ. Mech. Phys. Solids, 8, 100, 1960.

11) McCabe, D. E. and Heyer, R. H.
'R-Curve Determination using a crack-line-wedge-loaded (CLWL) specimen',
Fracture toughness evaluation by R-curve methods,
A.S.T.M., STP527, pp.17-35, 1973.

12) Rice J. R.

Journal of Applied Mechanics, Transactions of the American society of mechanical engineers, June, pp.379-386, 1968.

13) Begley, J. A. and Landes, J. D.
'The J Integral as a Fracture Criterion',
Fracture Toughness, Proceedings of the 1971 National Symposium on Fracture Mechanics, Part II, A.S.T.M., STP514.

14) 'Tentative Method of Test for Plane-strain Fracture Toughness of Metallic Materials'.
A.S.T.M. Designation: E399-70T.

15) Kaplan, M. F.
'Crack propagation and fracture of concrete',
Journ. Am. Con. Inst., Vol. 58(28), pp 591-610, 1961.

16) Lott, J. and Kesler, C. E.
'Crack propagation in plain concrete',
Symp. on structure of portland cement paste and concrete. Wastington D.C. Highway Research Board Special Report No.90, pp.204-218, 1966.

17) Moavenzadeh, F. and Kuguel, R.
'Fracture of concrete',
Journ, Mate., vol.4(3), pp.497-519, 1969.

18) Naus, S. J. and Lott, J. L.
'Fracture toughness of portland cement concretes',
Journ. Am. Conc. Inst., vol.66(6), pp.481-489, 1969.

19) Brown, J. H.
'Measuring the fracture toughness of cement paste and mortar',
Maz. Conc. Research, vol.24(81), pp.185-196, 1972.

20) Higgins, D. and Bailey, J.
'Fracture measurements on cement paste',
Journ. of Materials Science, vol.11, pp.1195-2003, 1976.

21) Barr, B. and Bear, T.
'Fracture Toughness',
Concrete, pp.30-32, April 1977.

22) Javan, L. and Dury, B. L.
'Fracture toughness of fibre reinforced concrete',
concrete, pp.31-33, Dec.1979.

23) Swamy, R. N.
'Fracture toughness applied to concrete',
Developments in concrete technology, Edited by F.D.
Lydon. Applied Science Publishers Ltd. London.
pp.221-281, 1979.

24) A.C.I. Committee 544.
'State-of the-Art Report on Fibre reinforced concrete',
A.C.I. Journal, pp.729-743, Nov. 1973.

25) 'Fibre Concrete Materials'. A report prepared by RILEM
Technical Committee 19-FRC.
Material et constructions, section 7, vol.10(56),
pp.103-119, 1977.

26) Hannant, D. J.
'Fibre cements and fibre cement composites',
John Willey and Sons, 1978.

27) Grimer, F. J. and Ali, M. A.
'The strengths of cements reinforced with glass
fibres',
Mag. of concrete research, vol.21(66), pp.23-30,
March 1969.

28) Harris, B., Varlow, J. and Ellis, C. D.
'The fracture behaviour of fibre reinforced concrete',

Cement and Concrete Research, vol.2, pp.447-461, 1972.

29) Takagi, J.
'Some properties of glass fibre reinforced concrete',
Fibre reinforced concrete, Publ. SP-44 (Detroit:
American Concrete Institute) pp.93-111, 1974.

30) Hughes, B. P. and Fattuhi, N. I.
'Improving the toughness of high strength cement paste
with fibre reinforcement',
Composite, pp.185-188. July 1976.

31) Hughes, B. P. and Fattihi, N. I.
'Load-deflection curves for fibre-reinforced concrete
beams in flexural',
Mag. of Concrete Reasearch, vol.29(101), pp.199-206,
Dec. 1977.

32) Hibbert, A. P. and Hannant, D. J.
'The design of an instrumented impact test machine for
fibre concretes',
Rilem Symp. on testing and test methods of fibre cement
composites, pp.107-120, 1978.

33) Patterson, W. A. and Chan, H. C.
'Fracture toughness of glass fibre-reinforced cement',
Composites, pp.102-104, May, 1975.

34) Mindess, S.
'The fracture of fibre-reinforced and polymer impregnated concretes',
International Journal of Cement Composites, vol.2, pp.3-11, 1980.

35) Nishioka, K., Yamakawa, S., Hisakawa, K., Akihama, S.
'Test mathod for the evaluation of the fracture toughness of steel fibre',
Rilem Symp. on Testing and test methods of fibre cement composites, pp.87-98, 1978.

36) Ohigashi, T.
'Measurement of effective fracture energy of glass fibre reinforced cement',
Rilem Symp. on Testing and test methods of fibre cement composites, pp.67-78, 1978.

37) Velazco, G., Visalvanich, K., and Shah, S. P.
'Fracture behaviour and analysis of fibre reinforced concrete beams',
Cement and Concrete Research, vol.10, pp.41-51, 1980.

38) Swamy, R. N.
'Influence of slow crack growth on the fracture resistance of fibre cement composites',
International Journal of Cement Composites, vol.2, pp.43-53, 1980.

39) Dowers, R. C.
'The fracture toughness of concretes',
A thesis submitted for the degree of Master of Philosophy, C.N.A.A., London, 1980.

40) Barr, B., Evans, W. T., Dowers, R. C., Sabir, B. B.
'The fracture toughness of concrete',
2nd. Int. Conference on Num. methods in fracture mechanics, Swansea, 1980.

41) Kobayashi, A. S., Maiden, D. E., Simon, B. J., Iida, S.
'Application of finite element analysis method to two-dimansional problems in fracture mechanics',
Office of Naval Research, Contract no.447(39) NR064 478, Technical Report 5.

42) Chan, S. K., Tuba, I. S., Wilson, W. K.
'On the Finite Element Method in Linear Fracture Mechanics',
Eng. Fracture Mechanics, pp.1-17, vol.2, 1970.

43) Watwood, V. B.
'The Finite Element Method for prediction of Crack Behaviour',
Nuclear Eng. Design, vol.11, 1969.

44) Dixon, J. R., Strannigan, J. S.

'Determination of Energy Release Rates and Stress-Intensity Factors by the Finite-Element Method',
Journal of Strain Analysis, vol.7, no.2, 1972.

45) Erdogan, F., Sih, G. C.
'On the crack extension in plates under plane loading and Transverse shear',
Transactions of the A.S.M.E., Dec. 1963.

46) Nowbray, D. F.
'A note on the Finite Element Method in Linear Fracture Mechanics',
Eng. Fracture Mechanics, vol.2, pp.173-176, 1970.

47) Swamy, R. N., Rao, C. V. S. K.
'Toughness and ductility of fibre reinforced concrete composites in flexure ',
Paper10 , Fibre reinforced materials. Inst. Civ. Eng., London, 1977.

48) Henager, C. M.
'A toughness index for fibre concrete',
Rilem Symp. on Testing and test methods of fibre cement composites, pp.79-86, 1978.

49) Majumdar, A. J., Ali, M. A., Singh, B.
'Properties of glass fibre cement — the effect of fibre length and content',

Fibre Reinforced Materials, BRE Building Research Series, vol.2, pp.69-76, 1978.

50) Singh, B., Walton, P. L., Stuck, M. S.
'Test method used to measure the mechanical properties of fibre cement composites at BRE',
Rilem Symp. on Testing and test methods of fibre cement composites. pp.371-387, 1978.

51) Oakley, D. R., Unsworth, M. A.
'Shear strength testing for glass reinforced cement',
Rilem Symp. on Testing and test methods of fibre cement Composites, 1978.

52) Sabir, B. B.
'The application of the finite element method to fracture mechanics problems',
Thesis submitted to the CNAA, London, for the degree of Doctor of Philosophy, 1980.

53) Coughlan, J.
'Crack propagation in isotropic materials',
Thesis submitted to the CNAA, London, for the degree of Doctor of Philosophy, 1973.

54) Chisholm, D. E., Jones, D. L.
'An analytical and experimental stress analysis of a practical Mode II fracture test specimen',

Experimental Mechanics, pp.7-13, Jan. 1977.

55) Liu, K.
'General properties of polypropylene fibre-reinforced concretes',
Final year undergraduate project, The Polytechnic of Wales, Treforest, 1979.

56) Neville, A. M.
'Properties of concrete',
Pitman, 1972.

57) Knott, J. F.
'Fundamental of fracture mechanics',
Butterworth, 1973.

58) Kesler, C., Naus, D., and Lott, J.
'Fracture mechanics — Its applicability to concrete',
Proceedings of the 1971 International Conference on Mechanical Behaviour of Materials.
Vol.IV, Japan, 1972, pp.113-124.

59) Saouma, V, E., Ingraffea, A. R., Catalano, D. M.
'Fracture Toughness of Concrete — K_{Ic} Revisited.'
Journal of the Engineering Mechanics Division,
American Society of Civil Engineers, October 1980.

60) Sharples, J. K.

'Finite Element Methods applied to two Fracture Test Specimens'.
Department of Industry, NEL Report no.675, June 1981.

61) Agarwal, B.D. and Giare, G. S.
'Fracture toughness of short fibre composites'.
Engineering Fracture Mechanics, vol.15, no.1-2,
pp.219-230, 1981.